UNIVERSITÀ DEGLI STUDI DELLA CALABRIA
Facoltà di Scienze Matematiche Fisiche e Naturali
Dipartimento di Chimica

Dottorato di ricerca in Metodologie Chimiche Inorganiche
XXII ciclo

AREA 03 –Scienze Chimiche, SSD-CHIM03/Chimica generale ed inorganica

Studio Teorico dei Dettagli Meccanicistici di Reazioni Organiche Catalizzate da Oro

Supervisore
Prof. Emilia Sicilia

Coordinatore
Ch.mo Prof. Nino Russo

Candidata
Gloria Mazzone

A.A. 2008-2009

Indice

Abstract

The catalytic chemistry of gold has had a relatively belated development with respect to other late transition metals, and this has been attributed to the preconception that gold is expensive and unreactive. The interest in gold has grown over the last thirty years, because both of these conceptions have been proven false, and successful applications of gold catalysis have emerged in chemical processing, pollution control, fuel cells design, and many others fields. These evidences have sparked a veritable "gold rush" in the field of catalysis, both homogeneous and heterogeneous.

We investigated the role of gold in both homogeneous and heterogeneous catalytic processes. In fact, the theoretical study of mechanistic details for reactions, that involves and underline the characteristics of gold, have been the subjects of this thesis. Density functional theory (DFT) is the method of choice in this kind of studies.

Regarding heterogeneous catalysis the synthesis of vinylacetate is the reaction on which we have focused our attention. In particular, a bimetallic catalyst containing low Pd coverage on Au surface (100 and 111) has been selected to outline the reaction mechanism of VAM formation. We have studied in detail both mechanisms proposed in literature, in order to selected the more active surface and the more likely mechanism.

The homogeneous catalytic process that has been selected to point out the catalytic activity of gold is the hydration of 1,2-diphenylacetylene to yield benzyl phenyl ketone, catalyzed by a complex of Au(I) with triphenylposphine. This cationic complex coordinates to the alkyne in the first step of the catalytic cycle, thus rendering it more susceptible for a nucleophilic attack. That reaction is a relatively new synthetic strategy that have recently studied experimentally. Our aim is to elucidate the mechanism of the whole reaction.

1

L'oro fa il suo debutto come catalizzatore

Introduzione

L'*oro* è un metallo nobile che per lungo tempo è stato considerato inerte dal punto di vista catalitico. Dalla seconda metà del secolo scorso, alcuni esperimenti condotti sull'*oro* hanno però evidenziato l'attività catalitica di piccole particelle del metallo. Tuttavia, l'*oro* manifesta le sue proprietà catalitiche solo in circostanze specifiche. Sono comunque necessari alcuni requisiti, quali la dimensione delle particelle, i materiali di supporto, la struttura e i metodi di preparazione, tutte importanti proprietà per la creazione di un buon catalizzatore.

Nonostante l'*oro*, paragonato agli altri metalli del gruppo del platino, abbia un prezzo contenuto e soprattutto stabile, il suo utilizzo dal punto di vista industriale è ancora fortemente limitato. Negli ultimi anni la percezione dell'*oro* è però notevolmente cambiata.

1.1 Sviluppo dell'*oro* come catalizzatore

Durante tutto il XX secolo sono state condotte una serie di ricerche per stabilire l'esistenza di un'attività catalitica per l'*oro*[1]. Nei primi anni del '900 le scoperte importanti in questo campo furono essenzialmente due. La prima, nel 1906 fatta da Bone e Wheeler, i quali osservarono l'ossidazione dell'idrogeno su una garza di *oro*[2]. Successivamente, nel 1925, Andrew, insieme con Bone, fu il primo ad effettuare l'ossidazione del monossido di carbonio catalizzata dall'*oro*[3]. Nel corso degli anni '50 e '60, invece, l'attenzione si è concentrata sull'attività catalitica dell'*oro* nelle reazioni di idrogenazione.

Una svolta importante in questo campo si ebbe con il lavoro di Wood e Wise, i quali mostrarono che un film di *Au* risultava attivo per l'idrogenazione del cicloesene e dell'1-butene se gli atomi di H dissociati venivano forniti da una lega del tipo Pd-Ag.[4]

Il primo indizio che l'*Au* potesse essere attivo cataliticamente se disperso in piccole particelle si ebbe negli anni '70. Bond and Sermon[5,6] riportarono i risultati ottenuti riguardo la deidrogenazione di alcheni e alchini a temperature inferiori a 473K, utilizzando *Au*/SiO_2 come supporto. Parravano a collaboratori[7,8] hanno, invece, riferito in merito a reazioni di trasferimento di idrogeno e ossigeno catalizzati da supporti del tipo *Au*/MgO e *Au*/Al_2O_3. I risultati ottenuti hanno così evidenziato un'attività catalitica selettiva, di alcuni di questi campioni, per l'idrogenazione di alcheni lineari a basse temperature, anche se l'efficienza risultava essere inferiore a quella riscontrata con altri metalli nobili.[9,10]

A metà di quegli anni ’70 McIntosh e Ozin[11] studiarono invece i fattori che potevano influenzare il “binding mode” dell’ossigeno molecolare nella formazione di complessi metallo-ossigeno. I risultati ottenuti utilizzando l’Au come metallo consentirono di sviluppare un modello per il meccanismo della reazione di ossidazione del CO catalizzata eterogeneamente.[11,12] L’importanza di queste osservazioni non venne però subito riconosciuta. Solo nella seconda metà degli anni ’80, Hutchings,[13] confermò la migliore attività catalitica svolta dall’Au nella reazione di idroclorinazione dell’acetilene a vinil cloruro.

Intorno al 1987 M. Haruta[14] fu invece in grado di dimostrare che l’ossidazione del CO poteva essere realizzata a temperatura ambiente utilizzando l’Au disperso su superfici di ossidi. Sulla base di tale evidenza, durante gli ultimi vent’anni l’interesse nei confronti di reazioni catalizzate da Au è aumentato notevolmente.

1.2 Gli stati di ossidazione dell’Au

I comuni stati di ossidazione dell’Au sono essenzialmente *I* e *III*, mentre *V* è stato osservato solo in composti di oro con fluoro. La coordinazione locale è in generale lineare (*I*), planare quadrata (*III*) e ottaedrica (*V*), rispettivamente. È stato osservato che, la maggiore destabilizzazione relativistica ed espansione degli orbitali *5d* della terza riga di transizione, dovrebbe favorire stati di ossidazione più alti, rispetto ai corrispondenti orbitali *4d* della seconda riga di transizione.[15] Il ruolo della relatività nel cambio dello stato di ossidazione dell’Au da *I* a *III*[16,17] o da *III* a *V*[17] in complessi alogenuri è stato esplicitamente dimostrato da Schwerdtfeger e collaboratori. Nel caso particolare di $(AuX_2)^q$, X = Cl,Br, sia gli studi teorici che gli esperimenti di spettroscopia di massa mostrano che l’oro può avere tre stati di ossidazione (*I*, *II*, *III*) corrispondenti alla carica totale *q* di -1, 0 e +1 rispettivamente.[18]

Sono noti composti paramagnetici closed-shell di Au^{II} per i quali la natura del legame è stata discussa dal gruppo di Hoffmann[19] e confermata con studi teorici a livello ab initio.[20]

Sperimentalmente, è stato sintetizzato da Yam e collaboratori[21] un legame senza ponti P-Au^{II}-Au^{II}-P con una lunghezza di legame Au-Au di 261pm. Successivamente, il gruppo di Fackler[22] sintetizzò dei sistemi a doppio ponte con una distanza Au^{II}-Au^{II} pari a 247pm.

Puddephatt e Vittal[23] hanno, invece, osservato l’esistenza di un complesso di Au^{IV}.

Esistono naturalmente esempi di sistemi contenenti Au in stato di ossidazione *0*, non solo in solidi o in cluster neutri, ma anche in altri composti, alcuni dei quali sembrano contenere nascosta l'unità Au_2.

Infine, per quanto riguarda lo stato di ossidazione Au^{-1}, sono stati condotti numerosi studi a livello ab initio su auridi solidi o molecolari.[24] In particolare per il CsAu liquido sono state effettuate anche simulazioni a livello di dinamica molecolare.[25,26]

1.3 L'utilizzo dell'oro in catalisi omogenea

I benefici dell'Au in catalisi omogenea si sono manifestati solo negli ultimi dieci anni.[27,28,29,30,31] La maggiore virtù dei sali di oro, in catalisi omogenea, è la singolare abilità degli stessi di attivare legami multipli C-C come acido di Lewis carbofilico, permettendo la formazione di nuovi legami C-C, C-O, C-N e C-S per attacco nucleofilico a questi substrati attivati. Per di più, l'oro risulta essere un eccellente catalizzatore per l'attivazione di legami C-H, come per esempio di composti aromatici. Come conseguenza si apre, ancora una volta, un percorso di reazione senza precedenti per la formazione di un legame carbonio-carbonio. Occasionalmente, i sali di oro negli stati di ossidazione più stabili, Au(I) e Au(III), sono capaci di catalizzare la stessa trasformazione, e molto spesso non è chiaro quale stato di ossidazione rappresenti effettivamente la specie cataliticamente attiva. Inoltre, i composti di oro hanno il vantaggio di essere facilmente ridotti, ma difficili da ossidare, e non tendono a subire eliminazioni di idrogeno in posizione β.

1.3.1 Effetti relativistici

La determinazione della relazione esistente tra struttura e funzione è ormai diventata di fondamentale importanza per la comprensione dei processi chimici e biochimici, per cui, lo studio teorico della struttura elettronica dell'Au costituisce un punto cruciale per stabilire a priori il modo in cui esso funge da catalizzatore e determina il percorso reattivo più accessibile.[32]

Gorin e Toste[31] hanno ampiamente studiato gli effetti relativistici dell'Au in catalisi omogenea raccogliendo un mole di dati sperimentali e computazionali che fanno luce sulla reattività e sulle potenziali applicazioni dei catalizzatori a base di Au.

Le più importanti caratteristiche della struttura elettronica dell'oro sono la conseguenza di forti effetti relativistici.[31,33] Il termine "effetti relativistici" si riferisce a qualsiasi fenomeno risultante dalla necessità di considerare la velocità come significativa rispetto alla velocità della luce. L'espressione della massa corretta *m* risulta quindi essere

$$m = \frac{m_0}{\sqrt{1-\left(\frac{v}{c}\right)^2}}$$ con m_0 massa non relativistica e v la velocità

I fenomeni di maggiore rilievo derivanti dagli effetti relativistici[34,35] sono essenzialmente tre. Innanzitutto, la contrazione dell'orbitale *1s*, la quale risulta significativa solo per gli elementi in cui gli orbitali *4f* e *5d* sono pieni; tale contrazione si applica anche agli altri orbitali *s* e agli orbitali *p*. La seconda manifestazione degli effetti relativistici è dovuta al fatto che gli elettroni che occupano gli orbitali *d* ed *f* sono maggiormente schermati dagli elettroni negli orbitali contratti *s* e *p*, risentendo così di una minore attrazione nucleare. Il terzo effetto è l'accoppiamento spin-orbita.

Un'evidenza sperimentale spiegata dagli effetti relativistici è il colore dell'oro. Quest'ultimo è dovuto all'eccitazione egli elettroni *5d* dal livello di Fermi, che corrisponde ad un *bandgap* di *2.38eV*, il quale risulta abbastanza piccolo a causa della contrazione relativistica degli orbitali 6*s* e 6*p* e l'espansione degli orbitali 5*d*, da provocare l'assorbimento di luce blu nella zona del visibile. La differenza è per esempio evidente rispetto all'Ag, per il quale non si osserva l'assorbimento di alcuna radiazione nella zona del visibile.

Tale contrazione relativistica dell'orbitale *6s* risulta particolarmente evidente nei legami Au-L (dove L è il legante)[36]. Al di là della lunghezza di legame Au-L osservata, che risulta essere più lunga del previsto, l'ulteriore conferma sperimentale di questa distorsione dalla struttura elettronica prevista risiede nel fenomeno dell'"aurofilicità",[37] nella tendenza cioè delle interazioni Au-Au ad essere energeticamente stabilizzate dello stesso ordine di grandezza

dei legami a idrogeno, e anche nel valore del potenziale di prima ionizzazione osservato per l'Au (*9.22eV* contro i *7.57eV* per l'Ag).

Un'importante caratteristica dell'Au che lo differenzia dagli altri elementi dell'undicesimo gruppo (generalmente complessi tricoordinati e tetracoordinati di Cu(I) e Ag(I)) è la coordinazione lineare in geometria bicoordinata prevalentemente adottata dall'Au(I).[38,39] La conseguenza pratica del tipo di coordinazione tipicamente osservato nella chimica dell'Au(I) è la necessità di estrarre un legante da un complesso neutro bicoordinato di Au(I) in modo da indurre la reattività catalitica. Inoltre, i complessi organo aurati(I) non sono particolarmente nucleofili rispetto ai corrispondenti complessi di rame. Questa evidenza è stata motivata attraverso studi teorici, i quali hanno evidenziato che gli elettroni *5d* dell'Au sono più fortemente trattenuti rispetto agli elettroni *3d* del Cu a causa della diminuzione della repulsione elettrone-elettrone negli orbitali diffusi *5d*, risultanti in specie metalliche meno nucleofile che non tendono a subire addizione ossidativa.[40] Studi computazionali e sperimentali condotti su complessi di Au(III) del tipo $LR_3Au(III)$[41,42] hanno confermato la più ampia reattività osservata per i complessi di Au(I) e Au(III), i quali non vengono coinvolti facilmente nei cicli che comportano una variazione dello stato di ossidazione.[43]

Le specie di Au(I) sono generalmente tolleranti nei confronti dell'ossigeno, per cui le reazioni catalizzate dall'oro possono essere realizzate in condizioni meno drastiche, senza precauzioni per l'esclusione dell'aria. Inoltre, l'apparente stabilità redox dei complessi di Au(I), a temperatura e pressione ambiente, consente lo sviluppo di nuovi modi di reattività in modo da precludere i tradizionali cicli di addizione ossidativa/eliminazione riduttiva prevalenti nei meccanismi di catalisi degli altri metalli di transizione.

1.3.2 Caratteristiche dei complessi di Au(I)

La più comune stechiometria e struttura dei complessi di oro(I) può essere espressa dalla formula L-Au-X. Tale schematizzazione indica, innanzitutto, la presenza di un legante donatore neutro L e di un legante anionico X, ed evidenzia, poi, un'asse molecolare lineare che connette i leganti all'atomo metallico.

La forte acidità di Lewis dell'Au(I) cationico, accoppiata con il suo potenziale di stabilizzare gli intermedi di reazione cationici, impartisce una reattività unica a questi catalizzatori, che è stata sfruttata per lo sviluppo di nuovi metodi di sintesi. Agli studi

sperimentali che continuano ad evidenziare la reattività dei complessi di Au(I), vengono affiancati studi teorici che giustifichino e consolidino le osservazioni fatte sperimentalmente. Gli effetti relativistici forniscono un quadro teorico per la razionalizzazione della reattività osservata (come visto nel paragrafo **1.3.1**); l'orbitale *6s* contratto e gli orbitali *5d* espansi costituiscono un'importante caratteristica del metallo nel potenziale catalitico dei complessi di Au(I). Così, integrando lo studio teorico con quello sperimentale si è riusciti ad ottenere una più profonda comprensione delle proprietà fondamentali dell'Au(I).

Le specie cationiche di Au(I) sono acidi di Lewis molto più forti rispetto alle analoghe specie degli altri metalli dell'undicesimo gruppo. Una forte acidità di Lewis è generalmente accompagnata da una forte elettronegatività. Nel caso particolare dell'Au, l'elettronegatività è il risultato della contrazione relativistica degli orbitali di valenza *6s* e *6p*; in questo modo, l'analisi degli effetti relativistici non si limita a confermare l'analisi basata sull'elettronegatività, ma fornisce in realtà un base teoria per capirlo.

Tra i complessi particolarmente attivi nei confronti di reazioni in fase omogenea vi è certamente $AuPH_3^+$. Sulla base di confronti fatti con il corrispondente complesso di Ag,[39,44] tramite la *natural bond orbital (NBO) population analysis*, è stato possibile osservare, innanzitutto, che il legame Au-fosfina ha più carattere covalente del legame Ag-fosfina. Successivamente, con l'aggiunta di un secondo legante fosfinico, è stata misurata l'occupazione degli orbitali *6s* e *5s*, la quale ha suggerito una reibridizzazione degli orbitali molecolari nel complesso fosfinaAu(I) per giungere alla formazione di un legame tipo a 3-centri e 4-elettroni che innalza enormemente l'occupazione dell'orbitale *s*. Gli altri orbitali che potrebbero accettare elettroni, i *6p*, rimangono in gran parte inoccupati. Sebbene semplicistica, questa considerazione, se generalizzata, può essere in grado di razionalizzare la superiore acidità di Lewis dell'Au, poiché l'orbitale *s* dovrebbe essere responsabile dell'associazione di legame nel complesso fosfinaAuL^+. Inoltre, poiché $Au(I)^+$ è piuttosto grande, ci si potrebbe aspettare che sia l'orbitale, piuttosto che le interazioni di carica, a dominare la coordinazione del secondo legante. Pertanto, il complesso fosfine$Au(I)^+$ può essere considerato un acido di Lewis 'soft', che attiva preferenzialmente elettrofili 'soft', come per esempio i sistemi π.

1.3.3 La tendenza dell'oro all' "*Alchinofilicità*"

Molti degli studi condotti sulla reattività catalitica dell'oro hanno mostrato una propensione dei complessi cationici di Au(I) e di Au(III) ad attivare gli alchini verso l'addizione nucleofila.[29,30] Gli alchini costituiscono infatti un'importante classe di substrati ampiamente studiati per la loro caratteristica reattività. Le caratteristiche che li rendono particolarmente interessanti dal punto di vista della reattività sono essenzialmente due. Da un lato, hanno due orbitali π ortogonali occupati alti in energia, ciascuno con due elettroni, i quali possono facilmente reagire con composti elettrofili come alogeni, nel campo della sintesi organica, oppure con centri metallici elettrofili come l'Au, nel campo della catalisi con metalli di transizione.[45,46] Nell'interazione con un centro metallico, sia gli orbitali π nel piano di coordinazione con il metallo che gli orbitali π perpendicolari a tale piano, sono in grado di interagire con gli orbitali *d* del metallo. Dall'altro lato, l'orbitale non occupato si trova a più bassa energia e quindi reagisce con forti nucleofili come l'acetilene, con l'apporto catalitico di alcolati, nella sintesi di Reppe dei vinileteri.[47]

Sfortunatamente i nucleofili deboli non reagiscono direttamente con gli alchini, questi ultimi possono però essere attivati tramite coordinazione a complessi elettrofili di oro. Questa coordinazione attrae la densità elettronica dall'alchino rendendolo meno elettrofilo consentendo così anche l'attacco di nucleofili deboli.

Alcuni studi teorici condotti sui complessi Au(I)-etilene e Au(I)-etino indicano che è presente una retrodonazione, la quale è pari, però, ad una frazione molto piccola dell'energia di legame rispetto agli analoghi complessi di Cu.[48,49] Per cui, l'$Au(I)^+$ non può essere considerato significativamente partecipe all'interazione di legame del tipo Chatt-Dewar-Duncanson[50,51] poiché gli orbitali di antilegame sono apparentemente troppo alti in energia per verificarsi una significativa retrodonazione, considerando che la bassa energia degli orbitali *p* di non legame può essere più adatta per la sovrapposizione con gli orbitali pieni *5d* dell'Au. Questo può risultare rilevante per l'acidità di Lewis dell'Au(I); la mancanza di retrodonazione dall'Au(I) negli orbitali π dei leganti può rendere questi ultimi più elettron deficienti, contribuendo così a facilitare l'addizione nucleofila.

1.4 Il fenomeno dell' "Aurofilicità"

Il termine aurofilicità e "legame aurofilico" sono ormai ampiamente utilizzati per descrivere vari tipi di interazioni Au-Au con e tra composti di oro e le conseguenze di tali interazioni sulle proprietà dei sistemi considerati.

Nel caso generale, l'aurofilicità sembra essere operativa tra i centri metallici closed-shell nello stato di ossidazione formale Au^{+1} (con una configurazione elettronica di valenza $5d^{10}$) e nello stato linearmente bicoordinato. Il minore numero di coordinazione è un'importante prerequisito, dal momento che minimizza le repulsioni steriche tra i leganti negli aggregati. L'attrazione è quindi raramente osservata per numeri di coordinazioni maggiori di 2, anche se vi sono delle eccezioni.

Per molecole mononucleari indipendenti o ioni, l'approccio dei centri metallici avviene verticalmente all'asse molecolare fino a raggiungere una distanza di equilibrio Au-Au di circa 3Å (*Figura 1.1 a-c*). La conformazione degli aggregati può essere *staggered* (crossed) o *eclipsed* (parallel) (*Figura 1.1 d-f*) in base alla carica (+1, 0, -1) delle unità considerate.

Un centro metallico di Au(I) può instaurare uno o più contatti aurofilici. Gli arrangiamenti più comuni sono dimeri e polimeri chain-like (lineare, zig-zag o elicoidali), ma sono noti anche oligomeri con una disposizione lineare e compatta (*Figura 1.1 a,g-j*). Se però i leganti impongono delle restrizioni, allora la geometria può essere anche differente. Ciò è particolarmente comune quando diversi atomi di Au sono radunati attorno ad un atomo centrale comune (*Figura 1.1 k-l*). Per queste unità, gli angoli di legame Au-E-Au (spesso <90°) sono indicativi degli effetti di aurofilicità. Strutture alternative alla forma ciclica (*Figura 1.1 c*) ma con la stessa stechiometria sono costituite da polimeri (*Figura1 m*) o arrangiamenti macrociclici piegati (*Figura 1.1 n*).

L'energia associata al legame aurofilico è stata stimata sulla base di dati ottenuti con metodi differenti, ma con i quali risultati si è giunti a conclusioni molto simili. Tali dati inquadrano l'aurofilicità nella categoria delle forze deboli, paragonabili a quelle del legame a idrogeno e sicuramente più forti delle standard forze di Van der Walls. Il profilo energetico dell'approccio reciproco di due centri di Au sembra essere relativamente piatto, permettendo così una vasta gamma di distanze (*2.8-3.5Å*) per cui l'interazione di legame può essere ancora considerata. L'energia di legame di un solo atomo di oro (*Figura 1.1 a*) non è molto differente

da quella dell'atomo di oro misurata in aggregati multinucleari (*Figura 1.1 g-j*). La geometria delle unità individuali (L-Au-X) mostra solo lievi scostamenti dalla linearità presente negli aggregati, ma le lievi variazioni osservate sono tutte nella direzione che porta gli atomi di Au più vicini, indicando attrazione e non repulsione tra i centri. Questo tipo di descrizione esclude i legami tra atomi di Au con configurazioni elettroniche di valenza parzialmente aperte, in particolare il legame tra centri di Au^{2+} con configurazione $5d^9$, il quale può essere descritto come un regolare legame singolo metallo-metallo a due centri e due elettroni.

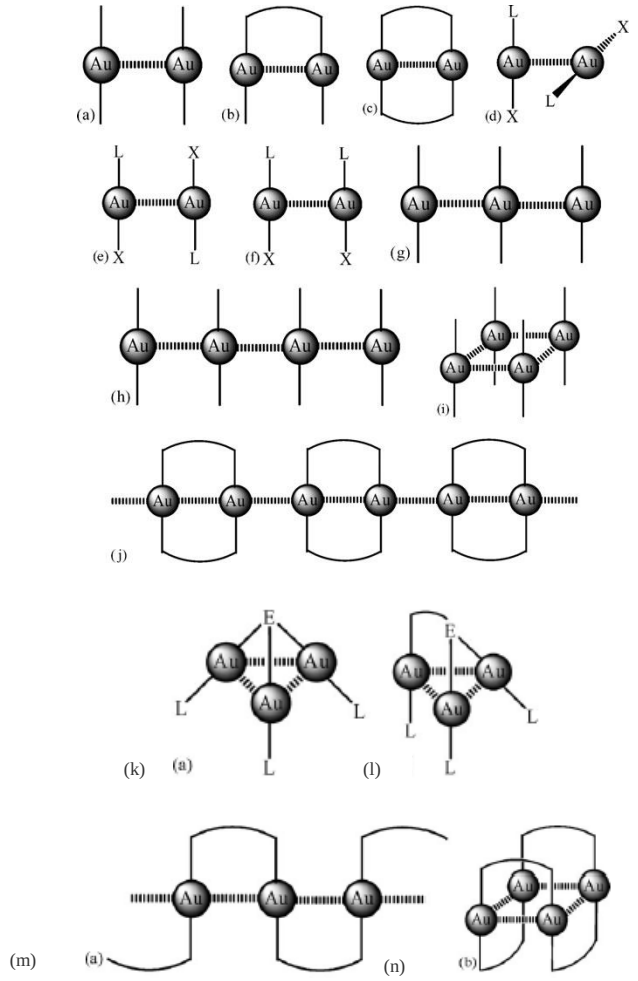

Figura 1.1: strutture schematiche per descrivere l'interazione tra centri metallici per molecole mononucleari indipendenti o ioni[52]

Uno dei più forti legami regolari Au-Au è presente nella molecola Au_2 in fase gassosa, derivante dalle interazioni degli stati $5d^{10}6s^1$ dell'Au^0. Va inoltre sottolineato il fatto che la maggior parte dei cluster di Au conosciuti sino ad ora contengono atomi di oro in stati di ossidazione misti, con componenti Au^0 e Au^+, il cui legame metallo-metallo può essere descritto nello stesso modo in cui è descritto il legame nell'oro metallico bulk. In tutti questi casi il legame aurofilico può rendere alcuni contributi assai lievi rispetto al legame complessivo del cluster che è generalmente molto più forte.

Sono stati pubblicati numerosi studi teorici a diversi livelli di sofisticazione, per sistemi modello semplici, che forniscono dati in buon accordo con i risultati sperimentali, anche se per il problema specifico dell'aurofilicità le procedure e i risultati di chimica computazionale non sono sempre molto chiari. Ma, nonostante non esista ancora alcuna immagine semplice dell'interazione, descrizioni come "super Van der Waals" e altre sono state comunque utilizzate. A prescindere da questo, sono stati trovati sempre più elementi di prova riguardo la rilevanza degli effetti, e il concetto è stato, di conseguenza, rapidamente impiegato con successo in molti settori della chimica dell'oro.

Dalla dettagliata descrizione delle possibili interazioni aurofiliche tra i centri metallici riportata in *Figura 1.1* risultano oltremodo evidenti i risultati ottenuti da studi combinati (sperimentali e computazionali) in diversi tipi di aggregati.

Evidenze di interazioni aurofiliche sono state infatti riscontrate in un gran numero di complessi polinucleari non ciclici con leganti polifunzionali flessibili[53] così come in complessi polinucleari ciclici. In questi due casi particolari di interazioni *intra*molecolari, l'identificazione di legami aurofilici risulta ancora più semplice. Tali contatti *intra*molecolari non sono associati ad una grave perdita di entropia, e in molti casi sono meno compromessi da effetti di congestioni steriche periferiche. I casi più comuni sono complessi di oro(I) con un numero di atomi di oro pari al numero di atomi donatori dei leganti, con catene flessibili a breve e media lunghezza, tra i centri donatori. Per ponti molto brevi, in particolare con un atomo che funge da centro comune dei donatori (*Figura 1.1 k,l*), un clustering può risultare praticamente obbligatorio, rendendo così l'effetto dell'aurofilicità meno evidente. Mentre, la presenza di leganti a ponte piuttosto lunghi, a causa dei contributi entropici e di packing molecolare, può favorire i contatti *inter*molecolari più che quelli *intra*molecolari. Molti complessi di oro(I) con

leganti bifunzionali formano dimeri con strutture cicliche mostrando interazioni aurofiliche trans anulari.[54]

Un'altra caratteristica particolarmente interessante riguardante l'interazione aurofilica è la sua influenza nel *self-assembly* di molecole[55] e ioni[56] all'interno di cristalli (*Figura 1.1 g-j*). Nello stato cristallino, composti di Au(I) del tipo L-Au-X, nella maggior parte dei casi si aggregano per formare oligomeri e polimeri. I più comuni oligomeri sono dimeri (*Figura 1.1 d-j*), trimeri (*Figura 1.1 g-j*) e tetrameri (*Figura 1.1 h-i*), mentre le catene *1D* sono i più comuni polimeri (*Figura 1.1 h*). È stato ampiamente evidenziato come in questo tipo di sistemi vengano preferiti i contatti Au-Au rispetto a quelli del tipo Au-X o Au-L, ad eccezione di alcune interazioni Au-S nei tiolati di oro(I), i quali riflettono chiaramente l'alta affinità dell'oro per i solfuri.[57,58]

In generale, le componenti ioniche, sia *omo*lettiche che *etero*lettiche, di segno opposto, si aggregano per formare cristalli ionici, ma per i complessi di oro(I) il modo di aggregazione è eccezionale. I leganti sono organizzati tutti in catene con contatti inter-ionici, tra gli atomi di Au, più brevi. Tale *self-assembly* è particolarmente comune per combinazioni di cui almeno una specie ionica ha forma allungata, e per i quali un approccio nei pressi degli atomi metallici non è impedito dall'ingombro sterico. Esempi di questo tipo di complessi scoperti recentemente sono le strutture a catena di $[(Me_3P)_2Au]^+[Au(C{\equiv}CPh)_2]^-$[59] o di $[(4\text{-}Me_2NC_5H_4N)_2Au]^+[AuCl_2]^-$.[60]

1.5 Il ruolo dell'oro in catalisi eterogenea

Il potenziale catalitico dei catalizzatori a base di oro è stato ampiamente discusso per la loro azione in numerose reazioni in fase eterogenea, quali l'ossidazione selettiva, la decomposizione ossidativa di composti alogeni, la combustione catalitica di idrocarburi, l'idrogenazione degli ossidi di carbonio, la riduzione degli ossidi di azoto con propano, monossido di carbonio e idrogeno.[61]

Tuttavia, l'idroclorurazione dell'acetilene e l'ossidazione del monossido di carbonio con catalizzatori d'oro sono gli esempi più significativi. Entrambe le reazioni sono state infatti ampiamente riviste.[62,63,64]

1.5.1 Idroclorinazione dell'acetilene

L'acetilene viene utilizzato per la produzione di vinil cloruro in un processo catalizzato da cloruro di mercurio sfruttando il carbonio come supporto ($HgCl_2$/C). Il cloruro di mercurio presenta però come svantaggi la rapida disattivazione per sublimazione, nelle condizioni di reazione, del componente attivo e la tossicità. È, per questo motivo, risultata di fondamentale importanza l'individuazione di un catalizzatore, altrettanto efficiente che fosse in grado di sostituirlo. Sulla base dei risultati dello studio dettagliato di Shinoda[65] si è osservato che un certo numero di metallo-cloruri supportati da carbonio potevano essere attivi per questo tipo di reazione, in base alla correlazione dell'attività con il potenziale dell'elettrodo[64]. Da tali studi l'*oro* è risultato essere il catalizzatore più attivo, e in particolare lo stato di ossidazione Au^{3+} risulta essere la forma attiva dell'*oro*. Rispetto alla reazione con il cloruro di mercurio, quella catalizzata da *oro* risulta, oltretutto, anche più stabile poiché esso viene disattivato lentamente con il tempo e la velocità di disattivazione è dipendente dalla temperatura.[66] La riattivazione è, comunque, facilmente effettuata *in situ* mediante la contemporanea aggiunta di NO diluito nel reattore delle materia prime.[67] Questa è stata la prima dimostrazione della possibilità di riattivare in situ i catalizzatori di *oro* ed anche la prima chiara evidenza che l'*oro* cationico potesse essere efficientemente attivo in catalisi eterogenea.

1.5.2 Ossidazione del monossido di carbonio

Nei primi anni '80 Haruta e collaboratori[14] hanno riconosciuto che nano-cristalli di *oro* supportati da ossidi risultavano attivi, a temperature molto basse, per la reazione di ossidazione del monossido di carbonio; in particolare, a temperature minori di 0 °C.[68] Si tratta di un'attività sorprendentemente elevata e che non è replicata da altri metalli. Questa attività a bassa temperatura ha fortemente stimolato l'interesse della ricerca nei confronti dell'*oro* nel campo della catalisi eterogenea. La reazione di ossidazione è infatti ormai utilizzata come reazione test standard.

Il meccanismo della reazione è ancora poco conosciuto. Il percorso di reazione più probabile vede l'interazione tra il CO e le nanoparticelle di *oro* tramite l'atomo di carbonio; l'ossido del metallo di supporto adsorbe l'O_2 con un legame intramolecolare parallelo alla superficie, attivando il legame O-O. Entrambe le molecole sono mobili e possono quindi muoversi sull'interfaccia del substrato di *Au* assumendo un'orientazione ideale per reagire.[9] Dal

momento che questo tipo di meccanismo richiede un substrato di Au all'interfaccia, risulta chiaro che particelle piccole, con un'area superficiale piuttosto grande, sono più attive.

In letteratura sono presenti numerose teorie, proposte per spiegare l'attivazione dell'Au nei confronti dell'ossidazione. Alcune riguardano semplicemente la dimensione delle piccole particelle di oro; altre, invece, si concentrano sull'interazione delle particelle di oro con il supporto. Si è, infatti, discusso molto sulla natura del sito attivo di questi catalizzatori, e, all'inizio dell'ultimo decennio, Bond e Thompson[63] hanno proposto un modello in cui hanno individuato gli atomi di Au, all'interfaccia tra le particelle di Au, e l'ossido come i centri attivi per l'ossidazione, anche se rimane da chiarire se sia Au^{3+} o Au la forma attiva dell'oro. Tale modello deve però essere ancora sperimentalmente verificato.

Bibliografia

1. Bond, G. The Catalytic Properties of Gold. *Gold Bull.* **5**, 11-13(1972).
2. Bone, W. & Wheeler, R. The Combination of Hydrogen and Oxygen in Contact with Hot Surfaces. *Phil. Trans. R. Soc. Lond. A* **206**, 1-67(1906).
3. W.A. Bone & G. W. Andrew*Proc. Roy. Soc. A* **109**, 409(1925).
4. Yolles, R.S., Wood, B.J. & Wise, H. Hydrogenation of alkenes on gold. *Journal of Catalysis* **21**, 66-69(1971).
5. Bond, G.C. et al. Hydrogenation over supported gold catalysts. *J. Chem. Soc., Chem. Commun.* 444b-445(1973).
6. Bond, G. et al.*J. Chem. Soc., Chem. Comm.* 444-445(1973).
7. Cha, D.Y. & Parravano, G. Surface reactivity of supported gold : I. Oxygen transfer between CO and CO2. *Journal of Catalysis* **18**, 200-211(1970).
8. Galvagno, S. & Parravano, G. Chemical reactivity of supported gold : IV. Reduction of NO by H2. *Journal of Catalysis* **55**, 178-190(1978).
9. Haruta, M. Catalysis of Gold Nanoparticles Deposited on Metal Oxides. *CATTECH* **6**, 102-115(2002).
10. Bond, G.C. Gold: a relatively new catalyst. *Catalysis Today* **72**, 5-9(2002).
11. McIntosh, D. & Ozin, G.A. Direct synthesis using gold atoms. Monodioxygen gold, Au(O2). *Inorganic Chemistry* **15**, 2869-2871(1976).
12. McIntosh, D. & Ozin, G.A. Synthesis of binary gold carbonyls, Au(CO)n (n=1 or 2). Spectroscopic evidence for isocarbonyl(carbonyl)gold, a linkage isomer of bis(carbonyl)gold. *Inorganic Chemistry* **16**, 51-59(1977).
13. Nkosi, B. et al. Hydrochlorination of acetylene using carbon-supported gold catalysts reactivation. *Journal of Catalysis* **128**, 378-386(1991).
14. Haruta, M. et al. Novel Gold Catalysts for the Oxidation of Carbon Monoxide at a Temperature far Below 0 °C. *Chem. Lett.* **16**, 405-408(1987).
15. Pyykkö, P.*Adv. Quantum Chem.* **11**, 353-409(1978).
16. Schwerdtfeger, P. Relativistic effects in gold chemistry. 2. The stability of complex halides of gold(III). *Journal of the American Chemical Society* **111**, 7261-7262(1989).
17. Schwerdtfeger, P. et al. Relativistic effects in gold chemistry. 4. Gold(III) and gold(V) compounds. *Inorganic Chemistry* **31**, 3411-3422(1992).
18. Schroder, D. et al. Gold dichloride and gold dibromide with gold atoms in three different oxidation states. *Ang. Chemie Int. Ed.* **42**, 311-+(2003).
19. Jiang, Y., Alvarez, S. & Hoffmann, R. Binuclear and polymeric gold(I) complexes. *Inorganic Chemistry* **24**, 749-757(1985).
20. Pyykko, P. & Mendizabal, F. Theory of d10−d10 Closed-Shell Attraction. III. Rings. *Inorganic Chemistry* **37**, 3018-3025(1998).
21. Yam, V.W., Choi, S.W. & Cheung, K. Synthesis, photophysics and thermal redox reactions of a [{Au(dppn)Cl}2]2+ dimer with an unsupported AuII-AuII bond. *Chem. Commun.* 1173-1174(1996).
22. Irwin, M.D. et al. Synthesis and X-ray structures of silver and gold guanidinate-like complexes. A Au(II) complex with a 2.47 AAu-Au distance. *Chem. Commun.* 2882-2883(2003).
23. Puddephatt, R.J. & Vittal, J. Encyclopedia of Inorganic Chemistry. 1320-1331(1994).
24. Watson, R.E. & Weinert, M. Charge transfer in gold–alkali-metal systems. *Phys. Rev. B* **49**, 7148(1994).
25. Costa Cabral, B.J. & Silva Fernandes, F.M.S.*AIP Conf. Proc.* **381**, 129-133(1995).

26. Matsunaga, S. Structural Study on Liquid Au–Cs Alloys by Computer Simulations. *J. Phys. Soc. Jpn.* **69**, 1712-1716(2000).
27. Dyker, G. Ein Eldorado für die homogene Katalyse? *Angewandte Chemie* **112**, 4407-4409(2000).
28. Dyker, G. An Eldorado for Homogeneous Catalysis? *Angewandte Chemie* **39**, 4237-4239(2000).
29. Hashmi, A. Homogeneous Gold Catalysts and Alkynes: A successfull liaison. *Gold Bull.* **36**, 3-9(2003).
30. Hashmi, A. Homogeneous Catalysis by Gold. *Gold Bull.* **37**, 51-65(2004).
31. Gorin, D.J. & Toste, F.D. Relativistic effects in homogeneous gold catalysis. *Nature* **446**, 395-403(2007).
32. Pyykkö, P. Theoretical chemistry of gold. II. *Inorganica Chimica Acta* **358**, 4113-4130(2005).
33. McKelvey, D.R. Relativistic Effects on Chemical Properties. *Journal of Chemical Education* **60**, 112-16(1983).
34. Pyykko, P. & Desclaux, J.P. Relativity and the periodic system of elements. *Accounts of Chemical Research* **12**, 276-281(1979).
35. Pyykko, P. Relativistic effects in structural chemistry. *Chemical Reviews* **88**, 563-594(1988).
36. Desclaux, J.P. & Pyykkö, P. Dirac-Fock one-centre calculations. The molecules CuH, AgH and AuH including p-type symmetry functions. *Chemical Physics Letters* **39**, 300-303(1976).
37. Scherbaum, F. et al. ldquoAurophilicityrdquo as a Consequence of Relativistic Effects: The Hexakis(triphenylphosphaneaurio)methane Dication. *Angewandte Chemie International Edition in English* **27**, 1544-1546(1988).
38. Carvajal, M.A., Novoa, J.J. & Alvarez, S. Choice of Coordination Number in d10 Complexes of Group 11 Metals. *Journal of the American Chemical Society* **126**, 1465-1477(2004).
39. Schwerdtfeger, P., Hermann, H.L. & Schmidbaur, H. Stability of the Gold(I)−Phosphine Bond. A Comparison with Other Group 11 Elements. *Inorganic Chemistry* **42**, 1334-1342(2003).
40. Nakanishi, W., Yamanaka, M. & Nakamura, E. Reactivity and Stability of Organocopper(I), Silver(I), and Gold(I) Ate Compounds and Their Trivalent Derivatives. *Journal of the American Chemical Society* **127**, 1446-1453(2005).
41. Komiya, S. & Kochi, J.K. Electrophilic cleavage of organogold complexes with acids. The mechanism of the reductive elimination of dialkyl(aniono)gold(III) species. *Journal of the American Chemical Society* **98**, 7599-7607(1976).
42. Komiya, S. et al. Reductive elimination and isomerization of organogold complexes. Theoretical studies of trialkylgold species as reactive intermediates. *Journal of the American Chemical Society* **98**, 7255-7265(1976).
43. Tamaki, A. & Kochi, J.K. Oxidative addition in the coupling of alkylgold(I) with alkyl halides. *Journal of Organometallic Chemistry* **64**, 411-425(1973).
44. Schwerdtfeger, P. et al. Relativistic effects in gold chemistry. 3. Gold(I) complexes. *Inorganic Chemistry* **29**, 3593-3607(1990).
45. Collman, J. et al. Principles and Applications of Organotransition Metal Chemistry. *University Science Books* 42, 156(1987).
46. Melikyan, G.G. & Nicholas, K.M. The Chemistry of Metal - Alkyne Complexes. *Modern Acetylene Chemistry* 99-138(2007).
47. Jäger , V. & Viehe, H. Houben-Weyl. **5/2a**, 738(1977).

48. Hertwig, R.H. et al. A Comparative Computational Study of Cationic Coinage Metal−Ethylene Complexes (C2H4)M+ (M = Cu, Ag, and Au). *The Journal of Physical Chemistry* **100**, 12253-12260(1996).
49. Nechaev, M.S., Rayon, V.M. & Frenking, G. Energy Partitioning Analysis of the Bonding in Ethylene and Acetylene Complexes of Group 6, 8, and 11 Metals: (CO)5TM−C2Hx and Cl4TM−C2Hx (TM = Cr, Mo, W), (CO)4TM−C2Hx (TM = Fe, Ru, Os), and TM+−C2Hx (TM = Cu, Ag, Au). *The Journal of Physical Chemistry A* **108**, 3134-3142(2004).
50. Dewar, J. A review of the pi-complex theory. *Bull. Soc. Chim. Fr.* **18**, C71-C79(1951).
51. Chatt, J. & Duncanson, L. Olefin co-ordination compounds. 3. Infra-red spectra and structure-attempted preparation of acetylene complexes. *J. Chem. Soc.* 2939-2947(1953).
52. Pyykkö, P. Theoretical Chemistry of Gold. *Angewandte Chemie International Edition* **43**, 4412-4456(2004).
53. Zank, J. & Schier, A. Different connectivies in supramolecular aggregates, aggregates of trinuclear Gold(I) complexes with the Sacconi-ligand N(CH2CH2PPH2)3. *Zeitschrift für Naturforschung. B, A journal of chemical sciences* **52**, 1471-1476(1997).
54. Schuster, O., Schier, A. & Schmidbaur, H. The Quest for Complexes with a Coordinative Gold−Bismuth Bond. *Organometallics* **22**, 4079-4083(2003).
55. Pathaneni, S.S. & Desiraju, G.R. Database analysis of Au Au interactions. *J. Chem. Soc., Dalton Trans.* 319-322(1993).
56. Rombke, P., Schier, A. & Schmidbaur, H. Gold(I) organosulfinate and organosulfonate complexes. *J. Chem. Soc., Dalton Trans.* 2482-2486(2001).
57. Preisenberger, M., Schier, A. & Schmidbaur, H. (Phosphine)gold(I) trifluoromethanesulfonates, trifluoroacetates and trichlorothioacetates. *J. Chem. Soc., Dalton Trans.* 1645-1650(1999).
58. Mathieson, T., Schier, A. & Schmidbaur, H. Supramolecular chemistry of gold(I) thiocyanate complexes with thiophene, phosphine and isocyanide ligands, and the structure of 2,6-dimethylphenyl isocyanide. *J. Chem. Soc., Dalton Trans.* 1196-1200(2001).
59. Schuster, O. et al. Unexpected Structural Preference for Aggregates with Metallophilic Ag- - -Au Contacts in (Trimethylphosphine)silver(I) and -gold(I) Phenylethynyl Complexes. An Experimental and Theoretical Study. *Organometallics* **25**, 1004-1011(2006).
60. Lin, J.C.Y. et al. Structural, Photophysical, and Catalytic Properties of Au(I) Complexes with 4-Substituted Pyridines. *Inorganic Chemistry* **47**, 2543-2551(2008).
61. Thompson, D. New advances in gold catalysis Part II . *Gold Bull.* **32**, 12(1999).
62. Hutchings, G.J. Catalysis by gold. *Catalysis Today* **100**, 55-61(2005).
63. Bond, G.C. & Thompson, D. Gold-Catalysed Oxidation of Carbon Monoxide. *Gold Bull.* **33**, 41-51(2000).
64. Hutchings, G. Catalysis: A golden future. *Gold Bulletin* **29**, 123-130(1996).
65. Shinoda, K. The vapor-phase hydroclorination of acetylene over metal chlorides supported on activated carbon. *Chem. Lett.* 219(1975).
66. Sermon, P.A., Bond, G.C. & Wells, P.B. Hydrogenation of alkenes over supported gold. *J. Chem. Soc., Faraday Trans. 1:* **75**, 385-394(1979).
67. Bailie, J.E. & Hutchings, G.J. Promotion by sulfur of gold catalysts for crotyl alcohol formation from crotonaldehyde hydrogenation. *Chem. Commun.* 2151-2152(1999).
68. Haruta, M. et al. Gold catalysts prepared by coprecipitation for low-temperature oxidation of hydrogen and of carbon monoxide. *Journal of Catalysis* **115**, 301-309(1989).

2

Approccio teorico

Introduzione

La chimica teorica è il campo in cui i metodi matematici sono combinati con le leggi fondamentali della fisica per studiare i problemi chimici. La meccanica quantistica è la teoria più potente utilizzata per descrivere i sistemi chimici microscopici, in particolare il movimento degli elettroni in una molecola. In meccanica quantistica, l'equazione generale è quella di Schröedinger dipendente dal tempo, dalla cui risoluzione è possibile, in linea di principio, ottenere tutte le proprietà del sistema, specialmente l'energia. Per la chimica dello stato fondamentale è sufficiente l'utilizzo della forma indipendente dal tempo dell'equazione di Schröedinger. Purtroppo l'equazione di Schrödinger, esattamente risolvibile nel caso dell'atomo di idrogeno e, con grandi sforzi, di altri sistemi molto semplici, si trasforma in un complicato insieme di equazioni differenziali man mano che il sistema in esame aumenta le sue dimensioni. Per trattare i sistemi multielettronici è necessaria l'introduzione di alcune approssimazioni.

L'applicazione della chimica teorica nel campo della catalisi è di fondamentale utilità per la comprensione dei comportamenti chimici delle specie coinvolte nei processi catalitici. La catalisi, in particolare quella eterogenea, è ampiamente utilizzata nell'industria chimica per produrre enormi quantità di migliaia di prodotti differenti. Su scala globale, l'importanza tecnologica ed economica della catalisi eterogenea è enorme, in quanto fornisce gli strumenti per la realizzazione di importanti processi chimici. La complessità dei sistemi catalitici ha portato all'applicazione della procedura per "tentativi ed errori" come approccio comune per lo sviluppo di nuovi e più efficienti catalizzatori. Sfortunatamente, questo tipo di approccio, benché possa risultare fruttuoso per l'individuazione di catalizzatori più specifici, non consente di comprendere a fondo la vera natura dei processi chimici coinvolti. Nonostante lo sviluppo di nuove tecniche sperimentali atte ad individuare i catalizzatori più efficienti, è praticamente impossibile, sulla base di soli dati sperimentali, comprendere il meccanismo molecolare che governa un particolare processo catalitico. È a questo punto che la sinergia tra tecniche sperimentali e calcoli teorici risulta di fondamentale importanza per la comprensione della catalisi eterogenea a livello molecolare.

2.1 Metodi quantomeccanici

La prima approssimazione, applicata in ogni metodo teorico, è certamente l'*approssimazione di Born-Oppenheimer*,[1] secondo la quale, considerata la differenza tra in

peso tra nuclei ed elettroni, è possibile disaccoppiare il moto dei nuclei da quello degli elettroni e considerare i nuclei fissi. Suddividendo il sistema molecolare in due sottosistemi (elettronico e nucleare), l'espressione dell'equazione di Schröedinger viene semplificata, in quanto è possibile trascurare l'energia cinetica dei nuclei e mantenere costante l'interazione nucleo-nucleo.

La ricerca di metodi teorici atti a fornire delle soluzioni approssimate dell'equazione di Schröedinger ha dato vita ai metodi HF, post-HF e DFT. L'accuratezza che i metodi post-HF garantiscono li rendono utili per la trattazione di sistemi semplici. Per sistemi più complessi, quali sono quelli catalitici, si palesa la necessità di utilizzare la teoria del funzionale della densità.

2.2 La teoria del funzionale della densità

La teoria del funzionale della densità ha trovato un suo solido fondamento teorico nell'enunciazione dei due teoremi *Hohenberg-Koh.* Hohenberg e Kohn dimostrarono che la densità dello stato fondamentale non degenere di un sistema di elettroni permette di determinare univocamente tutte le proprietà dello stato fondamentale. Quindi ogni grandezza fisica osservabile di stato fondamentale, come ad esempio l'energia totale dello stato fondamentale, può essere espressa come un funzionale della densità, $E[\rho]$. L'energia $E[\rho]$ è infatti un funzionale della densità elettronica $\rho(\mathbf{r})$, la quale è a sua volta una funzione delle coordinate spaziali (x, y, z). Inoltre per il funzionale $E[\rho]$ vale un principio di minimizzazione che si deduce direttamentamente dal principio di minima energia valido per il valore di aspettazione dell'hamiltoniano del sistema.

Il funzionale energia elettronica $E[\rho]$ viene generalmente suddiviso in diversi contributi che tengano conto separatamente dell'energia cinetica elettronica $T[\rho]$, dell'energia potenziale di interazione elettrone-elettrone $V_{ee}[\rho]$ e dell'energia potenziale di interazione elettrone-nucleo $V_{Ne}[\rho]$. I primi due contributi sono indipendenti dalle posizioni nucleari e possono quindi essere raggruppati insieme nel *funzionale universale* della densità $F[\rho]$:

$$E[\rho] = F[\rho] + V_{Ne}[\rho] \qquad 2.1$$

La determinazione esatta del funzionale $F[\rho]$ non è di fatto possibile.

Riconosciuta la limitazione di questa equazione[2] Kohn e Sham introdussero un set di orbitali (analogo agli orbitali di HF) utilizzando i quali l'energia cinetica può essere divisa in due parti, l'energia cinetica (T_S) di un sistema di N elettroni non-interagenti (con la stessa densità del sistema reale interagente) e una parte residua T_C (che è la parte mancante alla descrizione accurata del sistema reale interagente)[3]. Anche l'energia di repulsione elettrone-elettrone $V_{ee}[\rho]$, può essere separata in due differenti contributi, l'interazione classica di Coulomb (J) ed una parte non-classica contenente lo scambio e la correlazione. Viene così introdotto nell'equazione dell'energia totale del sistema il cosiddetto funzionale di scambio e correlazione $E_{XC}[\rho]$, dove viene incluso il contributo della parte residuale dell'energia cinetica ed i termini di scambio e correlazione:

$$E[\rho] = T_S[\rho] + J[\rho] + V_{Ne}[\rho] + E_{XC}[\rho] \qquad 2.2$$

I primi tre termini possono essere calcolati esplicitamente. Il termine di scambio e correlazione $E_{XC}[\rho]$ raggruppa tutti i contributi all'energia totale non conosciuti.

2.2.1 Approssimazioni per il Funzionale di Scambio e Correlazione

Un approccio per calcolare l'energia di scambio e correlazione è basato sull'assunzione che la densità varia solo localmente e lentamente e può, quindi, essere trattata come un gas elettronico omogeneo.[4] L'energia di scambio di un gas di elettroni con densità uniforme può essere calcolata esattamente, ed è su questa evidenza che fonda le sue basi l'Approssimazione della Densità di Spin Locale (LSDA). Sono stati sviluppati differenti funzionali per calcolare l'energia di correlazione di un gas di elettroni uniforme. Uno dei più popolari è certamente il funzionale di correlazione Vosko-Wilk-Nusair (VWN)[5].

Mentre l'assunzione della distribuzione omogenea di elettroni è adatta per alcuni sistemi, per molti sistemi di interesse chimico non è di particolare utilità, quelli, cioè, per i quali la distribuzione elettronica è ben lungi dall'essere uniforme.[6]

Un importante miglioramento in tal senso si ha con l'introduzione di un gradiente della densità elettronica, nasce così l'Approssimazione del Gradiente Generalizzato (GGA), il quale non tiene soltanto conto della densità in un dato punto, ma anche della sua derivata.[6] Becke ha introdotto un funzionale corretto per il gradiente per l'energia di scambio denominato B88[7]. Tale funzionale contiene un parametro semi-empirico, che è stato fittato sullo scambio di Hartree-Fock dei sei atomi di gas nobili. Un popolare funzionale di correlazione corretto per il

gradiente è stato sviluppato da Lee, Yang e Parr, dalle iniziali dei quali iniziali è stato coniato il nome di LYP.[8] La combinazione dei due funzionali dà vita ad un funzionale ampiamente utilizzato come il BLYP.[2] Successivamente Becke sostenne che poteva essere realizzato un ulteriore sviluppo nello schema GGA se fosse stata inclusa nel funzionale una certa quantità dello scambio di Hartree-Fock esatto,[9] portando così alla definizione di funzionali ibridi, trai quali il più popolare è certamente il B3LYP.

2.2.1.1 B3LYP

Il B3LYP è un funzionale ibrido che contiene i funzionali di scambio e correlazione B88, LYP e VWN,[5,7,8] insieme con il 20% dello scambio HF esatto:

$$E_{XC}^{B3LYP} = (1-a)E_X^{LSDA} + aE_X^{HF} + bE_X^{B88} + cE_C^{LYP} + (1-c)E_C^{VWN} \qquad 2.3$$

I coefficienti $a = 0.20$, $b = 0.72$ e $c = 0.81$ sono stati presi dal funzionale ibrido B3PW91.[2,9] I loro valori sono stati ottimizzati per B3PW91 attraverso un fit lineare dei minimi quadrati per 116 energie determinate sperimentalmente (56 energie di atomizzazione, 42 potenziali di ionizzazione, 8 affinità protoniche e 10 energie atomiche totali).

In questo lavoro di tesi, il funzionale B3LYP è stato scelto per lo studio della reazione di idratazione dell'1,2-difenilacetilene (la quale verrà discussa nel Capitolo 4, *manoscritto II*) e per valutare dettagliatamente il protocollo computazionale ottimale per l'applicabilità dell'approccio cluster (il quale verrà discusso nel capitolo 3, *pubblicazione I*) utilizzato per lo studio della reazione di formazione del vinilacetato.

2.2.1.2 BP86

Il funzionale BP86, invece, è un funzionale non ibrido che contiene il funzionale di scambio corretto per il gradiente B88,[7] l'espressione del funzionale di correlazione VWN per la correzione del UEG[5] e la correzione al gradiente di Perdew per VWN del 1986.[10]

Come conseguenza degli studi di convergenza sui cluster bimetallici di Pd e Au, il funzionale BP86 è risultato essere il più idoneo a riprodurre i dati sperimentali ed è stato, quindi, selezionato per lo studio dettagliato della reazione di formazione del vinilacetato sulle superfici PdAu(100) e PdAu(111) (*pubblicazioni II, III, manoscritto I*).

2.2.2 Set di funzioni di base e pseudopotenziali

In linea di principio il set di funzioni di base in cui sviluppare gli orbitali è completamente arbitrario, purché sia finito. Il criterio variazionale stabilisce solo che più esso è grande, maggiore è la flessibilità variazionale e migliori sono i risultati. Poiché per tempi computazionali limitati il set di funzioni di base deve essere piuttosto piccolo, è, quindi, importante che le funzioni abbiano un senso fisico.

La formazione di legami chimici può essere interpretata come una alterazione delle distribuzioni elettroniche presenti negli atomi isolati. Pertanto, le nuove distribuzioni possono essere rappresentate come combinazioni lineari di orbitali atomici (LCAO, *linear combination of atomic orbitals*), in modo che le funzioni di base rappresentino abbastanza fedelmente orbitali atomici. L'utilizzo di orbitali atomici garantisce la "portabilità" delle funzioni, in quanto si può costruire un insieme di base per qualsiasi molecola usando una quantità limitata di set di base noti e classificati, corrispondenti all'identità degli atomi costituenti.

La minimizzazione del numero di funzioni di base (a parità di qualità dei risultati) non può essere l'unico criterio guida, bisogna considerare la semplicità e la velocità di calcolo. In base, soprattutto, a quest'ultima considerazione il set di base che si sceglie di utilizzare è un set di funzioni gaussiane (GTO, *Gaussian Type Orbital*).

In realtà, le funzioni gaussiane non sono le funzioni ottimali per rappresentare gli orbitali atomici che risulterebbero da calcoli HF esatti, in quanto la dipendenza esponenziale è quadratica, per cui tali funzioni decrescono più rapidamente con l'aumentare della distanza. Le funzioni STO, *Slater Type Orbitals* riproducono in modo migliore la dipendenza esponenziale dalla distanza dai nuclei, simile a quello di semplici esponenziali idrogeno idi. Sono, inoltre, funzioni che con l'aumentare del numero di funzioni assicurano una convergenza rapida e sono, però, difficili da integrare. Il loro utilizzo si restringe quindi a sistemi atomici e biatomici. Per sistemi poliatomici la scelta che si fa è di descrivere le funzioni STO come combinazioni lineari delle GTO, in quanto vengono mantenuti i vantaggi di entrambe.

Per ridurre il numero di funzioni di base senza abbassare la qualità nella descrizione di quelle funzioni atomiche meno modificate dalla formazione dei legami chimici (orbitali atomici di core) ciascuna funzione è definita da una combinazione lineare di gaussiane. Le gaussiane importanti per la descrizione di orbitali interni, vicini ai nuclei, contribuiscono trascurabilmente alla descrizione di orbitali di valenza e viceversa. Inoltre, poiché i coefficienti di combinazione degli orbitali del sistema molecolare non sono molto differenti da quelli dell'atomo isolato, i coefficienti vengono normalmente determinati da calcoli sugli atomi isolati.

I parametri che caratterizzano le funzioni di base, nonché il loro ottimale numero complessivo (nel senso di un compromesso fra praticabilità computazionale e qualità dei risultati), dipendono ovviamente in linea di principio dal particolare sistema fisico e potrebbero essere trattati come ulteriori parametri variazionali insieme ai coefficienti di combinazione; per ragioni di praticità si preferisce, però, determinare il set di base a priori secondo criteri consolidati.

Nei sistemi di grandi dimensioni, contenenti metalli, è possibile applicare un'ulteriore approssimazione agli LCAO, tramite l'utilizzo di *pseudopotenziali o potenziali effettivi di core*. L'introduzione di uno pseudopotenziale ha principalmente lo scopo di abbassare sensibilmente il costo computazionale, in quanto corrisponde alla diminuzione del numero di elettroni che le funzioni LCAO devono rappresentare. Tale metodologia di calcolo è supportata da una delle assunzioni principali in chimica, la quale stabilisce che gli elettroni dei livelli energetici più interni (e di core) siano relativamente inerti e non perturbati dall'intorno molecolare, in quanto molte delle proprietà chimiche più importanti degli atomi e delle molecole sono determinate dalle interazioni dei loro elettroni di valenza con gli elettroni di valenza di altri atomi o molecole. L'utilizzo di potenziali di core effettivi o pseudopotenziali in principio non influenza la qualità della riproduzione delle proprietà molecolari, ma permette, come detto, di ridurre i tempi e le risorse di calcolo.

Nel caso specifico in cui i sistemi da trattare coinvolgano metalli pesanti, per i quali è necessario tenere conto dell'influenza degli effetti relativistici, si introducono i cosiddetti *potenziali effettivi di core relativistici* (*RECP*). Le correzioni relativistiche tendono ovviamente ad essere più significative nella regione che immediatamente circonda il nucleo poiché l'energia cinetica di questi elettroni è maggiore. Pertanto, è ragionevole assumere che gli elettroni più interni risentano in misura maggiore degli effetti della relatività rispetto a quelli più esterni che hanno una probabilità molto più bassa di trovarsi vicino al nucleo. Le interazioni degli elettroni di valenza con i nuclei e con gli altri elettroni dovrebbero essere sufficientemente ben descritte da un hamiltoniano non-relativistico. Anche se gli elettroni di valenza non risentono di effetti relativistici diretti significativi, i cambiamenti degli elettroni di core hanno conseguenze dirette sullo schermo nucleare e sull'ortogonalità. Poiché il comportamento degli elettroni di core non cambia in maniera significativa nel passaggio dall'ambiente atomico a quello molecolare, un metodo basato sull'utilizzo degli *ECP* che incorpora gli effetti relativistici risentiti dagli elettroni di core è di grande utilità pratica.

2.2.2.1 RECP di tipo Stuttgart/Dresden per l'oro

La scelta dello pseudopotenziale che meglio rappresentasse il comportamento dei 60 elettroni di core dell'Au è ricaduta sul potenziale effettivo di core relativistico (RECP) di tipo Stuttgart/Dresden.[11]

I vantaggi nell'utilizzo di questo tipo di pseudopotenziale per l'oro sono stati osservati in numerosi studi condotti su differenti composti di Au,[12-15] ed è per questo motivo stato utilizzato anche per reazioni catalizzate dal metallo.[16,17]

Nel caso specifico dello studio della reazione di formazione del VAM (*pubblicazioni I, II, III, manoscritto I*), lo stesso pseudopotenziale è stato utilizzato per descrivere il comportamento dei 28 elettroni di core del palladio.

2.3 Metodi quantomeccanici in catalisi eterogenea

Lo studio teorico dei fenomeni catalitici eterogenei necessita della messa a punto di modelli atti a descrivere in dettaglio le caratteristiche di catalizzatori specifici per determinate reazioni, in modo da riprodurre in maniera sufficientemente accurata le interazioni del catalizzatore stesso con i reagenti coinvolti nella reazione considerata. La catalisi è, infatti, controllata da una stretta sinergia tra l'arrangiamento atomico del sito attivo e l'ambiente di reazione che circonda il sito stesso. In particolare per la catalisi eterogenea, le informazioni circa i siti attivi su materiali di supporto possono essere ricavate per analogia degli stessi fenomeni eterogenei con quelli in fase omogenea. Le reazioni catalitiche eterogenee che si svolgono su uno o due centri metallici somigliano agli analoghi sistemi omogenei e tendono ad essere insensibili alla struttura. È per questo motivo che l'impiego di leghe metalliche per aumentare la selettività del catalizzatore per uno specifico prodotto evitando così la formazione di sottoprodotti, consente di che la reazione avvenga senza modificarne la reattività.

La reattività e la selettività di un catalizzatore omogeneo sono controllate dalle proprietà del centro metallico congiunte a quelle della sfera dei leganti. Queste includono stato di ossidazione, numero di coordinazione e geometria di coordinazione del metallo, così come le interazioni steriche ed elettroniche tra la sfera dei leganti e i potenziali reagenti.[18] Per progettare un sistema omogeneo è necessario ottimizzare il sito attivo metallico con il suo ambiente di reazione corrispondente alla sfera dei leganti. Le differenze tra i sistemi omogenei ed eterogenei molto spesso deriva dal livello di controllo più accurato che si ha nel sistema omogeneo di

manipolare la sua reattività. Inoltre, la sostanziale differenza di composizione del catalizzatore, un atomo metallico per il sistema omogeneo e un insieme di metalli organizzati in una particolare configurazione geometrica per un sistema eterogeneo, gioca un ruolo di fondamentale importanza, non solo sulle reattività di uno specifico processo, ma soprattutto sulla selettività nei confronti della formazione del prodotto desiderato. Analogamente ai catalizzatori omogenei, l'attività e la selettività dei sistemi eterogenei sono controllate dall'attività dell'ambiente di reazione che si trova nelle immediate vicinanze del sito attivo. Questo include non solo il metallo, ma anche il supporto sul quale si trova il sito attivo.

Dalla letteratura degli anni '90 risulta evidente lo sviluppo di numerosi metodi quantomeccanici capaci di studiare le proprietà chimiche e strutturali di una serie di catalizzatori eterogenei costituiti da diversi materiali di supporto.[19-30] La ricerca degli ultimi anni si è però concentrata sullo sviluppo di metodi che, oltre a consentire lo studio dei dettagli meccanicistici di uno specifico processo catalitico con costi computazionali non troppo elevati, garantissero parallelamente un certo grado di accuratezza, risultato sempre più necessario per la migliore fusione delle metodologie teoriche con le tecniche sperimentali. Le dimensioni del modello utilizzato per rappresentare la superficie del catalizzatore dovrebbero quindi essere scelte in base al grado di accuratezza desiderato.

Dal punto di vista computazionale, i calcoli sui sistemi catalitici vengono realizzati sfruttando i metodi basati sulla teoria del funzionale della densità. La DFT garantisce infatti una buona accuratezza nella riproduzione delle proprietà strutturali ed energetiche anche di sistemi quantomeccanici non semplici. L'utilizzo dei metodi semi-empirici è stato abbandonato per la scarsa precisione dei risultati ottenibili, mentre l'applicazione dei metodi CI (interazione di configurazione), i quali sono sicuramente molto più accurati, risulta ancora troppo costosa dal punto di vista computazionale.

2.4 Modelli catalitici

Nonostante molte reazioni di interesse industriale facciano ricorso a catalizzatori eterogenei, in quanto possono essere separati dai prodotti e dai reagenti residui abbastanza facilmente favorendo l'ottimizzazione dei processi produttivi, le motivazioni dettagliate che spiegano la loro attività in termini chimici, e più specificatamente meccanicistici, non sono note o comunque non certe anche nei più utilizzati processi di sintesi in cui essi sono coinvolti.

È in questo campo che si è sviluppata la ricerca di modelli computazionali, parallelamente a tecniche sperimentali in grado di indagare su scala microscopica, per rispondere alle esigenze dei ricercatori di descrivere in maniera dettagliata i meccanismi di reazione e di correlare specifiche caratteristiche strutturali (tipologia di supporto, specie metalliche, strategie di sintesi, condizioni di reazione) alle prestazioni catalitiche.

Il successo del *modeling* di sistemi catalitici non dipende solo dall'accuratezza del metodo impiegato, ma anche da quanto i sistemi modello riproducono le caratteristiche del sistema originale. Le tecniche utilizzate per modellare la struttura di un sito attivo sono essenzialmente tre: metodi *cluster*,[19,20,31] *embedded cluster*[21,22,31-33] e metodi *periodici*.[23-26,34] Ciascun metodo presenta naturalmente vantaggi e svantaggi. Per ogni sistema catalitico deve essere valutata l'idoneità di un metodo di modellizzazione in funzione delle caratteristiche del supporto, del metallo e del processo reattivo preso in considerazione.

2.4.1 I modelli cluster ed embedded cluster

Nell'approccio *cluster* viene considerato un numero finito di atomi per rappresentare la regione contenete il sito attivo. L'assunzione di base è che il chemisorbimento e la reattività sono fenomeni locali, quindi in linea di principio dipendenti dalla struttura della superficie nelle immediate vicinanze del sito attivo.

Il modello *embedded cluster* non è altro che un'estensione dell'approccio cluster, in cui si trattano i problemi connessi alla brusca terminazione dei cluster. Nell'approccio embedded cluster, per modellare la regione locale attorno al sito attivo si fa ricorso ad un metodo QM rigoroso. Questo cluster primario viene quindi incluso in sistema più grande in modo da simulare l'intorno elettronico esterno al cluster. Per il secondo modello viene impiegata una trattazione quantomeccanica più semplice o un campo di forza empirico per simulare l'ambiente esterno. Questo minimizza le limitazioni derivanti dalle dimensioni dei cluster. Il modello esterno può successivamente essere incorporato in un terzo modello che è costituito da cariche puntuali nelle posizioni definite dalla simmetria del bulk intorno alla porzione di solido costituente il cluster, in modo da riprodurre esattamente il potenziale di Madelung. Questo modeling avvicina il modello al sistema reale e mantiene la possibilità di trattare localmente il sito catalitico in maniera rigorosa e sufficientemente accurata.

Sia con il modello *cluster* che con quello *embedded cluster* la trattazione dei modelli al pari di sistemi molecolari presenta il vantaggio di descrivere localmente la struttura elettronica dei solidi (delocalizzata in bande). Pertanto, il problema della struttura elettronica e della

geometria molecolare dei solidi viene ridotto alla determinazione della struttura elettronica e della geometria di una molecola.

Dal punto di vista operativo, la costruzione del cluster viene realizzata tramite estrazione (cutting) di una porzione della superficie del solido contenente un numero discreto di atomi. Tale operazione genera dei legami pendenti (dangling) per quegli atomi direttamente strappati dal bulk e quindi anche la produzione di stati elettronici "spuri" ai bordi del cluster. Le condizioni in cui sono costretti gli atomi alla periferia del cluster determinano un riarrangiamento della struttura elettronica. Per ripristinare opportunamente tale struttura diviene spesso necessaria una procedura di embedding.[35-40] Le tipologie di embedding si distinguono in funzione del tipo di approssimazione dell'intorno che la procedura di cutting determina, il quale dipende dal tipo di solido costituente il sistema catalitico di supporto che si vuole simulare.

2.4.2 I modelli periodici

Il metodo *periodico* si differenzia dai precedenti in quanto in esso viene realizzata l'applicazione di teorie quantomeccaniche in grado di sfruttare le proprietà proprie di un cristallo reale. Tale caratteristica del modello periodico ha consentito lo sviluppo di metodi CO (*crystal orbital*),[32,41] i quali consentono di eliminare le difficoltà di riproduzione dell'intorno legate alle dimensioni ridotte dei modelli finiti.

In questo modello viene definita una cella unitaria che comprende un ensemble di superficie abbastanza grande. Si utilizzano quindi le condizioni periodiche al contorno per espandere la cella nelle tre dimensioni (x,y e/o z) in modo da simulare la condizione strutturale reale del catalizzatore. La modellizzazione estremamente realistica ottenibile con questi metodi non può che essere caratterizzata da una trattazione quantomeccanica meno rigorosa del sito attivo rispetto ai modelli molecolari. Questo comporta una perdita di informazioni accurate nella regione immediatamente vicina al sito attivo, ma anche un guadagno in termini di conoscenza del contributo dell'intorno all'attività catalitica del centro attivo.

I risultati ottenibili con un approccio periodico sono, quindi, complementari a quelli ottenibili con i metodi *cluster*, in quanto mentre il primo fornisce informazioni circa le dimensioni reali del sistema, i secondi forniscono i dati necessari per una descrizione locale dei fenomeni.

La scelta dei metodi teorici adatti a trattare i modelli di tipo periodico deve contemplare la necessità per la funzione d'onda di un sistema periodico di obbedire al Teorema di Bloch,[42] il quale viene applicato per ridurre il numero infinito di funzioni d'onda monoelettroniche da

calcolare al numero di funzioni necessario alla descrizione quantomeccanica degli elettroni presenti nella cella unitaria del cristallo. Per rappresentare tale funzione d'onda possono essere impiegati set di funzioni di base LCAO[43] (combinazioni lineari degli orbitali atomici) oppure onde piane.[34,44-46] L'utilizzo del set di funzioni LCAO, nonostante presenti il vantaggio di localizzare le funzioni di base, limitando così il numero di funzioni necessarie per una corretta descrizione dei *crystal orbital*, comporta uno sforzo computazionale piuttosto elevato. Il set di base di onde piane consente invece l'utilizzo di alcune funzioni matematiche più facili da trattare sia dal punto di vista teorico che computazionale. L'inconveniente risiede nella necessità di prendere in considerazione un gran numero di funzioni di base, in quanto necessario per una corretta descrizione della funzione d'onda che rappresenta gli oggetti quantomeccanici contenuti in una cella unitaria. Inconveniente che viene ovviato tramite l'utilizzo di pseudopotenziali di core,[47-49] i quali consentono così di utilizzare le onde piane necessarie per la descrizione della localizzazione dei soli elettroni di valenza degli atomi che sono contenuti nella cella unitaria.

L'applicazione dei metodi periodici, nati per lo studio delle proprietà di bulk dei solidi, è stata estesa allo studio dei fenomeni di superficie e quindi alla caratterizzazione dei processi che coinvolgono catalizzatori eterogenei. Il principale modello computazionale utilizzato per lo studio dei fenomeni chimici nei catalizzatori eterogenei è l'approccio *slab supercell*.[50] Tale modello prevede la costruzione di una cella unitaria contenente non solo una porzione di solido costituita da un certo numero di atomi (*slab*), ma anche uno spazio ben definito di vuoto sovrastante la superficie del solido. Tale cella viene per questo motivo definita "*supercella*" e, analogamente alla cella unitaria convenzionale, viene replicata nello spazio tridimensionale. Mentre nello spazio bidimensionale la replica della cella definisce l'estensione infinita di una superficie reale, nella terza dimensione ciascuna cella è separata dall'altra da un opportuno spazio vuoto. Per poter riprodurre correttamente le proprietà di una superficie è necessario scegliere un adeguato numero di strati di materiale sotto la superficie ed una porzione di vuoto opportuna che garantisca l'assenza di interazioni fittizie tra superfici opposte di due *slab* sovrapposte. Inoltre, lo spazio di vuoto che separa le due repliche lungo la terza dimensione deve essere scelto anche tenendo conto della presenza dei reagenti che verranno adsorbiti sulla superficie, i quali non dovranno in alcun modo interagire con la superficie sovrastante.

Bibliografia

1. Born, M. & Oppenheimer, R. Zur Quantentheorie der Molekeln. *Annalen der Physik* **389**, 457-484(1927).
2. Koch, W. & Holthausen, M.C. *A Chemist's Guide to Density Functional Theory*. (Wiley-VCH: Weinheim, 2001).
3. Kohn, W. & Sham, L.J. Self-Consistent Equations Including Exchange and Correlation Effects. *Phys. Rev.* **140**, A1133(1965).
4. Jensen, F. *Introduction to Computational Chemistry*. (John Wiley & Sons Ltd: England, 1999).
5. Vosko, S.H., Wilk, L. & Nusair, M. Accurate spin-dependent electron liquid correlation energies for local spin density calculations: a critical analysis. *Can. J. Phys.* **58**, 1200(1980).
6. Cramer, C.J. *Essentials of Computational Chemistry Theories and Models*. (Wiley, John & Sons, Incorporated: England, 2002).
7. Becke, A.D. Density-functional exchange-energy approximation with correct asymptotic behavior. *Phys. Rev. A* **38**, 3098(1988).
8. Lee, C., Yang, W. & Parr, R.G. Development of the Colle-Salvetti correlation-energy formula into a functional of the electron density. *Phys. Rev. B* **37**, 785(1988).
9. Becke, A. Density-functional thermochemistry. III. The role of exact exchange. *The Journal of Chemical Physics* **98**, 5648-5652(1993).
10. Perdew, J.P. Density-functional approximation for the correlation energy of the inhomogeneous electron gas. *Phys. Rev. B* **33**, 8822(1986).
11. Andrae, D. et al. Energy-adjustedab initio pseudopotentials for the second and third row transition elements. *Theoretical Chemistry Accounts: Theory, Computation, and Modeling (Theoretica Chimica Acta)* **77**, 123-141(1990).
12. Schwerdtfeger, P. et al. The accuracy of the pseudopotential approximation. III. A comparison between pseudopotential and all-electron methods for Au and AuH. (2000).
13. Mohr, F. & Schmidbaur, H. *Gold Chemistry*. 425(John Wiley and Sons: 2009).
14. Brown, J.R. et al. Experimental and theoretical studies of diatomic gold halides. *Journal of the American Society for Mass Spectrometry* **13**, 485-492(2002).
15. Sahu, B.R., Maofa, G. & Kleinman, L. Density-functional study of palladium-doped small gold clusters. *Phys. Rev. B* **67**, 115420(2003).
16. Roithová, J. et al. A gas-phase study of the gold-catalyzed coupling of alkynes and alcohols. *Inorganica Chimica Acta* **358**, 4287-4292(2005).
17. Fang, R. et al. DFT Study on the Mechanism and Regioselectivity of Gold(I)-Catalyzed Synthesis of Highly Substituted Furans Based on 1-(1-Alkynyl)cyclopropyl Ketones with Nucleophiles. *Organometallics* **28**, 741-748(2009).
18. Cornils, B. & Herrmann, W.A. *Applied homogeneous catalysis with organometallic compounds*. 448(Wiley-VCH: 2002).
19. Van Santen, R.A. & Neurock, M. Concepts in Theoretical Heterogeneous Catalytic Reactivity. *Catalysis Reviews: Science and Engineering* **37**, 557(1995).
20. van Santen, R.A. & Neurock, M.*Encyclopedia of Catalysis* (2001).
21. Sauer, J. Structure and reactivity of zeolite catalysts: Atomistic modelling using ab initio techniques. *Zeolites and Related Microporous Materials: State of the art 1994, Proceedings of the 10th International Zeolite Conference* **Volume 84, Part 3**, 2039-2057(1994).
22. Whitten, J.L. & Yang, H. Theory of chemisorption and reactions on metal surfaces. *Surface Science Reports* **24**, 55-124(1996).

23. Hammer, B. & Nørskov, J.K. Theoretical surface science and catalysis--calculations and concepts. *Impact of Surface Science on Catalysis* **Volume 45**, 71-129(2000).
24. Hafner, J. Atomic-scale computational materials science. *Acta Materialia* **48**, 71-92(2000).
25. Stampfl, C. et al.*Surf. Sci.* 500(2001).
26. Hammer, B. & Nørskov, J.K. *Chemisorption and Reactivity on Supported Clusters and Thin Films*. 285-351(R. M. Lambert, G. Pacchioni: Kluwer Academic, The Netherlands, 1997).
27. van Santen, R.A. & Neurock, M. *Theory of Surface-Chemical Reactivity*. (Wiley-VCH: Weinheim/New York, 1997).
28. Head-Gordon, M. Quantum Chemistry and Molecular Processes. *The Journal of Physical Chemistry* **100**, 13213-13225(1996).
29. van Santen, R.A. & Kramer, G.J. Reactivity Theory of Zeolitic Broensted Acidic Sites. *Chemical Reviews* **95**, 637-660(1995).
30. Pacchioni, G.*Heter. Chem. Rev.* **2**, 213-228(1995).
31. van Santen, R.A. The cluster approach to molecular heterogeneous catalysis. *Journal of Molecular Catalysis A: Chemical* **115**, 405-419(1997).
32. Sauer, J. Molecular models in ab initio studies of solids and surfaces: from ionic crystals and semiconductors to catalysts. *Chemical Reviews* **89**, 199-255(1989).
33. Sierka, M. & Sauer, J. Finding transition structures in extended systems: A strategy based on a combined quantum mechanics-empirical valence bond approach. *Journal of Chemical Physics* **112**, 6983-6996(2000).
34. Payne, M.C. et al. Iterative minimization techniques for ab initio total-energy calculations: molecular dynamics and conjugate gradients. *Rev. Mod. Phys.* **64**, 1045(1992).
35. Colbourn, E. & Mackrodt, W. A theoretical study of co chemisorption at {001} surfaces of non-defective and doped MgO. *Surface Science* **143**, 391-410(1984).
36. Pacchioni, G., Cogliandro, G. & Bagus, P.S. Molecular orbital cluster model study of bonding and vibrations of CO adsorbed on MgO surface. *International Journal of Quantum Chemistry* **42**, 1115-1139(1992).
37. Pacchioni, G., Cogliandro, G. & Bagus, P.S. Characterization of oxide surfaces by infrared spectroscopy of adsorbed carbon monoxide: a theoretical investigation of the frequency shift of CO on MgO and NiO. *Surface Science* **255**, 344-354(1991).
38. Pacchioni, G., Minerva, T. & Bagus, P.S. Chemisorption of CO on defect sites of MgO. *Surface Science* **275**, 450-458(1992).
39. Neyman, K.M. & Rösch, N. Bonding and vibration of CO molecules adsorbed on low-coordinated surface sites of MgO: a LCGTO-LDF cluster investigation. *Surface Science* **297**, 223-234(1993).
40. Mejías, J.A. et al. On modelling the interaction of CO on the MgO(100) surface. *Surface Science* **327**, 59-73(1995).
41. Ladik, J. & Suhai, S. *Theoretical Chemistry*. **4**, 49(C. Thomson: Royal Society of Chemistry, London, 1981).
42. Ashcroft, N.W. & Mermin, N.D. *Solid state physics*. 858(Saunders College: 1976).
43. Towler, M.D., Zupan, A. & Causà, M. Density functional theory in periodic systems using local Gaussian basis sets. *Computer Physics Communications* **98**, 181-205(1996).
44. Vanderbilt, D. Soft self-consistent pseudopotentials in a generalized eigenvalue formalism. *Phys. Rev. B* **41**, 7892(1990).
45. Laasonen, K. et al. Car-Parrinello molecular dynamics with Vanderbilt ultrasoft pseudopotentials. *Phys. Rev. B* **47**, 10142(1993).
46. Pasquarello, A. et al. Ab initio molecular dynamics for d-electron systems: Liquid copper at 1500 K. *Phys. Rev. Lett.* **69**, 1982(1992).

47. Hellmann, H.*J. Chem. Phys.* **3**, 61(1935).
48. Hellmann, H. & Kassatotchkin, W.*J. Chem. Phys.* **4**, 324(1936).
49. Fuchs, M. & Scheffler, M.*Comput. Phys. Commun.* **119**, 67(1999).
50. Wannier, N.K.*Rev. Mod. Phys.* **64**, 1045(1992).

3

L'oro in catalisi eterogenea: sintesi del Monomero del Vinil Acetato (VAM)

Introduzione

Il vinil acetato (VAc o VA) è utilizzato su larga scala nella produzione di una vasta gamma di polimeri. È, per esempio, uno dei componenti fondamentali per la produzione di pitture, adesivi, fibre e rivestimenti; oltre ad essere utilizzato per la sintesi di molte sostanze chimiche, quali il vinil alcool.

Fino alla fine degli anni '90 veniva prodotto industrialmente tramite un processo in fase eterogenea (processo Bayer), per acetossilazione dell'etilene in presenza di ossigeno su un catalizzatore a base di palladio. Nonostante la procedura illustrata sia stata scelta come la più vantaggiosa, in analogia agli altri processi di sintesi proposti presenta dei limiti non trascurabili, quali le condizioni di reazione e la formazione di sottoprodotti, per il cui smaltimento è necessaria una via alternativa.

Rimangono comunque da chiarire gli step chiave della reazione e le specie cataliticamente attive. In questa direzione si è mossa la ricerca degli ultimi dieci anni, grazie alla quale sono stati messi a punto catalizzatori più efficienti, costituiti da leghe metalliche a base di palladio in grado di limitare la formazione di sottoprodotti e, quindi, aumentare la resa della reazione.

In nostro lavoro si è concentrato sulla messa a punto di un modello computazionale in grado di riprodurre le evidenze sperimentali osservate per la reazione di formazione del VAM su superfici bimetalliche di Pd e Au, nel tentativo di far luce su molti dettagli concernenti il meccanismo di reazione, i siti di reazione ed il ruolo promozionale svolto dall'Au in questo tipo di leghe.

3.1 Sintesi del vinilacetato

Il metodo di produzione del VAc dal punto di vista industriale si è lentamente evoluto nel corso degli anni.[1-3] Le principali vie di sintesi comunemente utilizzate sono essenzialmente due: addizione di acido acetico all'acetilene (4.1) e coupling di acido acetico ed etilene (4.2).

$$C_2H_2 + CH_3COOH \rightarrow CH_2CHOOCCH_3 \qquad 4.1$$

$$C_2H_4 + CH_3COOH + \frac{1}{2}O_2 \rightarrow CH_2CHOOCCH_3 + H_2O \qquad 4.2$$

Entrambe le procedure possono essere realizzate sia in fase omogenea che eterogenea. Ad oggi, solo il processo eterogeneo viene utilizzato su scala industriale, sulla base delle maggiori rese che lo caratterizzano in confronto a quello omogeneo.[1-3]

Per i vari processi vengono coinvolti diversi catalizzatori. Per l'acetossilazione (4.2) viene generalmente utilizzato un catalizzatore a base di palladio (ioni di palladio nel processo omogeneo, palladio metallico in quello eterogeneo). La riossidazione del palladio viene poi realizzata per reazione dello stesso con ossigeno. In soluzione, tale reazione non avviene senza l'ausilio di un sale aggiuntivo (contenente rame o ferro) in grado di riossidare il palladio e di essere prontamente riossidato dall'ossigeno. Questo processo omogeneo, introdotto dal gruppo di Moiseev,[4] comporta la significativa formazione di acetaldeide (a causa della presenza di acqua nel solvente acido acetico). Il processo in fase gassosa, sviluppato da Hoechst e Bayer,[5] non presenta invece questo problema. Il principale sottoprodotto è il monossido di carbonio, il quale viene originato dalla combustione; si formano, però, anche tracce di altri prodotti di ossidazione.

3.1.1 Catalizzatori a base di Pd per la sintesi del VAc

I catalizzatori a base di palladio sono risultati essere i più selettivi nei confronti della reazione di formazione del VAM. Verranno discussi i due distinti processi, in fase omogenea (liquida) ed eterogenea (gassosa), che hanno segnato un passo importante verso la produzione del VAM su larga scala industriale.

All'inizio degli anni '60 è stato sviluppato da Moiseev e collaboratori,[4] un metodo di sintesi del VAc, in fase omogenea, molto simile al processo Wacker (ossidazione dell'etilene ad acetaldeide), nel quale è utilizzato il cloruro di palladio in acido acetico glaciale. La reazione omogenea dell'etilene con un acetato alchilico assistita da palladio cloruro vede la formazione dell'acqua come sottoprodotto, la quale viene rimossa dalla miscela di reazione tramite formazione di acetaldeide secondo il processo Wacker. La riossidazione del Pd viene realizzata dal rame in un ciclo redox, il quale può avvenire sia durante che nello step successivo alla formazione del vinilacetato. Nel corso della reazione si verifica la formazione di un gran numero di sottoprodotti, in funzione delle condizioni di reazione e delle specie presenti nella miscela di reazione. Il sottoprodotto in maggiore quantità è generalmente l'acetaldeide. La formazione di questo specifico sottoprodotto diviene più accentuata ad un'elevata concentrazione di acqua nella miscela di reazione; sicuramente non è tanto il processo Wacker

che contribuisce significativamente alla formazione dell'acetaldeide, quanto piuttosto l'idrolisi del vinilacetato. Tale processo omogeneo non è però particolarmente interessante dal punto di vista industriale, principalmente a causa dell'estrema corrosività della soluzione.

La produzione industriale del vinilacetato coinvolge, invece, come anticipato, il processo eterogeneo, il quale prevede il coupling di etilene e acido acetico. La miscela di reazione contiene ossigeno, necessario per rimuovere l'idrogeno attraverso la formazione di acqua. Il processo in fase gassosa è stato sviluppato da Hoechst e Bayer,[5] ma prima della loro scoperta sono stati condotti numerosi studi con lo scopo di perfezionare il catalizzatore più idoneo.[1-3] Tutti i catalizzatori impiegati sono, comunque, a base di palladio. Altri metalli, quali l'oro o il cadmio, vengono aggiunti come moderatori. La silice è, invece, generalmente utilizzata come materiale di supporto.

In letteratura sono proposti essenzialmente due meccanismi, uno dei quali prevede che la reazione avvenga sulla superficie metallica di palladio mentre l'altro coinvolge la reazione dell'etilene con la specie di palladio acetato sulla superficie. Nel primo meccanismo, proposto da Zaidi[6] e da Samanos e collaboratori,[7] il palladio viene ossidato a palladio acetato, il quale reagisce poi con l'etilene in maniera molto simile al processo omogeneo. L'ultimo step, che coinvolge l'inserzione dell'etilene nel legame palladio-acetato, è supposto essere il rate-determining step. L'altro meccanismo proposto coinvolge, invece, l'interazione delle specie adsorbite sulla superficie secondo una reazione del tipo Langmuir-Hinshelwood. Tale meccanismo è stato proposto alla fine degli anni '70 da Debellefontaine,[8] Nakamura e Yasui.[9] Questi ultimi suppongono che la formazione del palladio acetato sia sfavorita, in quanto contribuisce alla disattivazione del catalizzatore.[10] In questo meccanismo prima si formano le specie attive di etilene e acido acetico, vinile e acetato, e poi si ha il coupling tra queste due specie.

3.1.2 Meccanismi proposti per la reazione in fase eterogenea catalizzata da Palladio

La letteratura degli anni '60 e '70 sull'argomento rispecchia la smaniosa ricerca di catalizzatori attivi e selettivi nei confronti della produzione del monomero del vinil acetato (VAM). Per il metodo di sintesi di maggiore interesse dal punto di vista industriale, quello in fase eterogenea su superfici metalliche di palladio, sono stati delineati due meccanismi. Il primo, proposto da Moiseev,[4,11] Nakamura e Yasui[9] (*Figura 3.1 a*), prevede l'adsorbimento e la

successiva attivazione dell'etilene a vinile. L'acido acetico co-adsorbito reagisce rapidamente per formare l'acetato. Quest'ultimo e il vinile, entrambi adsorbiti sulla superficie di Pd, reagiscono per formare il vinilacetato che viene poi desorbito come prodotto. Il secondo meccanismo, proposto da Samanos[7] (*Figura 3.1 b*), prevede la diretta inserzione dell'etilene nel legame Pd-O dell'acetato adosorbito per formare un intermedio, il 2-etilacetato, che per β-H eliminazione porta alla formazione del prodotto. In addizione al percorso selettivo che porta alla formazione del vinilacetato, vi sono una serie di percorsi non selettivi che comportano la contemporanea formazione di sottoprodotti, i più importanti dei quali sono sicuramente CO e CO_2.

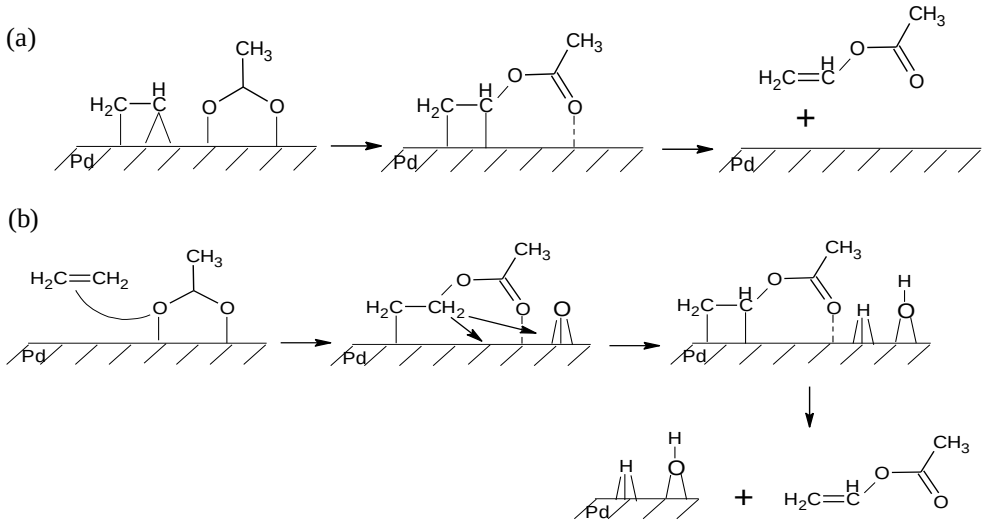

Figura 3.1: (a) meccanismo di tipo Moiseev, (b) meccanismo di tipo Samanos.

3.2 Catalizzatori bimetallici per la sintesi del VAM

In generale, l'impiego di catalizzatori bimetallici è di particolare utilità per migliorare la selettività di una reazione verso la formazione di uno specifico prodotto precludendo la genesi di percorsi alternativi che porterebbero alla formazione di sottoprodotti. Gli studi condotti su questo tipo di catalizzatori hanno evidenziato che l'attività delle reazioni su superfici bimetalliche rispetto alla superficie monometallica, non varia apprezzabilmente con la composizione della superficie stessa. E', pertanto, possibile agire sulla composizione del catalizzatore in modo da selezionare quello più efficiente senza variarne la reattività.

Nel caso specifico della sintesi del vinilacetato è stato osservato che l'aggiunta di Au al Pd aumenta significativamente la resa della reazione di formazione del vinilacetato.[12] Le superfici bimetalliche costituite da oro e palladio (silice come supporto) sono infatti ormai utilizzate a livello industriale per la sintesi del VAM.[7,9,12-15] La ricerca, però, dei dettagli meccanicistici è ancora aperta.

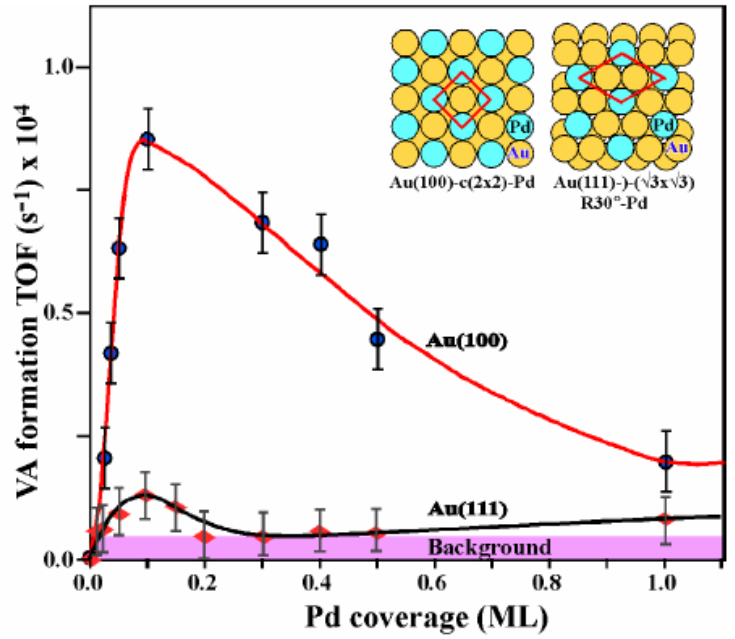

Figura 3.2: velocità di formazione del VAM in funzione del coverage di Pd sulle superfici Au(100) e Au(111).[16]

Goodman e collaboratori[16] hanno condotto uno studio sulla reazione di formazione del VAM realizzata su superfici bimetalliche di Pd e Au, nel quale è stato osservato il ruolo promozionale dell'Au in base al tipo di superficie esposta (*Figura 3.2*). Gli autori hanno individuato come composizione superficiale critica una coppia di monomeri di Pd non contigui, che avrebbe la funzione di inibire la formazione di sottoprodotti indesiderati. La velocità di formazione, maggiore sulla superficie PdAu(100) rispetto alla superficie PdAu(111), è stata giustificata sulla base di effetti di *ensemble*. Dovrebbe quindi essere la distanza tra gli atomi di Pd a controllare la catalitica formazione del VAM. Gli effetti di *ligand* sono stati invece considerati meno rilevanti rispetto a quelli di ensemble.

3.3 Approccio Cluster: modelli per le superfici PdAu(100) e PdAu(111)

Il modello cluster è stato scelto come approccio computazionale per interpretare i risultati sperimentali riguardanti la reazione di formazione del VAM e quindi giustificare l'intuizione che fossero gli effetti di *ensemble* a determinare la maggiore attività della superficie PdAu(100) rispetto alla superficie PdAu(111).

Nell'approccio cluster il sito di adsorbimento viene costruito tramite l'utilizzo di un numero finito di atomi metallici, la cui disposizione viene scelta in modo da riprodurre perfettamente i contributi all'interazione adsorbato-substrato che sono generati dai cambiamenti locali della struttura elettronica del substrato. Il modello è stato quindi costruito in modo che potesse descrivere le caratteristiche fondamentali del chemisorbimento di molecole semplici e, quindi, predire le proprietà locali, quali le geometrie di adsorbimento e le frequenze vibrazionali per coverages molto bassi.

Per modellare l'intorno di una coppia di monomeri di palladio sulle superfici PdAu(100) e PdAu(111), i cluster sono stati costruiti a partire da una coppia di atomi di Pd non contigui e due atomi di Au legati ad entrambi i monomeri di Pd. Per costruire il sito attivo, i primi vicini a questi quattro atomi sono stati aggiunti sia sul primo che sul secondo layer. I siti attivi sono quindi costituiti dai cluster Pd_2Au_{19} and Pd_2Au_{20}, denotati come Pd_2Au_{19}(12,9) e Pd_2Au_{20}(14,8) per indicare il numero di atomi che costituisce ciascun layer del cluster per le superfici Au(100) e Au(111) rispettivamente. Inizialmente, le posizioni atomiche sono state assegnate come nell'oro bulk quindi con una distanza Au-Au di 2.885 Å. Le dimensioni dei cluster sono state aumentate per aggiunta di un terzo layer, per ottenere i cluster Pd_2Au_{23}(12,9,4) e Pd_2Au_{28}(14,8,8). Come indica la notazione tra parentesi, nel caso della superficie PdAu(100) l'aggiunta di un terzo layer corrisponde all'aggiunta di quattro atomi di Au che vanno ad occupare le posizioni corrispondenti ai quattro atomi centrali del primo layer, come definito dall'impaccamento di tipo ABAB della superficie fcc(100). Per la superficie di oro fcc(111) con impaccamento ABCABC, l'aggiunta del terzo layer equivale all'aggiunta di 8 atomi in corrispondenza delle posizioni atomiche definite dai siti di adsorbimento hollow-fcc. A partire da questi modelli sono stati poi costruiti i due clusters più estesi considerati, completando così il set di atomi vicini per tutti gli atomi periferici del primo e del secondo layer. I cluster risultanti Pd_2Au_{55}(24,21,12) and Pd_2Au_{62}(30,21,13), per i sistemi PdAu(100) e PdAu(111)

rispettivamente, dovrebbero garantire l'impedimento di qualsiasi effetto di insaturazione indiretta per i siti attivi considerati.

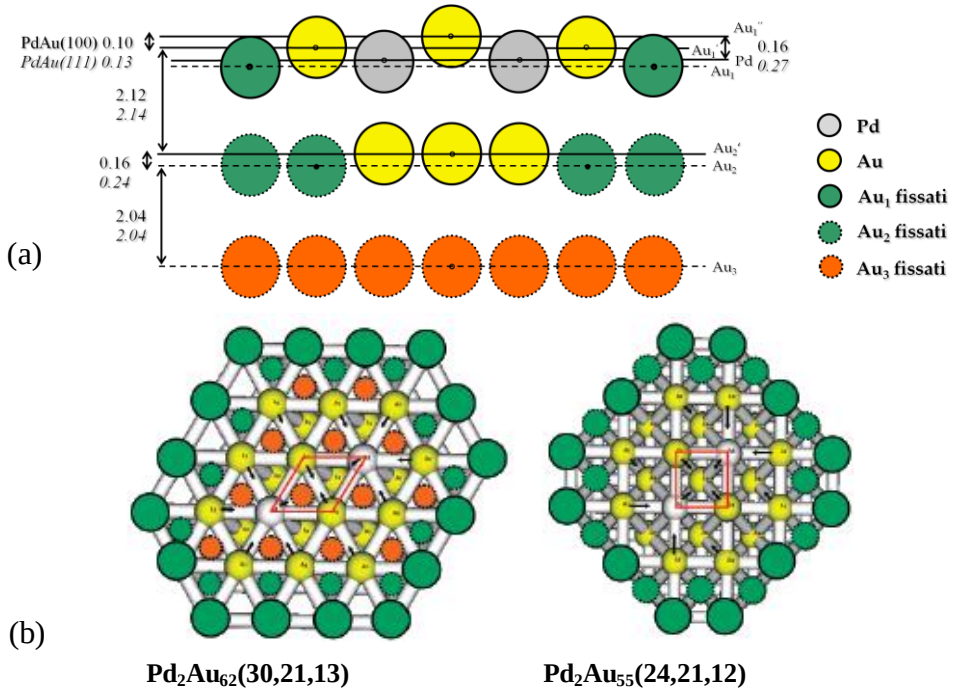

Figura 3.3: rappresentazione schematica dell'effetto di rilassamento nei cluster Pd_2Au_{55}(24,21,12) e Pd_2Au_{62}(30,21,13). (a) Rilassamento dei layer rispetto alle distanze tra i layer dell'oro bulk. (b) I cambiamenti delle posizioni atomiche dovuti al rilassamento locale sono indicati dalle frecce nere. Le celle unitarie sono delineate in rosso.

Per valutare e quindi analizzare gli effetti del rilassamento locale nelle vicinanze dei monomeri di Pd sono stati utilizzati i cluster di maggiori dimensioni presi in considerazione per il modello delle due superfici PdAu(100) e PdAu(111), in modo da ottenere un modello il più realistico possibile per lo studio dei fenomeni di adsorbimento del sistema probe e quindi dei reagenti. Le strutture rilassate localmente dei cluster bimetallici Pd_2Au_{55} e Pd_2Au_{62} sono state confrontate con le strutture dei cluster costituiti da soli atomi di oro (Au_{57} e Au_{64} rispettivamente), anch'esse rilassate, utilizzando il BP86 come funzionale di scambio e correlazione.

È stato così osservato un significativo riarrangiamento dei siti attivi come conseguenza della sostituzione dei due atomi superficiali di Au non contigui con due monomeri di Pd. Gli atomi di oro sulla superficie si muovono nella direzione dei monomeri di Pd (*Figura 3.3*),

mentre gli atomi di palladio si muovono lungo l'asse perpendicolare alla superficie verso l'interno (di 0.16-0.20 Å) rispetto al layer superficiale. Il risultato di questo rilassamento si traduce in una distanza di legame Pd-Au nel sito attivo più corta rispetto a quella Au-Au sulle superfici di soli atomi di oro, indice di una forte interazione Pd-Au, in accordo con i risultati degli studi condotti con l'approccio slab supercell.[17]

3.3.1 Adsorbimento di una molecola probe (*pubblicazione I*)

Lo studio delle proprietà di adsorbimento di una molecola probe per la caratterizzazione della composizione superficiale (che ha un ruolo chiave per la comprensione delle proprietà catalitiche di sistemi bimetallici) ha avuto come scopo la costruzione dei modelli cluster, appena descritti, che fossero in grado di simulare il processo catalitico preso in considerazione. Il monossido di carbonio è, contemporaneamente, sia un ideale sistema probe per la caratterizzazione della superficie sia un sottoprodotto di degradazione nella sintesi del VAc.

Per studiare l'influenza delle dimensioni dei cluster sulla geometria, sulle frequenze vibrazionali e sull'energetica delle molecole di CO adsorbite sulla coppia di monomeri di palladio non contigui, sono stati utilizzati, per entrambe le superfici, i tre cluster risultati dal processo di costruzione dei modelli. Gli atomi dei cluster sono però stati mantenuti fissi nelle loro posizioni ottimizzate nel processo di rilassamento, mentre le posizioni di C e O sono state interamente ottimizzate per tutti i siti di adsorbimento all'interno del sito attivo. Le proprietà energetiche, strutturali e vibrazionali sono state, quindi, valutate sia per l'adsorbimento di una sola molecola di CO on top ad uno dei due Pd che per due molecole di CO on top ai due monomeri di Pd non contigui. I calcoli sono stati effettuati nell'ambito della DFT utilizzando il BP86 come funzionale di scambio e correlazione, e le SVP come set di base. Per valutare gli effetti del funzionale e dei set di base è stato successivamente effettuato il confronto con il funzionale ibrido B3LYP e con le basi TZVP. A causa dell'aumento del costo computazionale utilizzando set di base più grandi e un funzionale ibrido di scambio e correlazione, le proprietà di chemisorbimento sono state valutate solo per i cluster minimali Pd_2Au_{19}(12,9) e Pd_2Au_{28}(14,8,8), scelti in base ai risultati degli studi di convergenza delle BE per entrambe le superfici. L'analisi dei risultati, in buon accordo con i dati sperimentali di riferimento, hanno portato all'individuazione del protocollo computazionale nel livello di teoria BP86/SVP, il quale è stato utilizzato per tutti gli studi successivi sui modelli prima descritti.

3.3.2 Adsorbimento dei reagenti (*pubblicazione II*)

Sulla base dei risultati ottenuti circa le proprietà del chemisorbimento del sistema probe, è stato effettuato l'adsorbimento dei reagenti coinvolti nel processo di sintesi del VAM. Gli studi sperimentali, condotti da Goodman e collaboratori,[16] hanno dimostrato che la formazione dei siti di Pd isolati influenza le proprietà dei reagenti adsorbiti. L'etilene, per esempio, si coordina al monomero di Pd tramite un'interazione meno forte in confronto a quella osservata con il sito contenente atomi di Pd contigui.[18,19] Sui siti di Pd contigui è stata osservata una coordinazione dell'etilene di-σ,[20] che si decompone comportando la formazione di carbonio, mentre sui monomeri di Pd circondati da atomi di Au è stata osservata una coordinazione dell'etilene sul Pd di tipo π.[16,19,20] L'addizione di oro inibendo la decomposizione dell'etilene aumenta l'attività del catalizzatore. Lo stesso tipo di effetto è stato dimostrato per la decomposizione dell'acido acetico e dell'acetato.[19,21] Risulta così oltremodo evidente il ruolo promozionale svolto dall'oro, il quale risulta necessario per l'isolamento dei monomeri di Pd e quindi la maggiore efficienza del catalizzatore nei confronti della specifica reazione.

Sulla base dei due meccanismi proposti (tipo Samanos e tipo Moiseev) per la medesima reazione su catalizzatori eterogenei a base di Pd, è stato effettuato l'adsorbimento, non solo dei due reagenti, etilene e acido acetico, ma anche delle loro specie attivate, quindi vinile e acetato sui monomeri di Pd non contigui (*Figura 3.4*). Per quanto riguarda l'adsorbimento dell'**etilene** sono state valutate tutte le possibili orientazioni della molecola rispetto alla superficie. I nostri studi hanno confermato il tipo di coordinazione osservata sperimentalmente. In accordo con il meccanismo di tipo Moissev la formazione del VAc si realizza tramite l'attivazione (deidrogenazione) dell'etilene a **vinile**, il quale poi reagisce direttamente con l'acetato co-adsorbito. Lo studio del chemisorbimento del vinile sulle due superfici ha evidenziato una coordinazione di tipo σ on top al monomero di Pd in orientazione verticale rispetto alla superficie. Questa specifica coordinazione è stata individuata anche on top all'Au, la quale risulta però molto meno stabile.

Lo stesso tipo di studio è stato condotto per l'adsorbimento dell'**acido acetico**, per il quale sono state valutate tutte le possibili coordinazioni (bi-dentate e mono-dentate) della molecola rispetto alla superficie. La coordinazione risultata più stabile è monodentata on top al Pd tramite l'ossigeno carbonilico, mentre il legame O-H punta verso il sito hollow della superficie, formando un legame a idrogeno molto debole con la superficie di atomi di Au che in qualche modo stabilizza questo modo di coordinazione. Le caratteristiche geometriche di questo stato di adsorbimento evidenziano la facile estrazione dell'H da parte della superficie per formare la

specie attiva dell'acido, l'**acetato**. Sulla base delle evidenze sperimentali, sono state valutate anche per l'acetato tutte le possibili conformazioni della molecola rispetto la superficie. In questo caso è stata individuata come coordinazione più stabile quella bidentata in cui i due atomi di ossigeno sono coordinati uno al monomero di Pd e l'altro all'atomo di Au adiacente sul sito attivo.

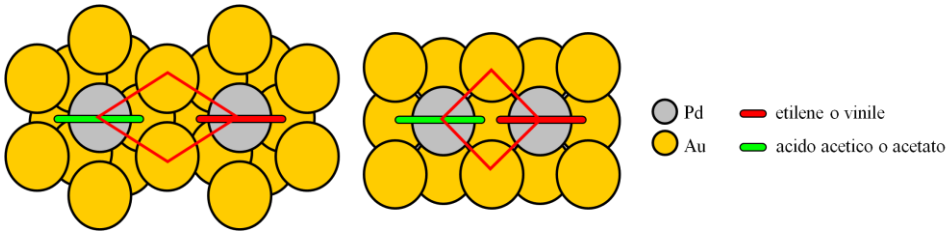

PdAu(111) **PdAu(100)**

Figura 3.4: rappresentazione schematica dei siti di adsorbimento dei reagenti e delle corrispondenti specie attivate.

In generale, l'adsorbimento delle quattro molecole sulle superfici PdAu (100) e PdAu(111) è risultato essere meno forte rispetto a quello osservato sulle corrispondenti superfici di Pd pure. L'effetto *ligand* degli atomi di oro suggerisce che i monomeri di Pd non contigui sulle superfici di Au comportino un abbassamento delle energie di adsorbimento.

3.3.3 Step di coupling per i due meccanismi (*pubblicazione III*)

Gli studi condotti sino ad ora sulla reazione di formazione del VAM, non solo su superfici di soli atomi di Pd[22] ma anche su superfici miste di Pd e Au,[23] hanno portato gli autori ad identificare lo step di **coupling** con il *rate-determining step*[4,7,9,11] ed a selezionare come processo favorito il meccanismo di tipo Samanos. Sulla base di tali osservazioni abbiamo condotto uno studio dettagliato di questo step chiave coinvolto in entrambi i meccanismi proposti, con lo scopo di interpretare i risultati sperimentali riportati da Goodman e collaboratori,[16] i quali hanno giustificato la maggiore velocità di formazione del VAM sulla superficie PdAu(100) sulla base di effetti di *ensemble*. Dal confronto dei risultati ottenuti a livello DFT con i cluster prima descritti, non emerge la maggiore attività della superficie PdAu(100) rispetto alla superficie PdAu(111). Gli effetti di ensemble sembrano essere rilevanti solo nel meccanismo di tipo Moiseev (*Figura 4.1a*), il coupling di vinile e acetato è, infatti, risultato più sfavorito sulla superficie PdAu(111). Per quanto riguarda, invece, il coupling

coinvolto nel meccanismo di tipo Samanos (*Figura 4.1b*), presenta barriere confrontabili per le due superfici, la distanza ottimale tra i due monomeri di Pd non sembra influire su tale step della reazione.

3.3.4 Deidrogenazione dell'etilene (*manoscritto I*)

I risultati sperimentali riguardo la reazione di formazione del VAM su superfici di soli atomi di Pd,[22] non solo hanno evidenziato la preferenza per il meccanismo di tipo Samanos sulla superficie Pd(111), hanno anche mostrato che la presenza dell'ossigeno non influisce significativamente sulla cinetica della reazione. Gli autori hanno però suggerito che l'ossigeno coadsorbito potrebbe giocare un ruolo importante nella sintesi del vinil acetato sulla superficie PdAu(100).[24] Per quanto il meccanismo di tipo Moiseev, il primo step del processo (**deidrogenazione dell'etilene**) è stato oggetto di studi teorici da parte di Yuan e collaboratori,[17] i quali hanno concluso che la deidrogenazione dell'etilene è improbabile che avvenga sulle superfici di PdAu. Sulla base di tali osservazioni, solo il meccanismo di tipo Samanos è stato oggetto di recenti studi teorici.[25,23] In questi lavori, gli autori hanno esaminato lo step di β-H eliminazione dell'intermedio 2-etilacetato in presenza di ossigeno[25] o del gruppo ossidrilico[23] mostrando come l'ossigeno coadsorbito promuova la deidrogenazione di tale intermedio per formare il vinil acetato. Tuttavia non è stato oggetto di alcuno studio l'analogo ruolo che intuitivamente l'ossigeno può svolgere nello step di deidrogenazione dell'etilene nel meccanismo di tipo Moiseev. Con l'obiettivo di valutare l'influenza delle specie promotrici O_s e OH_s sulla deidrogenazione dell'etilene, è stato condotto uno studio dettagliato di tale step della reazione su entrambe le superfici prese in considerazione sino ad ora, PdAu(100) e PdAu(111), utilizzando i modelli cluster Pd_2Au_{55} e Pd_2Au_{62} rispettivamente. Le barriere di attivazione calcolate mostrano come la presenza delle specie O_s e OH_s influenzi in maniera significativa la reazione di formazione del vinile su entrambe le superfici PdAu. Infatti, la facilità con cui si la formazione del vinile suggerisce che lo step di deidrogenazione sia coinvolto nel processo catalitico e che il coupling sia il rate-determining step per il meccanismo di tipo Moiseev.

Bibliografia

1. Miller, S.A. *Ethylene and its Industrail Derivatives*. (Ernest Benn Limited: London, 1969).
2. Summer, C.E. & Zoeller, J.R. *Acetic Acid and its Industrial Derivatives*. 225(Ernest Benn Limited: London, 1993).
3. Elvers, B. *Ullman's Encyclopedia of Industrial Chemistry*. **A27**, 419(Hawkins S.: VCH Verlagsgesellschaft mbH: Weinheim, 1996).
4. Moiseev, I.I., Vargaftick, M.N. & Syrkin, Y.K. Mechanism of the reaction of palladium salts with olefins in hydroxyl-containing solvents. *Dokl. Akad. Nauk SSSR* **133**, 377-380(1960).
5. Schwerdtel, W. Make Vinyl Acetate Via Ethylene. *Hydrocarbon Proc.* **47(11)**, 187(1968).
6. Zaidi, S.A.H. Gas phase acetoxylation of ethylene: palladium-on-carbon catalyst stability. **68**, 255-263(1981).
7. Samanos, B., Boutry, P. & Montarnal, R. The mechanism of vinyl acetate formation by gas-phase catalytic ethylene acetoxidation. *Journal of Catalysis* **23**, 19-30(1971).
8. Debellefontaine, H. & Besombes-Vaihé, J.*J. Chim. Phys. (trans)* **75**, 801-809(1978).
9. Nakamura, S. & Yasui, T. The mechanism of the palladium-catalyzed synthesis of vinyl acetate from ethylene in a heterogeneous gas reaction. *Journal of Catalysis* **17**, 366-374(1970).
10. Nakamura, S. & Yasui, T. Formation of palladous acetate and stability of catalyst in palladium-metal-catalyzed synthesis of vinyl acetate from ethylene. *Journal of Catalysis* **23**, 315-320(1971).
11. Moiseev, I.I. *Catalytic Oxidation*. 203(R. A. Sheldon: World Scientific, 1995).
12. Provine, W.D., Mills, P.L. & Lerou, J.J. Discovering the role of Au and KOAc in the catalysis of vinyl acetate synthesis. *11th International Congress On Catalysis-40th Anniversary, Proceedings of the 11th ICC* **Volume 101, Part 1**, 191-200(1996).
13. Macleod, N., Keel, J.M. & Lambert, R.M. The effects of ageing a bimetallic catalyst under industrial conditions: a study of fresh and used Pd-Au-K/silica vinyl acetate synthesis catalysts. *Applied Catalysis A: General* **261**, 37-46(2004).
14. Han, Y., Kumar, D. & Goodman, D. Particle size effects in vinyl acetate synthesis over Pd/SiO2. *Journal of Catalysis* **230**, 353-358(2005).
15. Stacchiola, D. et al. Vinyl Acetate Formation by the Reaction of Ethylene with Acetate Species on Oxygen-Covered Pd(111). *Journal of the American Chemical Society* **126**, 15384-15385(2004).
16. Chen, M. et al. The Promotional Effect of Gold in Catalysis by Palladium-Gold. *Science* **310**, 291-293(2005).
17. Yuan, D., Gong, X. & Wu, R. Ensemble effects on ethylene dehydrogenation on PdAu(001) surfaces investigated with first-principles calculations and nudged-elastic-band simulations. *Physical Review B - Condensed Matter and Materials Physics* **75**, (2007).
18. Luo, K. et al. Preparation and Characterization of Silica Supported Au−Pd Model Catalysts. *The Journal of Physical Chemistry B* **109**, 23517-23522(2005).
19. Calaza, F. et al. The adsorption of ethylene on Au/Pd(1 1 1) alloy surfaces. *Surface Science* **601**, 714-722(2007).
20. Chen, M. et al. The nature of the active site for vinyl acetate synthesis over Pd-Au. *Catalysis Today* **117**, 37-45(2006).
21. Owens, T.G. et al. The Effects of Gold and Co-adsorbed Carbon on the Adsorption and Thermal Decomposition of Acetic Acid on Pd{111}. *The Journal of Physical Chemistry B* **110**, 21152-21160(2006).

22. Stacchiola, D. et al. Elucidation of the Reaction Mechanism for the Palladium-Catalyzed Synthesis of Vinyl Acetate13. *Angewandte Chemie International Edition* **44**, 4572-4574(2005).
23. García-Mota, M. & López, N. Template Effects in Vinyl Acetate Synthesis on PdAu Surface Alloys: A Density Functional Theory Study. J*ournal of the American Chemical Society* 1**30,** 14406-14407(2008).
24. Li, Z., Gao, F. & Tysoe, W. Surface chemistry of acetic acid on clean and oxygen-covered Pd(1 0 0). S*urface Science* 6**02,** 416-423(2008).
25. Yuan, D., Gong, X. & Wu, R. Origin of High Activity and Selectivity of PdAu(001) Bimetallic Surfaces toward Vinyl Acetate Synthesis. T*he Journal of Physical Chemistry C* 1**12,** 1539-1543(2008).

4

L'oro in catalisi omogenea: catalizzatore alternativo per la reazione di idratazione degli alchini

Introduzione

L'interesse nei confronti dell'oro nel campo della catalisi omogenea è rimasto sopito per lungo tempo. Solo negli ultimi anni, l'abilità dei sali a base di oro di attivare legami multipli carbonio-carbonio come acidi di Lewis soft è stata considerata di grande utilità pratica nei processi di sintesi.

I sali di oro sono in particolare risultati efficienti per l'attivazione degli alchini nei confronti dell'attacco di un nucleofilo debole, come l'acqua o il metanolo. Il processo di idratazione degli alchini per dare i corrispondenti composti carbonilici rappresenta un modello di reazione piuttosto nuovo. Nonostante questa reazione sia conosciuta dal XIX secolo, il suo potenziale non è stato convenientemente sfruttato nei processi industriali, a causa delle drastiche condizioni di reazione richieste dal tipo di catalizzatore utilizzato, un catalizzatore a base di sali di mercurio considerato essere il composto più attivo per catalizzare questo tipo di reazioni.

4.1 L'oro in catalisi omogenea

La caratteristica di maggiore rilievo dei complessi di Au(I) e Au(III) è la loro capacità di attivare legami C-H e legami multipli C-C consentendo la formazione di nuovi legami C-C, C-O, C-N e C-S come acido soft di Lewis tramite attacco nucleofilo di tali substrati attivati. Grazie a questa peculiarità l'impiego dei sali di Au nei processi catalitici è stato ampiamente studiato.(rif) In particolare, l'attivazione di legami C-H in substrati quali alchini, alcheni o areni, chetoni α,β insaturi, β-dichetoni o alleni può avvenire ad opera di sali di Au(I) e Au(III). Una delle reazioni più interessanti nella quale l'Au manifesta le sue particolari caratteristiche nei confronti dell'attivazione di legami multipli C-C, è certamente la reazione di idratazione di alchini semplici.

La comprensione dell'attività catalitica mostrata dai complessi di Au può essere facilitata dall'analisi computazionale degli orbitali di frontiera, degli effetti relativistici e della π-acidità. Le proprietà di forti donatori σ e di deboli accettori π degli alchini rendono elettrofilici i complessi oro-alchini, facilitando così l'attacco da parte di un nucleofilo, quale l'acqua o il metanolo.

4.1.1 Natura del legame nel complesso Metallo-Alchino

Il primo step della trasformazione chimica catalitica di un alchino nel corrispondente composto carbonilico è senz'altro la complessazione e l'attivazione del legame multiplo. L'interazione metallo-legante, in cui il legante coinvolto è un alchino, può, almeno in prima istanza, essere giustificata sulla base del modello Dewar-Chatt-Duncanson[1,2] (*Figura 4.1*), il quale considera il legame come un'interazione donatore-accettore tra due frammenti closed-shell.[3] Secondo il modello DCD, il legame σ si instaura in seguito alla sovrapposizione del sistema π del legante con un orbitale vuoto del metallo, con simmetria opportuna. L'interazione π invece risulta dalla retro-donazione della densità elettronica da un orbitale *d* pieno del metallo nell'orbitale di antilegame π* dell'alchino.

Le principali componenti che possono contribuire all'interazione di legame di un alchino con i centri metallici, come l'Au(I), sono essenzialmente quattro (*Figura 4.1*). Gli orbitali sul piano $\pi_{//}$ sono responsabili della donazione σ-simmetrica M←L nonché della retro-donazione π-simmetrica.

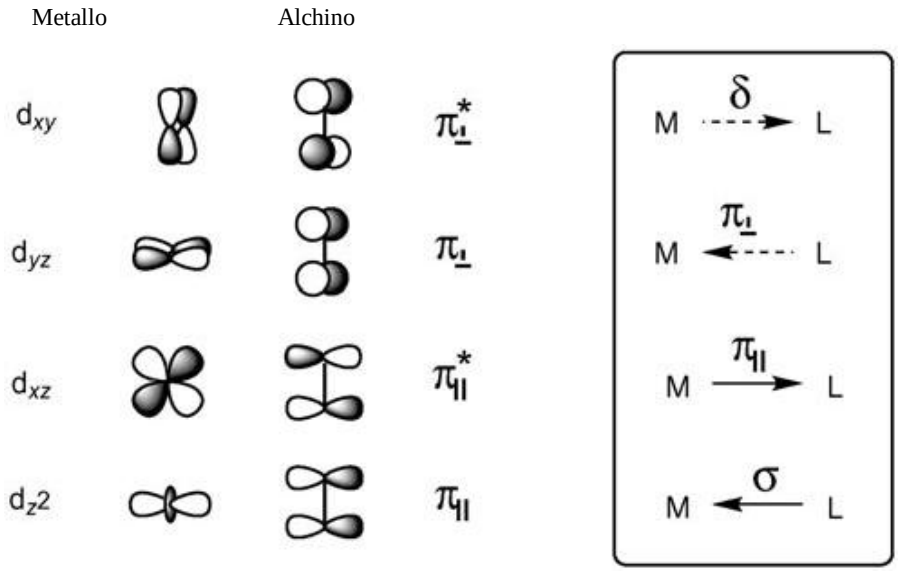

Figura 4.1: Diagramma qualitativo degli orbitali, esemplificativo dell'interazione tra un metallo di transizione e un alchino legante.[4]

Gli orbitali fuori dal piano, ortogonali, possono invece essere coinvolti nella donazione π (un'importante interazione nei complessi contenenti alchini in cui il quest'ultimo funge da donatore di quattro elettroni), mentre la combinazione di un orbitale *d* occupato del metallo e di

un orbitale $\pi_{\perp}^{*}$ vuoto dell'alchino può tradursi in un contributo addizionale alla retro-donazione M→L, quest'ultima interazione, che genera solo una debole sovrapposizione, ha simmetria δ e comporta un piccolo contributo alla formazione del legame.

Questa schematizzazione qualitativa del legame si adatta bene ai complessi di oro d^{10}. La formazione del complesso altera necessariamente le strutture dei frammenti metallici e del legante. Il modello DCD prevede un'elongazione del triplo legame come conseguenza del cambiamento netto della densità degli elettroni dagli orbitali π di legame agli orbitali π* di antilegame. Si verifica così una parziale flessione dell'alchino come conseguenza della successiva reibridizzazione. Di conseguenza il grado di distorsione della geometria del legante non coordinato può essere utilizzato come indicazione osservabile del grado di retro-donazione.

Gli studi teorici condotti per valutare la natura del legame nei complessi di Au(I) con alchini hanno portato alla conclusione che il metallo non partecipa in maniera significativa alla formazione del legame del tipo DCD in quanto gli orbitali di antilegame sono troppo alti in energia per realizzare una significativa retrodonazione. Questo tipo di interazione tra il metallo e il legante nella formazione del primo complesso è stata studiata in dettaglio per il complesso Au-difenilacetilene. L'analisi computazionale ha confermato l'impossibilità di un'efficiente retrodonazione dal metallo al legante.

4.2 Idratazione degli alchini

Il processo di idratazione degli alchini semplici non è solo una delle vie più filo- ambientali per trattare uno degli idrocarburi più diffusi, ma è soprattutto un'importante strategia di sintesi per la formazione di composti carbonilici.

L'addizione di acqua ad alchini ricchi di elettroni attivati, come gli alchinil eteri, alchinil tioeteri o inammine, avviene piuttosto facilmente in presenza di un catalizzatore acido.[5,6] La reazione di alchini semplici necessita, invece, dell'ausilio di un cocatalizzatore, tipicamente sali di mercurio(II), per aumentarne la reattività.[7,8] È noto che le reazioni di addizione ad alchini catalizzate da un acido di Brønsted richiedono condizioni di reazione piuttosto drastiche e sono ostacolate da una serie di processi collaterali che coinvolgono il carbocatione intermedio.[9] Sostituire il protone con il frammento isolobale Hg^{2+} costituisce appunto una classica soluzione al problema.[10] Il carattere soft di questi cationi grandi e polarizzabili assicura un'affinità molto maggiore per il substrato, che si traduce in condizioni di reazioni più miti e in un'elevata resa

del prodotto desiderato. I dati spettroscopici forniscono la prova evidente che il legante nel complesso π è carente di elettroni ed è quindi suscettibile all'attacco da parte di un nucleofilo nel classico modo trans.[11] Inoltre, le reazioni di addizione ad alchini si realizzano con quantità catalitiche di Hg(II),[10] ma rimane la chiara evidenza della tossicità di questi composti. Questo tipo di catalizzatori è stato infatti ampiamente utilizzato nei processi industriali fino alla scoperta della tossicità dei sali di mercurio.

Per lungo tempo si è tentato di individuare un catalizzatore alternativo per l'idratazione di alchini. Sono stati studiati complessi di metalli di transizione quali il Ru(II),[12-15] Ru(III),[16-18] Rh,[19,20] Pt,[21-23] Au(III),[24,25] e altri centri metallici,[26,27] ma nonostante nessuno di questi fosse in grado di riprodurre l'attività catalitica dei corrispondenti sistemi contenenti sali di mercurio, si è lentamente sviluppata la possibilità di utilizzare complessi di Au(I) per la sintesi di complessi carbonilici a partire dagli alchini corrispondenti. Infatti il frammento LAu^+ combina l'alta affinità del sistema π del substrato con il vantaggio di un legame carbonio-metallo cineticamente labile che può essere rapidamente scisso nelle condizioni di reazione, in modo da garantire un turnover efficiente. L'utilizzo della specie LAu^+ al posto del frammento isolobale H^+, oltre all'analogia nel comportamento chimico, suggerisce che il protone e il complesso siano equivalenti, ma che quest'ultimo possieda un maggiore carattere carbofilico. Questi studi iniziali hanno, infatti, spinto i ricercatori a sfruttare l'apparente insensibilità dell'Au a sviluppare una serie di reazioni collaterali in presenza di acqua o metanolo come solventi[28,29] per l'efficiente addizione di alcool ad alchini, la quale risulta la prima applicazione dell'oro come catalizzatore nella sintesi organica.

Alla fine degli anni '90 Teles e collaboratori hanno effettuato l'addizione di metanolo ad alchini catalizzata da complessi di Au(I), del tipo R_3PAu^+, con l'aiuto di un co-catalizzatore acido (acido di Brønsted o di Lewis).[30] Successivamente allo studio di Teles i complessi di Au(I) sono infatti stati considerati la tipologia di complesso metallico ottimale per riprodurre l'efficienza catalitica dei Sali di mercurio.

L'indagine sulla capacità dell'Au di catalizzare trasformazioni sintetiche, utilizzando alogenuri di Au(III), ha portato alla conclusione che un'ampia gamma di nucleofili potesse essere addizionata ad alchini sia in maniera intra-[31-34] che intermolecolare.[24] I risultati ottenuti da Teles hanno così contribuito ad un'estensione del potenziale catalitico dell'Au. Catalizzatori del tipo R_3PAuX (X=triflato o altri controioni debolmente coordinanti), formati in situ per estrazione di Cl_2 da R_3PAuCl da parte di un alogenuro di Ag o per potonolisi di R_3PAuCH_3 con un acido rilasciando CH_4, sono mostrati essere ottimi catalizzatori per una serie di reazioni che

portano alla formazione di legami C-C, incluse reazioni di conia-ene[35,36] e idroarilazione,[37-39] nonché reazioni che portano alla formazione di legami carbonio-eteroatomo.[40-42] Il principio comune di tutte queste reazioni è comunque l'attivazione elettrofila del legame multiplo C-C tramite coordinazione all'Au.

Un importante risultato del lavoro di Teles deriva da calcoli teorici, i quali mostrano come l'oro(I) direziona l'attacco dell'alcool nucleofilo dal lato del metallo coordinato, realizzando così un'addizione *sin*. Questo comportamento è diverso dal solito attacco del nucleofilo che in genere, per altri metalli elettrofili, avviene dal lato apposto al metallo coordinato (addizione *trans*).

4.3 Idratazione dell'1,2-fenilacetilene (Manoscritto II)

Come ampiamente discusso, l'importanza del processo di idratazione di alchini catalizzata da complessi di Au(I) è basata sulla capacità di questi ultimi di garantire condizioni di reazioni blande, in quanto non necessitano di cocatalizzatori o di riscaldamento per far avvenire la reazione. Con l'obiettivo di razionalizzare i dati sperimentali e confermare le supposizioni circa il meccanismo di reazione riportati da Leyva e Corma[43] abbiamo scelto di studiare in dettaglio il processo di idratazione con acqua di un alchino simmetrico, l'1,2-fenilacetilene, catalizzata da un complesso di Au(I), il $(Ph)_3PAu(I)$.

Il meccanismo proposto (Schema 4.1) coinvolge la coordinazione del triplo legame al complesso di Au(I), con la formazione del complesso **I** Au-π-alchino e il successivo attacco dell'acqua. La coordinazione dell'H_2O nel complesso **II** avviene direttamente sull'atomo di carbonio C1. Il trasferimento del protone dall'O all'atomo di carbonio C2 si realizza tramite la formazione di un intermedio **III** in cui il protone si coordina all'oro, fungendo così quest'ultimo da proton-shuttle. La reazione potrebbe a questo punto procedere senza l'ausilio di catalizzatore, con la formazione dell'isomero E dell'enolo. I calcoli energetici mostrano come l'ausilio del catalizzatore anche per l'addizione della seconda molecola d'acqua comporti un notevole guadagno. La formazione dell'isomero Z dall'isomero E si realizza con la rotazione attorno al doppio legame C-C. La reazione procede con la formazione del complesso **V** nel quale la seconda molecola d'acqua è stata addizionata. Nello step finale, la formazione del benzilfenilchetone può o meno essere assistita da una terza molecola d'acqua, il suo ruolo sarebbe quello di catturare un protone legato ad un atomo di O e contemporaneamente cederne

uno all'altro atomo di O, facilitando così l'uscita di due molecole d'acqua e quindi la formazione del prodotto. Questo ultimo step può realizzarsi senza l'intervento di una molecola d'acqua aggiuntiva, anche se la barriera calcolata è comunque più elevata.

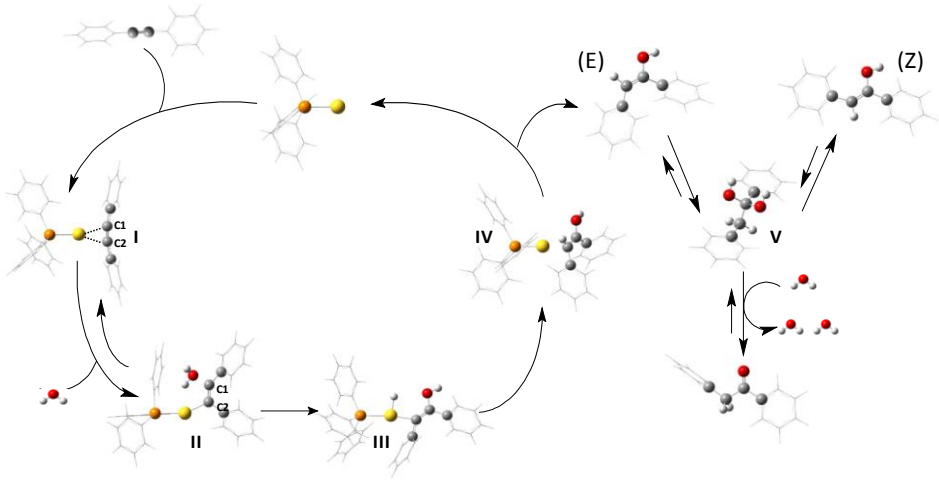

Schema I: Meccanismo di reazione per l'idratazione del difenilacetilene.

Bibliografia

1. Dewar, J. A review of the pi-complex theory. *Bull. Soc. Chim. Fr.* **18**, C71-C79(1951).
2. Chatt, J. & Duncanson, L. Olefin co-ordination compounds. 3. Infra-red spectra and structure-attempted preparation of acetylene complexes. *J. Chem. Soc.* 2939-2947(1953).
3. Mingos, D.M.P. *Comprehensive Organometallic Chemistry*. **3**, 1-88(G. Wilkinson, F. G. A. Stone, E. W. Abel: Pargamon, Oxford, 1982).
4. Fürstner, A. & Davies, P. Catalytic Carbophilic Activation: Catalysis by Platinum and Gold pi Acids. *Angewandte Chemie International Edition* **46**, 3410-3449(2007).
5. Drenth, W. & Hogeveen, H.*Recl. Trav. Chim. Pays-Bas* **79**, 1002(1960).
6. Allen, A.D. et al. Substituent effects on the acid hydration of acetylenes. *The Journal of Organic Chemistry* **47**, 775-779(1982).
7. Thomas, R.J., Campbell, K.N. & Hennion, G.F. Catalytic Hydration of Alkylacetylenes1. *Journal of the American Chemical Society* **60**, 718-720(1938).
8. Olah, G. & Meidar, D. Heterogenous Catalysis by Solid Superacids; 101. Mercury Impregnated Nafion-H Perfluorinated Resinsulfonic Acid Catalyzed Hydration of Alkynes. 671-672(1978).
9. Rosenfeld, D.C. et al. Hydroamination and Hydroalkoxylation Catalyzed by Triflic Acid. Parallels to Reactions Initiated with Metal Triflates. *Organic Letters* **8**, 4179-4182(2006).
10. Freeman, F. Possible criteria for distinguishing between cyclic and acyclic activated complexes and among cyclic activated complexes in addition reactions. *Chemical Reviews* **75**, 439-490(1975).
11. Olah, G.A. & Clifford, P.R. Organometallic chemistry. II. Direct mercuration of olefins to stable mercurinium ions. *Journal of the American Chemical Society* **93**, 2320-2321(1971).
12. Tokunaga, M. & Wakatsuki, Y. The First Anti-Markovnikov Hydration of Terminal Alkynes: Formation of Aldehydes Catalyzed by a Ruthenium(II)/Phosphane Mixture. *Angewandte Chemie International Edition* **37**, 2867-2869(1998).
13. Suzuki, T., Tokunaga, M. & Wakatsuki, Y. Ruthenium Complex-Catalyzed anti-Markovnikov Hydration of Terminal Alkynes. *Organic Letters* **3**, 735-737(2001).
14. Tokunaga, M. et al. Ruthenium-Catalyzed Hydration of 1-Alkynes to Give Aldehydes: Insight into anti-Markovnikov Regiochemistry. *Journal of the American Chemical Society* **123**, 11917-11924(2001).
15. Grotjahn, D.B., Incarvito, C.D. & Rheingold, A.L. Combined Effects of Metal and Ligand Capable of Accepting a Proton or Hydrogen Bond Catalyze Anti-Markovnikov Hydration of Terminal Alkynes13. *Angewandte Chemie International Edition* **40**, 3884-3887(2001).
16. Halpern, J., James, B.R. & Kemp, A.L.W. CATALYSIS OF THE HYDRATION OF ACETYLENIC COMPOUNDS BY RUTHENIUM(III) CHLORIDE. *Journal of the American Chemical Society* **83**, 4097-4098(1961).
17. Halpern, J., James, B.R. & Kemp, A.L.W. Formation and Properties of Some Chlorocarbonyl Complexes of Ruthenium(II) and Ruthenium(III)1. *Journal of the American Chemical Society* **88**, 5142-5147(1966).
18. Khan, M.M.T., Halligudi, S.B. & Shukla, S. Hydration of acetylene to acetaldehyde using K[RuIII(EDTA-H)Cl]2H2O. *Journal of Molecular Catalysis* **58**, 299-305(1990).
19. James, B.R. & Rempel, G.L. Hydration of acetylenes catalyzed by rhodium(III) chloride complexes. *Journal of the American Chemical Society* **91**, 863-865(1969).
20. Blum, J., Huminer, H. & Alper, H. Alkyne hydration promoted by RhCl3and quaternary ammonium salts. *Journal of Molecular Catalysis* **75**, 153-160(1992).
21. Hiscox, W. & Jennings, P.W. Catalytic hydration of alkynes with Zeise's dimer. *Organometallics* **9**, 1997-1999(1990).

22. Baidossi, W., Lahav, M. & Blum, J. Hydration of Alkynes by a PtCl4−CO Catalyst. *The Journal of Organic Chemistry* **62**, 669-672(1997).
23. Francisco, L.W., Moreno, D.A. & Atwood, J.D. Synthesis, Characterization, and Reaction Chemistry of PtCl2[P(m-C6H4SO3Na)3]2, an Alkyne Hydration Catalyst. *Organometallics* **20**, 4237-4245(2001).
24. Fukuda, Y. & Utimoto, K. Effective transformation of unactivated alkynes into ketones or acetals with a gold(III) catalyst. *The Journal of Organic Chemistry* **56**, 3729-3731(1991).
25. Fukuda, Y. & Utimoto, K. Efficient Transformation of Methyl Propargyl Ethers into α,β-Unsaturated Ketones. *Bull. Chem. Soc. Jpn* **64**, 2013-2015(1991).
26. Meier, I.K. & Marsella, J.A. Hydration of acetylenic compounds without using mercury. *Journal of Molecular Catalysis* **78**, 31-42(1993).
27. Imi, K., Imai, K. & Utimoto, K. Regioselective hydration of alkynones by palladium catalysis. *Tetrahedron Letters* **28**, 3127-3130(1987).
28. Yao, X. & Li, C. Water-Triggered and Gold(I)-Catalyzed Cascade Addition/Cyclization of Terminal Alkynes with ortho-Alkynylaryl Aldehyde. *Organic Letters* **8**, 1953-1955(2006).
29. Arcadi, A. et al. Gold catalysis in the reactions of 1,3-dicarbonyls with nucleophiles. *Green Chem.* **5**, 64-67(2003).
30. Teles, J.H., Brode, S. & Chabanas, M. Cationic Gold(I) Complexes: Highly Efficient Catalysts for the Addition of Alcohols to Alkynes. *Angewandte Chemie International Edition* **37**, 1415-1418(1998).
31. Fukuda, Y., Utimoto, K. & Nozaki, H. Preparation of 2,3,4,5-tetrahydropyridines from 5-alkynylamines under the catalytic action of Au(III). *Heterocycles* **25**, 297-300(1987).
32. Asao, N. et al. AuCl3-Catalyzed Benzannulation: Synthesis of Naphthyl Ketone Derivatives from o-Alkynylbenzaldehydes with Alkynes. *Journal of the American Chemical Society* **124**, 12650-12651(2002).
33. Hashmi, A.S.K., Frost, T.M. & Bats, J.W. Highly Selective Gold-Catalyzed Arene Synthesis. *Journal of the American Chemical Society* **122**, 11553-11554(2000).
34. Hashmi, A.S.K. et al. A New Gold-Catalyzed C-C Bond Formation13. *Angewandte Chemie International Edition* **39**, 2285-2288(2000).
35. Kennedy-Smith, J.J., Staben, S.T. & Toste, F.D. Gold(I)-Catalyzed Conia-Ene Reaction of β-Ketoesters with Alkynes. *Journal of the American Chemical Society* **126**, 4526-4527(2004).
36. Staben, S.T., Kennedy-Smith, J.J. & Toste, F.D. Gold(I)-Catalyzed 5-endo-dig Carbocyclization of Acetylenic Dicarbonyl Compounds13. *Angewandte Chemie International Edition* **43**, 5350-5352(2004).
37. Reetz, M.T. & Sommer, K. Gold-Catalyzed Hydroarylation of Alkynes. *European Journal of Organic Chemistry* **2003**, 3485-3496(2003).
38. Nevado, C. & Echavarren, A.M. Intramolecular Hydroarylation of Alkynes Catalyzed by Platinum or Gold: Mechanism and endo Selectivity. *Chemistry - A European Journal* **11**, 3155-3164(2005).
39. Ferrer, C. & Echavarren, A.M. Gold-Catalyzed Intramolecular Reaction of Indoles with Alkynes: Facile Formation of Eight-Membered Rings and an Unexpected Allenylation13. *Angewandte Chemie International Edition* **45**, 1105-1109(2006).
40. Antoniotti, S. et al. Highly Efficient Access to Strained Bicyclic Ketals via Gold-Catalyzed Cycloisomerization of Bis-homopropargylic Diols. *Journal of the American Chemical Society* **127**, 9976-9977(2005).
41. Buzas, A. & Gagosz, F. Gold(I)-Catalyzed Formation of 4-Alkylidene-1,3-dioxolan-2-ones from Propargylic tert-Butyl Carbonates. *Organic Letters* **8**, 515-518(2006).

42. Mizushima, E. et al. Highly Efficient Au(I)-Catalyzed Hydration of Alkynes13. *Angewandte Chemie International Edition* **41**, 4563-4565(2002).
43. Leyva, A. & Corma, A. Isolable Gold(I) Complexes Having One Low-Coordinating Ligand as Catalysts for the Selective Hydration of Substituted Alkynes at Room Temperature without Acidic Promoters. *The Journal of Organic Chemistry* **74**, 2067-2074(2009).

Appendice

Pubblicazione I

Interaction of CO with Pd$_{Au}$(111) and Pd$_{Au}$(100) Bimetallic Surfaces: A Theoretical Cluster Model Study

Gloria Mazzone, Ivan Rivalta, Nino Russo, Emilia Sicilia

J. Phys. Chem. C **2008**, 112, 6073-6081

J. Phys. Chem. C **2008,** *112,* 6073−6081

Interaction of CO with PdAu(111) and PdAu(100) Bimetallic Surfaces: A Theoretical Cluster Model Study

Gloria Mazzone, Ivan Rivalta, Nino Russo, and Emilia Sicilia*

Dipartimento di Chimica and Centro di Calcolo ad Alte Prestazioni per Elaborazioni Parallele e Distribuite−Centro d'Eccellenza MURST, Università della Calabria, I-87030 Arcavacata di Rende, Italy

Received: November 15, 2007; In Final Form: January 10, 2008

Structural parameters, binding energies, and bonding mechanism of CO molecules on PdAu(111) and PdAu(100) surface alloys have been investigated at the density functional level by employing a cluster model approach. Cluster models have been constructed to represent second-neighbor Pd pairs on both the exposed gold surfaces, given that special ensembles are able to confine reactants in a small region of bimetallic catalysts. Analysis of the cluster size dependence of the chemisorption properties has been carried out together with the study of the influence of exchange correlation functional and basis set quality. An accurate description of the bonding mechanism of CO on top of Pd monomers surrounded by gold atoms has been achieved by an atom-projected description of the surface bond. The remarkable agreement of computed results with available experimental information and previous periodic supercell calculations clearly indicates that the adopted cluster models are suitable for chemisorption studies on PdAu surface alloys.

1. Introduction

The selectivity and efficiency of catalytic processes can be largely enhanced by use of bimetallic instead of monometallic catalysts.[1−4] The concepts of "ensemble" (or geometric)[5,6] and "ligand" (or electronic)[7] effects are commonly used to rationalize this superior activity of bimetallic systems in electrochemistry and heterogeneous catalysis. The former concept refers to the fact that the addition of a second metal may block certain sites, reducing or eliminating the formation of an inhibiting species or an important intermediate. Thus, specific groupings of surface atoms are required to serve as active sites.[1,5,6] The latter effect refers to the formation of heteronuclear metal−metal bonds in binary alloys that involves a modification of the electronic structure, leading to a different (and, it is hoped, better) overall catalytic activity with respect to that of either of the constituent metals. Orbital rehybridization of one or both of the metals and/or charge transfer between the metals can substantially modify the catalytic performance by means of ligand effect.[1,7]

Among bimetallic systems, Pd−Au has received particular attention due to its use in a number of catalytic reactions (e.g., CO oxidation, cyclotrimerization of acetylene, synthesis of vinyl acetate monomer, selective oxidation of alcohols to aldehydes)[8−11] and applications (e.g., hydrogen fuel cells and pollution control systems).[12−13] A deeper understanding of the underlying physical reasons that determine the catalytic performance of Pd−Au alloys can thus be very beneficial for rational improvement of these catalysts.

The utility of single-crystal studies for understanding the role played by ensemble and ligand effects in bimetallic catalysts has been demonstrated[14] because they are simple enough for a systematic study of the relationship between the microscopic structure of the catalyst and its activity. At the same time, a broad variety of possible compositions and structures of increasing complexity can be examined. Therefore, well-defined bimetallic Pd−Au surfaces have been the subject of several investigations.[15−19]

Goodman and co-workers,[5] in their investigations of the promotional role of gold in a palladium−gold alloy catalyst used for the acetoxylation of ethylene to yield vinyl acetate (VA), have invoked ensemble effects to explain the significant enhancement of the VA formation rate. The ligand and eventually strain effects have been considered minimal and a pair of noncontiguous Pd monomer sites has been supposed to be the critical ensemble for the VA formation as inferred from the difference in the VA formation rates on Pd/Au(100) and Pd/Au(111) surfaces.

Surface composition is, therefore, the key to understanding the catalytic properties of bimetallic surface alloys, especially for the catalytic systems for which the efficiency and selectivity are dominated by the ensemble effect. In fact, the surface segregation in Pd−noble metal alloys is well-known by both experimental evidence for Pd−Cu,[21] Pd−Ag,[22] and Pd−Au[23,24] and theoretical periodic calculations.[25] Since the morphology of Pd−Au strongly depends on the experimental preparation in terms of deposition technique and annealing history, several Pd−Au surface compositions have been reported so far.[5,6,9,26−28]

The use of the in situ STM technique developed by Behm and co-workers[6] has allowed the determination of critical ensembles for adsorption of small molecules. Application of this technique has shown that the critical ensemble for CO adsorption on PdAu(111) surface-alloy electrodes is a Pd monomer.

The adsorption of small molecules, such as CO, is commonly used to obtain information concerning the properties of single-metal and alloy surfaces, including composition and electronic structure, by both experimental and theoretical studies.

The contribution given by first-principles calculations to better microscopic understanding of the catalytic activity of bimetallic systems has been recently reviewed by Gross,[29] showing how theoretical calculations can supply additional information for the rational design of robust bimetallic catalysts.[30−32]

* Corresponding author: e-mail siciliae@unical.it.

10.1021/jp710915g CCC: $40.75
Published on Web 03/20/2008

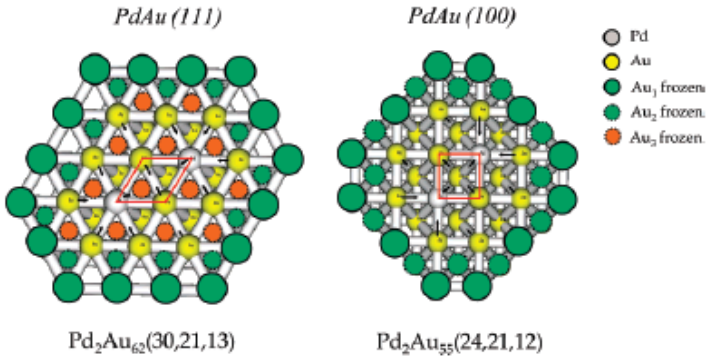

Figure 1. Schematic representation of Pd_2Au_n clusters used in this work to model the second-neighbor Pd pair ensemble on PdAu(100) and PdAu(111) surface alloys. From the top view, the positions of the frozen Au_3 atoms are not directly visible in the fcc(100) surface cluster model due to its ABAB packing, but they correspond to the unfrozen atoms in the first layer. Changes in the atomic positions due to the local relaxation are indicated by arrows. Unit cells of the Au(100) and Au(111) pure surfaces are depicted in red.

In the framework of density functional (DF) calculations, the periodic supercell approach using plane-waves has already been applied to PdAu surface alloys for the study of the surface segregation phenomenon and of the atomic configuration of Pd atoms in PdAu(111) bimetallic surfaces.[25,33] On the other hand, the cluster model approach has provided information about several catalytic systems[34] and has proved to be a useful tool for surface science studies. For the study of chemisorption properties of CO on low-index surfaces, cluster model calculations can be compared with periodic calculations[35] and can be used to focus on the chemical bonding between the surface atoms and the adsorbed molecule.[36,37] Nevertheless, few examples of the application of the cluster model approach in bimetallic systems can be found in literature, such as for PtRe,[38] PdCu,[39,40] and PdSn, RhSn, and RhZn[41] catalysts.

A DF cluster model approach has been applied here to the study of the adsorption properties of CO on the PdAu(111) and PdAu(100) surface alloys. In particular, cluster models have been built up to represent the ensemble with a second-neighbor Pd pair on both the exposed gold surfaces, given that ensembles with second-neighbor Pd appear to be seldom separated from isolated monomers.[42]

The calculated energetic, electronic, and vibrational properties will be compared with the recent periodic calculations for PdAu(111)[33] and with the available experimental data.

2. Methodology and Computational Details

In the cluster approach the adsorption site is modeled by a finite number of metal atoms whose arrangement is chosen to properly reproduce those contributions to the adsorbate–substrate interaction that are due to local changes in the substrate electronic structure. Thus, it is reasonable to expect that cluster models are able to capture the essential features of the chemisorption bond and to predict local properties such as adsorption geometries and vibrational frequencies for very low coverages.

In order to model the second-neighbor Pd pair ensemble on PdAu(100) and PdAu(111) surfaces, we have built up the clusters starting with a group of two noncontiguous Pd atoms and two Au atoms bonded to both of them. Then, the first neighbors of those four atoms have been added both in the first and in the second layer. In this way, the active sites are represented by Pd_2Au_{19} and Pd_2Au_{20} cluster models, denoted as $Pd_2Au_{19}(12,9)$ and $Pd_2Au_{20}(14,8)$ to indicate the number of atoms in each cluster layer for Au(100) and Au(111) surfaces, respectively.

Initially, the atomic positions have been assigned as in bulk gold, with the experimental lattice parameter of 4.08 Å, yielding an Au–Au (initially equal to Pd–Au) distance of 2.885 Å.

With these models a good description of the coordination of the two noncontiguous Pd monomers involved in the chemisorption sites for both low-index gold surfaces is obtained.

In order to study the influence of the cluster size on the geometry and energetics of adsorbed CO, we have used the strategies that will be illustrated below.

First, the size of the $Pd_2Au_{19}(12,9)$ model has been increased by adding a third layer in such a way to obtain for the PdAu(100) surface the $Pd_2Au_{23}(12,9,4)$ cluster, including in the third layer four gold atoms that lie in the positions corresponding to those of the four central atoms in the first layer, because of the ABAB packing of the fcc(100) surface. For the less open fcc(111) gold surface with ABCABC packing, eight atoms have been added in the third layer to the $Pd_2Au_{20}(14,8)$ model in correspondence to the atomic positions defining the fcc-hollow adsorption sites, giving rise to the larger $Pd_2Au_{28}(14,8,8)$ cluster.

Starting from these three-layer models, two more extended clusters have been constructed by completing the set of the first neighbor atoms for all the peripheral atoms of the first and the second layer. The resulting $Pd_2Au_{55}(24,21,12)$ and $Pd_2Au_{62}(30,21,13)$ large models for the Pd/Au(100) and the Pd/Au(111) systems, respectively, would prevent any indirect insaturation effect for the two noncontiguous Pd and the two Au atoms of the active sites. Moreover, these large models have been used to take into account local relaxation effects due to the substitution of two noncontiguous surface gold atoms with two Pd monomers. The positions of the atoms defining the $Pd_2Au_{19}(12,9)$ and $Pd_2Au_{20}(14,8)$ models have been fully optimized; in fact, within the $Pd_2Au_{55}(24,21,12)$ and $Pd_2Au_{62}(30,21,13)$ clusters the positions of the remaining atoms are frozen (Figure 1). Finally, the $Pd_2Au_{19}(12,9)$, $Pd_2Au_{23}(12,9,4)$ and the $Pd_2Au_{20}(14,8)$, $Pd_2Au_{28}(14,8,8)$ models have been pulled out from the corresponding partially optimized Pd_2Au_{55} and Pd_2Au_{62} clusters.

In summary, the relaxed Pd_2Au_{19}, Pd_2Au_{23}, and Pd_2Au_{55} models for the Pd/Au(100) surface and Pd_2Au_{20}, Pd_2Au_{28}, and Pd_2Au_{62} models for the Pd/Au(111) surface have been employed to study the chemisorption properties of CO.

In order to explore the variation of the electronic structure of gold surfaces due to the substitution of two noncontiguous gold atoms by two Pd monomers on Au(111) and Au(100) clean surfaces, six Au_{n+2} cluster models corresponding to the Pd_2Au_n models described above have been used. As for the bimetallic clusters, the largest Au_{n+2} cluster models have been locally relaxed, starting from the bulk gold atomic positions, and then the smaller Au_{n+2} models have been pulled out from them.

The calculations have been performed with the Turbomole package (version 5.8)[43] at the DF level, by use of the BP86 functional[44,45] within the resolution of the identity approximation for computing the electronic Coulomb interaction (RI-J). This approach expands the molecular electron density in a set of atom-centered auxiliary functions, improving the computational efficiency of large-scale calculations.[46,47]

The Stuttgart effective core potential[48] have been used to model the scalar relativistic effects, replacing the 28 and 60 core electrons of palladium and gold atoms, respectively. The valence electrons, 18 for Pd and 19 for Au, have been explicitly considered in the standard Turbomole SVP basis set.[49] For CO, the all-electron SVP basis set of Ahlrichs and co-workers,[49] featuring a split valence basis set with polarization functions, has been employed. The standard Turbomole SVP auxiliary basis set has been used for all the atoms.[47]

No symmetry constraints have been imposed for the relaxation of the positions of C and O atoms in the adsorption study of one and two CO molecules on the Pd_2Au_n cluster models.

For selected CO/Pd_2Au_{19}(12,9) and CO/Pd_2Au_{28}(14,8,8) cluster models, the influence of the exchange−correlation (xc) functional and basis set effect on vibrational frequencies, geometries, and binding energies of the adsorbate have also been investigated. Becke's three-parameter hybrid functional[50] combined with the Lee, Yang, and Parr (LYP)[51] correlation functional, the standard Turbomole TZVP basis set,[52] and the corresponding auxiliary basis set[47] for C and O atoms have been employed for this purpose. From now on, for the sake of clarity, the four levels of theory used in this work will be indicated as BP86/SVP and BP86/TZVP for the pure (i.e., nonhybrid) xc functional and B3LYP/SVP and B3LYP/TZVP for the hybrid B3LYP functional.

It should be emphasized that the Pd_2Au_{19}(12,9) and Pd_2Au_{28}(14,8,8) cluster models used to calculate the chemisorption properties of CO at the B3LYP level have been obtained by partially optimizing the larger Pd_2Au_{55} and Pd_2Au_{62} models at the same level of theory, following the same strategy described above.

All the C−O stretching frequencies reported in this work have been corrected by use of scaling factors, calculated with respect to the C−O vibrational frequency for the isolated CO molecule in the gas phase obtained at the corresponding level of theory. Scaling factors applied to the C−O frequencies in the chemisorbed systems are 1.0084 (BP86/SVP), 1.0197 (BP86/TZVP), 0.9679 (B3LYP/SVP), and 0.9792 (B3LYP/TZVP).

The total energies calculated after geometry optimizations have been corrected for basis-set superposition error (BSSE) by use of Boys−Bernardi counterpoise calculations[53] for all adsorbate/cluster models. This correction is 3.3 kcal/mol per bond for all the cluster models if the SVP basis set is used, whereas is only 1.0 kcal/mol when the triple-ζ quality basis set is used.

Atomic-projected density of states (DOS) has been calculated (as implemented in Turbomole) by broadening the discrete energy levels of each cluster model with Gaussians having width of 0.003 au and superimposing them.

3. Results and Discussion

3.1. Cluster Models and Local Relaxation Effects. The local relaxation effects in the vicinity of the Pd monomers on PdAu(111) and PdAu(100) clean surfaces have been studied by use of suitably large clusters in order to obtain more realistic models for the chemisorption study of CO molecules.

Locally relaxed structures obtained for the pure gold Au_{57} and Au_{64} cluster models and the bimetallic Pd_2Au_{55} and Pd_2Au_{62} large clusters were compared by use of the BP86 functional, and significant rearrangements have been observed in the active sites as a consequence of the substitution of two noncontiguous surface gold atoms with two Pd monomers. In the surface plane, the neighboring gold atoms move toward the palladium monomers (see Figure 1), whereas on the axis perpendicular to the surface, the Pd atoms move inward (by 0.16−0.20 Å) with respect to the surface gold layer.

As a result of these local relaxations, the Pd−Au distances in the active sites become shorter with respect to the Au−Au distances in the pure gold surfaces. In particular, Pd−Au distances are equal to 2.840 and 2.861 Å for the PdAu(100) and (111) surfaces, respectively. These values differ by 0.017−0.026 Å from the Au−Au distances found with the locally relaxed pure gold clusters. That is an indication of a stronger Pd−Au bond with respect to the Au−Au bond, which is in agreement with the outcome of the study carried out on Pd monomer formation on an Au(111) surface by the slab supercell approach.[33] Moreover, in line with the periodic calculations, weak hybridization between palladium and gold d-orbitals is deducible by the atomic-projected density of states (DOS) plots. In Figure 2, atomic-projected DOS plots of the gold and palladium d-bands, calculated with the BP86 xc functional, for the largest Pd_2Au_{55}(24,21,12) and Pd_2Au_{62}(30,21,13) clusters and the selected Pd_2Au_{19}(12,9) and Pd_2Au_{28}(14,8,8) models are depicted.

When the projected density of d-states for the Pd atom and the nearest gold neighbor atoms is plotted, a wide d-band for gold atoms and a narrow d-band well below the Fermi level for the Pd atom are visible for all cluster calculations.

The main peak of the Pd 4d-band lying at 1 eV below the Fermi level is visible in Figure 2a, whereas in panel b the 5d-band of gold is located between −6.5 and −1.0 eV. These plots, obtained by use of the Pd_2Au_{62}(30,21,13) cluster model, are nicely very close to the results found when a slab supercell was used to represent Pd monomers surrounded by Au atoms in the PdAu(111) surface alloy.[33] It should be noted that in both these DFT calculations a pure xc functional has been used.

When plots obtained for the largest cluster and for the smaller Pd_2Au_{28}(14,8,8) model are compared, both the Pd and Au d-bands appear to be compressed toward the Fermi level in the latter compared to the former. This narrowing of both the metal d-bands, however, does not really affect the overall description of the heterometallic bonds. In fact, for both models (Figure 2a,b) a sharp peak is visible at ∼1.0 eV below the Fermi level, whose low dispersion can be attributed to the strong localization of Pd 4d-electrons, suggesting that the Pd monomer(s) surrounded by gold atoms acquire such atomistic properties. Moreover, the broad 5d-band related to the first-neighbor gold atoms preserves almost the same shape in the two cases even if it shows a different width.

The gold 5d-bands of the Pd_2Au_{28}(14,8,8) and the corresponding Au_{30}(14,8,8) cluster models are depicted in Figure 2b.

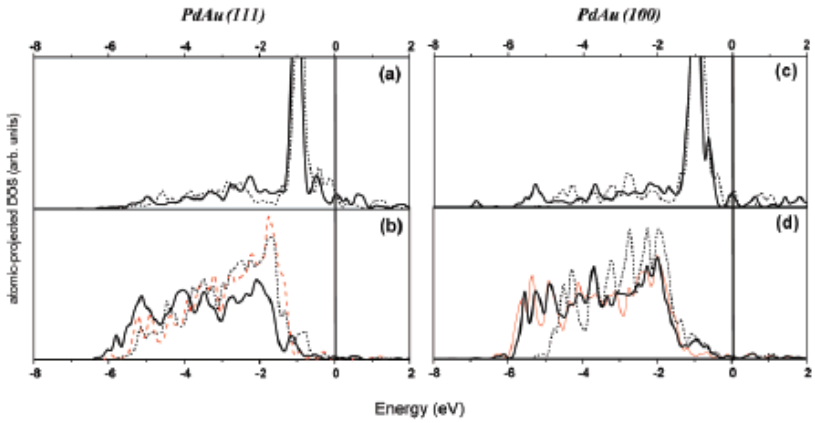

Figure 2. BP86 atomic-projected density of d-states (DOS) of Pd monomers (a, c) and adjacent Au atoms (b, d), calculated for PdAu(111) (a, b) and PdAu(100) (c, d) surface alloys. The largest Pd_2Au_{62}(30,21,13) and Pd_2Au_{55}(24,21,12) cluster models (bold black lines) are compared with selected Pd_2Au_{28}(14,8,8) and Pd_2Au_{19}(12,9) smaller clusters (dotted black lines). Atomic-projected DOS of gold d-states of the clean Au(111) and Au(100) surfaces are calculated for the exemplifying cases of Au_{30} (red dashed line in panel b) and Au_{57} (red thin line in panel d) cluster models. Zero energy is at the Fermi level.

The almost undisturbed Au d-band in the PdAu(111) surface alloy with respect to the pure gold surface (see red dotted line and black dotted line in Figure 2b) and the small overlapping of Pd and Au d-bands in the bimetallic system suggest that a weak orbital hybridization is involved in the Pd−Au bonds.

The projected density of d-states for palladium and gold atoms obtained at the BP86 level in the case of the PdAu(100) surface alloy are reported in Figure 2c,d). No evident differences exist between these plots and what is described above for the PdAu(111) binary system.

The atomic-projected DOS of gold d-band for the PdAu(100) surface alloy (Figure 2d), remains almost unaffected in comparison with the clean Au(100) surface, as in the (111) low-index surfaces.

For simplicity, only the results for the pure gold Au_{57}(24,21,12) and Au_{30}(14,8,8) clusters [modeling the Au(100) and Au(111) gold surfaces, respectively] are reported in Figure 2, but the same indications have been obtained for all remaining Au_{n+2} cluster models.

Comparison between the pictures obtained with the largest Pd_2Au_{55}(24,21,12) and the smallest Pd_2Au_{19}(12,9) cluster models of the PdAu(100) system (Figure 2d) shows a stronger narrowing of the d-bands with respect to the results achieved with the PdAu(111) models (Figure 2b). This comes as no surprise since the description of the electronic properties of the metal surface in the cluster approach is strongly dependent on the cluster size, which is different in these two cases.

3.2. Adsorption of CO Molecules. In order to study the influence of the cluster size on the geometry, vibrational frequencies, and energetics of CO molecules adsorbed on the Pd noncontiguous monomer pairs, a set of six cluster models, as described in the previous section, has been used. In these models the cluster atoms have been kept frozen at their optimized positions, whereas the C and O positions have been fully optimized for all the adsorption sites within the active site. As expected, most of the attempts to find local minima related to the adsorption sites different from those on top of Pd monomers were unsuccessful. This is due to the difference between the chemisorption properties of CO on Pd and Au surfaces, which can be simply explained by the d-band model of Hammer and Nørskov.[54−56] Indeed, the calculated chemisorption energies for CO adsorption atop a metal atom at the Pd(111) and Au(111) metal surfaces are 30.0 and 0.9 kcal/mol, respectively,[57] and then the preferred adsorption site for an ensemble constituted by a Pd monomer surrounded by gold atoms is expected to be the Pd on-top site.

Initially, we started studying the adsorption of one molecule of CO on the six Pd_2Au_n cluster models representing the PdAu(111) and PdAu(100) systems. Energetic, structural, and vibrational properties calculated at the BP86/SVP level of theory for one CO molecule adsorbed on top of one of the two Pd monomers, as a function of the cluster size, are reported in Table 1.

Both experimental data and theoretical results from periodic supercell calculations for adsorption of CO on PdAu(111) surface alloy are available for comparison with our cluster models. In a very recent work, Li et al.,[28] using the Redhead equation (assuming a desorption pre-exponential factor of 1×10^{13} s^{-1}), calculated the desorption activation energy for the Pd atop site on the Au/Pd(111) alloy to be between 18.2 and 20.5 kcal/mol. This result is in good agreement with the binding energies obtained with the Pd_2Au_{28} and the Pd_2Au_{62} cluster models. The corresponding infrared feature found in the RAIRS experiment lies between 2086 and 2089 cm^{-1}, which is comparable to the vibrational frequencies obtained with the Pd_2Au_{28} and Pd_2Au_{62} cluster models (2068 and 2073 cm^{-1}, respectively). In contrast to the work of Li et al.,[28] who deposited a thin film of gold onto a Pd(111) single crystal and heated it to various temperatures, PdAu surface alloys have been generated by other strategies.[5,26] The calculated vibrational and energetic properties obtained with the converged three-layer Pd_2Au_{28} and Pd_2Au_{62} cluster models are also in good agreement with the experimental results of Goodman and co-workers[5,26] reported in these two works.

The only available experimental value of the Pd−CO stretching frequency for PdAu(111) is given by Gleich et al.,[58] who assigned the 371 and 2080 cm^{-1} vibrational peaks of the HREEL spectra to the Pd−C and C−O stretching frequencies, respectively, for CO adsorbed on Pd atoms adjacent to one or more Au surface atoms. As well as for the other calculated properties, these experimental values of the Pd−CO stretching frequency are close to the calculated values obtained by use of

TABLE 1: BP86/SVP Results for Adsorption of One CO Molecule on PdAu Cluster Models[a]

cluster model	BE, kcal/mol	d(Pd−C), Å	ω(Pd−CO), cm^{-1}	d(C−O), Å	ω^{corr}(C−O), cm^{-1}
			hkl (111)		
Pd_2Au_{30}(14,8)	33.6	1.883	454	1.155	2070
Pd_2Au_{39}(14,8,8)	20.0	1.931	383	1.153	2073
Pd_2Au_{62}(30,21,13)	19.3	1.937	378	1.154	2068
exp[b−d]	18.2−20.5[b]		371[d]		2086−2089,[b] 2088,[c,e] 2080[d]
theory[f]	25.6−27.0				2043−2056
			hkl (100)		
Pd_2Au_{19}(12,9)	26.2	1.916	410	1.155	2069
Pd_2Au_{23}(12,9,4)	24.4	1.924	397	1.155	2068
Pd_2Au_{55}(24,21,12)	25.5	1.922	400	1.154	2065
exp[c]					2090−2104

[a] Binding energies (BE) are BSSE-corrected. Scaled C−O frequencies are indicated as ω^{corr}. [b] Reference 28. [c] Reference 5. [d] Reference 57. [e] Reference 59. [f] Reference 33.

the Pd_2Au_{28} and Pd_2Au_{62} cluster models (378 and 383 cm^{-1}, respectively).

The DFT results obtained very recently by Yuan et al.[33] using the slab supercell approach reveal the favorable existence of second-neighbor ensembles. For the adsorption of CO on top of Pd monomers and noncontiguous dimers and trimers, the calculated C−O stretching frequencies show a deviation of 40 cm^{-1} compared to the experimental value, which is twice the deviation obtained with our cluster models. The corresponding adsorption energies for CO adsorbed on the atop sites are 25.6−27.0 kcal/mol at the GGA-PW91 level of theory, which differs by ∼7 kcal/mol from experimental data and our cluster model results. As suggested by the authors, the overestimation of the adsorption energies at the GGA-PW91 level can be corrected by use of the RPBE functional, which is predicted to reduce the values by just 5−7 kcal/ mol.

As already mentioned above, any attempt to reach local minima for bridge or hpc and fcc hollow sites was unsuccessful in accordance with the preferred site found for CO adsorbed on Pd monomers and noncontiguous dimers and trimers by periodic calculations, which is always a Pd atop site.[33]

In view of the converged results reached with the Pd_2Au_{28} and Pd_2Au_{62} cluster models and the agreement with the available experimental data and theoretical results from periodic supercell calculations, one can conclude that the chemical properties of the CO molecule chemisorbed on a Pd monomer in the Pd/Au(111) surface alloy cannot be properly achieved by using the bilayer Pd_2Au_{30}(14,8) cluster model.

On the other hand, for the adsorption of a CO molecule on the more open PdAu(100) surface, we have found a nice convergence of the binding energies using all the cluster models built up for this system (see Table 1).

No local minima have been found for CO adsorbed on bridge Pd−Au sites on the cluster models used to represent the PdAu(100) system, whereas we have found a stable CO chemisorption state on the 4-fold hollow site, in contrast with what has been found for the 3-fold hollow sites in the PdAu(111) surface alloy. This is probably due to the fact that both the Pd monomers of the second-neighbor Pd pair are included in the 4-fold hollow site on the PdAu(100) surface, whereas on the PdAu(111) surface the 3-fold hpc and fcc hollow sites include only one Pd monomer. However, the calculated binding energy for CO adsorbed on the 4-fold hollow site on Pd_2Au_{55}(24,21,12) cluster, at BP86/SVP level, is only 12.2 kcal/mol and the perpendicular distance between the C atom and the surface plane is 1.150 Å, while the d(Pd−C) is 2.428 Å. The C−O distance is 1.182 Å and the corresponding stretching frequency (1788 cm^{-1}) is in the classical region of CO adsorbed on a multifold adsorption site.

As for the CO adsorption on top of a Pd monomer site, all the Pd_2Au_n cluster models built up for the PdAu(100) system give converged results for the CO chemisorption properties on the 4-fold hollow adsorption site. The chemisorption binding energies of CO on the hollow site resulting from all the PdAu(100) cluster models are always less than half the chemisorption energies calculated for the atop adsorption site.

Since no multifold chemisorbed states have been found on the PdAu(111) cluster models and only one less-preferred (4-fold) chemisorbed state has been found on the PdAu(100) cluster models, we will focus for the rest of this paper on the adsorption of CO on top of the Pd monomers.

The results for the adsorption of two CO molecules on top of two noncontiguous Pd monomers by use of our six cluster models are shown in Table 2.

Comparing these results with the chemisorption of one CO molecule, we practically look at two situations with two different CO coverages, and then a rough evaluation of the lateral interaction mediated by the surface can be achieved by calculating the differences between the binding energies per bond in the two cases.

As a first result, it is evident that the same considerations made for the adsorption of one CO molecule regarding the convergence properties of the used cluster models are still valid here and, in general, very small changes have been observed for all the geometrical and vibrational parameters when going from the adsorption of one to two CO molecules.

Since the calculated lateral interactions are, in general, less than 2 kcal/mol per bond (see Table 2) and the effect on the vibrational and geometrical parameters is negligible, all the calculated chemisorption properties of CO on top of Pd monomer are almost unaffected by the presence of other CO molecules on top of a second-neighbor Pd monomer. These results are in line with the experimental observation of very small dipole−dipole coupling between CO molecules on the PdAu surface alloys due to the relatively large intermolecular distance at low coverage regimes (<0.5 ML) and to the improbable adsorption on Au atoms surrounding Pd monomers at higher CO coverages.[59]

3.3. Analysis of the Chemisorption Bond. The Blyholder model[60] is the simplest and most commonly accepted picture for understanding the chemisorption mechanism of CO on metal surfaces. In the spirit of the frontier orbital theory, in that only the highest occupied and lowest unoccupied molecular orbitals (HOMO and LUMO) of the adsorbed molecule are involved in the chemisorption bonding, this model considers only the 5σ donation and the 2π^* back-donation contributions to the CO−metal interaction.

TABLE 2: BP86/SVP Results for the Adsorption of Two CO Molecules on PdAu Cluster Models[a]

cluster model	BE, kcal mol^{-1} (CO molecule)$^{-1}$	ΔBE	d(Pd−C), Å	ω(Pd−CO)$_{in}$, cm^{-1}	ω(Pd−CO)$_{out}$, cm^{-1}	d(C−O), Å	ω^{corr} (C−O)$_{in}$, cm^{-1}	ω^{corr} (C−O)$_{out}$, cm^{-1}
				hkl (111)				
Pd_2Au_{30}	24.6	9.0	1.894	460	394	1.155	2079	2065
Pd_2Au_{28}	18.8	1.2	1.938	384	364	1.153	2070	2060
Pd_2Au_{62}	17.0	1.3	1.936	372	360	1.154	2067	2057
exp[b−d]	18.2−20.5[b]			371[d]			2086−2089,[b] 2088,[c,e] 2080[d]	
theory[f]	25.6−27.0						2043−2056	
				hkl (100)				
Pd_2Au_{19}	23.5	2.7	1.924	391	371	1.155	2063	2056
Pd_2Au_{23}	22.6	1.8	1.927	383	373	1.155	2067	2055
Pd_2Au_{55}	23.9	1.6	1.922	406	399	1.154	2068	2056
exp[e]							2090−2104	

[a] BSSE-corrected binding energies per bond are calculated as BE = $[E_{(cluster-(CO)_n)} - nE_{(CO)} - E_{(cluster)}]/n$, where n is the number of CO molecules. With this definition, BE values are in kilocalories per mole per CO molecule. ΔBE is the difference from the BE values in Table 1. (in, out) In-phase and out-of-phase modes of Pd−CO (ω) and scaled C−O (ω^{corr}) stretching frequencies. [b] Reference 28. [c] Reference 5. [d] Reference 57. [e] Reference 59. [f] Reference 33.

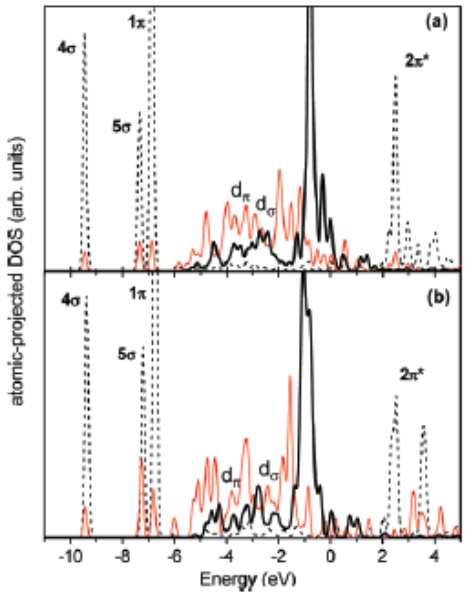

Figure 3. Atomic-projected DOS of Pd d-states (red thin lines) and CO (dotted black lines) in the (a) CO/Pd_2Au_{28}(14,8,8) and (b) CO/Pd_2Au_{19}(12,9) cluster models, together with the atomic-projected density of d-states of Pd (bold black lines) in the corresponding clean PdAu(111) and PdAu(100) surfaces. Zero energy is at the Fermi level.

The atomic-projected DOS for the CO/Pd_2Au_{28}(14,8,8) and the CO/Pd_2Au_{19}(12,9) cluster models, at the BP86/SVP level, are depicted in Figure 3. In both the CO/PdAu(111) and CO/PdAu(100) systems we have found that Pd d-states are strongly disturbed by CO (see Figure 3 a,b). Besides, a relevant shift to lower energies and depletion of the 5σ along with a broadening of the 2π^* peak are clearly visible, in accordance with the common donation and back-donation picture. The plots in Figure 3a are in line with the mechanism of CO−PdAu(111) interaction proposed by periodic calculations.[33]

But, as shown by several experimental and theoretical studies,[36,37,61,62] the Blyholder model has some deficiencies and lacks some important subtleties that would be taken into account.

The resonant features at −9.4 and −6.8 eV and in the region between −6.0 eV and the Fermi level in Figure 3 suggest that not only the HOMO and LUMO are involved in the Pd−CO chemical bond and that other minor contributions are given by the 4σ and the 1π CO molecular orbitals along with the formation of new orbital states below the Fermi level (d_σ and d_π bands).

Polarization of the CO−σ system has been observed that can be interpreted as due to a Pauli repulsion between the CO−σ system and the Pd states as already suggested for Ni and Cu clean metal surfaces.[36,37,63] More details on the atomic C and O contributions to the adsorbed CO states are provided as Supporting Information. On the other hand, the interaction between the CO−π system and the 4d Pd states is more complicated and spans three different energy ranges according to the position of bonding, nonbonding, and antibonding states. A detailed description of these contributions to the substrate−adsorbate bond can be found as Supporting Information.

For the Pd monomer ensemble in the PdAu(111) and PdAu(100) surface alloys, the same chemisorption mechanism has been singled out as it is deducible from the comparison of CO/Pd_2Au_{28}(14,8,8) and CO/Pd_2Au_{19}(12,9) systems in Figure 3. The different CO binding energies obtained for these two cluster models (20.0 and 26.2 kcal/mol at the BP86/SVP level, respectively) can be explained by looking at the different contributions of the Pd d-orbitals to the 4σ, 5σ, and 1π bonding orbitals, indicating a more efficient chemisorption process for the PdAu(100) system.

The same information on the chemisorption bond, mainly characterized by orbital overlaps of σ character and relatively small π contributions, has been obtained by analysis on the largest cluster models used for both the PdAu(111) and PdAu(100) surface alloys.

3.4. Exchange−Correlation Functional and Basis-Set Effects. In order to set up suitable quantum-mechanical models for the study of CO adsorption on PdAu bimetallic surfaces, we have studied the influence of the exchange−correlation functional on the electronic properties of PdAu cluster models and the calculated chemisorption properties. For this purpose we have employed the hybrid B3LYP functional. In addition, we have improved the description of the CO electrons by using the TZVP basis set for both BP86 and B3LYP computations.

When local relaxation effects are studied at the B3LYP level, almost the same results with respect to BP86 calculations are obtained. Indeed, Pd−Au distances are equal to 2.832 and 2.854 Å for the PdAu(100) and (111) surfaces, respectively. Moreover, nearly the same description of the Pd−Au bond is obtained, as showed in Figure 4, with the exception of a rigid downshift of both Pd and Au d-bands of 0.7−0.8 eV compared to the BP86 results.

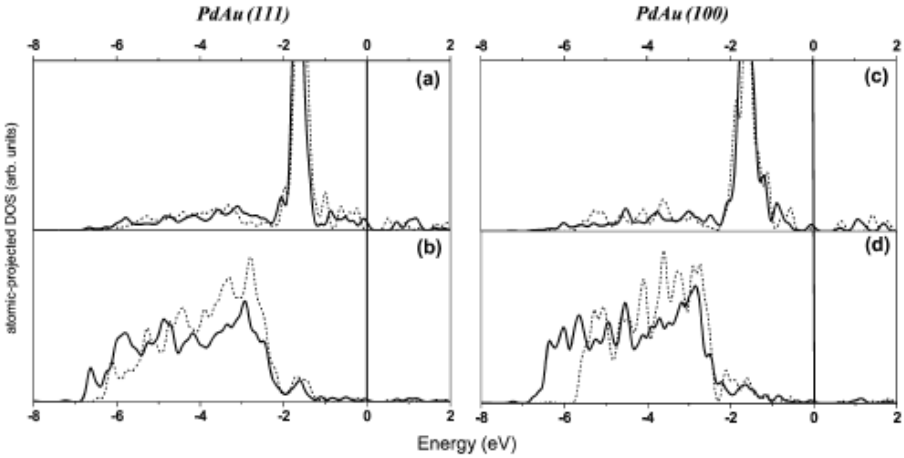

Figure 4. B3LYP atomic-projected density of d-states of Pd monomers (a, c) and adjacent Au atoms (b, d), calculated for PdAu(111) (a, b) and PdAu(100) (c, d) surface alloys. The largest Pd_3Au_{62}(30,21,13) and Pd_2Au_{63}(24,21,12) cluster models (bold black lines) are compared with selected Pd_2Au_{28}(14,8,8) and Pd_2Au_{19}(12,9) smaller clusters (dotted black lines). Zero energy is at the Fermi level.

TABLE 3: BP86/SVP, BP86/TZVP, B3LYP/SVP, and B3LYP/TZVP Results for Adsorption of One CO Molecule on Pd_2Au_{19}(12,9) and Pd_2Au_{28}(14,8,8) Cluster Models[a]

xc functional	basis set	BE, kcal/mol	d(Pd−C), Å	ω(Pd−C), cm^{-1}	d(C−O), Å	ω^{scm}(C−O), cm^{-1}	d(C−O),[b] Å	ω(C−O),[b] cm^{-1}
				Pd_2Au_{19}(12,9)				
BP86	SVP	26.2	1.916	410	1.155	2069	1.142	2152
BP86	TZVP	24.7	1.915	401	1.151	2077	1.138	2128
B3LYP	SVP	17.6	1.944	373	1.141	2069	1.130	2242
B3LYP	TZVP	15.9	1.956	355	1.136	2079	1.127	2216
exp[c,d]						2090−2104[e]	1.128[d]	2170[d]
				Pd_2Au_{28}(14,8,8)				
BP86	SVP	20.0	1.931	385	1.153	2073		
BP86	TZVP	18.5	1.938	370	1.149	2085		
B3LYP	SVP	13.7	1.952	362	1.139	2078		
B3LYP	TZVP	12.0	1.967	344	1.135	2090		
exp[c,e,f]		18.2−20.5[e]		371[f]		2086−2089,[e] 2088,[c] 2080[f]		
theory[g]		25.6−27.0				2043−2056		

[a] Binding energies (BE) are BSSE-corrected. [b] Values for the free CO molecule in the gas phase. [c] Reference 5. [d] Reference 65. [e] Reference 28. [f] Reference 57. [g] Reference 33.

This difference is exclusively due to the different evaluation of the exchange in these two xc functionals and has no effect on the description of the Pd−Au bonds in the surface alloys. Furthermore, by use of both pure and hybrid xc functionals, the electronic configurations and natural charges of the involved atoms in the studied cluster models suggest the same picture for the heterometallic bond; that is, a small amount (0.20−0.25 electron/atom) of Au-to-Pd charge transfer and a small gain of d electrons for Pd atoms in line with other theoretical[33] and experimental[64] works.

Due to the increased computational cost of using a larger basis set and a hybrid exchange−correlation functional, the study of the chemisorption properties has been performed only for the minimal reliable clusters chosen according to the results of the BE convergence studies for both the low-index surface alloys. Therefore, we have chosen the CO/Pd_2Au_{19}(12,9) and CO/Pd_2Au_{28}(14,8,8) cluster models for the PdAu(111) and PdAu(100) surface alloys, respectively. The results for this study are collected in Table 3.

The choice of a triple-ζ quality basis set has an influence of only 1.5 kcal/mol on BP86 binding energies and slightly affects the geometrical parameters. Calculated Pd−CO and C−O stretching frequencies are properly shifted, becoming very close to the experimental available data.

Using the hybrid B3LYP functional, we have found an overall underestimation of the binding energies with respect to the experimental data, whereas a small improvement of the calculated vibrational frequencies, with respect to the BP86 results, has been found.

The differences between the binding energies of CO adsorbed on top of a Pd monomer surrounded by gold atoms, using these two different exchange−correlation functionals, are mainly due to the differently calculated HOMO and LUMO of the CO molecule. In fact, the HOMO and LUMO gaps are smaller in BP86 than in B3LYP, and the HOMO and LUMO are closer to the Fermi energy (see Figure 5 a,b). Hence, following the Blyholder model, the use of the pure xc functional will favor more donation from the 5σ orbital to metal d-states and back-donation from them to the $2\pi^*$ orbital, since the interaction strength between two states is inversely proportional to their energy separation.

The atomic-projected DOS for the CO*−Pd_2Au_{19}(12,9) noninteracting system (where CO* indicates that the CO molecule is located at 4 Å above the substrate) (Figure 5 a,b) and the CO/Pd_2Au_{19}(12,9) adsorbate/cluster model (Figure 5 c,d) are compared in Figure 5, for both BP86/SVP and B3LYP/SVP levels of theory.

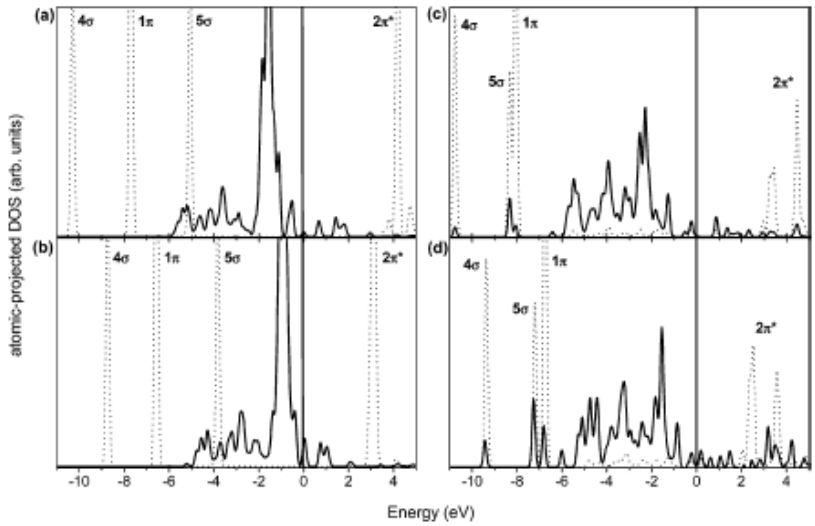

Figure 5. Atomic-projected DOS of Pd (bold lines) and CO (dotted lines) in the CO*/PdAu(100) noninteracting system (a, b) and the CO/PdAu-(100) chemisorbed system (c, d). CO* indicates the CO molecule located 4 Å above the Pd monomer in the PdAu(100) surface. Calculations have been performed with Pd_2Au_{19}(12,9) cluster models at the B3LYP/SVP (a, c) and the BP86/SVP (b, d) levels of theory. Zero energy is at the Fermi level.

In the noninteracting CO*−Pd_2Au_{19}(12,9) system, the energy separation between the 4σ, 5σ, and 1π CO molecular orbitals and the main peak of the Pd 4d-band is strongly dependent on the xc functional employed as well as on the position of the antibonding 2π* state above the Fermi level.

Although the overall chemisorption mechanism obtained with the pure xc functional is maintained, the addition of exact exchange seems to lead to a less efficient chemisorption process with a resulting decrease of the Pd−CO binding energies. A possible explanation of this behavior is given as Supporting Information.

The influence of the basis set on the theoretical results at B3LYP level is, in general, similar to what has been found with the BP86 functional. That is, binding energies slightly decrease for both surface alloy models, and C−O and Pd−CO vibrational frequencies come closer to the experimental values (Table 3).

In summary, the use of a more extended basis set is necessary only for an accurate calculation of the vibrational frequencies but is not strictly required for the prediction of chemisorption binding energy trends if the BSSE corrections are included. Moreover, both standard and extended basis sets give the same qualitative description of the chemisorption mechanism, whatever xc functional is used. The admixture of the exact exchange into the xc functional does not have a remarkable influence on the characterization of the heterometallic bond within PdAu surface alloys. The chemisorption binding energies, instead, are strongly dependent on the xc functional used, with the BP86 results better matching the experimental data.

4. Conclusions

In this work we have studied the adsorption properties of CO on the PdAu(111) and PdAu(100) surface alloys by the DF cluster model approach. In particular, cluster models have been built up to represent second-neighbor Pd pair ensembles on both the exposed surfaces.

The local relaxation effects in the active sites have been studied by use of suitably large clusters with sizes of around 60 metal atoms, in order to obtain the more realistic models for the chemisorption study of CO molecules.

Investigation of the chemical properties of the heterometallic bond in the PdAu surface alloys, using these very large clusters, has shown that the Pd−Au bond is stronger than the Au−Au bond and has a slightly ionic character, in line with previous observations.

The energetic and vibrational properties of the CO molecule adsorbed on the PdAu(111) and PdAu(100) surface alloys have been successfully compared with the available theoretical and experimental data. The convergence study of the chemisorption binding energies has showed good reliability of the models with medium cluster size for the calculation of CO chemisorption properties. That has allowed us to study the influence of the exchange−correlation functional and the basis-set quality on the theoretical results with a reasonable computational cost.

The chemisorption mechanism of CO on top of a Pd monomer surrounded by gold atoms has been analyzed by an atom-projected description of the surface chemical bond providing an accurate picture.

The success of the adopted strategy demonstrates that the cluster model approach can be fruitfully employed for the chemisorption study of small molecules on relatively simple critical ensembles of bimetallic surfaces, such as second-neighbor Pd pairs on palladium−gold catalysts.

Acknowledgment. We thank the Università della Calabria for financial support.

Supporting Information Available: Details on the chemisorption mechanism of CO on PdAu(100) surface, influence of the exact exchange on the Pd−CO interaction strength, and metal contribution to the Pd−CO orbitals as a function of the xc functional. This material is available free of charge via the Internet at http://pubs.acs.org.

References and Notes

(1) Sinfelt, J. H. *Bimetallic Catalysts: Discoveries, Concepts and Applications*; Wiley: New York, 1983.
(2) Moss, R. L.; Whally, L. *Advances in Catalysis*; Academic Press: New York, 1972.
(3) Ponec, V. *Adv. Catal.* **1983**, *32*, 149.
(4) Nascimento, M. A. C. *Theoretical aspects of heterogeneous catalysis*; Kluwer Academic Publishers: Dordrecht, The Netherlands, 2001; Vol. 8.
(5) Chen, M.; Kumar, D.; Yi, C. W.; Goodman, D. W. *Science* **2005**, *310*, 291 and supporting online material.
(6) Maroun, F.; Ozanam, F.; Magnussen, O. M.; Behm, R. J. *Science* **2001**, *293*, 1811.
(7) Bligaard, T.; Norskov, J. K. *Electrochim. Acta* **2007**, *52*, 5512.
(8) Baddeley, C. J.; Tikhov, M.; Hardacre, C.; Lomas, J. R.; Lambert, R. M. *J. Phys. Chem.* **1996**, *100*, 2189.
(9) Baddeley, C. J.; Ormerod, R. M.; Stephenson, A. W.; Lambert, R. M. *J. Phys. Chem.* **1995**, *99*, 5146.
(10) Han, Y. F.; Kumar, D.; Goodman, D. W. *J. Catal.* **2005**, *230*, 353.
(11) Enache, D. I.; Edwards, J. K.; Landon, P.; Solsona-Espriu, B.; Carley, A. F.; et al. *Science* **2006**, *311*, 362.
(12) Trimm, D. L.; Onsan, Z. I. *Catal. Rev.* **2001**, *43*, 31.
(13) Bonarowska, M.; Malinowski, A.; Juszczyk, W.; Karpinski, Z. *Appl. Catal., B* **2001**, *30*, 187.
(14) Rodriguez, J. A. *Surf. Sci. Rep.* **1996**, *24*, (7−8), 225.
(15) Sarkany, A.; Horvath, A.; Beck, A. *Appl. Catal., A* **2002**, *229*, 117.
(16) Hilaire, L.; Legare, P.; Holl, Y.; Maire, G. *Surf. Sci.* **1981**, *103*, 125.
(17) Jablonski, A.; Overbury, S. H.; Somorjai, G. A. *Surf. Sci.* **1977**, *65*, 578.
(18) Swartzfager, D. G.; Ziemecki, S. B.; Kelley, M. J. *J. Vac. Sci. Technol.* **1981**, *19*, 185.
(19) Wood, B. J.; Wise, H. *Surf. Sci.* **1975**, *52*, 151.
(20) Michaelson, H. B. *J. Appl. Phys.* **1977**, *48*, 4729.
(21) Lambert, S.; Heinrichs, B.; Brasseur, A.; Rulmont, A.; Pirard, J. P. *Appl. Catal., A* **2004**, *270*, 201.
(22) Wouda, P. T.; Schmid, M.; Nieuwenhuys, B. E.; Varga, P. *Surf. Sci.* **1998**, *417*, 292.
(23) Kuntze, J.; Speller, S.; Heiland, W.; Deurinck, P.; Creemers, C.; Atrei, A.; Bardi, U. *Phys. Rev. B* **1999**, *60*, 9010.
(24) Kaszkur, Z. *Phys. Chem. Chem. Phys.* **2004**, *6*, 193.
(25) Lovvik, O. M. *Surf. Sci.* **2005**, *583*, 100.
(26) Yi, C. W.; Luo, K.; Wei, T.; Goodman, D. W. *J. Phys. Chem. B* **2005**, *109*, 18535.
(27) Baddeley, C. J.; Barnes, C. J.; Wander, A.; Ormerod, R. M.; King, D. A.; Lamerod, R. M. *Surf. Sci.* **1994**, *1*, 314.
(28) Li, Z.; Gao, F.; Wang, Y.; Calaza, F.; Burkholder, L.; Tysoe, W. T. *Surf. Sci.* **2007**, *601*, 1898.
(29) Gross, A. *Top. Catal.* **2006**, *37*, 1.
(30) Besenbacher, F.; Chorkendorff, I.; Clausen, B. S.; Hammer, B.; Molenbroek, A. M.; Norskov, J. K.; Stensgaard, I. *Science* **1998**, *279*, 1913.
(31) Kratzer, P.; Hammer, B.; Norskov, J. K. *J. Chem. Phys.* **1996**, *105*, 5595.
(32) Larsen, J. H.; Chorkendorff, I. *Surf. Sci.* **1999**, *35*, 165.
(33) Yuan, D.; Gong, X.; Wu, R. *Phys. Rev. B* **2007**, *75*, 085428.
(34) Siegbahn, P. E. M.; Wahlgren U.; Schustorovich, E. *Metal−Surface Reaction Energetics*; VCH Publishers: New York, 1991.
(35) Gil, A.; Clotet, A.; Ricart, J. M.; Kresse, G.; Garcia-Hernández, M.; Rosch, N.; Sautet, P. *Surf. Sci.* **2003**, *530*, 71.
(36) Fohlisch, A.; Nyberg, M.; Hasselstrom, J.; Karis, O.; Pettersson, L. G. M.; Nilsson, A. *Phys. Rev. Lett.* **2000**, *85*, 3309.
(37) Fohlisch, A.; Nyberg, M.; Bennich, P.; Triguero, L.; Hasselstrom, J.; Karis, O.; Pettersson, L. G. M.; Nilsson, A. *J. Chem. Phys.* **2000**, *112*, 1946.
(38) Swang, O.; Baerends, E. J.; Fægri, K., Jr.; Gropen, O. *J. Mol. Struct.: THEOCHEM* **1996**, *388*, 321.
(39) Illas, F.; Lòpez, N.; Clotet, A.; Ricart, J. M.; Fernàndez-Garcia, M.; Conesa, J. C. *J. Phys. Chem. B* **1998**, *102*, 8017.
(40) Sousa, C.; Bertin, V.; Illias, F. *J. Phys. Chem. B* **2001**, *105*, 1817.
(41) Rochefort, A.; Andzelm, J.; Russo, N.; Salahub, D. R. *J. Am. Chem. Soc.* **1990**, *112*, 8239.
(42) Kumar, D.; Chen, M. S.; Goodman, D. W. *Catal. Today* **2007**, *123*, 77.
(43) Ahlrichs, M. Bär; Häser, M.; Horn, H.; Kölmel, C. *Chem. Phys. Lett.* **1989**, *162*, 165.
(44) Becke, A. D. *Phys. Rev. A* **1988**, *38*, 3098.
(45) Perdew, J. P. *Phys. Rev. B* **1986**, *33*, 8822.
(46) Eichkorn, K.; Treutler, O.; Öhm, H.; Häser, M.; Ahlrichs, R. *Chem. Phys. Lett.* **1995**, *240*, 283.
(47) Eichkorn, F.; Weigend, O.; Treutler, Ahlrichs, R. *Theor. Chem. Acc.* **1997**, *97*, 119.
(48) Andrae, D.; Hæussermann, U.; Dolg, M.; Stoll, H.; Preuss, H. *Theor. Chim. Acta* **1990**, *77*, 123.
(49) Schäfer, A.; Horn, H.; Ahlrichs, R. *J. Chem. Phys.* **1992**, *97*, 2571.
(50) Becke, A. D. *J. Chem. Phys.* **1993**, *98*, 5648.
(51) Stephens, P. J.; Devlin, F. J.; Chabalowski, C. F.; Frisch, M. J. *J. Phys. Chem.* **1994**, *98*, 11623.
(52) Schäfer, A.; Huber, C.; Ahlrichs, R. *J. Chem. Phys.* **1994**, *100*, 5829.
(53) Boys, S. F.; Bernardi, F. *Mol. Phys.* **1970**, *19*, 553.
(54) Hammer, B.; Norskov, J. K. *Surf. Sci.* **1995**, *343*, 211.
(55) Pallassana, V.; Neurock, M.; Hansen, L. B.; Hammer, B.; Nørskov, J. K. *Phys. Rev. B* **1999**, *60*, 6146.
(56) Hammer, B. *Topics Catal.* **2006**, *37*, 3.
(57) Hammer, B.; Morikawa, Y.; Nørskov, J. K. *Phys. Rev. Lett.* **1996**, *60*, 2141.
(58) Gleich, B.; Ruff, M.; Behm, R. J. *Surf. Sci.* **1997**, *386*, 48.
(59) Wei, T.; Wang, J.; Goodman, D. W. *J. Phys. Chem. C* **2007**, *111*, 8781.
(60) Blyholder, G. *J. Phys. Chem.* **1964**, *68*, 2772.
(61) Nilsson, A.; Weinelt, M.; Wiell, T.; Bennich, P.; Karis, O.; Wassdahl, N. *Phys. Rev. Lett.* **1997**, *78*, 2847.
(62) Hammer, B.; Norskov, J. K. *Adv. Catal.* **2000**, *45*, 71.
(63) Bagus, P. S.; Hermann, K. *Phys. Rev. B* **1986**, *33*, 2987.
(64) Nascente, P. A. P.; de Castro, S. G. C.; Landers, R.; Kleiman, G. G. *Phys. Rev. B* **1991**, *43*, 4659.
(65) Huber, K. P.; Herzberg, G. *Molecular Spectra and Molecular Structure, Constants of Diatomic Molecules*; Van Nostrand: Princeton, NJ, 1979; Vol. IV.

SUPPORTING INFORMATION

On the interaction of CO with PdAu(111) and PdAu(100) bimetallic surfaces. A theoretical cluster model study

*Gloria Mazzone, Ivan Rivalta, Nino Russo, Emilia Sicilia**

Dipartimento di Chimica and Centro di Calcolo ad Alte Prestazioni per Elaborazioni Parallele e Distribuite-Centro d'Eccellenza MURST, Università della Calabria, I-87030 Arcavacata di Rende, Italy

siciliae@unical.it

.

Figure S1. Full orbital character of the Pd-CO orbitals.

Chemisorption mechanism of CO on PdAu(100) surface: CO-σ and CO-π system.

Figure S2. Metal contribution to the Pd-CO orbitals as a function of the xc-functional.

Influence of the exact exchange on the Pd-CO interaction strength.

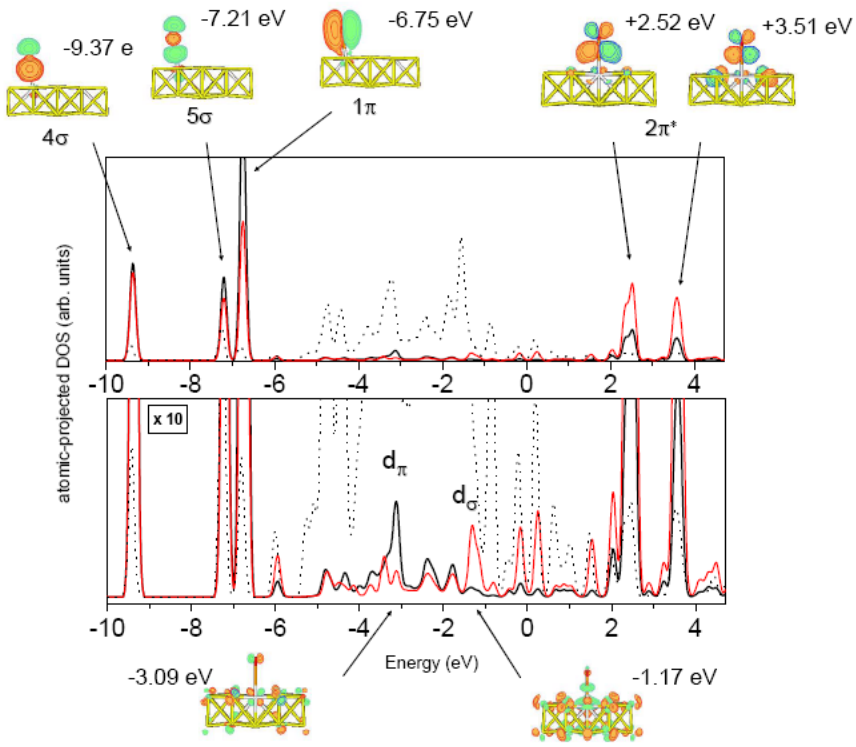

Figure S1. The atomic-projected DOS of C atom (red line), O atom (black line) and Pd (dotted line) in the $CO/Pd_2Au_{19}(12,9)$ cluster model calculated at BP86/SVP level. The insets display the full orbital character (contour factor 0.03) of the 4σ, 5σ and 1π and $2\pi^*$ peaks (top panel) and of the low intense d_π and d_σ bands (bottom panel). The zero of energy is at the Fermi level.

Chemisorption mechanism of CO on PdAu(100) surface.

CO-σ system: Looking at the molecular orbitals of the $CO/Pd_2Au_{19}(12,9)$ cluster model depicted in Figure S1 one can observe that the 5σ CO HOMO hybridizes with the d_{z^2} states and remarkably shifts to lower energies (-7.21 eV) even below the orbital states with 1π character. Due to the symmetry, this is the major orbital interaction for a-top site adsorption of CO molecule on metals. Upon adsorption, the 5σ orbital, which is strongly polarized to the carbon in the free molecule, moves towards the oxygen atom showing an important redistribution. Similarly, but in the opposite direction, a remarkable polarization of the 4σ towards the carbon atom is present in the CO/Pd_2Au_{19} system although the interaction of the d_{z^2} states with the 4σ molecular orbital (at -9.37 eV) is characterized by weaker hybridization compared to the 5σ case. Since almost fully occupied states interact, the polarization between the CO-σ system can be interpreted as due to a Pauli repulsion between the CO-σ system and the Pd states. Additional σ-states with low intensity have been found between 5σ and the Fermi level that are strongly located on the metal and have only weak contributions on the adsorbate and are denoted as d_σ band. In the orbital plots within the Figure S1 the full orbital character is depicted for a d_σ state located at 1.17 eV below the Fermi level revealing the antibonding nature between the metal and carbon atoms.

CO-π system: The interaction between CO-π system and the 4*d* Pd states is more complicated and spans three different energy ranges. An almost perturbed 1π orbital is located at low energies (around -6.8 eV) shifted down, by some tenths of eV, with respect to the free molecule by a weak hybridization with the d_{xz} and the d_{yz} states. The polarization of 1π orbital towards the carbon atom (by $2\pi^*$ contribution) upon CO adsorption has not been observed but in the medium energy range, between -6.0 and the Fermi level, hybrid states of the unperturbed 1π and $2\pi^*$ orbitals exist. Since these states are largely derived from the Pd *d*-band they are named d_π band. This band is essentially constituted by nonbonding oxygen lone pair orbitals as exemplified in Figure S1 in the orbital plot of the state located at -3.09 eV. Since the partial occupation of the $2\pi^*$ orbital increases with the coordination and decreases with *d*-band filling the intensity of the d_π band is reasonably low in the examined case. Finally, in the range of 2-4 eV above the Fermi level the antibonding $2\pi^*$-d_{yz} and $2\pi^*$-d_{xz} hybrid orbitals are visible.

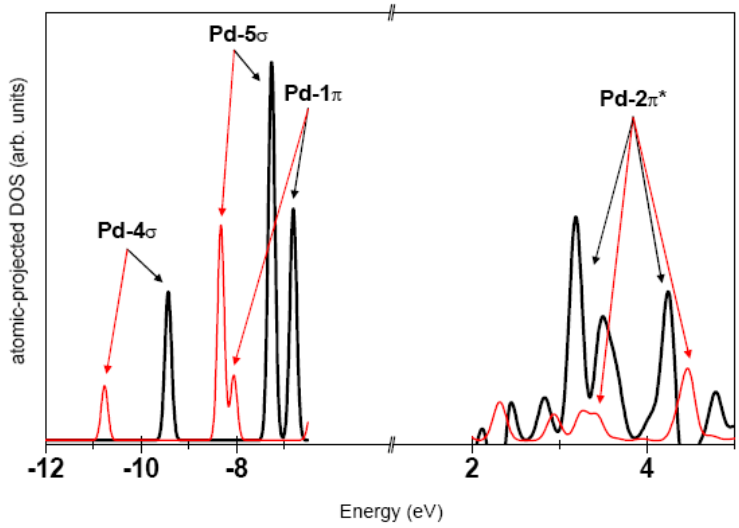

Figure S2. The atomic-projected DOS of Pd atom in the CO/Pd_2Au_{19}(12,9) cluster model calculated at BP86/SVP level (black line) and at B3LYP/SVP level (red line). The contribution of the metal to the newly formed Pd-4σ, Pd-5σ, Pd-1π and Pd-2π^*orbitals is strongly dependent on the xc-functional.

Influence of the exact exchange on the Pd-CO interaction strength.

Even if the general downshift of the CO molecular orbitals upon the adsorption is almost identical in both BP86/SVP and B3LYP/SVP calculations, showing that the adsorbed CO molecule get similar chemical properties, the chemisorption bond formation is much more favored at BP86 than at B3LYP level. Looking at the overlapping of the CO orbitals with the broadened 4*d*-band of the Pd atom in Figures S2, it is evident how the contribution of the metal to the newly formed Pd-4σ, Pd-5σ and Pd-1π orbitals halves when exact exchange is added. This is an indication of a weaker interaction strength between the Pd monomer and the adsorbate which is further emphasized by a less efficient back-donation process due to the position of the empty $2\pi^*$ CO orbital. As expected, employing the hybrid functional, the $2\pi^*$ orbital at B3LYP/SVP lies more than 1 eV above the calculated $2\pi^*$ at BP86/SVP level in the non-interacting system, making the occupation of this empty orbital more difficult. This is corroborated by the less intense broadening of the $2\pi^*$ states (below the Fermi level) and the less metal contribution to the Pd-$2\pi^*$orbitals (above the Fermi level) in the interacting system (Figure S2).

Pubblicazione II

The geometric effect in palladium–gold catalysis. Is the coupling the rate-determining step in the vinyl-acetate synthesis?

Gloria Mazzone, Ivan Rivalta, Nino Russo, Emilia Sicilia

Chem. Commun. **2009**, 1852–1854

1350 J. Chem. Theory Comput. 2009, 5, 1350–1360

JCTC Journal of Chemical Theory and Computation

Adsorption of Ethylene, Vinyl, Acetic Acid, and Acetate Species on PdAu(111) and PdAu(100) Surface Alloys: A Cluster Model Study

Ivan Rivalta, Gloria Mazzone, Nino Russo, and Emilia Sicilia*

Dipartimento di Chimica and Centro di Calcolo ad Alte Prestazioni per Elaborazioni Parallele e Distribuite-Centro d'Eccellenza MURST, Università della Calabria, I-87030 Arcavacata di Rende, Italy

Received January 7, 2009

Abstract: The adsorption properties on PdAu surface alloys of ethylene and acetic acid molecules along with their derived vinyl and acetate surface species have been investigated by density functional theory calculations. Large clusters have been used to model second-neighbor Pd monomer pair ensembles on PdAu(100) and PdAu(111) surface alloys. Ethylene and acetic acid are weakly bonded to the Pd monomers, while vinyl and acetate are strongly bonded to both Pd and Au atoms being very stable surface species. The ligand effect of the gold atoms surrounding the Pd monomers has been shown to be stronger in the more dense PdAu(111) surface alloy. Cluster model results are in good agreement with experimental evidence providing important insight on the adsorption bonding modes, the assignment of the infrared features, and the preferred adsorption sites.

1. Introduction

Bimetallic systems constitute a broad class of selective catalysts that attempt to exploit and combine the different chemical properties of various metals toward a given chemical reaction.[1−4] Among the several binary systems that are often used in basic and applied research, PdAu provides an example of a rather versatile catalytic system. Mixtures of Pd and Au are frequently used as catalysts for a number of reactions (e.g., CO oxidation, cyclotrimerization of acetylene, synthesis of vinyl acetate monomer, selective oxidation of alcohols to aldehydes)[5−8] and applications including hydrogen fuel cells and pollution control.[9,10] It has been shown that the addition of Au to Pd significantly enhances the catalytic activity, selectivity, and stability of Pd-based catalysts; therefore, Pd−Au surface alloys have been the subject of many investigations.[6,7,11−18]

One of the major uses of gold/palladium catalysis is for vinyl acetate monomer (VAM) production. Indeed, the synthesis of vinyl acetate monomer from ethylene, acetic acid, and oxygen is catalyzed by both supported palladium and palladium−gold alloys, but alloying with gold leads to a substantial increase in selectivity.[19] Although this process is a mature industrial reaction, the nature of the key reaction intermediates and mechanism as well as the promotional role of Au are still unresolved questions. Two different surface reaction mechanisms, both invoking coupling of acetate and ethylenic species as the rate-limiting step, have been proposed for VAM synthesis. The one proposed by Samanos et al. involves the coupling of ethylene with adsorbed acetate to form, as intermediate, ethyl acetate that undergoes β-hydride elimination to form VAM (Samanos-type mechanism).[20] Alternatively, as suggested by both Moiseev[21,22] and Nakamura and Yasui,[23] ethylene could adsorb and subsequently dehydrogenate to form a vinyl species that couples with the coadsorbed acetate to give VAM directly (Moiseev-type mechanism). Although support to the pathway proposed by Samanos et al. comes from the experimental results by Tysoe et al. on Pd(111) surface,[24] the reaction mechanism for VAM synthesis remains essentially uncertain.

Goodman and co-workers[25] recently demonstrated that the critical ensemble for VAM formation on a PdAu(100) surface alloy is a pair of noncontiguous, suitably spaced, Pd monomers. They have also used ultra-high-vacuum (UHV)

* To whom correspondence should be addressed. E-mail: siciliae@unical.it.

10.1021/ct9000137 CCC: $40.75
Published on Web 04/20/2009

scanning tunnelling microscopy (STM) to image the Pd monomer pairs on AuPd(100) bulk alloy surface and presented a method for increasing the concentration of these active sites.[26]

The formation of isolated Pd monomer sites influences the properties of adsorbed reagents (ethylene, acetic acid, and their derived surface species) as well. Indeed, temperature-programmed desorption (TPD) experiments have shown that ethylene binds significantly less strongly to a Pd monomer compared to a site containing contiguous Pd atoms.[27,28] On contiguous Pd sites a di-σ-bonded ethylene species and an ethylidyne species have been observed,[29] which decompose leading to the formation of carbon, while on Pd monomers surrounded by gold atoms a π-ethylene surface species has been observed.[25,28,29] The addition of Au inhibits the decomposition of ethylene, consequently forming less carbon and extending the activity of the catalyst.[25] The same effect of gold addition to Pd surfaces has been demonstrated for the acetic acid and acetate decompositions.[30,31] High-resolution electron energy loss spectroscopy (HREELS) experiments[25,29] have shown the presence of a bidentate acetate species on isolated and contiguous Pd sites on PdAu(111) surfaces at high temperatures (350 K). By use of reflection−absorption infrared spectroscopy (RAIRS),[31] intact acetic acid molecules that form catemers have been detected for Au-rich PdAu(111) surface, whereas both bidentate and monodentate acetate species have been observed on surface alloys containing small mole fractions of gold. Recently, the effect on the adsorption of reactants (in VAM synthesis) has been demonstrated to be an important factor in determining the structure sensitivity of PdAu surface alloys.[32]

Since accurate knowledge of the binding sites and of the orientation of the molecules adsorbed on surfaces is an important component of any effort to describe heterogeneously catalyzed reactions with mechanistic detail, here we present the outcome of a density functional cluster model study of the adsorption properties of ethylene, vinyl, acetic acid, and acetate species on the PdAu(111) and PdAu(100) surface alloys. Ethylene and acetic acid (along with molecular oxygen) are the starting reagents in the VAM synthesis and the species that deposit from the gas phase on the catalyst surface. Their derived species, acetate and vinyl, are the most relevant surface species if both Samanos-type and Moiseev-type mechanisms are considered viable on PdAu surfaces.

The focus of the present paper is on the local features of the interaction between adsorbed molecules and PdAu surface alloys. Consequently, we adopted for our investigation the cluster model approach as more suitable, with respect to alternative slab models, to capture the essential features of the chemisorption bond and to predict local properties such as adsorption geometries and vibrational frequencies at low coverages. In particular, cluster models have been built up to represent the second-neighbor Pd pair ensembles on both surfaces given that these are the critical ensembles in the synthesis of vinyl-acetate monomer catalyzed by PdAu alloys and supposed to be crucial for the different catalytic activities of PdAu(100) and PdAu(111) surfaces.

Results have been compared with previous periodic slab supercell calculations for the PdAu(001) surface[33,34] and also with helpful information concerning the adsorption properties of acetic acid-derived species and ethylene on Au/Pd(111) alloys as a function of temperature and alloy composition comprised in a recent series of systematic experimental studies carried out by Tysoe's group.[11,28,31]

2. Methodology and Computational Details

In order to model the second-neighbor Pd pair ensembles on PdAu(100) and PdAu(111) surfaces we have built up cluster models of large size having 57 and 64 metal atoms, respectively, in order to prevent any indirect insaturation effect for the surface atoms directly involved in the adsorbate−surface bonds. A schematic representation of the Pd_2Au_n clusters used in this work is reported in Figure 1.

Since these models have been successfully adopted for the study of CO adsorption on the PdAu surface alloys, a more detailed description of the Pd_2Au_{55}(24,21,12) and Pd_2Au_{62}(30,21,13) cluster models used here along with the cluster size dependence of the chemisorption properties can be found elsewhere.[35] The employed clusters are three-layer models centered in the active site that contains two noncontiguous Pd atoms and two Au atoms bonded to both of them. The atomic positions of the clusters have been assigned, initially, as in bulk gold, with the experimental lattice parameter of 4.08 Å. For the adsorption studies, the positions of the molecules, adsorbed on these cluster models, have been fully relaxed without symmetry constraints. Cluster atoms involved in the adsorption bonds and their first neighbors in the first and second layers have been also relaxed. The calculations have been performed with the Turbomole package[36] at the DF level, by use of the BP86 functional[37,38] within the resolution of the identity approximation for computing the electronic Coulomb interaction (RI-J).[39,40] The Stuttgart effective core potential[41] has been used to model the scalar relativistic effects replacing the 28 and 60 core electrons of palladium and gold atoms, respectively. The valence electrons of metal atoms, 18 for Pd and 19 for Au, and all electrons for C, O, and H atoms have been explicitly considered by use of the Turbomole's TZVP basis set[42] along with the corresponding TZVP auxiliary basis set.[40] The electronic ground states of bare PdAu clusters and adsorbate/cluster models (including ionic adsorbates) have been checked by studying different spin multiplicities. The lowest energy states have always shown the smallest multiplicity values (i.e., singlet or doublet states). The total energies calculated after geometry optimization have been corrected for basis set superposition error (BSSE) by use of Boys−Bernardi counterpoise calculations[43] for all adsorbate/cluster models. This correction is less than 4.0 kcal/mol per bond for the strong chemisorption of acetate radical and vinyl species on the cluster models, whereas is around 1.0−1.3 kcal/mol for the weak adsorption of ethylene and acetic acid molecules. As expected, for the absorption of charged species, i.e., CH_3COO anion, the correction is larger up to ~7−8 kcal/mol. All the vibrational frequencies reported in this work have been corrected by use of the scaling factor (1.004) suggested for the BP86 functional in combination

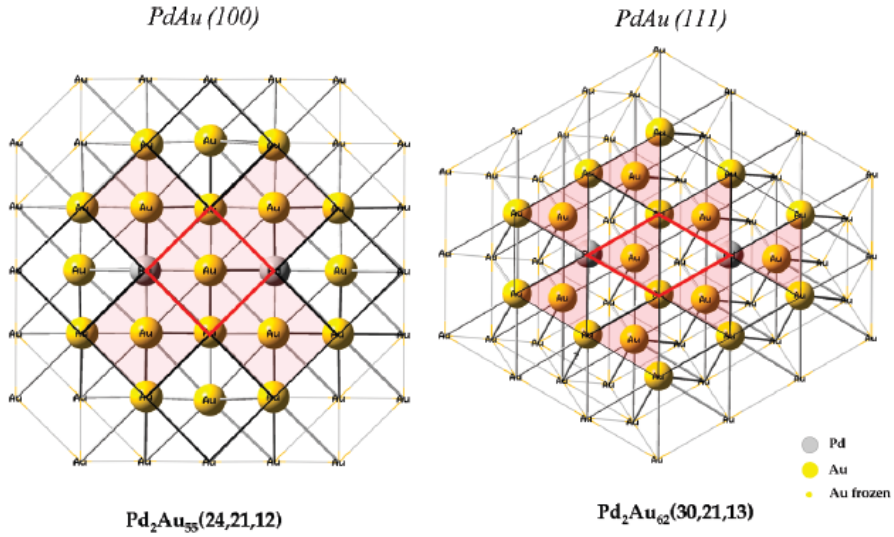

Figure 1. Schematic representation of the Pd_2Au_n clusters used in this work to model the second-neighbor Pd pair ensemble on the PdAu(100) and PdAu(111) surface alloys. Frozen Au atoms are shown as spots, while Pd and Au atoms in the first and second layer that are allowed to relax are depicted as spheres. Four-fold and three-fold (hcp) hollow sites associated with the relaxed atoms in the first layer are evidenced by planes (in red). Unit cells of the Au(100) and Au(111) pure surfaces are depicted in red.

with the TZVP basis set.[44] The atom-projected density of states (DOS) has been calculated (as implemented in Turbomole) by broadening the discrete energy levels of each cluster model with Gaussians having a width of 0.003 au and superimposing them.

3. Results and Discussion

3.1. Adsorption of Ethylene. Experimental studies by both Goodman's[25,29] and Tysoe's[28] groups have demonstrated that on gold−palladium alloys at low palladium coverages only π-bonded adsorbed ethylene on isolated Pd atoms, completely surrounded by gold, is present as surface species.

In accordance with this experimental evidence, the DF cluster model calculations performed in this study have shown that there are no stable adsorption states for a di-σ-bonded ethylene on second-neighbor Pd monomer pairs. Indeed, despite the numerous attempts to find on both PdAu(100) and PdAu(111) surface alloys a stable adsorption geometry having Pd−C and Au−C σ bonds, the ethylene molecule always moves to an atop configuration (π-bonded-type) on a Pd atom completely surrounded by gold.

The energetic, structural, and vibrational properties calculated for the π-bonded ethylene molecule adsorbed on top of Pd monomer are reported in Table 1 for both PdAu(100) and PdAu(111) palladium−gold surface alloys.

For the PdAu(100) surface, the calculated binding energy (BE) of ethylene is 13.0 kcal/mol, in good agreement with the values obtained by use of a plane-wave-based method[33] for isolated Pd monomers (12.9 kcal/mol) and second-neighbor Pd monomer pairs (15.2 kcal/mol). The geometry of the adsorbed ethylene molecule with the C−C bond along the [011] axis of the PdAu(100) surface is energetically preferred by only 0.7 kcal/mol with respect to that along the [010] axis, analogously to what has been obtained with the periodic slab supercell approach.[33]

Since the experimental BE of the π-bonded ethylene on the Pd(100) clean surface is ~19 kcal/mol[45] and this value

Table 1. BSSE-Corrected Binding Energies (BE, in kcal/mol), Equilibrium Bond Distances (d, in Angstroms), Angles (in degrees), and Scaled Vibrational Frequencies (in cm^{-1}) of the π-Bonded Ethylene Molecule on the Pd_2Au_{55}(24,21,12) and Pd_2Au_{62}(30,21,13) Cluster Models[a]

	PdAu(100)	PdAu(111)
BE	13.0	5.5
d(C−C)	1.383	1.374
d(Pd−C)	2.299	2.383
θ(CCH)	120.6	121.1
ϕ_{tilt}	8.4	5.1
ν(C−H)	3184 (w)	3178 (w)
	3159 (w)	3152 (w)
	3083 (w)	3083 (w)
	3080 (w)	3076 (w)
ν(C−C) + δ(CH_2)	1530 (w)	1607 (w)
	1422 (w)	1430 (w)
	1276 (w)	1336 (w)
	1203 (w)	1206 (w)
ω(CH_2)	958 (w)	1005 (w)
	922 (s)	938 (vs)
	900 (s)	925 (s)
	818 (w)	811 (w)
ν(Pd−C)	175 (w)	158 (w)

[a] The ϕ_{tilt} angle indicates the tilting angle between the ethylene molecular plane and the surface plane. ν stretching; δ in-plane bending, scissoring and rocking; ω out of plane bending, twisting and wagging. (vs) very strong; (s) strong; (w) weak.

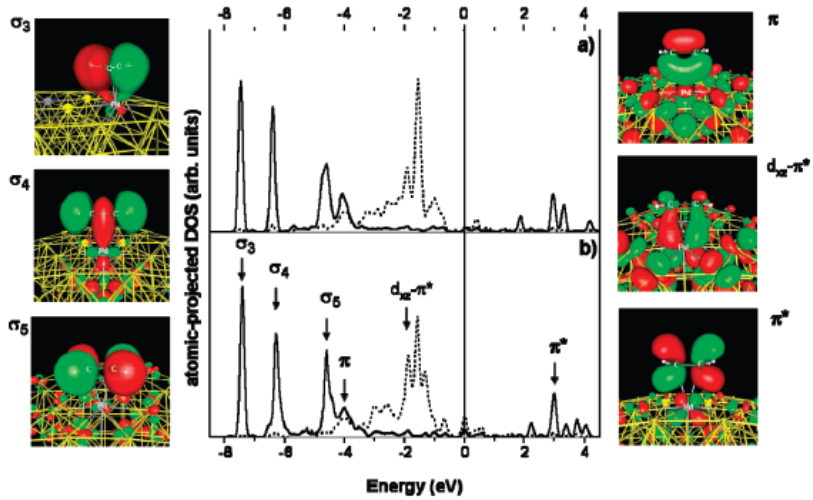

Figure 2. Atom-projected DOS of ethylene molecule (black lines) and Pd d states (dotted black lines) in the C_2H_4/Pd_2Au_{55} (a) and C_2H_4/Pd_2Au_{62} (b) systems. The insets display the full orbital character (contour factor 0.03) of the σ_3, σ_4, and σ_5 peaks (left) and π, π^*, and $d_{\pi z}-\pi^*$ bands (right) of the C_2H_4/Pd_2Au_{62} cluster model. The zero of energy indicates the highest occupied molecular orbital.

significantly decreases by gold addition due to the ligand effect,[33,34] the interaction of the π-bonded ethylene with Pd monomers finally is in the energy regime of the chemisorption/physisorption limit.

Unsurprisingly, this effect has been also observed for the adsorption of C_2H_4 on the PdAu(111) surface. The BE value for this adsorption, calculated with the cluster model used in this study, is 5.5 kcal/mol and is just a little lower than the calculated BEs for the Pd(111) surface, which are in the range of 6.4−7.2 kcal/mol.[45−47] These results are in line with the observations made in the TPD experiments on PdAu(111) surface alloy,[28] which indicated that the heat of adsorption of ethylene decreases monotonically as the gold coverage increases. On the other hand, a desorption activation energy of 13.6−14.8 kcal/mol has been estimated experimentally[28] for the ethylene adsorption on PdAu(111) with medium−high gold coverage (between ~0.5 and ~0.7). The computed BE is, therefore, underestimated by about 7−9 kcal/mol with respect to the experimental value. However, it is worth underlining that this discrepancy, beside the DFT limits in the description of such long-range interactions, can be due to the uncertainty associated with the experimental estimation of the heat of adsorption. Indeed, peak broadness, in the TPD spectra, is observed for the ethylene adsorption on PdAu(111) surface at gold coverage higher than 0.73 ML. Furthermore, the stronger interaction between ethylene and the PdAu(100) surface with respect to the PdAu(111) surface is in line with the behavior observed for the adsorption of other organic molecules (such as CO[45,48] and other adsorbed species studied here) on these two surfaces alloys.

The different adsorption orientations for the π-bonded ethylene on the PdAu(111) surface (i.e., with the carbon−carbon axis along the $0\bar{1}0$, $\bar{1}01$, and $\bar{2}11$ directions) explored in this study have practically shown the same energetics, proving to be adsorption degenerate states.

The main infrared features of π-bonded ethylene have been detected in the range between 900 and 960 cm^{-1} by both RAIRS[28] and HREELS[25,29] experiments and assigned to the CH_2 wagging modes. In the same spectral region we found the most intense infrared vibrations that just correspond to the in-phase wagging vibrational mode, where in phase indicates the simultaneous wagging of the two CH_2 groups out of the molecular plane. In particular, in the case of the PdAu(111) surface alloys the main infrared feature (with the highest peak intensity, see Table 1) is calculated to lie at 938 cm^{-1}. This value is in excellent agreement with the main experimental feature detected at 931 cm^{-1} by RAIRS[28] for the π-bonded ethylene adsorbed on a PdAu(111) surface with a 0.73 ML gold coverage and annealed to 120 K (to prevent the interference of ethylene molecules adsorbed on Au atoms).

Further remarks regarding the analysis of the π-bonded ethylene vibrational spectra will be given in the next paragraph for a comparison with the calculated vibrational properties of the surface vinyl species.

The fundamental features of ethylene π-bonded adsorption on the Pd noncontiguous pairs can be described in the framework of the classic Dewar−Chatt−Duncanson model of orbital interactions.[49,50] The filled bonding π orbital of ethylene transfers charge to the empty metal d states at the surface, while the occupied metal d band back-donates electron density into the ethylene antibonding π^* orbital. This model is confirmed by our calculations, in agreement with the periodic slab supercell-projected DOS,[33] as shown by the atom-projected DOS for the C_2H_4/Pd_2Au_{55} and the C_2H_4/Pd_2Au_{62} cluster models depicted in Figure 2a and 2b.

In the noninteracting system (where the ethylene molecule is located 4 Å above the substrate) the highest occupied molecular orbital (HOMO) of ethylene and the lowest unoccupied molecular orbital (LUMO) lie at −1.2 and 3.9 eV, respectively. In the equilibrium structure of adsorbed ethylene on PdAu clusters, a relevant depletion of the π-orbital peak of ethylene (HOMO) can be observed at −4.0 eV along with a broadening of the π^* peak (LUMO) into a wide energy range, in accordance with the common donation and back-donation picture (see Figure 2). In general, small bonding and antibonding overlaps between Pd d bands and σ and π states of ethylene have been detected, in line with a Dewar−Chatt−Duncanson description of a weak chemical interaction. The main contribution to the adsorption bond comes from the coupling of the HOMO of ethylene with the empty d_{z^2} orbital of the Pd monomer.

As confirmed by the orbital plot at −2.0 eV (d_{xz}−π^*), some orbital states with π^* character appear to be occupied, but the feeble overlapping with the metal d states indicates a back-donation mechanism with a limited charge transfer.

According to this description of the Pd−ethylene interaction, a very small elongation of the C−C bond by 0.05 and 0.04 Å with respect to the gas-phase ethylene (1.333 Å) has been observed (see Table 1) on the PdAu(100) and PdAu(111) surfaces, respectively. The calculated Pd−C distances (about 2.3−2.4 Å) and the planar and tilt angles (θ and ϕ, respectively), whose values confirm a negligible distortion of the sp^2 hybridization of the C atoms, confirm the weak chemical interaction between ethylene and Pd atoms in the gold-rich PdAu surface alloys.

3.2. Adsorption of Vinyl. According to the Moiseev-type mechanism[21−23] the vinyl acetate formation involves a surface vinyl species that couples with the coadsorbed acetate. This radical species is a surface intermediate of the dehydrogenation reaction of an adsorbed ethylene molecule. However, it has been generally observed that ethylene decomposition leads to the formation of the stable surface intermediate ethylidyne on the close-packed fcc (111) and hcp (0001) metal surfaces,[51,52] while adsorbed vinylic (vinyl or vinylidene) species seem to be more favorable intermediates only on the more open fcc (100) surfaces.[51−54] On the other hand, the density functional study of the ethylene dehydrogenation pathways over Pd(111)[55] has strongly suggested that the surface vinyl species is even formed on this closed packed surface, but it is unlikely to be detected spectroscopically because it quickly reacts along other surface reaction paths (e.g., rehydrogenation of ethylene or ethylidyne formation[56]). These theoretical results are corroborated by low-energy electron diffraction (LEED) analysis of ethylene decomposition over Pd(111) at low temperature,[57] which suggests the presence of ∼15% of tilted species in the surface layer having the same geometry of a di-σ ($\eta^1\eta^2$) vinyl surface species.

The surface vinyl species formation from adsorbed ethylene, instead, seems to be inhibited over PdAu(001) surface alloys due to the high activation barrier of this elementary step, as recently suggested by slab supercell calculations.[33] It is worthwhile underlining that surface oxygen and hydroxyl groups should be present in the reaction conditions of VAM synthesis[25] leading to water formation. Since surface oxygen atoms promote the β-hydrogen elimination from ethyl acetate-like species (in the Samanos-type mechanism), lowering the activation barrier,[34] these surface species should also facilitate the formation of surface vinyl species by hydrogen abstraction from ethylene (in the Moiseev-type mechanism). Therefore, the theoretical predictions on the adsorption properties of vinyl radical on PdAu surface alloys are not meaningless and have been carefully carried out in this study in order to be possibly compared with future experimental studies.

On the clean Pd(111) surface the vinyl species prefers to adsorb with an $\eta^1\eta^2$(C,C) fashion, showing an approximate sp^3 hybridization at each C atom with a BE of 56−61 kcal/mol, whereas the η^1-atop adsorption mode (sp^2) is less favorable by about 10 kcal/mol, as indicated by both periodic slab and cluster model calculations.[55] All attempts to find local minima related to the $\eta^1\eta^2$ adsorption mode of vinyl on the cluster models of PdAu(100) and PdAu(111) surfaces have been unsuccessful, indicating that the absence of contiguous Pd monomers determines the destabilization of such an $\eta^1\eta^2$ (C,C) adsorption.

The most stable adsorption mode of vinyl on second-neighbor Pd monomer pairs is the σ-bonded η^1-vinyl on top of Pd monomer (denoted as η^1-Pd) with the vinyl molecule vertically adsorbed. The full geometry optimizations starting from the η^1-bridge and η^1-hollow adsorption modes relax to the η^1-atop one. Besides, a stable η^1-vinyl species adsorbed on top of the Au atom (denoted as η^1-Au) has been obtained on both the PdAu(100) and PdAu(111) surfaces having an adsorption energy 10−11 kcal/mol lower than the η^1-Pd vinyl species.

The vinyl radical adsorption properties on the Pd monomers and the Au atoms of both Pd_2Au_{55} and Pd_2Au_{62} cluster models in the stable η^1-atop configurations are listed in Table 2.

For the η^1-atop adsorption mode, all the orientations of the C−C axis with respect to the surface directions have shown the same adsorption energy. The BEs for the η^1-Pd vinyl on PdAu(100) and PdAu(111) surfaces alloys are 44.1 and 41.4 kcal/mol, respectively. These values are slightly lower than the calculated value of 49.5 kcal/mol for the same adsorption mode on the Pd(111) clean surface.[55] Therefore, even if the ligand effect of gold weakens the interaction between the Pd atom and the adsorbed vinyl, this radical species remains strongly bonded to the surface alloys. The C−C bond distance in the adsorbed vinyl species is, in fact, elongated with respect to the gas-phase vinyl molecule (1.309 Å), becoming similar to that of the gas-phase ethylene (1.333 Å). The sp^2 hybridization of both the C atoms in the surface vinyl species is also revealed by the θ(PdCC) angle, whose values (around 127°) are close to the 120° of ethylene. The small values of the tilting angle ϕ_{tilt} (between 2° and 7°) confirm the planarity of the Pd−vinyl system, which always is perpendicular to the surface plane.

Due to the loss of symmetry by the presence of the Pd−C bond instead of the H−C bond and to the different adsorption modes of the ethylene and vinyl surface species, the calculated vibrational spectra for the η^1-vinyl adsorbed

Table 2. BSSE-Corrected Binding Energies (BE, in kcal/mol), Equilibrium Bond Distances (*d*, in Angstroms), Angles (θ and ϕ, in degrees), and Scaled Vibrational Frequencies (in cm^{-1}) of the η^1-Pd and η^1-Au Vinyl Surface Species on the Pd_2Au_{55}(24,21,12) and Pd_2Au_{62}(30,21,13) Cluster Models[a]

	PdAu(100)		PdAu(111)	
	η^1-Pd	η^1-Au	η^1-Pd	η^1-Au
BE	44.1	34.6	41.4	30.3
d(C−C)	1.336	1.331	1.333	1.338
d(S−C)	2.007	2.071	2.016	2.113
θ(SCC)	127.7	125.7	127.5	125.5
ϕ_{tilt}	6.9	2.3	1.6	7.8
$\nu(CH_2)$asymm + ν(CH)	3126(w)	3149(w)	3124(w)	3128(w)
$\nu(CH_2)$symm + $\nu(CH)_{in}$	3099(w)	3119(w)	3090(w)	3114(w)
$\nu(CH_2)$symm + $\nu(CH)_{out}$	3026(w)	3040(w)	3027(w)	3030(w)
ν(CC)	1561(s)	1580(s)	1560(s)	1551(s)
(CH_2) sciss	1356(m)	1366(m)	1352(m)	1361(m)
CH_2CH $rock_{in}$	1154(vs)	1174(vs)	1145(vs)	1177(vs)
CH_2CH $rock_{out}$	929(w)	948(w)	909(w)	954(w)
CH_2CH wag_{in}	905(m)	938(m)	901(m)	952(m)
CH_2CH wag_{out}	842(w)	877(w)	841(w)	895(w)
ν(S−C)	443(w)	475(w)	449(w)	437(w)

[a] The ϕ_{tilt} angle indicates the tilting angle between the vinyl molecular plane and the plane normal to the surface. S indicates the surface atom involved in the adsorption bond (Pd for η^1-Pd and Au for η^1-Au). ν: stretching. Subscript in and out indicate the in-phase and out-of-phase motions of the CH_2 and CH groups. (vs) very strong; (s) strong; (m) medium; (w) weak.

molecule are, obviously, different with respect to those calculated for the π-bonded adsorbed ethylene (compare Table 1 with Table 2). In particular, the main infrared feature for the η^1-Pd vinyl is calculated at 1154 and 1145 cm^{-1} on PdAu(100) and PdAu(111), respectively, and is associated with the in-phase rocking vibration of CH_2 and CH groups, whereas, as already discussed, the main peak of the π-bonded ethylene on the two surface alloys corresponds to the in-phase wagging of CH_2 groups and lies at 922 and 938 cm^{-1}, respectively.

For both PdAu surface alloys, a significant red shift of the vinyl vibration features with respect to the ethylene-adsorbed case has been observed in all regions of the calculated spectra. The C−C stretching and in-plane CH_2 bending modes are largely coupled in a wide-frequency range (1203−1607 cm^{-1}) for the π ethylene, whereas they are red shifted in the range 929−1561 cm^{-1} and become less coupled in the vibrational spectra of the adsorbed vinyl. Furthermore, the C−C stretching mode at about 1560 cm^{-1} appears to be particularly intense in the calculated vibrational spectra of surface vinyl species and should be clearly visible experimentally. The stretching modes of C−H bonds and the out-of-plane bending modes are generally red shifted by 50−100 cm^{-1}. The former modes move from 3080−3184 cm^{-1} in the π-bonded ethylene to 3026−3126 cm^{-1} in the η^1-Pd vinyl, whereas the latter ones move from 841−905 to 811−1005 cm^{-1}. The most consistent red shift has been observed for the Pd−C stretching and moves from 158−175 cm^{-1} for the weak π interaction of ethylene with Pd monomer to 443−449 cm^{-1} for the strong σ bond involved in the Pd−vinyl interaction.

Very similar adsorption geometries have been obtained for the η^1-vinyl adsorbed on Au atoms, as it is shown in Table 2. The main difference in the calculated vibrational spectra concerns a blue shift by 20−30 cm^{-1}, which should be experimentally detectable in the case of the most intense vibrational frequency.

3.3. Adsorption of Acetic Acid. Experimental studies have shown that acetic acid adsorbs molecularly on Pd(111) surfaces and forms η^2-acetate species on heating, even if the formation of η^1-acetate species has not been excluded.[58] In this section we focus on the adsorption of acetic acid molecules on PdAu surface alloys by comparing theoretical results and experimental data.

Indications on the adsorption features of intact acetic acid molecules on PdAu(111) come from RAIRS experiments combined with TPD data.[31] One of the main conclusions of the combined TPD and RAIRS experiments, carried out as a function of gold content, is that acetic acid adsorbs molecularly and desorbs intact for gold mole fractions greater than ∼0.5. TPD spectra collected as a function of gold coverage show that the presence of gold does not change significantly the desorption activation energy (at about 200 K) of the acetic acid intact molecules. Indeed, the acetic acid desorption from the monolayer on Pd-rich PdAu(111) surface[31] and clean Pd(111)[58] and Pd(100)[59] surfaces occurs at about 200 K corresponding to a desorption activation energy of about 12 kcal/mol.

The BE for a di-σ-(O,O)-bonded acetic acid molecule on bridge sites of Pd(111) surface, calculated by use of both cluster and periodic slab supercell models, is in the range of 4.8−6.0 kcal/mol[60] and underestimated with respect to the experimental desorption activation energy.[58] On both Pd and PdAu the predominant form of surface acetic acid species is surface catemers, and the nature of the catemer is gold coverage dependent.[31,58] Since in the theoretical models, both here and in previous studies on Pd surfaces,[60] only the monomeric acetic acid species have been considered, a perfect agreement between the theoretical and experimental results is unlikely.

The acetic acid molecule can adsorb on Pd surfaces in both monodentate and bidentate ways, but periodic slab model calculations[60] have indicated that the bidentate η^2-(O,O) surface species is more stable with respect to the monodentate η^1-(O_C) one (where O_C indicates the carbonyl oxygen atom involved in the Pd−O bond) on the Pd(111) surface.

In our study all possible adsorption geometries of acetic acid on second-neighbor Pd monomer pairs have been considered (see Figure 3). In particular, both the η^2-(O,O) atop (Pd-chelating) and the μ_2-η^2-(O,O) bridge (Pd−Au, not chelating) bidentate adsorption modes have been examined. All attempts to find stable adsorption states having these geometries have been unsuccessful, indicating that bidentate adsorption of acetic acid monomer on isolated Pd sites is really improbable. Moreover, the possibility to find a μ_2-η^2-(O,O)-CH_3COOH bonded to both second-neighbor Pd monomers can be excluded due to the too long Pd−Pd distance in these ensembles (at least 4.08 Å) with respect to the O−O distance in the acetic acid molecule (2.270 Å). All the η^2-CH_3COOH adsorption modes force the adsorbate to obtain its high-energy isomeric configuration (the cis conformer).

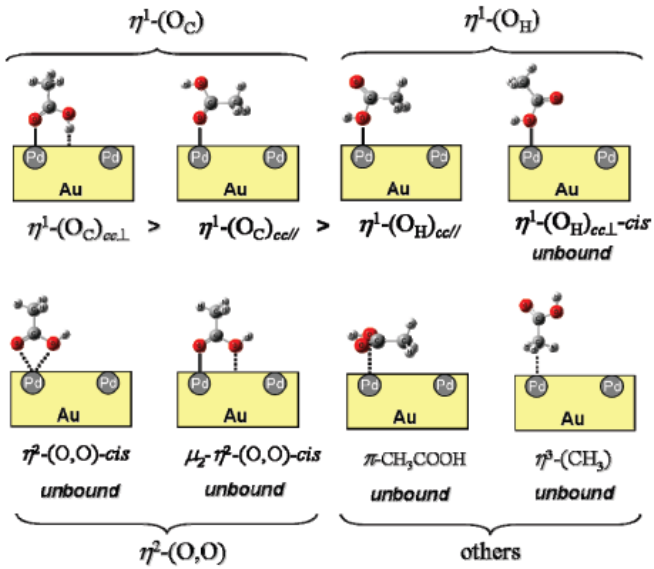

Figure 3. Adsorption geometries of acetic acid on second-neighbor Pd monomer pairs considered in this study. The stability trend on the PdAu surface alloys has been indicated. O_H and O_C specify the oxygen atom involved in the Pd−O bond in the monodentate adsorption, hydroxyl oxygen atom, and the carbonyl oxygen, respectively. The label *cis* indicates the less stable acetic acid conformer; *trans* is omitted.

Table 3. BSSE-Corrected Binding Energies (BE, in kcal/mol), Equilibrium Bond Distances (d, in Angstroms), Angles (θ, in degrees), and Scaled Vibrational Frequencies (in cm^{-1}) of the η^1 Adsorption Modes of Acetic Acid on the Pd_2Au_{55}(24,21,12) and Pd_2Au_{62}(30,21,13) Cluster Models[a]

			PdAu(100)			PdAu(111)		
	gas-phase CH_3COOH	exp[b]	η^1-$(O_C)_{cc\perp}$	η^1-$(O_C)_{cc//}$	η^1-$(O_H)_{cc//}$	η^1-$(O_C)_{cc\perp}$	η^1-$(O_C)_{cc//}$	η^1-$(O_H)_{cc//}$
BE		~12.0	9.0	5.1	2.9	5.6	3.0	2.1
d(Pd−O_C)			2.330	2.374		2.451	2.475	
d(Pd−O_H)					2.549			2.806
d(O−H)	0.980		1.011	0.991	0.988	1.010	0.990	0.990
d(H−S)			1.930		2.510	2.090		2.691
d(C−C)	1.513		1.508	1.501	1.504	1.510	1.504	1.509
d(C−O_C)	1.215		1.239	1.232	1.210	1.233	1.229	1.213
d(C−O_H)	1.365		1.332	1.346	1.388	1.338	1.350	1.376
θ(COH)	105.6		109.6	106.9	106.7	109.1	106.8	107.6
ν(O−H)	3622(m)		3243(vs)	3607(m)	3612(m)	3250(vs)	3611(m)	3607(m)
ν(C=O)	1820(s)	1720 (s)	1677(vs)	1714(vs)	1829(s)	1697(vs)	1727(vs)	1817(s)
$\delta_s(CH_3)$	1422(m), 1415(m)	1426 (br)	1420(w), 1410(m)	1435(m), 1415(m)	1412(m), 1402(m)	1422(w), 1411(m)	1431(m), 1413(m)	1422(m), 1414(m)
ν(C−O)	1371(m), 1309(m)	1294 (br)	1389(s), 1327(w)	1359(s), 1328(m)	1356(m), 1267(m)	1377(s), 1322(w)	1359(s), 1321(m)	1361(m), 1278(m)
γ(OH)	1184(s)	923/958 (s)	1201(m)	1199(s)	1151(s)	1199(m)	1197(s)	1148(s)
$\rho(CH_3)$	1035(m)	1052 (m)	1031(w)	1032(w)	1027(w)	1030(w)	1031(w)	1032(w)

[a] Geometrical parameters and vibrational frequencies for the free acetic acid molecule and available experimental data on PdAu(111) are reported for comparison. [b] Reference 31. ν, stretching; δ, deformation; γ, bending; ρ, rocking modes. For detailed assignments, see ref 61. (vs) very strong; (s) strong; (m) medium; (w) weak; (br) broad.

On the other hand, three monodentate adsorption modes are local minima having different stability on second-neighbor Pd monomer pairs. The adsorption properties of these monodentate acetic acid molecules are listed in Table 3.

Other explored adsorption geometries, such as those with the acetic acid molecular plane parallel to the surface or the methyl group forming a surface bond, are very unstable on the surface alloys studied here (Figure 3).

The monodentate CH_3COOH can bond to the Pd monomers through the hydroxyl oxygen atom (O_H) or the carbonyl oxygen (O_C). On both PdAu(100) and PdAu(111), the η^1-(O_C)-CH_3COOH geometry is more stable than the η^1-(O_H)-CH_3COOH (see Figure 3).

In particular, the η^1-(O_C)-CH_3COOH having the C−C axis perpendicular to the surface plane (denoted as η^1-$(O_C)_{cc\perp}$) is the most stable adsorption state and shows BE values of 5.6

and 9.0 kcal/mol on the PdAu(111) and (100) surfaces, respectively.

In this adsorption geometry the O−H bond points to the hollow site of the surface, forming a very weak hydrogen bond with the gold surface that to some extent stabilizes this adsorption state. The O−H bond is, in fact, slightly elongated to 1.010 Å with respect to the 0.980 Å of the free acetic acid molecule.

The hydrogen−surface distances are about 2.0 Å on both surface alloys, indicating that this adsorption state should also facilitate hydrogen abstraction from acetic acid, leading to the formation of surface acetate species.

The contributions to the adsorbate−surface bonds in the η^1-$(O_C)_{cdl}$ and η^1-$(O_H)_{cdl}$ surface species are the weak interactions between the Pd surface atom and the sp^2 and sp^3 oxygen lone pairs of carbonyl and hydroxyl oxygen atoms, respectively. Indeed, on both PdAu surface alloys the binding energies of η^1-$(O_C)_{cdl}$ and η^1-$(O_H)_{cdl}$ adsorption states are 2−3 kcal/mol lower than the BEs of η^1-$(O_C)_{cc\perp}$, suggesting that the hydrogen−surface bond in the latter geometry has this strength. The η^1-$(O_H)_{cc\perp}$-CH_3COOH is not stable on the surface alloys because in this adsorption geometry the acetic acid molecule is forced in its *cis* isomeric configuration.

Let us compare now the calculated vibrational spectra of the stable η^1-CH_3COOH adsorption states with the RAIRS spectra collected from the adsorption of acetic acid on the Au-rich PdAu(111) surface alloys[31] and with the gas-phase free molecule vibrations, see Table 3.

First, in the experimental RAIRS spectra[31] two main features appear at 1720 and 923 cm^{-1} corresponding to the carbonyl C−O stretching, denoted as ν(C═O), and the hydroxyl group bending motions, denoted as γ(OH), respectively. The calculated ν(C═O) frequencies for both the η^1-$(O_C)_{cdl}$ and the η^1-$(O_H)_{cc\perp}$ adsorption states show strong intensities at 1697−1727 cm^{-1}, in accordance with the observed experimental features. On the contrary, for η^1-(O_H)-CH_3COOH the carbonyl C−O stretching is almost 100 cm^{-1} blue shifted (1817 cm^{-1}), becoming very similar to the ν(C═O) in the free acetic acid molecule (1820 cm^{-1}).

On the other hand, the calculated γ(OH) bending frequencies of all the stable η^1-CH_3COOH adsorption states are close to those of gas-phase acetic acid (at 1184 cm^{-1}) and therefore far away from the experimentally observed features between 923 and 958 cm^{-1}. This result comes as no surprise since the RAIRS peaks in this spectral region are exclusively due to the presence of catemeric and dimeric acetic acid species that form on PdAu(111) surface alloy at the considered acetic acid coverage (i.e., 1.2 L). Although it is not the aim of the present paper to follow the variation of the vibrational frequencies of acetic acid due to formation of dimeric or catemeric species, we carried out a test calculation on the acetic acid dimer on the PdAu(111) surface. The calculated γ(OH) bending frequency for one of the possible acetic acid dimer configurations is 942 cm^{-1}, which falls in the range of the experimental values.

Moreover, the C−O_H stretching and the symmetric deformation of the CH_3 group, denoted as ν (C−O) and $\delta_s(CH_3)$, respectively, appear as broad RAIRS peaks at 1294 and 1426 cm^{-1}, and this is in good agreement with the calculated spectra. For all the adsorption states, in fact, these two vibrational modes have medium intensities and are strongly coupled in a wide frequency range between 1267 and 1435 cm^{-1}.

Finally, the stretching mode of the hydroxyl group, ν(O−H), has not been observed in the RAIRS spectra collected for the PdAu(111) surface alloy, while in the HREELS spectra of acetic acid adsorbed on Pd(111) surface[62] a broad peak at 2525 cm^{-1} has been assigned to this stretching mode. The large frequency shift of this mode with respect to the gas-phase acetic acid molecule (calculated at 3622 cm^{-1}) has been suggested to be indicative of the formation of catemers on the clean Pd surface. In the calculated vibrational spectra, as expected, this large frequency shift is not observed. The ν(O−H) vibrations lie at about 3610 cm^{-1} for the η^1-$(O_C)_{cdl}$ and the η^1-$(O_H)_{cdl}$ surface species. For the η^1-$(O_H)_{cc\perp}$-CH_3COOH, where a weak hydrogen bond is involved, a significant red shift has been observed in the 3243−3250 cm^{-1} range.

The theoretical cluster model results, therefore, confirm the RAIRS assignments of the ν(C═O), ν(C−O), and $\delta_s(CH_3)$ modes and support the indication of acetic acid catemers formation on PdAu surface alloys because surface acetic acid monomers do not show essential features at 920−960 and ca. 2525 cm^{-1} corresponding to the hydroxyl γ(OH) and ν(O−H) vibrational modes, respectively.

3.4. Adsorption of Acetate. The surface chemistry of acetic acid has been studied on a number of single-crystal surfaces including Pd(111),[58] Pd(110),[63] and clean and oxygen-covered Pd(100)[59] and Pd−Au alloys.[25,29,31] These experiments have indicated that acetate surface species are easily formed, even at room temperature, after acetic acid adsorption on the Pd and PdAu surfaces. Both mono- and bi-dentate spectroscopically detected acetate surface species can decompose to form CO and CO_2 or rehydrogenate to give acetic acid again. The role of Au addition to Pd surfaces is to stabilize the adsorbed acetic acid and acetate surface species by decreasing their decomposition tendency.

Theoretical studies combined with LEED measurements have shown that the preferred adsorption mode of acetate on Pd(111) surface is the bidentate species di-σ-bonded to two Pd atoms on a bridge site having the C−C axis perpendicular to the surface.[64] Binding energies of 50.7 and 52.6 kcal/mol have been calculated by use of cluster and slab supercell models, respectively.[60]

Periodic slab supercell calculations performed on second-neighbor Pd monomer pairs of PdAu(001)[34] surface alloy have shown that the preferred adsorption mode of the acetate is the di-σ-bonded on the PdAu bridge site, denoted as η^2-(O,O), having a BE equal to 47.5 kcal/mol. The π-bonded geometry, with both oxygen atoms bonded to Pd monomer in a bidentate chelating fashion, is less stable by about 13 kcal/mol.

According to these slab supercell calculations, metastable states with chelating geometry that lie approximately 11−12 kcal/mol higher in energy than the corresponding bridge adsorptions have been found on both PdAu(111) and PdAu(100) surfaces by use of cluster models. However, they

Table 4. BSSE-Corrected Binding Energies (BE, in kcal/mol), Equilibrium Bond Distances (*d*, in Angstroms), and Scaled Vibrational Frequencies (in cm^{-1}) of the η^1- and η^2-Acetate on the Pd_2Au_{55}(24,21,12) and Pd_2Au_{62}(30,21,13) Cluster Models[a]

	adsorption mode	BE	d(Pd−O_1)	d(Au−O_2)	d(C−C)	d(C−O_1)	d(C−O_2)
PdAu(100)	η^2-(O,O)	46.4	2.135	2.271	1.523	1.273	1.271
	η^1-(O)	30.5	2.114		1.514	1.321	1.234
slab supercell[b]	η^2-(O,O)	47,5	2.134	2.243			
PdAu(111)	η^2-(O,O)	34.1	2.145	2.356	1.525	1.281	1.265
	η^1-(O)	16.6	2.128		1.512	1.314	1.238

	adsorption mode	ν_{as}(OCO)	ν_s(OCO)	δ_{as}(CH_3)
PdAu(100)	η^2-(O,O)	1482 (m) +24]	1327 (s) [-5]	1417−1437 (m) [+4]
	η^1-(O)	1613 (s)	1210 (w)	1403−1425(m)
PdAu(111)	η^2-(O,O)	1480 (w) [+23]	1315 (s) [−2]	1421−1439 (w) [+4]
	η^1-(O)	1597 (s)	1232 (w)	1410−1434 (m)
PdAu(111) RAIRS[c]	η^2-(O,O)		∼1402(s)	
	η^1-(O)	∼1653 (s)		1426 (s)
PdAu(111) HREELS[d]	η^2-(O,O)	1420(br)		

[a] Differences between negatively charged ($q = -1$) and neutral acetate/cluster systems are reported in brackets. (s) strong; (m) medium; (w) weak; (br) broad. ν_{as} asymmetric stretching; ν_s symmetric stretching; δ deformation; γ bending; ρ rocking modes. [b] Reference 34. [c] Reference 31. [d] References 25 and 29.

do not result as stable local minima because they easily relax to the more stable PdAu-bridge site geometries.

Since the η^1-acetate, which can be spectroscopically distinguished from the bidentate η^2-species, has been experimentally observed to be a stable surface species, the monodentate adsorption mode, denoted as η^1-(O), has also been considered in this study. The adsorption properties, including binding energies, geometrical parameters, and vibrational frequencies, of both bidentate and monodentate modes are listed in Table 4.

It is necessary to underline that the acetate molecule has two stable rotamers having one of the HCC planes perpendicular (staggered) or parallel (eclipsed) to the OCO plane. As already shown for the adsorption of acetate on Au[65] and Ag[66] surfaces, the internal rotation of methyl group has a marginal influence on the calculated vibrational spectra. Therefore, only the more stable staggered isomer has been considered in this study.

η^2-(O,O) is strongly bonded to the palladium−gold surface alloys with binding energies of 46.4 and 34.1 kcal/mol for PdAu(100) and PdAu(111), respectively. The former BE value is in very good agreement with the previous calculated BE on PdAu(100) by the slab supercell approach,[34] while the lower BE value for the more dense PdAu(111) surface is in line with the results obtained for the other adsorbates studied here. According to the decrease of the binding energy, the Pd−O and Au−O distances increase from 2.135 to 2.145 Å and 2.271 to 2.356 Å for the PdAu(100) and the PdAu(111) surfaces, respectively.

The BE differences between the η^2-(O,O) bridge and the η^1-(O) on top adsorptions are around 16−18 kcal/mol, indicating that monodentate acetate is significantly less stable than the bidentate one on PdAu surface alloys. The only stable monodentate adsorption state has the C−C axis parallel to the surface plane.

Despite this trend in BE, shorter Pd−O bond lengths have been observed in the η^1-(O)-acetate (2.114 and 2.128 Å for the PdAu(100) and PdAu(111), respectively) with respect to the η^2-(O,O)-acetate (2.135 and 2.145 Å, respectively). These results suggest that the Au−O bond provides an important contribution to the chemisorption bond of the bidentate surface species. This argument is important since the bidentate adsorbed acetate is a key surface species in the VAM synthesis on PdAu surfaces.[25] The presence of the Au−O bond in the adsorbed surface acetate can offer further (or different) explanations for the promotional role of gold in these Pd-based catalysts and for the different reactivity observed on PdAu(100) and PdAu(111) surfaces. Indeed, the breaking of the Au−O bond instead of the Pd−O bond in the ethylene−acetate coupling reaction on PdAu(001) has been indicated as the primary motivation of the higher reactivity of second-neighbor Pd pairs with respect to contiguous Pd ensembles.[34]

Let us consider now the calculated vibrational spectra of the bidentate and monodentate acetate surface species that can be compared with previous RAIRS[31] and HREELS[25,29] experiments. The major infrared features for the surface acetate species that generally allow distinguishing between bidentate and monodentate species are the symmetric and asymmetric stretching frequencies of the carboxylic group, namely, ν_s(OCO) and ν_{as}(OCO), and the asymmetric deformations of the CH_3 group, i.e., δ_{as}(CH_3).

In the RAIRS experiments the bidentate acetate has been recognized following the ν_s(OCO) symmetric stretching feature at about 1400 cm^{-1}, whereas in the HREELS spectra a broader peak centered at 1420 cm^{-1}, assigned to the coupled (OCO) stretching frequencies and CH_3 deformation modes, has been observed. This difference can be ascribed to the compositions of the surface alloys in these experiments, namely, Pd-rich surfaces in RAIRS (the η^2-acetate is detected only at a Au mole fraction < 0.33)[31] and isolated Pd sites in HREELS.[25,29]

The calculated ν_s(OCO) stretching frequencies on PdAu surfaces are shifted to lower frequencies, at 1315−1327 cm^{-1}, with respect to the experimental features for bidentate acetate, at about 1400 cm^{-1}. On both clean Pd surfaces[58] and Pd-rich PdAu alloys[31] as well as on clean Au surfaces[65] the observed and calculated ν_s(OCO) stretching frequencies

lie at about 1400 cm^{-1}. The difference between the asymmetric di-σ bonds on the Pd−Au bridge site (see Pd−O and Au−O distances in Table 4) and the symmetrical di-σ bonds on the homonuclear Pd−Pd and Au−Au bridge sites can explain this discrepancy. In fact, the calculated ν_s(OCO) at 1315−1327 cm^{-1}, the $\delta_{as}(CH_3)$ in the 1417−1439 cm^{-1} frequency range, and the ν_{as}(OCO) at about 1480 cm^{-1} (see Table 4) are in good agreement with the broad HREELS band of the "ν (OCO) + $\delta(CH_3)$" modes, centered at 1420 cm^{-1}, observed for the Pd isolated sites.[25,29]

The formation of monodentate acetate on PdAu(111) has been recognized by RAIRS experiments[31] by means of two features at 1653 and 1426 cm^{-1} assigned to the asymmetric ν_{as}(OCO) stretching and the asymmetric methyl deformation $\delta_{as}(CH_3)$, respectively.

In accordance with Tysoe et al.[31] we found that in the monodentate adsorption mode the C−C axis is parallel to the surface plane. Indeed, the asymmetric CH_3 deformation modes lie at 1403−1434 cm^{-1} (about 1426 cm^{-1} in the RAIRS experiments), whereas the symmetric $\delta_s(CH_3)$ deformations are very weak and lie at about 1350 cm^{-1}.

The ν_{as}(OCO) stretching frequencies in the η^1-acetate become strong in intensity and blue shifted to 1597−1613 cm^{-1} with respect to those of the bidentate acetate.

For the most stable η^2-(O,O) adsorption states on PdAu(100) and PdAu(111) surfaces, both the radical and anionic acetate species have been considered in order to evaluate the effect of surface acetate species discharge on the vibrational properties. As already obtained for acetate adsorption on gold[65] and silver[66] surfaces the frequency shifts due to the cluster charge variation are small for the ν_s(OCO) stretching frequencies (~20 cm^{-1}) and negligible for the $\delta_{as}(CH_3)$ modes (2−5 cm^{-1}).

4. Conclusions

In this work we studied the adsorption properties of ethylene, vinyl, acetic acid, and acetate species on the PdAu(111) and PdAu(100) surface alloys by the density functional cluster model approach. In particular, cluster models have been built up to represent second-neighbor Pd pairs on both surfaces since these are the critical Pd ensembles in the vinyl acetate monomer synthesis, which involves the surface species under study.

In accordance with experimental evidence and previous slab supercell calculations, our cluster model study has shown that ethylene is π bonded on Pd monomers, whereas acetate adsorbs in a bidentate fashion on a palladium−gold bridge site.

The presence of a gold−oxygen bond in the adsorbed surface acetate is confirmed by our cluster model results and should stimulate further rationalizations of the promotional role of gold in the PdAu-catalyzed VAM synthesis.

The calculated binding energies for ethylene and acetate are in very good agreement with preceding slab supercell calculations on the PdAu(100) surface, and the calculated vibrational spectra confirm the experimental frequency assignments, giving more details regarding all the involved vibrational modes.

Even if the surface vinyl species has not been detected on PdAu surface alloys, theoretical predictions on the adsorption properties of the vinyl radical on second-neighbor Pd pairs have been reported in order to be possibly compared with future experimental studies. The surface vinyl species has shown, in fact, strong interactions with Pd monomers and also with Au surface atoms. The calculated vibrational spectra are quite different from those of the adsorbed ethylene molecules.

Density functional cluster model results on the adsorption of acetic acid monomers have confirmed the experimental assignments of the major vibrational modes in the infrared spectra, supporting the indication that acetic acid catemers form on PdAu surface alloys. However, at very low acetic acid coverages, monomeric species should be present on PdAu surfaces, and our results suggest that it adsorbs in a monodentate fashion, forming a weak hydrogen bond with the surface.

In general, the adsorption of all molecules on the bimetallic PdAu surfaces is a less efficient process with respect to the clean Pd surfaces. The ligand effect of the gold atoms surrounding the Pd monomers lowers the adsorption energies. This effect is more pronounced for the more dense PdAu(111) surface alloy.

Finally, the adopted cluster models have been demonstrated to be sufficiently reliable by giving accurate results on the adsorption properties, including binding energies, preferred adsorption sites, stable bonding modes, geometrical parameters, and vibrational frequencies, in full agreement with available slab supercell calculations and the experimental evidence.

Acknowledgment. The authors thank the Università della Calabria for financial support.

References

(1) Sinfelt, J. H. *Bimetallic Catalysts: Discoveries, Concepts and Applications*; Wiley: New York, 1983.

(2) Somorjai, G. *Introduction to Surface Chemistry and Catalysis*; John Wiley & Sons: New York, 1994.

(3) Rodriguez, J. A. *Surf. Sci. Rep.* **1996**, *24*, 223–287.

(4) Moss, R. L.; Whally, L., *Advances in Catalysis*; Academic Press: New York, 1972.

(5) Baddeley, C. J.; Tikhov, M.; Hardacre, C.; Lomas, J. R.; Lambert, R. M. *J. Phys. Chem.* **1996**, *100*, 2189–2194.

(6) Baddeley, C. J.; Ormerod, R. M.; Stephenson, A. W.; Lambert, R. M. *J. Phys. Chem.* **1995**, *99*, 5146–5151.

(7) Han, Y. F.; Kumar, D.; Goodman, D. W. *J. Catal.* **2005**, *230*, 353–358.

(8) Enache, D. I.; Edwards, J. K.; Landon, P.; Solsona-Espriu, B.; Carley, A. F.; et al. *Science* **2006**, *311*, 362–365.

(9) Trimm, D. L.; Önsan, Z. I. *Catal. Rev.* **2001**, *43*, 31–84.

(10) Bonarowska, M.; Malinowski, A.; Juszczyk, W.; Karpinski, Z. *Appl. Catal., B* **2001**, *30*, 187–193.

(11) Li, Z.; Gao, F.; Wang, Y.; Calaza, F.; Burkholder, L.; Tysoe, W. T. *Surf. Sci.* **2007**, *601*, 1898–1908.

(12) Yi, C. W.; Luo, K.; Wei, T.; Goodman, D. W. *J. Phys. Chem. B* **2005**, *109*, 18535–18540.

(13) Legawiec-Jarzyna, M.; Srebowata, A.; Karpinski, Z. *React. Kinet. Catal. Lett.* **2003**, *79*, 157–161.

(14) Venezia, A. M.; La Parola, V.; Pawelec, B.; Fierro, J. L. G. *Appl. Catal., A* **2004**, *264*, 43–51.

(15) Maroun, F.; Ozanam, F.; Magnussen, O. M.; Behm, R. J. *Science* **2001**, *293*, 1811–1814.

(16) Sarkany, A.; Horvath, A.; Beck, A. *Appl. Catal., A* **2002**, *229*, 117–125.

(17) Hilaire, L.; Legare, P.; Holl, Y.; Maire, G. *Surf. Sci.* **1981**, *103*, 125–140.

(18) Jablonski, A.; Overbury, S. H.; Somorjai, G. A. *Surf. Sci.* **1977**, *65*, 578–592.

(19) Provine, W. D.; Mills, P.; Lerov, J. J. *Stud. Surf. Sci. Catal.* **1996**, *101*, 191–200.

(20) Samanos, B.; Boutry, P.; Montarnal, R. *J. Catal.* **1971**, *23*, 19–30.

(21) Moiseev, I.; Vargaftic, M. N.; Syrkin, Y. L. *Dokl. Akad. Nauk SSSR* **1960**, *133*, 377–380.

(22) Moiseev, I. *Catalytic Oxidation*; Sheldon, R. A., Ed.; World Scientific, 1995; p 203.

(23) Nakamura, S.; Yasui, T. *J. Catal.* **1970**, *17*, 366–374.

(24) Stacchiola, D.; Calaza, F.; Burkholder, L.; Tysoe, W. T. *J. Am. Chem. Soc.* **2004**, *126*, 15384–15385.

(25) Chen, M.; Kumar, D.; Yi, C. W.; Goodman, D. W. *Science* **2005**, *310*, 291–293, including supporting online material.

(26) Han, P.; Axnanda, S.; Lyubinetsky, I.; Goodman, D. W. *J. Am. Chem. Soc.* **2007**, *129*, 14355–14361.

(27) Luo, K.; Wei, T.; Yi, C. W.; Axnanda, S.; Goodman, D. W. *J. Phys. Chem. B* **2005**, *109*, 23517–23522.

(28) Calaza, F.; Gao, F.; Li, Z.; Tysoe, W. T. *Surf. Sci.* **2007**, *601*, 714–722.

(29) Chen, M. S.; Luo, K.; Wei, Z.; Yan, Z.; Kumar, D.; Yi, C. W.; Goodman, D. W. *Catal. Today* **2006**, *117*, 37–45.

(30) Owens, T. G.; Jones, T. E.; Noakes, T. C. Q.; Bailey, P.; Baddeley, C. J. *J. Phys. Chem. B* **2006**, *110*, 21152–21160.

(31) Calaza, F.; Gao, F.; I, Z; Tysoe, W. T. *Surf. Sci.* **2007**, *601*, 1351–1357.

(32) García-Mota, M.; Lopez, N. *J. Am. Chem. Soc.* **2008**, *130*, 14406–14407.

(33) Yuan, D.; Gong, X.; Wu, R. *Phys. Rev. B* **2007**, *75*, 233401–233404.

(34) Yuan, D.; Gong, X.; Wu, R. *J. Phys. Chem. C* **2008**, *112*, 1539–1543.

(35) Mazzone, G.; Rivalta, I.; Russo, N.; Sicilia, E. *J. Phys. Chem. C* **2008**, *112*, 6073–6081.

(36) Ahlrichs, R.; Bär, M.; Häser, M.; Horn, H.; Kölmel, C. *Chem. Phys. Lett.* **1989**, *162*, 165–169.

(37) Becke, A. D. *Phys. Rev. A* **1988**, *38*, 3098–3100.

(38) Perdew, J. P. *Phys. Rev. B* **1986**, *33*, 8822–8824.

(39) Eichkorn, K.; Treutler, O.; Öhm, H.; Häser, M.; Ahlrichs, R. *Chem. Phys. Lett.* **1995**, *240*, 283–289.

(40) Eichkorn, K.; Weigend, F.; Treutler, O.; Ahlrichs, R. *Theor. Chem. Acc.* **1997**, *97*, 119–124.

(41) Andrae, D.; Hæussermann, U.; Dolg, M.; Stoll, H.; Preuss, H. *Theor. Chim. Acta* **1990**, *77*, 123–141.

(42) Schäfer, A.; Huber, C.; Ahlrichs, R. *J. Chem. Phys.* **1994**, *100*, 5829–5835.

(43) Boys, S. F.; Bernardi, F. *Mol. Phys.* **1970**, *19*, 553–566.

(44) Neugebauer, J.; Hess, B. A. *J. Chem. Phys.* **2003**, *118*, 7215–7225.

(45) Ge, Q.; Neurock, M. *Chem. Phys. Lett.* **2002**, *358*, 377–382.

(46) Neurock, M.; van Santen, R. A. *J. Phys. Chem. B* **2000**, *104*, 11127–11145.

(47) Mei, D.; Hansen, E. W.; Neurock, M. *J. Phys. Chem. B* **2003**, *107*, 798–810.

(48) Yuan, D.; Gong, X.; Wu, R. *Phys. Rev. B* **2007**, *75*, 085428–085432.

(49) Dewar, M. J. S. *Bull. Soc. Chim. Fr.* **1951**, *18*, C71–C79.

(50) Chatt, J.; Duncanson, L. A. *J. Chem. Soc.* **1953**, *75*, 2939–2947.

(51) Masel, R. I. *Principles of Adsorption and Reaction on Solid Surfaces*; John Wiley and Sons: New York, 1996.

(52) Yagasaki, E.; Masel, R. *Catalysis* **1994**, *11*, 165–222.

(53) Stuve, E. M.; Madix, R. J. *J. Phys. Chem.* **1985**, *89*, 105–112.

(54) Zaera, F.; Hall, R. B. *Surf. Sci.* **1987**, *180*, 1–18.

(55) Pallassana, V.; Neurock, M.; Lusvardi, V. S.; Lerou, J. J.; Kragten, D. D.; van Santen, R. A. *J. Phys. Chem. B* **2002**, *106*, 1656–1669.

(56) Azad, S.; Kaltchev, M.; Stacchiola, D.; Wu, G.; Tysoe, W. T. *J. Phys. Chem. B* **2000**, *104*, 3107–3115.

(57) Stacchiola, D.; Calaza, F.; Zheng, T.; Tysoe, W. T. *J. Mol. Catal A: Chem.* **2005**, *228*, 35–45.

(58) Haley, R. D.; Tikhov, M. S.; Lambert, R. M. *Catal. Lett.* **2001**, *76*, 125–130.

(59) Li, Z.; Gao, F.; Tysoe, W. T. *Surf. Sci.* **2008**, *602*, 416–423.

(60) Pallassana, V.; Neurock, M. *J. Catal.* **2002**, *209*, 289–305.

(61) Burneau, A.; Génin, F.; Quilès, F. *Phys. Chem. Chem. Phys.* **2000**, *2*, 5020–5029.

(62) Davis, J. L.; Barteau, M. A. *Langmuir* **1989**, *5*, 1299–1309.

(63) Bowker, M.; Morgan, C.; Couves, J. *Surf. Sci.* **2004**, *555*, 145–156.

(64) James, J.; Saldin, D. K.; Zheng, T.; Tysoe, W. T.; Sholl, D. S. *Catal. Today* **2005**, *105*, 74–77.

(65) Bernà, A.; Delgado, J. M.; Orts, J. M.; Rodes, A.; Feliu, J. M. *Electrochim. Acta* **2008**, *53*, 2309–2321.

(66) Delgado, J. M.; Rodes, A.; Orts, J. M. *J. Phys. Chem. C* **2007**, *111*, 14476–14483.

CT9000137

Pubblicazione III

Adsorption of Ethylene, Vinyl, Acetic Acid, and Acetate Species on Pd$_{Au}$(111) and Pd$_{Au}$(100) Surface Alloys: A Cluster Model Study

Ivan Rivalta, Gloria Mazzone, Nino Russo, Emilia Sicilia

J. Chem. Theory Comput. **2009**, Vol. 5, No. 5, 1350-1360

COMMUNICATION www.rsc.org/chemcomm | ChemComm

The geometric effect in palladium–gold catalysis. Is the coupling the rate-determining step in the vinyl-acetate synthesis?†

Gloria Mazzone, Ivan Rivalta, Nino Russo* and Emilia Sicilia*

Received (in Cambridge, UK) 5th January 2009, Accepted 26th January 2009
First published as an Advance Article on the web 20th February 2009
DOI: 10.1039/b823207e

First-principles calculations support the hypothesis that the appropriate spacing between Pd monomers controls the catalytic activity of Pd/Au catalysts in the vinyl acetate formation only if a vinyl surface species is involved in the rate-determining step of the reaction, opening new questions on these relevant catalytic systems.

Since gold catalysis manifests itself only under quite specific circumstances,[1,2] the interest in the gold catalytic power has dramatically grown only in the last twenty years. For example, gold has demonstrated industrial potential with its use in the production of vinyl acetate monomer (VAM) as a component of bimetallic catalysts due to the ability of Pd–Au catalyst to significantly improve the reactivity in comparison to pure Pd catalysts.[3–5] Although acetoxylation of ethylene on Pd–Au bimetallic silica-supported catalysts promoted with potassium acetate (KOAc) is a mature commercial process for VAM synthesis,[6–10] many details concerning the reaction mechanism and the surface reaction site, as well as the promotional role played by gold have not yet been elucidated.

Theoretical investigations are essential towards providing a better microscopic understanding of the catalytic activity of bimetallic systems and, moreover, to supply additional information for the rational design of robust bimetallic catalysts.

Two reaction mechanisms are proposed for VAM synthesis. The first proposed by Samanos *et al.* involves the coupling of ethylene with adsorbed acetate to form, as an intermediate, ethyl-acetate that undergoes β-H elimination to form VAM.[8] Alternatively, as suggested by both Moiseev[11,12] and Nakamura and Yasui[7] ethylene could adsorb and subsequently dehydrogenate to form a vinyl species, which then couples with the co-adsorbed acetate to give VAM directly. Both mechanisms, the former designated as the Samanos-type and the latter as the Moiseev-type, assume that the coupling of a surface ethylenic and acetate species is the rate determining step for VAM formation. Although support for the Samanos-type mechanism comes from a recent experimental study by Tysoe *et al.*[13] on the VAM synthesis on Pd(111) clean surface, many details of the reaction mechanism remain uncertain.

Goodman and co-workers[14] have investigated the promotional effect of gold in palladium Pd–Au alloy catalysts and invoked ensemble effects to explain the significant enhancement of the VAM formation rate on Pd/Au(100) compared with Pd/Au(111). They have demonstrated that the critical ensemble for VAM formation on a Pd/Au(100) surface alloy is a pair of non-contiguous, suitably spaced, Pd monomers. It should be, indeed, the distance between Pd atoms that controls the catalytic formation of VAM by PdAu catalysts lowering the barrier of the rate determining step. The pair of isolated Pd sites has also been proposed to suppress the undesirable formation of reaction by-products, such as CO, CO_2 and surface carbon, thus improving the overall selectivity.

In an attempt to interpret the experimental results outlined above and to provide further insight into the elementary steps of the VAM formation mechanism, we report here the outcome of a theoretical density functional (DF) cluster model study of VAM synthesis. Specifically, the key step involving coupling of the surface reacting species for both Samanos- and Moiseev-type mechanisms on both Pd/Au(111) and Pd/Au(100) surface alloys has been examined in detail.

A cluster model approach has been chosen to properly reproduce those contributions to the adsorbate–substrate interaction, which are due to local changes in the substrate electronic structure. Computational details, along with the strategy used to select the size of the clusters and the computational protocol,[15] are presented in the ESI.†

In the framework of DF calculations, the periodic supercell approach using plane-waves has already been applied to PdAu surface alloys for the study, on the Pd/Au(100) surface, of both the ethylene dehydrogenation[16] and of the three separate steps of the Samanos mechanism: coupling of ethylene and acetate, β-H elimination, and VAM desorption.[17]

As a result of such calculations, the conclusion the authors come to is that the Samanos-type mechanism is the most probable one. Indeed, on Pd/Au(100), it appears that dehydrogenation of ethylene does not occur and becomes the rate-determining step of the Moiseev mechanism. On the contrary, the energy barriers are low for both ethylene and acetate coupling and β-H elimination steps. In the latter case, the barrier further lowers in presence of oxygen, according to experimental detections.[14] Very recently a new paper has appeared in the literature concerning the same topic.[18] Assuming the Samanos-type mechanism as the preferred one, the authors have theoretically investigated, by using a plane-waves slab supercell approach, the steps of the reaction mechanism on both (100) and (111) surfaces. Work comparing potential energy surfaces for both mechanisms on both surfaces at the same level of theory has not been carried out until now.

We have started our investigation comparing on both the (100) and (111) exposed gold surfaces the rate-determining step of the Samanos mechanism, which involves the coupling of ethylene directly with chemisorbed acetate, on the critical ensemble represented by a pair of non-contiguous Pd monomers.

A plot of the potential energy surface for the coupling step on both Pd/Au(100) and Pd/Au(111) is shown in Fig. 1.

Dipartimento di Chimica, Università della Calabria, 87036 Arcavacata di Rende (CS), Italy. E-mail: nrusso@unical.it. E-mail: siciliae@unical.it
† Electronic supplementary information (ESI) available: Computational details. See DOI: 10.1039/b823207e

Selected geometrical parameters of optimized structures for co-adsorbed ethylene and acetate, transition states and ethyl-acetate like intermediates are reported in Table 1. At a first glance, it clearly appears from the data in Table 1 that the geometrical parameters that we can consider critical for the transition state formation show similar changes on both Pd/Au(100) and Pd/Au(111). Initially, ethylene is only weakly π-bonded to the Pd monomer and its C–C bond is only slightly longer than gas-phase value (1.333 Å). Acetate adsorbs in a di-σ configuration with the two oxygen atoms bound separately on one Pd and one Au atom of the substrate. In the transition state, owing to the forthcoming insertion of ethylene into the adsorbed acetate, the bond of the closest ethylene carbon (C_1 in Scheme 1) with the palladium monomer is broken and the carbon hybridization is switching from sp^2 to sp^3. On the other hand, the bonds of acetate oxygen atoms with gold and palladium atoms weaken only slightly while the molecule turns around the Pd_2–O_1 bond of few degrees approaching the adjacent ethylene molecule. The C_1–O_2 distance shortens and the bond begins to form. The calculated energy barriers that it is necessary to overcome in order to obtain the ethyl-acetate product are 21.5 and 19.2 kcal mol^{-1} on Pd/Au(100) and Pd/Au(111) surface alloys, respectively. All the pending changes in the transition state become definitive in the ethylacetate product as shown in Table 1. It is worth underlining that the value of 21.5 kcal mol^{-1} calculated for the activation energy on Pd/Au(100) is close enough to the theoretical value (26.9 kcal mol^{-1}) found by Yuan *et al.*[17] The results outlined above are inconsistent with the proposed speculation that the optimum distance between the Pd monomers, which promotes the coupling of reacting species on the exposed gold surfaces, could be responsible for the enhanced VAM formation rate on Pd/Au(100) compared with Pd/Au(111). Indeed, the height of the barriers is comparable as well as the values of the critical geometrical parameters of the transition state structures show very similar changes. We have carried out an analogous exploration, on both Pd/Au(100) and Pd/Au(111) surface alloys, of the coupling step for the Moiseev-type mechanism, which involves a vinyl species interacting with an adsorbed acetate species to form VAM.

A plot of the energy changes, along the Langmuir–Hinshelwood-type pathway that leads from the co-adsorbed vinyl and acetate moieties to the formation of vinyl acetate, is shown in Fig. 2 for both Pd/Au(100) and Pd/Au(111) surface alloys. The most significant geometrical parameters of reactants, transition states and products are reported in the same Table 1.

Table 1 Selected geometrical parameters (bond lengths (Å) and angles (°)) of reactants (R, R′), TS and product (P, P′) for the coupling step between ethyl and acetate (Samanos-type mechamism) and vinyl and acetate (Moiseev-type mechamism) on both Pd/Au(100) (left) and Pd/Au(111) surface alloys.

	Pd/Au(100)			Pd/Au(111)		
	Samanos-type					
	R	TS	P	R	TS	P
$d(C_1–C_2)$	1.377	1.415	1.508	1.360	1.415	1.506
$d(Pd_1–C_1)$	2.301	3.255	3.180	2.651	3.451	3.224
$d(Pd_1–C_2)$	2.707	2.283	2.147	2.612	2.386	2.167
$\angle(C_1C_2H)$	119.8	116.1	109.6	120.2	118.2	107.0
$d(Pd_2–O_1)$	2.158	2.224	2.454	2.192	2.300	3.883
$d(Au–O_2)$	2.330	2.467	3.179	2.369	2.613	2.817
$d(C_1–O_2)$	3.175	1.904	1.465	3.213	1.917	1.450
	Moiseev-type					
	R′	TS	P′	R′	TS	P′
$d(C_1–C_2)$	1.336	1.362	1.329	1.335	1.350	1.330
$d(Pd_1–C_1)$	2.029	2.080	4.344	2.055	2.204	4.732
$\angle(Pd_1C_2C_1)$	130.2	107.7	71.8	129.6	114.7	110.9
$\angle(C_1C_2H)$	119.2	118.7	121.4	125.3	118.3	121.5
$d(Pd_2–O_1)$	2.162	2.263	2.372	2.182	2.626	2.539
$d(Au–O_2)$	2.314	2.454	3.434	2.384	2.337	3.317
$d(C_1–O_2)$	3.238	1.957	1.398	3.246	1.996	1.397

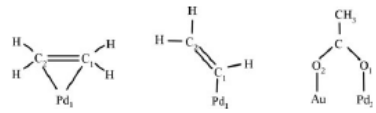

Scheme 1

The vinyl species, in the beginning, is strongly bonded to the surface Pd monomer and is anchored at the surface by means of the carbon atom involved in the coupling. Co-adsorbed acetate is in the same configuration described above for the mechanism proposed by Samanos. In the transition state vinyl and acetate species approach one another to couple. As a consequence, the Pd_1–C_1 and Au–O_2 bonds begin to break, whereas the C_1–O_2 distance significantly shortens.

The normal mode associated to the transition state structure imaginary frequency involves also the stretching of the Pd_2–O_1 bond to facilitate the coupling. Among the structural changes

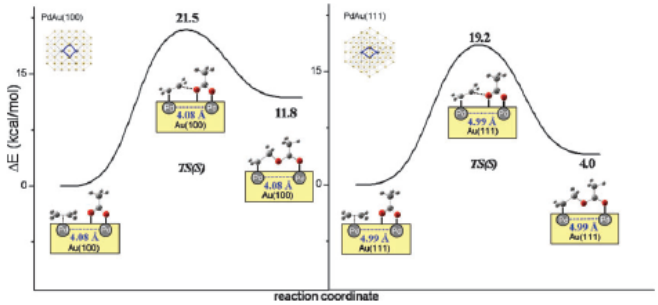

Fig. 1 Potential energy surface for the coupling step between ethylene and acetate of Samanos-type mechanism on both Pd/Au(100) (left) and Pd/Au(111) (right) critical ensembles of two non-contiguous Pd monomers.

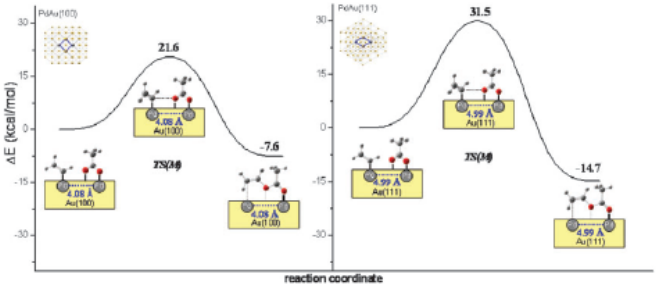

Fig. 2 Potential energy surface for the coupling step between vinyl and acetate of Moiseev-type mechanism on both Pd/Au(100) (left) and Pd/Au(111) (right) critical ensembles of two non-contiguous Pd monomers.

involved by the formation of the transition state structures it is worthwhile focusing on the most significant ones, that is the elongation of the Pd_2–O_1 bond and the shortening of the C_1–O_2 distance. In going from the co-adsorbed molecules to the transition state the Pd_2–O_1 bond changes from 2.162 to 2.263 Å and from 2.182 to 2.626 Å on Pd/Au(100) and Pd/Au(111), respectively. The length of the forming C_1–O_2 bond goes from 3.238 to 1.957 Å on Pd/Au(100) and from 3.242 to 1.996 Å on Pd/Au(111). The transition states collapse into vinyl acetate product by the definitive formation of the bond between C_1 and O_2 atoms. Formation of the product takes place by overcoming an energy barrier of 21.1 and 30.7 kcal mol^{-1} on Pd/Au(100) and Pd/Au(111), respectively, which means that the process on the Pd/Au(100) surface occurs with a much higher rate compared with Pd/Au(111). The different spacing between the two neighbouring Pd monomers, in this case, can be the reason for the more favourable coupling conditions between the reacting species on the Au(100) critical ensemble, whereas on Au(111) the Pd monomers distance, much larger than the ideal one, causes the described bond stretching which is responsible for the high energy barrier.

When comparing the results of our computational analysis, no clear explanation of the significantly higher VAM formation rate at Pd monomer sites on Au(100) emerges.

The height of the barrier for the Moiseev-type mechanism on Pd/Au(100) is significantly lower than that on Pd/Au(111), but is comparable to both the energy barriers that is necessary to overcome to yield the Samanos-type ethyl-acetate product on Pd/Au(100) and Pd/Au(111). Moreover, the suitability of the distance between the two non-contiguous Pd monomers in the critical ensemble seems to influence the course of the reaction only once the Moiseev-type mechanism is taken into account. On the other hand, on the basis of the outcome of their first-principles calculations carried out to investigate the dehydrogenation step of ethylene on Pd/Au(100) bimetallic surfaces, Yuan *et al.*[17] have already proven the inability of the Pd second neighbour ensemble to promote ethylene dehydrogenation that becomes the rate-determining step of the Moiseev mechanism. However, it is of great importance to recall that the experimental data clearly show how the presence of oxygen atoms strongly influences[19] and promotes[13] the VAM synthesis process. For that reason the β-H elimination step has been examined[17] under coexistence of O showing how the oxygen atoms presence drastically promotes dehydrogenation lowering the energy barrier. Intuitively, it cannot be excluded *a priori* that oxygen atoms play the same promotional role in lowering the energy barrier of the ethylene dehydrogenation step of the Moiseev-type mechanism. According to this hypothesis both mechanisms have to be deeply investigated avoiding to focus to one of them only, with the aim to identify the reaction step which is strongly influenced by the fact that the reaction is carried out on Pd/Au(100) surface alloys rather than on Pd/Au(111).

In conclusion, the speculation that the different spacing of Pd monomers in the critical reaction site could be responsible for the experimentally detected enhancement of the VAM formation rate on Pd/Au(100) compared to Pd/Au(111) cannot be supported by the results of our computational analysis. The data reported here, however, will help open questions concerning the role of gold in this catalytic process to be properly addressed.

Notes and references

1 M. Haruta, T. Kobayashi, H. Sano and N. Yamada, *Chem. Lett.*, 1987, **16**, 405.
2 G. J. Hutchings, *J. Catal.*, 1985, **96**, 292.
3 Y.-F. Han, D. Kumar and D. W. Goodman, *J. Catal.*, 2005, **230**, 353–358.
4 D. J. Gulliver and J. S. Kitchen, *Eur. Pat.*, 0 654 301, BP. Chem. Int. Ltd., 1995.
5 W. D. Provine, P. L. Mills and J. J. Lerou, *Stud. Surf. Sci. Catal.*, 1996, **101**, 191.
6 E. G. Allison and G. C. Bond, *Catal. Rev.*, 1972, **7**, 233.
7 S. Nakamura and T. Yasui, *J. Catal.*, 1970, **17**, 366.
8 B. Samanos and P. Boutry, *J. Catal.*, 1971, **23**, 19–30.
9 N. Macleod, J. M. Keel and R. M. Lambert, *Appl. Catal. A*, 2004, **261**, 37.
10 M. S. Chen, K. Luo, T. Wei, Z. Yan, D. Kumar, C.-W. Yi and D. W. Goodman, *Catal. Today*, 2006, **117**, 37.
11 I. I. Moiseev, M. N. Vargaftic and Y. L. Syrkin, *Dokl. Akad. Nauk SSSR*, 1960, **133**, 377.
12 I. I. Moiseev, in *Catalytic Oxidation*, ed. R. A. Sheldon, World Scientific, 1995, p. 203.
13 D. Stacchiola, F. Calaza, L. Burkholder, A. W. Schwabacher, M. Neurock and W. T. Tysoe, *Angew. Chem., Int. Ed.*, 2005, **44**, 4572.
14 M. Chen, D. Kumar, C. W. Yi and D. W. Goodman, *Science*, 2005, **310**, 291; including supporting online material.
15 G. Mazzone, I. Rivalta, N. Russo and E. Sicilia, *J. Phys. Chem. C*, 2008, **112**, 6073.
16 D. W. Yuan, X. G. Gong and R. Q. Wu, *Phys. Rev. B*, 2007, **75**, 233401.
17 D. W. Yuan, X. G. Gong and R. Q. Wu, *J. Phys. Chem. C*, 2008, **112**, 1539.
18 M. García-Mota and N. López, *J. Am. Chem. Soc.*, 2004, **130**, 14406.
19 F. Calaza, L. Burkholder and W. T. Tysoe, *J. Am. Chem. Soc.*, 2004, **126**, 15384.

Supplementary Material (ESI) for Chemical Communications

Supplementary Information

The Geometric Effect in Palladium-Gold Catalysis. Is the Coupling the Rate-Determining Step in the Vinyl-Acetate Synthesis?

Gloria Mazzone, Ivan Rivalta, Nino Russo, Emilia Sicilia**

Dipartimento di Chimica and Università della Calabria, I-87030 Arcavacata di Rende, Italy

Methodology and Computational Details

Figure S1.

Cartesian coordinates of all intermediates and transition states

Imaginary frequencies of transition states

Supplementary Material (ESI) for Chemical Communications

Methodology and computational details

In order to model the second neighbor Pd pair ensemble on PdAu(100) and PdAu(111) surfaces we have built-up the clusters starting with a group of two non-contiguous Pd atoms and two Au atoms bonded to both of them. Then, the first neighbors of those four atoms have been added both in the first and in the second layer. In this way, the active sites are represented by Pd_2Au_{19} and Pd_2Au_{20} cluster models, or Pd_2Au_{19}(12,9) and Pd_2Au_{20}(14,8) to indicate the number of atoms in each cluster layer, for Au(100) and Au(111) surfaces, respectively.

Initially, the atomic positions have been assigned as in bulk gold, with the experimental lattice parameter of 4.08 Å, yielding an Au-Au (initially equal to Pd-Au) distance of 2.885 Å.

With these models a good description of the coordination of the two non-contiguous Pd monomers involved in the chemisorption sites for both low-index gold surfaces is obtained.

First, the size of the Pd_2Au_{19}(12,9) model has been increased by adding a third layer in such a way as to obtain for the PdAu(100) surface the Pd_2Au_{23}(12,9,4) cluster including in the third layer four gold atoms which lie in the positions corresponding to that of the four central atoms in the first layer, because of the ABAB packing of the fcc(100) surface. For the less open fcc(111) gold surface with the ABCABC packing, eight atoms have been added in the third layer to the Pd_2Au_{20}(14,8) model in correspondence to the atomic positions defining the fcc-hollow adsorption sites, giving rise to the larger Pd_2Au_{28}(14,8,8) cluster.

Starting from these three-layer models, other two more extended clusters have been constructed completing the set of the first neighbor atoms for all the peripheral atoms of the first and the second layer. The resulting Pd_2Au_{55}(24,21,12) and Pd_2Au_{62}(30,21,13) large models for the Pd/Au(100) and the Pd/Au(111) systems, respectively, would prevent any indirect insaturation effect for the two non-contiguous Pd and the two Au atoms of the active sites. Moreover, these large models have been used to take into account local relaxation effects due to the substitution of two non-contiguous surface gold atoms with two Pd monomers. The positions of the atoms defining the Pd_2Au_{19}(12,9) and Pd_2Au_{20}(14,8) models have been fully optimized, in fact, within the Pd_2Au_{55}(24,21,12) and Pd_2Au_{62}(30,21,13) clusters freezing the positions of the remaining atoms (see Figure S1).

Due to relaxation effects in the surface plane the neighboring gold atoms move towards the palladium monomers (see Figure S1 (a)) whereas, on the axis perpendicular to the surface, the Pd atoms move inward (of 0.16-0.20 Å) with respect to the surface gold layer (see Figure S1 (b)). As a result of these local relaxations, the Pd-Au distances in the active sites become shorter with respect to the Au-Au distances in the pure gold surfaces. In particular, Pd-Au distances are equal to 2.840 and 2.861 Å for the

Supplementary Material (ESI) for Chemical Communications
This journal is (c) The Royal Society of Chemistry 2009

PdAu(100) and (111) surfaces, respectively. These values differ by 0.017-0.026 Å from the Au-Au distances found with the locally relaxed pure gold clusters.

The calculations have been performed with the Turbomole package (version 5.9)[1] at the DF level, using the BP86 functional[2] within the resolution of the identity approximation for computing the electronic Coulomb interaction (RI-J). This approach expands the molecular electron density in a set of atom-centered auxiliary functions improving the computational efficiency of large-scale calculations.[3,4]

The Stuttgart effective core potential[5] has been used to model the scalar relativistic effects replacing the 28 and 60 core electrons of palladium and gold atoms, respectively. The valence electrons of metal atoms, 18 for Pd and 19 for Au, and all electrons for C, O and H atoms have been explicitly considered by use of the Turbomole's TZVP basis set[6] along with the corresponding TZVP auxiliary basis set.[7]

Supplementary Material (ESI) for Chemical Communications
This journal is (c) The Royal Society of Chemistry 2009

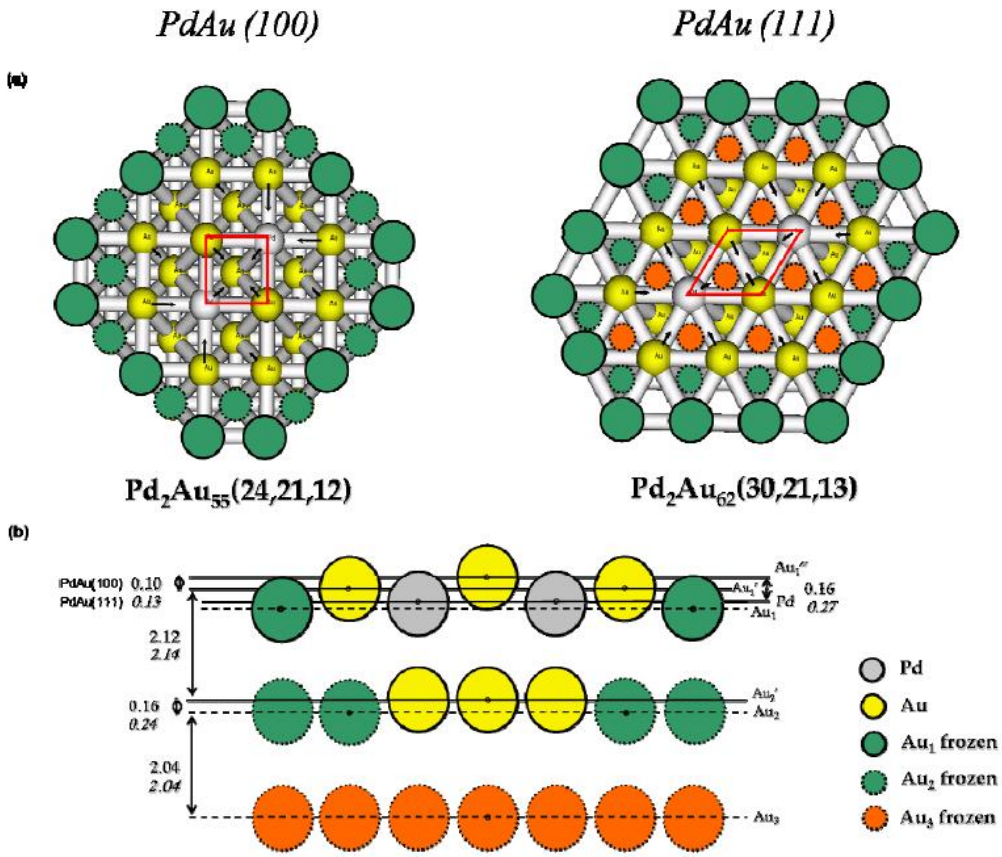

Figure S1. Schematic representation of the Pd_2Au_n clusters used to model the critical ensemble of two non-contiguous Pd monomers on the PdAu(100) and PdAu(111) surface alloys. Top view (a) shows unit cells of the Au(100) and Au(111) pure surfaces in red and changes in the atomic positions due to the local relaxation by arrows. Side view (b) indicates surface layers relaxation with respect to bulk gold interlayer distances.

1 Ahlrichs, M. Bär; Häser, M.; Horn, H.; Kölmel, C. *Chem. Phys. Lett.* **1989**, *162*, 165.

2 Becke, A.D. *Physical Reviews A* **1988**, *38*, 3098.

3 Perdew, J.P. *Physical Review B* **1986**, *33*, 8822.

4 Eichkorn, K.; Treutler, O.; Öhm, H.; Häser M.; Ahlrichs, R. *Chem. Phys. Lett.* **1995**, *240*, 283.

5 Eichkorn, F.; Weigend, O.; Treutler; Ahlrichs, R. *Theor. Chem. Acc.* **1997**, *97*, 119.

6 Andrae, D.; Hæussermann, U.; Dolg, M.; Stoll, H.; Preuß, H. *Theor. Chim. Acta* **1990**, 77, 123. Schäfer, A.; Horn, H.; Ahlrichs, R. *J. Chem. Phys.* **1992**, 97, 2571.

7 Schäfer, A.; Huber, C.; Ahlrichs, R. *J. Chem. Phys.* **1994**, 100, 5829.

Supplementary Material (ESI) for Chemical Communications
This journal is (c) The Royal Society of Chemistry 2009

Cartesian Coordinates of all minima and transition states

Samanos-type mechanism

PdAu(100) – Pd_2Au_{55} cluster model

	R			TS(S)			P		
	x	*y*	*z*	*x*	*y*	*z*	*x*	*y*	*z*
Au	4,0800	-2,0400	-2,4695	4,0800	-2,0400	-2,4695	4,0800	-2,0400	-2,4695
Au	2,0400	-4,0800	-2,4695	2,0400	-4,0800	-2,4695	2,0400	-4,0800	-2,4695
Au	4,0800	2,0400	-2,4695	4,0800	2,0400	-2,4695	4,0800	2,0400	-2,4695
Au	2,0400	0,0000	-2,4695	2,0400	0,0000	-2,4695	2,0400	0,0000	-2,4695
Au	0,0000	-2,0400	-2,4695	0,0000	-2,0400	-2,4695	0,0000	-2,0400	-2,4695
Au	-2,0400	-4,0800	-2,4695	-2,0400	-4,0800	-2,4695	-2,0400	-4,0800	-2,4695
Au	2,0400	4,0800	-2,4695	2,0400	4,0800	-2,4695	2,0400	4,0800	-2,4695
Au	0,0000	2,0400	-2,4695	0,0000	2,0400	-2,4695	0,0000	2,0400	-2,4695
Au	-2,0400	0,0000	-2,4695	-2,0400	0,0000	-2,4695	-2,0400	0,0000	-2,4695
Au	-4,0800	-2,0400	-2,4695	-4,0800	-2,0400	-2,4695	-4,0800	-2,0400	-2,4695
Au	-2,0400	4,0800	-2,4695	-2,0400	4,0800	-2,4695	-2,0400	4,0800	-2,4695
Au	-4,0800	2,0400	-2,4695	-4,0800	2,0400	-2,4695	-4,0800	2,0400	-2,4695
Au	6,1200	-2,0400	-0,4295	6,1200	-2,0400	-0,4295	6,1200	-2,0400	-0,4295
Au	4,0800	-4,0800	-0,4295	4,0800	-4,0800	-0,4295	4,0800	-4,0800	-0,4295
Au	2,0400	-6,1200	-0,4295	2,0400	-6,1200	-0,4295	2,0400	-6,1200	-0,4295
Au	6,1200	2,0400	-0,4295	6,1200	2,0400	-0,4295	6,1200	2,0400	-0,4295
Au	4,1303	0,0000	-0,4335	4,1303	0,0000	-0,4335	4,1303	0,0000	-0,4335
Au	2,0104	-2,0092	-0,2598	2,0104	-2,0092	-0,2598	2,0104	-2,0092	-0,2598
Au	-0,0005	-4,1513	-0,4582	-0,0005	-4,1513	-0,4582	-0,0005	-4,1513	-0,4582
Au	-2,0400	-6,1200	-0,4295	-2,0400	-6,1200	-0,4295	-2,0400	-6,1200	-0,4295
Au	4,0800	4,0800	-0,4295	4,0800	4,0800	-0,4295	4,0800	4,0800	-0,4295
Au	2,0105	2,0093	-0,2596	2,0105	2,0093	-0,2596	2,0105	2,0093	-0,2596
Au	-0,0001	0,0000	-0,2763	-0,0001	0,0000	-0,2763	-0,0001	0,0000	-0,2763
Au	-2,0115	-2,0087	-0,2588	-2,0115	-2,0087	-0,2588	-2,0115	-2,0087	-0,2588
Au	-4,0800	-4,0800	-0,4295	-4,0800	-4,0800	-0,4295	-4,0800	-4,0800	-0,4295
Au	2,0400	6,1200	-0,4295	2,0400	6,1200	-0,4295	2,0400	6,1200	-0,4295
Au	-0,0005	4,1509	-0,4580	-0,0005	4,1509	-0,4580	-0,0005	4,1509	-0,4580
Au	-2,0116	2,0087	-0,2587	-2,0116	2,0087	-0,2587	-2,0116	2,0087	-0,2587
Au	-4,1298	0,0000	-0,4334	-4,1298	0,0000	-0,4334	-4,1298	0,0000	-0,4334
Au	-6,1200	-2,0400	-0,4295	-6,1200	-2,0400	-0,4295	-6,1200	-2,0400	-0,4295
Au	-2,0400	6,1200	-0,4295	-2,0400	6,1200	-0,4295	-2,0400	6,1200	-0,4295
Au	-4,0800	4,0800	-0,4295	-4,0800	4,0800	-0,4295	-4,0800	4,0800	-0,4295
Au	-6,1200	2,0400	-0,4295	-6,1200	2,0400	-0,4295	-6,1200	2,0400	-0,4295
Au	6,1200	-4,0800	1,6105	6,1200	-4,0800	1,6105	6,1200	-4,0800	1,6105
Au	4,0800	-6,1200	1,6105	4,0800	-6,1200	1,6105	4,0800	-6,1200	1,6105
Au	6,1200	0,0000	1,6105	6,1200	0,0000	1,6105	6,1200	0,0000	1,6105
Au	4,0420	-2,0081	1,8525	4,0420	-2,0081	1,8525	4,0420	-2,0081	1,8525
Au	2,0068	-4,0368	1,8579	2,0068	-4,0368	1,8579	2,0068	-4,0368	1,8579
Au	0,0000	-6,1200	1,6105	0,0000	-6,1200	1,6105	0,0000	-6,1200	1,6105
Au	6,1200	4,0800	1,6105	6,1200	4,0800	1,6105	6,1200	4,0800	1,6105
Au	4,0419	2,0082	1,8523	4,0419	2,0082	1,8523	4,0419	2,0082	1,8523
Pd	2,0426	0,0000	1,7918	2,0426	0,0000	1,7918	2,0426	0,0000	1,7918
Au	0,0000	-1,9640	1,9533	0,0000	-1,9640	1,9533	0,0000	-1,9640	1,9533
Au	-2,0073	-4,0364	1,8578	-2,0073	-4,0364	1,8578	-2,0073	-4,0364	1,8578
Au	-4,0800	-6,1200	1,6105	-4,0800	-6,1200	1,6105	-4,0800	-6,1200	1,6105
Au	4,0800	6,1200	1,6105	4,0800	6,1200	1,6105	4,0800	6,1200	1,6105
Au	2,0068	4,0367	1,8576	2,0068	4,0367	1,8576	2,0068	4,0367	1,8576
Au	0,0001	1,9640	1,9530	0,0001	1,9640	1,9530	0,0001	1,9640	1,9530
Pd	-2,0432	0,0000	1,7922	-2,0432	0,0000	1,7922	-2,0432	0,0000	1,7922
Au	-4,0427	-2,0083	1,8524	-4,0427	-2,0083	1,8524	-4,0427	-2,0083	1,8524
Au	-6,1200	-4,0800	1,6105	-6,1200	-4,0800	1,6105	-6,1200	-4,0800	1,6105
Au	0,0000	6,1200	1,6105	0,0000	6,1200	1,6105	0,0000	6,1200	1,6105
Au	-2,0073	4,0363	1,8574	-2,0073	4,0363	1,8574	-2,0073	4,0363	1,8574
Au	-4,0426	2,0084	1,8521	-4,0426	2,0084	1,8521	-4,0426	2,0084	1,8521
Au	-6,1200	0,0000	1,6105	-6,1200	0,0000	1,6105	-6,1200	0,0000	1,6105
Au	-4,0800	6,1200	1,6105	-4,0800	6,1200	1,6105	-4,0800	6,1200	1,6105
Au	-6,1200	4,0800	1,6105	-6,1200	4,0800	1,6105	-6,1200	4,0800	1,6105
O	2,0482	0,2169	3,9392	2,1767	0,1743	4,0046	2,3952	0,1957	4,2118
C	1,4128	1,0862	4,6271	1,2029	0,5038	4,7243	1,3703	0,4066	4,8573
O	0,5516	1,9202	4,2166	0,1284	1,0698	4,2487	0,2125	-0,0836	4,3738
C	1,7177	1,0798	6,1200	1,2991	0,2220	6,2103	1,3640	1,1859	6,1456
H	2,7816	0,8767	6,2893	2,3537	0,1438	6,4950	2,3956	1,3242	6,4826
H	1,1424	0,2685	6,5898	0,8215	-0,7457	6,4292	0,7736	0,6828	6,9233
H	1,4251	2,0318	6,5756	0,8029	1,0000	6,8029	0,9139	2,1764	5,9735
C	-1,9637	0,0061	4,0879	-1,5953	0,6641	4,9477	-1,0983	0,4125	4,8009
C	-3,0516	-0,8361	4,1531	-2,3587	-0,1195	4,0503	-2,1704	-0,1874	3,9273
H	-0,9623	-0,3908	4,2601	-1,1832	0,1863	5,8367	-3,1240	0,3126	4,1436
H	-2,0863	1,0828	4,2172	-1,8593	1,7144	5,0740	-2,2790	-1,2611	4,1172
H	-2,9178	-1,9051	4,3291	-2,3648	-1,1952	4,2361	-1,2511	0,0944	5,8494
H	-4,0625	-0,4408	4,2566	-3,3506	0,3119	3,8485	-1,0999	1,5102	4,7482

Supplementary Material (ESI) for Chemical Communications
This journal is (c) The Royal Society of Chemistry 2009

PdAu(111) – Pd_2Au_{62} cluster model

	R			TS(S)			P		
	x	*y*	*z*	*x*	*y*	*z*	*x*	*y*	*z*
Au	7,2125	7,4954	0,0000	7,2125	7,4954	0,0000	7,2125	7,4954	0,0000
Au	8,6550	9,9939	0,0000	8,6550	9,9939	0,0000	8,6550	9,9939	0,0000
Au	10,0975	12,4924	0,0000	10,0975	12,4924	0,0000	10,0975	12,4924	0,0000
Au	11,5400	14,9909	0,0000	11,5400	14,9909	0,0000	11,5400	14,9909	0,0000
Au	10,0975	7,4954	0,0000	10,0975	7,4954	0,0000	10,0975	7,4954	0,0000
Au	11,5400	9,9939	0,0000	11,5400	9,9939	0,0000	11,5400	9,9939	0,0000
Au	12,9825	12,4924	0,0000	12,9825	12,4924	0,0000	12,9825	12,4924	0,0000
Au	14,4250	14,9909	0,0000	14,4250	14,9909	0,0000	14,4250	14,9909	0,0000
Au	12,9825	7,4954	0,0000	12,9825	7,4954	0,0000	12,9825	7,4954	0,0000
Au	14,4250	9,9939	0,0000	14,4250	9,9939	0,0000	14,4250	9,9939	0,0000
Au	15,8675	12,4924	0,0000	15,8675	12,4924	0,0000	15,8675	12,4924	0,0000
Au	15,8675	7,4954	0,0000	15,8675	7,4954	0,0000	15,8675	7,4954	0,0000
Au	17,3100	9,9939	0,0000	17,3100	9,9939	0,0000	17,3100	9,9939	0,0000
Au	5,7700	8,3283	2,3556	5,7700	8,3283	2,3556	5,7700	8,3283	2,3556
Au	7,2125	10,8267	2,3556	7,2125	10,8267	2,3556	7,2125	10,8267	2,3556
Au	8,6550	13,3252	2,3556	8,6550	13,3252	2,3556	8,6550	13,3252	2,3556
Au	10,0975	15,8237	2,3556	10,0975	15,8237	2,3556	10,0975	15,8237	2,3556
Au	7,2125	5,8298	2,3556	7,2125	5,8298	2,3556	7,2125	5,8298	2,3556
Au	8,6470	8,3235	2,5240	8,6470	8,3235	2,5240	8,6470	8,3235	2,5240
Au	10,0773	10,8180	2,5362	10,0773	10,8180	2,5362	10,0773	10,8180	2,5362
Au	11,5300	13,3021	2,5347	11,5300	13,3021	2,5347	11,5300	13,3021	2,5347
Au	12,9825	15,8237	2,3556	12,9825	15,8237	2,3556	12,9825	15,8237	2,3556
Au	10,0975	5,8298	2,3556	10,0975	5,8298	2,3556	10,0975	5,8298	2,3556
Au	11,5223	8,3153	2,5359	11,5223	8,3153	2,5359	11,5223	8,3153	2,5359
Au	12,9630	10,8161	2,5315	12,9630	10,8161	2,5315	12,9630	10,8161	2,5315
Au	14,4360	13,3114	2,5370	14,4360	13,3114	2,5370	14,4360	13,3114	2,5370
Au	15,8675	15,8237	2,3556	15,8675	15,8237	2,3556	15,8675	15,8237	2,3556
Au	12,9825	5,8298	2,3556	12,9825	5,8298	2,3556	12,9825	5,8298	2,3556
Au	14,4000	8,3317	2,5355	14,4000	8,3317	2,5355	14,4000	8,3317	2,5355
Au	15,8602	10,8439	2,5366	15,8602	10,8439	2,5366	15,8602	10,8439	2,5366
Au	17,3100	13,3252	2,3556	17,3100	13,3252	2,3556	17,3100	13,3252	2,3556
Au	15,8675	5,8298	2,3556	15,8675	5,8298	2,3556	15,8675	5,8298	2,3556
Au	17,3100	8,3283	2,3556	17,3100	8,3283	2,3556	17,3100	8,3283	2,3556
Au	18,7525	10,8267	2,3556	18,7525	10,8267	2,3556	18,7525	10,8267	2,3556
Au	4,3275	9,1611	4,7112	4,3275	9,1611	4,7112	4,3275	9,1611	4,7112
Au	5,7700	11,6596	4,7112	5,7700	11,6596	4,7112	5,7700	11,6596	4,7112
Au	7,2125	14,1581	4,7112	7,2125	14,1581	4,7112	7,2125	14,1581	4,7112
Au	8,6550	16,6565	4,7112	8,6550	16,6565	4,7112	8,6550	16,6565	4,7112
Au	5,7700	6,6626	4,7112	5,7700	6,6626	4,7112	5,7700	6,6626	4,7112
Au	7,2418	9,1521	5,1036	7,2418	9,1521	5,1036	7,2418	9,1521	5,1036
Au	8,6544	11,6193	5,0736	8,6544	11,6193	5,0736	8,6544	11,6193	5,0736
Au	10,0998	14,1188	5,0136	10,0998	14,1188	5,0136	10,0998	14,1188	5,0136
Au	11,5400	16,6565	4,7112	11,5400	16,6565	4,7112	11,5400	16,6565	4,7112
Au	7,2125	4,1641	4,7112	7,2125	4,1641	4,7112	7,2125	4,1641	4,7112
Au	8,6623	6,6923	5,1047	8,6623	6,6923	5,1047	8,6623	6,6923	5,1047
Pd	10,1032	9,1645	4,9167	10,1032	9,1645	4,9167	10,1032	9,1645	4,9167
Au	11,5442	11,6202	5,1198	11,5442	11,6202	5,1198	11,5442	11,6202	5,1198
Au	13,0014	14,1110	5,0369	13,0014	14,1110	5,0369	13,0014	14,1110	5,0369
Au	14,4250	16,6565	4,7112	14,4250	16,6565	4,7112	14,4250	16,6565	4,7112
Au	10,0975	4,1641	4,7112	10,0975	4,1641	4,7112	10,0975	4,1641	4,7112
Au	11,5045	6,6819	5,0731	11,5045	6,6819	5,0731	11,5045	6,6819	5,0731
Au	12,9509	9,1839	5,1197	12,9509	9,1839	5,1197	12,9509	9,1839	5,1197
Pd	14,4040	11,6472	4,9093	14,4040	11,6472	4,9093	14,4040	11,6472	4,9093
Au	15,8672	14,1271	5,0513	15,8672	14,1271	5,0513	15,8672	14,1271	5,0513
Au	17,3100	16,6565	4,7112	17,3100	16,6565	4,7112	17,3100	16,6565	4,7112
Au	12,9825	4,1641	4,7112	12,9825	4,1641	4,7112	12,9825	4,1641	4,7112
Au	14,3912	6,6835	5,0142	14,3912	6,6835	5,0142	14,3912	6,6835	5,0142
Au	15,8357	9,1997	5,0366	15,8357	9,1997	5,0366	15,8357	9,1997	5,0366
Au	17,2831	11,6733	5,0509	17,2831	11,6733	5,0509	17,2831	11,6733	5,0509
Au	18,7525	14,1581	4,7112	18,7525	14,1581	4,7112	18,7525	14,1581	4,7112
Au	15,8675	4,1641	4,7112	15,8675	4,1641	4,7112	15,8675	4,1641	4,7112
Au	17,3100	6,6626	4,7112	17,3100	6,6626	4,7112	17,3100	6,6626	4,7112
Au	18,7525	9,1611	4,7112	18,7525	9,1611	4,7112	18,7525	9,1611	4,7112
Au	20,1950	11,6596	4,7112	20,1950	11,6596	4,7112	20,1950	11,6596	4,7112
C	13,8947	10,6144	7,8198	13,4884	11,0884	7,9005	14,4547	9,8996	8,3801
C	14,0609	10,8042	9,3241	13,5652	11,1625	9,4091	12,3230	9,5917	7,8370
O	14,3512	11,5600	7,0989	14,3835	11,6235	7,2096	13,3183	10,3083	8,4737
O	13,3225	9,5488	7,4308	12,4762	10,4702	7,3446	12,9204	11,5633	9,2154
H	13,5076	11,7007	9,6370	12,7271	11,7617	9,7946	12,5357	12,3154	8,5095
H	15,1208	10,9767	9,5519	14,5086	11,6285	9,7095	13,8081	11,9642	9,7128
H	13,6947	9,9297	9,8707	13,4889	10,1588	9,8493	12,1338	11,3707	9,9585
C	9,8827	9,7766	7,4469	10,9989	9,6167	8,2182	10,9347	10,0013	7,9176
C	10,2919	8,4799	7,4717	10,0283	9,1483	7,3011	10,0662	9,0965	7,0829
H	9,5710	7,6635	7,5386	9,0891	9,7043	7,2897	9,01521	9,3284	7,2895
H	8,8263	10,0430	7,5003	11,6411	8,8838	8,7081	10,25584	8,0441	7,3187
H	10,6051	10,5875	7,5507	10,7686	10,5067	8,8052	10,82371	11,0603	7,6353

Moiseev -type mechanism

PdAu(100) – Pd_2Au_{55} cluster model

	R'			TS(M)			P'		
	x	*y*	*z*	*x*	*y*	*z*	*x*	*y*	*z*
Au	4,0800	-2,0400	-2,4695	4,0800	-2,0400	-2,4695	4,0800	-2,0400	-2,4695
Au	2,0400	-4,0800	-2,4695	2,0400	-4,0800	-2,4695	2,0400	-4,0800	-2,4695
Au	4,0800	2,0400	-2,4695	4,0800	2,0400	-2,4695	4,0800	2,0400	-2,4695
Au	2,0400	0,0000	-2,4695	2,0400	0,0000	-2,4695	2,0400	0,0000	-2,4695
Au	0,0000	-2,0400	-2,4695	0,0000	-2,0400	-2,4695	0,0000	-2,0400	-2,4695
Au	-2,0400	-4,0800	-2,4695	-2,0400	-4,0800	-2,4695	-2,0400	-4,0800	-2,4695
Au	2,0400	4,0800	-2,4695	2,0400	4,0800	-2,4695	2,0400	4,0800	-2,4695
Au	0,0000	2,0400	-2,4695	0,0000	2,0400	-2,4695	0,0000	2,0400	-2,4695
Au	-2,0400	0,0000	-2,4695	-2,0400	0,0000	-2,4695	-2,0400	0,0000	-2,4695
Au	-4,0800	-2,0400	-2,4695	-4,0800	-2,0400	-2,4695	-4,0800	-2,0400	-2,4695
Au	-2,0400	4,0800	-2,4695	-2,0400	4,0800	-2,4695	-2,0400	4,0800	-2,4695
Au	-4,0800	2,0400	-2,4695	-4,0800	2,0400	-2,4695	-4,0800	2,0400	-2,4695
Au	6,1200	-2,0400	-0,4295	6,1200	-2,0400	-0,4295	6,1200	-2,0400	-0,4295
Au	4,0800	-4,0800	-0,4295	4,0800	-4,0800	-0,4295	4,0800	-4,0800	-0,4295
Au	2,0400	-6,1200	-0,4295	2,0400	-6,1200	-0,4295	2,0400	-6,1200	-0,4295
Au	6,1200	2,0400	-0,4295	6,1200	2,0400	-0,4295	6,1200	2,0400	-0,4295
Au	4,1303	0,0000	-0,4335	4,1303	0,0000	-0,4335	4,1303	0,0000	-0,4335
Au	2,0104	-2,0092	-0,2598	2,0104	-2,0092	-0,2598	2,0104	-2,0092	-0,2598
Au	-0,0005	-4,1513	-0,4582	-0,0005	-4,1513	-0,4582	-0,0005	-4,1513	-0,4582
Au	-2,0400	-6,1200	-0,4295	-2,0400	-6,1200	-0,4295	-2,0400	-6,1200	-0,4295
Au	4,0800	4,0800	-0,4295	4,0800	4,0800	-0,4295	4,0800	4,0800	-0,4295
Au	2,0105	2,0093	-0,2596	2,0105	2,0093	-0,2596	2,0105	2,0093	-0,2596
Au	-0,0001	0,0000	-0,2763	-0,0001	0,0000	-0,2763	-0,0001	0,0000	-0,2763
Au	-2,0115	-2,0087	-0,2588	-2,0115	-2,0087	-0,2588	-2,0115	-2,0087	-0,2588
Au	-4,0800	-4,0800	-0,4295	-4,0800	-4,0800	-0,4295	-4,0800	-4,0800	-0,4295
Au	2,0400	6,1200	-0,4295	2,0400	6,1200	-0,4295	2,0400	6,1200	-0,4295
Au	-0,0005	4,1509	-0,4580	-0,0005	4,1509	-0,4580	-0,0005	4,1509	-0,4580
Au	-2,0116	2,0087	-0,2587	-2,0116	2,0087	-0,2587	-2,0116	2,0087	-0,2587
Au	-4,1298	0,0000	-0,4334	-4,1298	0,0000	-0,4334	-4,1298	0,0000	-0,4334
Au	-6,1200	-2,0400	-0,4295	-6,1200	-2,0400	-0,4295	-6,1200	-2,0400	-0,4295
Au	-2,0400	6,1200	-0,4295	-2,0400	6,1200	-0,4295	-2,0400	6,1200	-0,4295
Au	-4,0800	4,0800	-0,4295	-4,0800	4,0800	-0,4295	-4,0800	4,0800	-0,4295
Au	-6,1200	2,0400	-0,4295	-6,1200	2,0400	-0,4295	-6,1200	2,0400	-0,4295
Au	6,1200	-4,0800	1,6105	6,1200	-4,0800	1,6105	6,1200	-4,0800	1,6105
Au	4,0800	-6,1200	1,6105	4,0800	-6,1200	1,6105	4,0800	-6,1200	1,6105
Au	6,1200	0,0000	1,6105	6,1200	0,0000	1,6105	6,1200	0,0000	1,6105
Au	4,0420	-2,0081	1,8525	4,0420	-2,0081	1,8525	4,0420	-2,0081	1,8525
Au	2,0068	-4,0368	1,8579	2,0068	-4,0368	1,8579	2,0068	-4,0368	1,8579
Au	0,0000	-6,1200	1,6105	0,0000	-6,1200	1,6105	0,0000	-6,1200	1,6105
Au	6,1200	4,0800	1,6105	6,1200	4,0800	1,6105	6,1200	4,0800	1,6105
Au	4,0419	2,0082	1,8523	4,0419	2,0082	1,8523	4,0419	2,0082	1,8523
Pd	2,0426	0,0000	1,7918	2,0426	0,0000	1,7918	2,0426	0,0000	1,7918
Au	0,0000	-1,9640	1,9533	0,0000	-1,9640	1,9533	0,0000	-1,9640	1,9533
Au	-2,0073	-4,0364	1,8578	-2,0073	-4,0364	1,8578	-2,0073	-4,0364	1,8578
Au	-4,0800	-6,1200	1,6105	-4,0800	-6,1200	1,6105	-4,0800	-6,1200	1,6105
Au	4,0800	6,1200	1,6105	4,0800	6,1200	1,6105	4,0800	6,1200	1,6105
Au	2,0068	4,0367	1,8576	2,0068	4,0367	1,8576	2,0068	4,0367	1,8576
Au	0,0001	1,9640	1,9530	0,0001	1,9640	1,9530	0,0001	1,9640	1,9530
Pd	-2,0432	0,0000	1,7922	-2,0432	0,0000	1,7922	-2,0432	0,0000	1,7922
Au	-4,0427	-2,0083	1,8524	-4,0427	-2,0083	1,8524	-4,0427	-2,0083	1,8524
Au	-6,1200	-4,0800	1,6105	-6,1200	-4,0800	1,6105	-6,1200	-4,0800	1,6105
Au	0,0000	6,1200	1,6105	0,0000	6,1200	1,6105	0,0000	6,1200	1,6105
Au	-2,0073	4,0363	1,8574	-2,0073	4,0363	1,8574	-2,0073	4,0363	1,8574
Au	-4,0426	2,0084	1,8521	-4,0426	2,0084	1,8521	-4,0426	2,0084	1,8521
Au	-6,1200	0,0000	1,6105	-6,1200	0,0000	1,6105	-6,1200	0,0000	1,6105
Au	-4,0800	6,1200	1,6105	-4,0800	6,1200	1,6105	-4,0800	6,1200	1,6105
Au	-6,1200	4,0800	1,6105	-6,1200	4,0800	1,6105	-6,1200	4,0800	1,6105
O	1,9943	0,1730	3,9465	1,8061	-0,0823	4,0403	2,3925	0,0665	4,1375
C	1,2993	0,9907	4,6347	0,7239	0,1371	4,6377	1,6364	0,0558	5,1009
O	0,4899	1,8729	4,2127	-0,2403	0,8609	4,1319	0,3198	-0,1998	4,8830
C	1,4432	0,8635	6,1461	0,5272	-0,4067	6,0342	2,1147	0,3036	6,5062
H	2,4717	0,5947	6,4127	1,2655	-1,1843	6,2550	3,2084	0,2949	6,5066
H	0,7815	0,0505	6,4806	-0,4942	-0,7945	6,1508	1,7287	-0,4543	7,2022
H	1,1410	1,7921	6,6416	0,6461	0,4198	6,7506	1,7716	1,2894	6,8566
C	-2,0745	-0,0636	3,8204	-2,0765	0,2416	3,8583	-0,6348	-0,1102	5,9011
C	-2,2808	-1,0913	4,6483	-2,5023	-0,9312	4,4059	-1,7462	-0,8361	5,8239
H	-1,8653	0,9414	4,1992	-2,4610	1,2178	4,1473	-0,4306	0,6271	6,6781
H	-2,2749	-0,9140	5,7323	-3,4216	-0,9319	5,0031	-2,5193	-0,7177	6,5807
H	-2,4632	-2,1175	4,3254	-1,9743	-1,8785	4,3004	-1,9121	-1,5389	5,0076

Supplementary Material (ESI) for Chemical Communications
This journal is (c) The Royal Society of Chemistry 2009

PdAu(111) – Pd_2Au_{62} cluster model

	R'			TS(M)			P'		
	x	*y*	*z*	*x*	*y*	*z*	*x*	*y*	*z*
Au	7,2125	7,4954	0,0000	7,2125	7,4954	0,0000	7,2125	7,4954	0,0000
Au	8,6550	9,9939	0,0000	8,6550	9,9939	0,0000	8,6550	9,9939	0,0000
Au	10,0975	12,4924	0,0000	10,0975	12,4924	0,0000	10,0975	12,4924	0,0000
Au	11,5400	14,9909	0,0000	11,5400	14,9909	0,0000	11,5400	14,9909	0,0000
Au	10,0975	7,4954	0,0000	10,0975	7,4954	0,0000	10,0975	7,4954	0,0000
Au	11,5400	9,9939	0,0000	11,5400	9,9939	0,0000	11,5400	9,9939	0,0000
Au	12,9825	12,4924	0,0000	12,9825	12,4924	0,0000	12,9825	12,4924	0,0000
Au	14,4250	14,9909	0,0000	14,4250	14,9909	0,0000	14,4250	14,9909	0,0000
Au	12,9825	7,4954	0,0000	12,9825	7,4954	0,0000	12,9825	7,4954	0,0000
Au	14,4250	9,9939	0,0000	14,4250	9,9939	0,0000	14,4250	9,9939	0,0000
Au	15,8675	12,4924	0,0000	15,8675	12,4924	0,0000	15,8675	12,4924	0,0000
Au	15,8675	7,4954	0,0000	15,8675	7,4954	0,0000	15,8675	7,4954	0,0000
Au	17,3100	9,9939	0,0000	17,3100	9,9939	0,0000	17,3100	9,9939	0,0000
Au	5,7700	8,3283	2,3556	5,7700	8,3283	2,3556	5,7700	8,3283	2,3556
Au	7,2125	10,8267	2,3556	7,2125	10,8267	2,3556	7,2125	10,8267	2,3556
Au	8,6550	13,3252	2,3556	8,6550	13,3252	2,3556	8,6550	13,3252	2,3556
Au	10,0975	15,8237	2,3556	10,0975	15,8237	2,3556	10,0975	15,8237	2,3556
Au	7,2125	5,8298	2,3556	7,2125	5,8298	2,3556	7,2125	5,8298	2,3556
Au	8,6470	8,3235	2,5240	8,6470	8,3235	2,5240	8,6470	8,3235	2,5240
Au	10,0773	10,8180	2,5362	10,0773	10,8180	2,5362	10,0773	10,8180	2,5362
Au	11,5300	13,3021	2,5347	11,5300	13,3021	2,5347	11,5300	13,3021	2,5347
Au	12,9825	15,8237	2,3556	12,9825	15,8237	2,3556	12,9825	15,8237	2,3556
Au	10,0975	5,8298	2,3556	10,0975	5,8298	2,3556	10,0975	5,8298	2,3556
Au	11,5223	8,3153	2,5359	11,5223	8,3153	2,5359	11,5223	8,3153	2,5359
Au	12,9630	10,8161	2,5315	12,9630	10,8161	2,5315	12,9630	10,8161	2,5315
Au	14,4360	13,3114	2,5370	14,4360	13,3114	2,5370	14,4360	13,3114	2,5370
Au	15,8675	15,8237	2,3556	15,8675	15,8237	2,3556	15,8675	15,8237	2,3556
Au	12,9825	5,8298	2,3556	12,9825	5,8298	2,3556	12,9825	5,8298	2,3556
Au	14,4000	8,3317	2,5355	14,4000	8,3317	2,5355	14,4000	8,3317	2,5355
Au	15,8602	10,8439	2,5366	15,8602	10,8439	2,5366	15,8602	10,8439	2,5366
Au	17,3100	13,3252	2,3556	17,3100	13,3252	2,3556	17,3100	13,3252	2,3556
Au	15,8675	5,8298	2,3556	15,8675	5,8298	2,3556	15,8675	5,8298	2,3556
Au	17,3100	8,3283	2,3556	17,3100	8,3283	2,3556	17,3100	8,3283	2,3556
Au	18,7525	10,8267	2,3556	18,7525	10,8267	2,3556	18,7525	10,8267	2,3556
Au	4,3275	9,1611	4,7112	4,3275	9,1611	4,7112	4,3275	9,1611	4,7112
Au	5,7700	11,6596	4,7112	5,7700	11,6596	4,7112	5,7700	11,6596	4,7112
Au	7,2125	14,1581	4,7112	7,2125	14,1581	4,7112	7,2125	14,1581	4,7112
Au	8,6550	16,6565	4,7112	8,6550	16,6565	4,7112	8,6550	16,6565	4,7112
Au	5,7700	6,6626	4,7112	5,7700	6,6626	4,7112	5,7700	6,6626	4,7112
Au	7,2418	9,1521	5,1036	7,2418	9,1521	5,1036	7,2418	9,1521	5,1036
Au	8,6544	11,6193	5,0736	8,6544	11,6193	5,0736	8,6544	11,6193	5,0736
Au	10,0998	14,1188	5,0136	10,0998	14,1188	5,0136	10,0998	14,1188	5,0136
Au	11,5400	16,6565	4,7112	11,5400	16,6565	4,7112	11,5400	16,6565	4,7112
Au	7,2125	4,1641	4,7112	7,2125	4,1641	4,7112	7,2125	4,1641	4,7112
Au	8,6623	6,6923	5,1047	8,6623	6,6923	5,1047	8,6623	6,6923	5,1047
Pd	10,1032	9,1645	4,9167	10,1032	9,1645	4,9167	10,1032	9,1645	4,9167
Au	11,5442	11,6202	5,1198	11,5442	11,6202	5,1198	11,5442	11,6202	5,1198
Au	13,0014	14,1110	5,0369	13,0014	14,1110	5,0369	13,0014	14,1110	5,0369
Au	14,4250	16,6565	4,7112	14,4250	16,6565	4,7112	14,4250	16,6565	4,7112
Au	10,0975	4,1641	4,7112	10,0975	4,1641	4,7112	10,0975	4,1641	4,7112
Au	11,5045	6,6819	5,0731	11,5045	6,6819	5,0731	11,5045	6,6819	5,0731
Au	12,9509	9,1839	5,1197	12,9509	9,1839	5,1197	12,9509	9,1839	5,1197
Pd	14,4040	11,6472	4,9093	14,4040	11,6472	4,9093	14,4040	11,6472	4,9093
Au	15,8672	14,1271	5,0513	15,8672	14,1271	5,0513	15,8672	14,1271	5,0513
Au	17,3100	16,6565	4,7112	17,3100	16,6565	4,7112	17,3100	16,6565	4,7112
Au	12,9825	4,1641	4,7112	12,9825	4,1641	4,7112	12,9825	4,1641	4,7112
Au	14,3912	6,6835	5,0142	14,3912	6,6835	5,0142	14,3912	6,6835	5,0142
Au	15,8357	9,1997	5,0366	15,8357	9,1997	5,0366	15,8357	9,1997	5,0366
Au	17,2831	11,6733	5,0509	17,2831	11,6733	5,0509	17,2831	11,6733	5,0509
Au	18,7525	14,1581	4,7112	18,7525	14,1581	4,7112	18,7525	14,1581	4,7112
Au	15,8675	4,1641	4,7112	15,8675	4,1641	4,7112	15,8675	4,1641	4,7112
Au	17,3100	6,6626	4,7112	17,3100	6,6626	4,7112	17,3100	6,6626	4,7112
Au	18,7525	9,1611	4,7112	18,7525	9,1611	4,7112	18,7525	9,1611	4,7112
Au	20,1950	11,6596	4,7112	20,1950	11,6596	4,7112	20,1950	11,6596	4,7112
C	13,9166	10,6294	7,8188	12,8452	10,5401	7,9393	14,5682	11,7148	7,4422
C	14,0854	10,8391	9,3199	12,3936	10,8330	9,3517	13,8868	11,3631	8,3925
O	14,3513	11,5814	7,08927	13,7705	11,1878	7,4161	12,6624	10,8158	8,1374
O	13,3652	9,5516	7,43933	12,2559	9,5217	7,3255	14,3445	11,4903	9,8231
H	13,4459	11,6757	9,63485	12,7423	11,8224	9,6647	11,7663	10,4669	9,1516
H	15,1245	11,1179	9,5373	12,8250	10,0710	10,0181	10,8462	9,5342	8,9228
H	13,8090	9,9352	9,87184	11,3003	10,7569	9,4324	13,7416	12,2371	10,3613
C	10,1859	9,0967	6,96885	9,5312	10,1726	7,7151	15,3883	11,8168	9,8181
C	9,1934	9,0290	7,8589	10,2917	9,2338	7,1122	14,2509	10,5338	10,3568
H	8,1320	8,9641	7,61655	10,3526	8,1960	7,4274	11,8406	11,0470	10,0721
H	11,2271	9,1447	7,29921	8,7168	9,8414	8,3707	10,1075	9,3068	9,6886
H	9,4509	9,0412	8,92656	9,6379	11,2473	7,5592	10,7987	8,9995	7,9732

Supplementary Material (ESI) for Chemical Communications

Imaginary frequencies (cm^{-1}) of transition states

	PdAu(100)	**PdAu(111)**
TS(S) Samanos-type	-357*i*	-428*i*
TS(M) Moiseev-type	-396*i*	-454*i*

Manoscritto I

The influence of surface oxygen and hydroxyl group on the dehydrogenation of ethylene on Pd$_{Au}$ surface alloys. A theoretical cluster model study

Ivan Rivalta, Gloria Mazzone, Nino Russo, Emilia Sicilia

Submitted

The influence of surface oxygen and hydroxyl group on the dehydrogenation of ethylene on PdAu surface alloys. A theoretical cluster model study

Ivan Rivalta,[a] *Gloria Mazzone,*[a] *Nino Russo*[a] and Emilia Sicilia*[a]*

The outcomes of a density functional cluster model study of the dehydrogenation of ethylene on Pd second-neighbor ensembles of both PdAu(100) and PdAu(111) surface alloys in presence of oxygen and hydroxyl groups corroborates the hypothesis that ethylene dehydrogenation can easily occur during VAM synthesis on PdAu surface alloys and the formed vinyl can couple with acetate following a Langmuir-Hinshelwood-type mechanism.

Vinyl acetate monomer (VAM) is an important chemical intermediate, which is essential in the manufacture of emulsion-based paints, wallpaper paste and wood glue.

Currently approximately 3000 metric tonnes of VAM are produced annually from the coupling of acetic acid and ethylene in oxygen ambient, according to the following reaction:

$$CH_3COOH + C_2H_4 + 0{,}5\ O_2 \rightarrow CH_3COOCHCH_2 + H_2O$$

The VAM synthesis is catalyzed by both supported palladium and palladium-gold alloys, but alloying with gold leads to a substantial increase in selectivity.[1]

Acetoxylation of ethylene on Pd-Au bimetallic catalysts is a mature commercial route for the industrial production of VAM.[2-8] However, the nature of key reaction intermediates, the mechanism by which the reaction occurs and the role played by gold are still matter of debate. The comprehension of the mechanism and the role of Au on the surface of the catalyst can lead to further improvements of such an industrial production process.

Two alternative reaction pathways were proposed for VAM synthesis. Coupling of adsorbed ethylene with adsorbed acetate to form an ethyl-acetate-like intermediate that then undergoes β-H elimination to form VAM is one mechanism proposed by Samanos et al.[9] The second mechanism, suggested by both Moiseev[10,11] and Nakamura and Yasui,[12] involves, dehydrogenation of adsorbed ethylene to form a vinyl species which then couples with the coadsorbed acetate to give VAM directly. Mopping up of hydrogen atoms by oxygen completes the reaction. Both mechanisms, designated as Samanos-type and Moiseev-type, respectively

assume that the rate determining step of the whole process is the coupling of a surface ethylenic and acetate species.

The experimental results of a study by Tysoe et al.[13] on the VAM synthesis on Pd(111) clean surface provide clear evidence that the reaction proceeds by the Samanos-type mechanism. Furthermore, in the same paper it is shown how the presence of coadsorbed oxygen does not affect significantly the reaction kinetics. On the contrary, Tyose and collaborators suggested that surface oxygen plays a crucial role in the vinyl acetate synthesis reaction on Pd(100) clean surface.[14] Nevertheless, an analogous clear indication on the preferred mechanism on Pd(100) clean surfaces does not exist in literature.

In their investigation of the promotional effect of gold in palladium Pd-Au alloy catalysts Goodman and coworkers[15] invoked ensemble effects to explain the significant enhancement of the VAM formation rate on Pd/Au(100) compared with Pd/Au(111) and demonstrated that the critical ensemble for VAM formation on a Pd/Au(100) surface alloy is a pair of non-contiguous, suitably spaced, Pd monomers. Indeed, the role of Au should be to isolate single Pd atoms, being the distance between them the key factor, to facilitate coupling of the reactants and to suppress the undesirable formation of reaction by-products.

Based on the conclusion of the first principle theoretical investigation of Yuan et al. that the dehydrogenation of ethylene is unlikely to occur on PdAu surfaces,[16] only one of the two reaction mechanisms proposed for this reaction (Samanos-type) was taken into consideration by theoretical investigations on this subject[17,18]. In that studies the β-H elimination from the ethyl-acetate-like intermediate was examined under coexistence of surface oxygen[18] (or hydroxyl groups[17]) showing how the O atoms drastically promotes dehydrogenation lowering the energy barrier. Nevertheless, the analogous role that intuitively could be played by surface oxygen species in the ethylene dehydrogenation step involved in Moiseev-type mechanism was not investigated so far.

Very recently, in an attempt to interpret the experimental results outlined above[15], we examined in detail the key step involving coupling of the surface reacting species considering both Samanos- and Moiseev-type mechanisms.[19] The main conclusion of our work is that the suitability of the distance between Pd monomers in the critical ensemble can influence the course of the reaction only once it is assumed that the reaction occurs following the Moiseev-type mechanism. Indeed, the barriers that is necessary to overcome in order to form the ethyl-acetate-like intermediate along the Samanos-type pathway are calculated to be 21.5 and 19.2 kcal mol^{-1} on Pd/Au(100) and Pd/Au(111) surface alloys, respectively. On the contrary, the

height of the barrier for the coupling step between coadsorbed vinyl and acetate, in the Moiseev-type mechanism, is significantly lower on Pd/Au(100) (21.1 kcal mol^{-1}) than that on Pd/Au(111) (30.7 kcal mol^{-1}).

In this work, adding another piece to the intricate puzzle, we present the outcomes of a theoretical density functional cluster model study of the dehydrogenation of ethylene on Pd second-neighbor ensembles of both PdAu(100) and PdAu(111) surface alloys and the influence of oxygen and hydroxyl groups surface species (i.e. O_s and OH_s) on this process.

To this aim we used large cluster models (containing up to 64 atoms, see Figure 1) to represent second-neighbor Pd ensembles given that they are the active sites for VAM synthesis[15] and the most stable ensembles[16,20,21] on PdAu surfaces. Computational details, along with the strategy used to select the size of the clusters[22] are presented in the Supporting Information.

As a first step, we studied the adsorption properties of reactant surface species involved in the ethylene dehydrogenation reaction (i.e. ethylene, O, and OH). Ethylene is weakly π-bonded on top of Pd monomers on clean PdAu surface alloys[23,24] whereas O_s atoms and OH_s groups are strongly bonded to the bimetallic surfaces preferring multifold PdAu sites. In particular, on clean PdAu(111) O_s atoms are sited on the three-fold (both fcc and hcp) hollows (with a BE of ~60 kcal/mol) while on clean PdAu(100) they site preferentially on the four-fold hollows (BE is 68.0 kcal/mol). O_s atoms adsorbed on bridge PdAu sites show BEs close to those calculated on hollow sites, being 58.1 and 67.3 kcal/mol on PdAu(111) and (100), respectively. Instead, the preferred adsorption sites for OH_s groups on clean surface alloys are the bridge PdAu sites with the O atom forming a covalent bond with the Pd monomers. On clean PdAu(111) and PdAu(100) surfaces cluster model calculations indicate values of BEs equal to 45.7 and 40.0 kcal/mol, respectively (see Supporting Information for further details).

In the initial state (IS) of the dehydrogenation reaction, ethylene is adsorbed, or coadsorbed with O_s or OH_s species, on the PdAu surfaces (see Figure 1). In the active site of the (111) bimetallic surface there are two three-fold hollow sites and one of them can be occupied by an O_s atom even if an ethylene molecule is coadsorbed. Conversely, in the (100) surface there is only one hollow in the active site and that forces an O_s atom to site on a bridge PdAu site. When an OH_s group is adsorbed together with the π-bonded ethylene in the active site, it still occupies the PdAu bridge site, on both surface alloys.

The potential energy surfaces (PESs) for the activation of the C-H bond of ethylene and the transition state (TS) structures on clean and covered PdAu surfaces are depicted in Figure 2.

By use of the CI-NEB method,[16] for the C-H bond breaking TS structure showing both H and vinyl on PdAu bridge sites, an high energy barrier of 41.9 kcal mol^{-1} was previously calculated on clean PdAu(100) surface, indicating that ethylene molecules are unlikely to be decomposed in such a situation.

In our work, we have intercepted an energetically more stable TS structure that corresponds to a typical TS complex for the C-H activation on a metal surface[25] in which the C atom sits on top of a single metal center (see Figure 2). The C-H bond is elongated with respect to the adsorbed ethylene molecule by ~0.7 Å, up to 1.844-1.882 Å, whereas a Pd-H bond is formed having bond distances in the range 1.707-1.714 Å. Both vinyl molecule and H atom lie in their preferred adsorption sites (vinyl on top and H on PdAu bridge) in these TS structures. The corresponding activation barriers for the (100) and (111) surfaces calculated to be 33.2 and 34.9 kcal mol^{-1}, respectively are by about 9 kcal mol^{-1} lower than the barrier calculated by CI-NEB method. Even if these results clearly show that the H-abstraction on Pd second-neighbor ensembles can be more accessible than thought, the calculated barriers, if compared with the coupling step barriers, are high enough to still consider the ethylene dehydrogenation as the rate-determining step (in the Moiseev-type mechanism) for VAM synthesis on clean PdAu surfaces. The heights of the barriers for C-H activation on clean PdAu surfaces appear to be more affected by the ligand effect than by the ensemble effect, since similar barrier are observed for (100) and (111) bimetallic surfaces being significantly lower than that calculated on Pd(100) clean surface.[16]

When the ethylene C-H bond is activated by coadsorbed O_s groups, the corresponding TS structures and activation barriers are significantly altered with respect to clean surfaces (see Figure 2 and 3).

A surface oxygen atom, strongly bonded on the PdAu bridge site, acts as attraction center for the H atom of adsorbed π-ethylene. This leads to a TS structure with an H atom almost equally shared by C and O_s atoms (C-H and O-H distances are 1.333-1.388 Å and 1.279-1.296 Å, respectively). Due to different surface geometries, the (*quasi*-formed) vinyl molecule sits on different positions depending on the exposed surfaces, indicating that the ensemble effect is more pronounced on O-covered than on clean surfaces.

The activation barriers for the O-assisted C-H activation are almost halved with respect to the reaction on clean surfaces, being 19.1 and 15.0 kcal mol^{-1} on PdAu(111) and (100) surfaces, respectively.

The abstraction of H atoms from ethylene by OH_s group leads to the formation of adsorbed water molecules. Since water molecules are sited preferentially on top of Pd monomers, the TS structures of the OH-assisted process holds vinyl molecules in the PdAu bridge sites, no matter what is the exposed surfaces. The activation barriers corresponding to these transition states are even lower than in the O-assisted case, being 13.1 and 11.0 kcal mol^{-1} for the PdAu(111) and (100) surfaces, respectively.

The calculated activation barriers and reaction energies (see Table 1) clearly indicate that presence of O_s and OH_s species drastically influences the vinyl formation reaction on PdAu surface alloys. Since O_s and OH_s groups are present in the experimental conditions of VAM synthesis, our study strongly suggests that vinyl is formed during the catalytic process. As a consequence, ethylene dehydrogenation cannot be considered the rate-determining step in the Moiseev-type mechanism since coupling step shows higher barriers.

In conclusion, the ease with which ethylene can form vinyl in the presence of surface oxygen and hydroxyl groups supports the hypothesis that ethylene dehydrogenation can occur during VAM synthesis on PdAu surface alloys and the formed vinyl can couple with acetate following a Moiseev-type reaction mechanism. In light of the results presented here, further theoretical investigation on this catalytic system should be performed covering all the possible elementary steps and comparing the two reaction mechanisms. The possibility that different mechanisms operate on different surface alloys should be also taken into consideration. Additional information coming from experimental studies on the characterization of the short life reaction intermediates, such as the highly reactive vinyl or ethyl-acetate surface species, should be welcome to unequivocally determine the microscopic behavior of the surface reaction and the promotional role of gold.

Notes and references

[a] *Dipartimento di Chimica, Università della Calabria, 87036 Arcavacata di Rende (CS), Italy; E-mail:nrusso@unical.it, E-mail:siciliae@unical.it.*

† Electronic Supplementary Information (ESI) available: Computational details. See DOI: 10.1039/b000000x/

1 *Cat. Gold News*, 2003, **4** Spring.
2 Y.-F. Han, D. Kumar, D.W. Goodman, *J. Catal*. 2005, **230**, 353-358.
3 D. J. Gulliver, and J. S. Kitchen, *Eur. Pat.* 0654301, BP. Chem. Int. Ltd., 1995.
4 W.D. Provine, P.L. Mills, J.J. Lerou, *Stud. Surf. Catal*. 1996, **101**, 191.
5 E.G. Allison, G.C. Bond, *Catal. Rev*. 1972, **7**, 233.
6 N. Macleod, J.M. Keel, R.M. Lambert, *Appl. Catal. A* 2004, **261**, 37.
8 M.S. Chen, K. Luo, T. Wei, Z. Yan, D. Kumar, C.-W. Yi, D.W. Goodman *Catalysis Today* 2006, **117**, 37.
9 B. Samanos, P. Boutry, *J. Catal.* 1971, **23**, 19-30.
10 I. I. Moiseev, M. N. Vargaftic, Y. L. Syrkin, *Dokl. Akad. Nauk SSSR* 1960, **133**, 377.
11 M. Haruta, T. Kobayashi, H. Sano, N. Yamada, *Chem. Lett.* 1987, **16**, 405.
12 S. Nakamura, T. Yasui, *J. Catal.* 1970, **17**, 366.
13 D. Stacchiola, F. Calaza, L. Burkholder, A. W. Schwabacher, M.Neurock, W.T. Tysoe, *Ang. Chem. Int. Ed.* 2005, **44**, 4572
14 Z. Li, F. Gao, W.T. Tysoe, *Surf. Sci*. 2008, **602**, 416.
15 M. Chen, D. Kumar, C.W.Yi, D.W. Goodman, *Science* 2005, **310**, 291; including supporting online material.
16 D.W. Yuan, X. G. Gong; R.Q. Wu *Phys. Rev. B* 2007, **75**, 233401.
17 García-Mota M.; López N. *J. Am. Chem. Soc*. 2008, **130**, 14406.
18 Yuan, D. W.; Gong, X. G.; Wu, R. Q. *J. Phys. Chem. C* 2008, **112**, 1539.
19 Mazzone G.; Rivalta I.; Russo N.; Sicilia E. *Chem. Commun.* 2009, **14**, 1852.
20 P. Han, S. Axnanda, I. Lyubinetsky, D. W. Goodman, *J. Am. Chem. Soc.* 2007, **129**, 14355.
21 H. J. Gotsis, I. Rivalta, N. Russo, E. Sicilia. *Chem. Phys. Lett.* 2009, **468**, 162.
22 For the convergence study see: G. Mazzone, I. Rivalta; N. Russo, E. Sicilia *J. Phys. Chem. C* 2008, **112**, 6073.
23 F. Calaza, F. Gao, Z. Li, W. T. Tysoe *Surf. Sci.* 2007, **601**, 714.
24 I. Rivalta, G. Mazzone, N. Russo, E. Sicilia *J. Chem. Theory Comput.*, 2009, **5**, 1350.
25 M. Neurock M. *Applied Catalysis, A* 1997, **160**, 169.

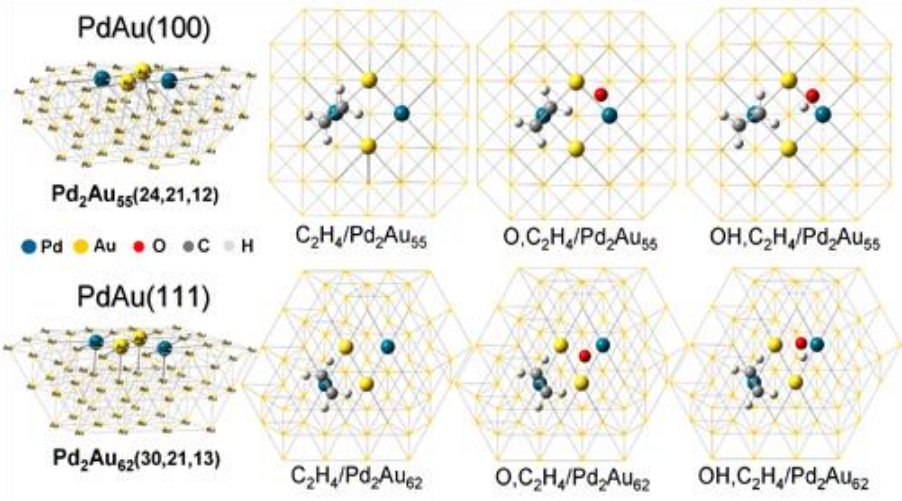

Figure 1. Cluster models used for Pd second-neighbor ensembles on PdAu(100) and (111) surface alloys and top view of the initial state configurations calculated for clean, O- and OH-covered PdAu surfaces.

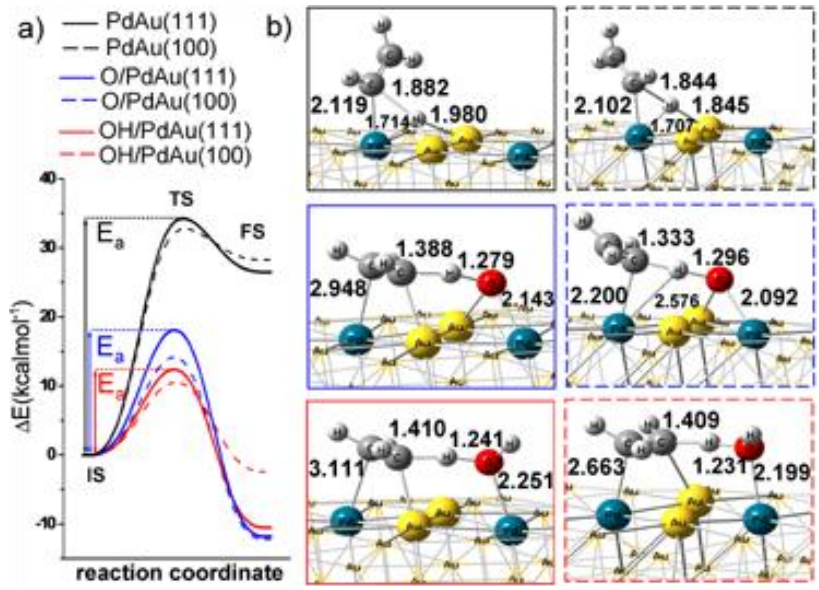

Figure 2. (a) Potential energy surfaces for ethylene dehydrogenation on clean, O- and OH-covered PdAu(111) and (100) surfaces. (b) Selected geometrical parameters for TS structures are reported.

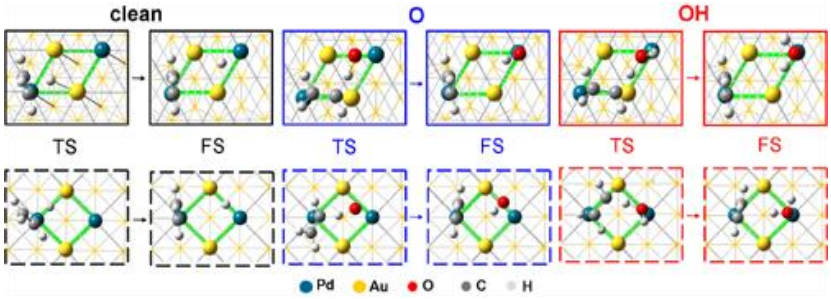

Figure 3. Transition and final states (TS, FS) for ethylene dehydrogenation on clean, O- and OH-covered PdAu(111) and (100) surfaces (colors and lines follow the PESs in Figure 2).

Table 1. Activation (E_a, kcal mol^{-1}) and reaction energies (ΔE, kcal mol^{-1}) calculated as $E_a = E_{TS} - E_{IS}$ and $\Delta E = E_{FS} - E_{IS}$.

	(111)		**(100)**	
	E_a	**ΔE**	**E_a**	**ΔE**
PdAu	34.9	26.5	33.2	28.6
O/PdAu	19.1	-11.8	15.0	-12.2
OH/PdAu	13.1	-10.5	11.0	-2.4

The influence of surface oxygen and hydroxyl group on the dehydrogenation of ethylene on PdAu surface alloys. A theoretical cluster model study

Ivan Rivalta,[a] Gloria Mazzone,[a] Nino Russo[a] and Emilia Sicilia*[a]*

SUPPORTING INFORMATION

-S1-

Computational tool (including building strategy for cluster models)

The calculations have been performed with the Turbomole package[1] at the DF level, using the BP86 functional[2] within the resolution of the identity approximation for computing the electronic Coulomb interaction (RI-J).[3,4]

The Stuttgart effective core potential[5] has been used to model the scalar relativistic effects replacing the 28 and 60 core electrons of palladium and gold atoms, respectively. The valence electrons of metal atoms, 18 for Pd and 19 for Au, and all electrons for C, O and H atoms have been explicitly considered by use of the Turbomole's TZVP basis set[6] along with the corresponding TZVP auxiliary basis set.[7]

Initially, the atomic positions have been assigned as in bulk gold, with the experimental lattice parameter of 4.08 Å, yielding an Au-Au (initially equal to Pd-Au) distance of 2.885 Å.

We have built-up the clusters starting with a group of two non-contiguous Pd atoms and two Au atoms bonded to both of them since they represent the active sites for VAM synthesis on both PdAu(100) and PdAu(111) surface alloys. The first neighbors of those four atoms have been added both in the first and in the second layer. In this way, the active sites are represented by the Pd_2Au_{19}(12,9) and Pd_2Au_{20}(14,8) cluster models, for Au(100) and Au(111) surfaces, respectively. The size of the Pd_2Au_{19}(12,9) and the Pd_2Au_{23}(12,9,4) has been increased by adding a third layer in such a way as to obtain the larger Pd_2Au_{23}(12,9,4) and Pd_2Au_{28}(14,8,8) cluster models.

Finally, starting from these three-layer models, the largest clusters Pd_2Au_{55}(24,21,12) and Pd_2Au_{62}(30,21,13) have been constructed completing the set of the first neighbor atoms for all the peripheral atoms of the first and the second layer of PdAu(100) and PdAu(111) surfaces, respectively. Within these two large model the position of the inner atoms (corresponding to the atoms included in the Pd_2Au_{19}(12,9) and Pd_2Au_{20}(14,8) models) have been optimized.

In these models any indirect unsaturation effect for the two non-contiguous Pd and the two Au atoms of the active sites is prevented, as showed by previous convergence studies.[8,9]

-S2-

Adsorption properties (O, OH, H and H_2O)

The BE of O, OH, H and H_2O on PdAu(100) and PdAu(111) have been calculated for different adsorption sites according to the equation:

$$BE = (E_A + E_s) - E_{A\text{-}S} \qquad (1)$$

where E_A and E_S are the total energies of the isolated adsorbate species and cluster model, respectively, and $E_{A\text{-}S}$ is the total energy of the interacting system for a given adsorption configuration.

Due to the high computational cost of the calculations, the trends in BE for all the adsorption sites have been obtained by use of the SVP basis set.[10-11] However, for the preferred adsorption sites the TZVP basis set has been used to calculate the BEs and the corresponding BSSE corrections.[12] The atomic position of the adsorbates have been optimized without geometric constrains allowing adsorbates to move from unstable initial adsorption positions to the preferred adsorption sites.

	PdAu(100)		**PdAu(111)**	
	adsorption site	**BE (kcal mol^{-1})**	*adsorption site*	**BE (kcal mol^{-1})**
H				
	Hollow	58.3	***fcc Hollow***	**50.5**
	Bridge Pd-Au	**61.5**	*hcp Hollow*	49.9
	Top Pd→BridgePdAu	-	*Bridge Pd-Au→fcc Hollow*	-
	Top Au→ BridgePdAu	-	*Top Pd→fcc Hollow*	-
		-	*TopAu→fcc Hollow*	-
O				
	Hollow	**68.0**	***fcc Hollow***	**60.2**
	Bridge Pd-Au	67.3	*hcp Hollow*	58.1
	Top Pd	56.5	*Bridge Pd-Au→fcc Hollow*	-
			Top Pd→fcc Hollow	-
OH				
	Hollow	35.2	*fcc Hollow→Bridge PdAu*	-
	Bridge Pd-Au	**40.2**	*hcp Hollow→Bridge PdAu*	-
	Top Pd	33.6	***Bridge Pd-Au***	**45.7**
			Top Pd	44.6
H_2O				
	Hollow→ Top Pd	-	*fcc Hollow→ Top Pd*	-
	Bridge Pd-Au	13.8	*hcp Hollow→Top Pd*	-
	Top Pd	**17.2**	*Bridge Pd-Au*	13.1
			Top Pd	**14.9**

Table. Calculated BEs (SVP basis set) for different adsorption sites (*initial→final* position). BEs for the preferred adsorption sites are reported in bold.

-S3-

Geometric parameters for stationary points (IS,TS and FS) and imaginary vibrational frequencies for TS structures.

Distances are in Å, angles in degrees and vibrational frequencies in cm^{-1}.
The labels listed in the tables are assigned according to the following scheme:

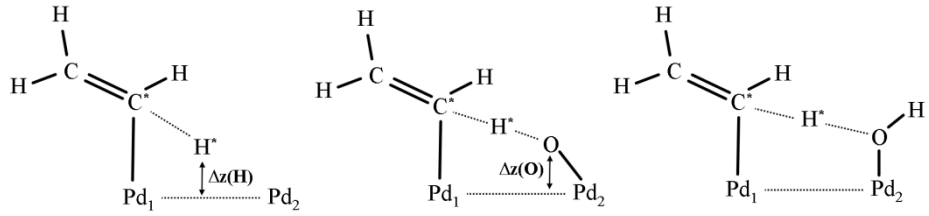

PdAu(100)

	C-C*	C-H*	Pd_1-C*	Pd_1-H*	Δz(H)	Pd_2-H*	C*-Pd_1-H*	*ν*
IS	1.375	1.091	2.376	-	-	-	-	-
TS	1.337	1.844	2.102	1.707	1.140	-	50.7	*i*360.1
FS	1.336	-	2.042	-	-	1.694	-	-

O/PdAu(100)

	C-C*	C-H*	Pd_1-C*	Pd_2-O	Δz(O)	O-H*	Pd_1-C	C*-Pd_1-H*	Pd_2-O-H*	*ν*
IS	1.373	1.093	2.386	1.984	1.478	-	-	-	-	-
TS	1.365	1.333	2.200	2.093	-	1.296	2.886	31.1	126.1	*i*1396.2
FS	1.340	-	2.035	2.151	-	0.981	-	-	108.0	-

OH/PdAu(100)

	C-C*	C-H*	Pd_1-C*	Pd_2-O	O-H*	O-H	Pd_1-C	H-O-H*	Pd_2-O-H*	*ν*
IS	1.370	1.092	2.351	2.147	-	0.975	-	-	106.8	-
TS	1.399	1.409	2.663	2.199	1.231	0.975	2.260	112.8	105.0	*i*1215.2
FS	1.345	-	2.047	2.438	-	0.986	-	104.5	103.2	-

PdAu(111)

	C-C*	C-H*	Pd_1-C*	Pd_1-H*	Δz(H)	Pd_2-H*	C*-Pd_1-H*	ν
IS	1.375	1.091	2.376	-	-	-	-	-
TS	1.337	1.844	2.102	1.707	1.140	-	50.7	*i*557.9
FS	1.336	-	2.042	-	-	1.695	-	-

O/PdAu(111)

	C-C*	C-H*	Pd_1-C*	Pd_2-O	Δz(O)	O-H*	Pd_1-C	C*-Pd_1-H*	Pd_2-O-H*	ν
IS	1.373	1.092	2.385	1.983	1.477	-	-	-	-	--
TS	1.365	1.332	2.200	2.092	-	1.296	2.886	31.1	126.1	*i*1527.7
FS	1.339		2.035	2.151	-	0.981	-	--	108.0	-

OH/PdAu(111)

	C-C*	C-H*	Pd_1-C*	Pd_2-O	O-H*	O-H	Pd_1-C	H-O-H*	Pd_2-O-H*	ν
IS	1.370	1.092	2.351	2.147	-	0.975	-	-	106.8	-
TS	1.399	1.408	2.663	2.199	1.230	0.974	2.260	112.7	105.0	*i*1318.3
FS	1.345	--	2.046	2.438	-	0.986	-	104.5	103.2	-

-S4-

Cartesian Coordinates (including adsorption study), in Å

Ethylene dehydrogenation on PdAu(111)

	IS			TS			FS		
	x	*y*	*z*	*x*	*y*	*z*	*x*	*y*	*z*
Au	7,2125	7,4954	0,0000	7,2125	7,4954	0,0000	7,2125	7,4954	0,0000
Au	8,6550	9,9939	0,0000	8,6550	9,9939	0,0000	8,6550	9,9939	0,0000
Au	10,0975	12,4924	0,0000	10,0975	12,4924	0,0000	10,0975	12,4924	0,0000
Au	11,5400	14,9909	0,0000	11,5400	14,9909	0,0000	11,5400	14,9909	0,0000
Au	10,0975	7,4954	0,0000	10,0975	7,4954	0,0000	10,0975	7,4954	0,0000
Au	11,5400	9,9939	0,0000	11,5400	9,9939	0,0000	11,5400	9,9939	0,0000
Au	12,9825	12,4924	0,0000	12,9825	12,4924	0,0000	12,9825	12,4924	0,0000
Au	14,4250	14,9909	0,0000	14,4250	14,9909	0,0000	14,4250	14,9909	0,0000
Au	12,9825	7,4954	0,0000	12,9825	7,4954	0,0000	12,9825	7,4954	0,0000
Au	14,4250	9,9939	0,0000	14,4250	9,9939	0,0000	14,4250	9,9939	0,0000
Au	15,8675	12,492	0,0000	15,8675	12,492	0,0000	15,8675	12,492	0,0000
Au	15,8675	7,4954	0,0000	15,8675	7,4954	0,0000	15,8675	7,4954	0,0000
Au	17,3100	9,9939	0,0000	17,3100	9,9939	0,0000	17,3100	9,9939	0,0000
Au	5,7700	8,3283	2,3556	5,7700	8,3283	2,3556	5,7700	8,3283	2,3556
Au	7,2125	10,8268	2,3556	7,2125	10,8268	2,3556	7,2125	10,8268	2,3556
Au	8,6550	13,3252	2,3556	8,6550	13,3252	2,3556	8,6550	13,3252	2,3556
Au	10,0975	15,8237	2,3556	10,0975	15,8237	2,3556	10,0975	15,8237	2,3556
Au	7,2125	5,8298	2,3556	7,2125	5,8298	2,3556	7,2125	5,8298	2,3556
Au	8,6470	8,3235	2,5240	8,6470	8,3235	2,5240	8,6470	8,3235	2,5240
Au	10,0773	10,8180	2,5362	10,0773	10,8180	2,5362	10,0773	10,8180	2,5362
Au	11,5300	13,3021	2,5347	11,5300	13,3021	2,5347	11,5300	13,3021	2,5347
Au	12,9825	15,8237	2,3556	12,9825	15,8237	2,3556	12,9825	15,8237	2,3556
Au	10,0975	5,8298	2,3556	10,0975	5,8298	2,3556	10,0975	5,8298	2,3556
Au	11,5223	8,3153	2,5359	11,5223	8,3153	2,5359	11,5223	8,3153	2,5359
Au	12,9630	10,8161	2,5315	12,9630	10,8161	2,5315	12,9630	10,8161	2,5315
Au	14,4360	13,3114	2,5370	14,4360	13,3114	2,5370	14,4360	13,3114	2,5370
Au	15,8675	15,8237	2,3556	15,8675	15,8237	2,3556	15,8675	15,8237	2,3556
Au	12,9825	5,8297	2,3556	12,9825	5,8297	2,3556	12,9825	5,8297	2,3556
Au	14,4000	8,3317	2,5355	14,4000	8,3317	2,5355	14,4000	8,3317	2,5355
Au	15,8602	10,8439	2,5366	15,8602	10,8439	2,5366	15,8602	10,8439	2,5366
Au	17,3100	13,3252	2,3556	17,3100	13,3252	2,3556	17,3100	13,3252	2,3556
Au	15,8675	5,8298	2,3556	15,8675	5,8298	2,3556	15,8675	5,8298	2,3556
Au	17,3100	8,3283	2,3556	17,3100	8,3283	2,3556	17,3100	8,3283	2,3556
Au	18,7525	10,8268	2,3556	18,7525	10,8268	2,3556	18,7525	10,8268	2,3556
Au	4,3275	9,1611	4,7112	4,3275	9,1611	4,7112	4,3275	9,1611	4,7112
Au	5,7700	11,6596	4,7112	5,7700	11,6596	4,7112	5,7700	11,6596	4,7112
Au	7,2125	14,1581	4,7112	7,2125	14,1581	4,7112	7,2125	14,1581	4,7112
Au	8,6550	16,6565	4,7112	8,6550	16,6565	4,7112	8,6550	16,6565	4,7112
Au	5,7700	6,6626	4,7112	5,7700	6,6626	4,7112	5,7700	6,6626	4,7112
Au	7,2418	9,1521	5,1036	7,2418	9,1521	5,1036	7,2418	9,1521	5,1036
Au	8,6544	11,6193	5,0736	8,6544	11,6193	5,0736	8,6544	11,6193	5,0736

Au	10,0998	14,1188	5,0136	10,0998	14,1188	5,0136	10,0998	14,1188	5,0136
Au	11,5400	16,6565	4,7112	11,5400	16,6565	4,7112	11,5400	16,6565	4,7112
Au	7,2125	4,1641	4,7112	7,2125	4,1641	4,7112	7,2125	4,1641	4,7112
Au	8,6623	6,6923	5,1047	8,6623	6,6923	5,1047	8,6623	6,6923	5,1047
Pd	10,1032	9,1645	4,9167	10,1032	9,1645	4,9167	10,1032	9,1645	4,9167
Au	11,5442	11,6202	5,1198	11,5442	11,6202	5,1198	11,5442	11,6202	5,1198
Au	13,0014	14,1110	5,0369	13,0014	14,1110	5,0369	13,0014	14,1110	5,0369
Au	14,4250	16,6565	4,7112	14,4250	16,6565	4,7112	14,4250	16,6565	4,7112
Au	10,0975	4,1641	4,7112	10,0975	4,1641	4,7112	10,0975	4,1641	4,7112
Au	11,5045	6,6819	5,0731	11,5045	6,6819	5,0731	11,5045	6,6819	5,0731
Au	12,9509	9,1839	5,1197	12,9509	9,1839	5,1197	12,9509	9,1839	5,1197
Pd	14,4040	11,6472	4,9093	14,4040	11,6472	4,9093	14,4040	11,6472	4,9093
Au	15,8672	14,1271	5,0513	15,8672	14,1271	5,0513	15,8672	14,1271	5,0513
Au	17,3100	16,6565	4,7112	17,3100	16,6565	4,7112	17,3100	16,6565	4,7112
Au	12,9825	4,1641	4,7112	12,9825	4,1641	4,7112	12,9825	4,1641	4,7112
Au	14,3912	6,6835	5,0142	14,3912	6,6835	5,0142	14,3912	6,6835	5,0142
Au	15,8357	9,1997	5,0366	15,8357	9,1997	5,0366	15,8357	9,1997	5,0366
Au	17,2831	11,6733	5,0509	17,2831	11,6733	5,0509	17,2831	11,6733	5,0509
Au	18,7525	14,1581	4,7112	18,7525	14,1581	4,7112	18,7525	14,1581	4,7112
Au	15,8675	4,1641	4,7112	15,8675	4,1641	4,7112	15,8675	4,1641	4,7112
Au	17,3100	6,6626	4,7112	17,3100	6,6626	4,7112	17,3100	6,6626	4,7112
Au	18,7525	9,1611	4,7112	18,7525	9,1611	4,7112	18,7525	9,1611	4,7112
Au	20,1950	11,6596	4,7112	20,1950	11,6596	4,7112	20,1950	11,6596	4,7112
C	10,5659	8,5897	7,8944	10,2968	9,0324	7,0273	10,1964	9,1902	6,9646
C	9,8890	9,7505	7,8824	9,3347	8,7862	7,9195	10,1588	10,2079	7,8305
H	8,7983	9,7760	7,8772	11,3349	9,1457	7,3445	10,2638	8,1647	7,3342
H	10,4017	10,7129	7,9262	9,6097	8,64178	8,9714	10,2069	9,9898	8,9053
H	11,6555	8,5634	7,9452	8,2754	8,7103	7,6708	10,0778	11,2610	7,5559
H	10,0510	7,6273	7,8957	9,8609	10,5007	5,9829	13,2209	10,9740	5,9284

Ethylene dehydrogenation on O/PdAu(111)

	IS			**TS**			**FS**		
	x	*y*	*z*	*x*	*y*	*z*	*x*	*y*	*z*
Au	7,2125	7,4954	0,0000	7,2125	7,4954	0,0000	7,2125	7,4954	0,0000
Au	8,6550	9,9939	0,0000	8,6550	9,9939	0,0000	8,6550	9,9939	0,0000
Au	10,0975	12,4924	0,0000	10,0975	12,4924	0,0000	10,0975	12,4924	0,0000
Au	11,5400	14,9909	0,0000	11,5400	14,9909	0,0000	11,5400	14,9909	0,0000
Au	10,0975	7,4954	0,0000	10,0975	7,4954	0,0000	10,0975	7,4954	0,0000
Au	11,5400	9,9939	0,0000	11,5400	9,9939	0,0000	11,5400	9,9939	0,0000
Au	12,9825	12,4924	0,0000	12,9825	12,4924	0,0000	12,9825	12,4924	0,0000
Au	14,4250	14,9909	0,0000	14,4250	14,9909	0,0000	14,4250	14,9909	0,0000
Au	12,9825	7,4954	0,0000	12,9825	7,4954	0,0000	12,9825	7,4954	0,0000
Au	14,4250	9,9939	0,0000	14,4250	9,9939	0,0000	14,4250	9,9939	0,0000
Au	15,8675	12,492	0,0000	15,8675	12,492	0,0000	15,8675	12,492	0,0000
Au	15,8675	7,4954	0,0000	15,8675	7,4954	0,0000	15,8675	7,4954	0,0000
Au	17,3100	9,9939	0,0000	17,3100	9,9939	0,0000	17,3100	9,9939	0,0000
Au	5,7700	8,3283	2,3556	5,7700	8,3283	2,3556	5,7700	8,3283	2,3556
Au	7,2125	10,8268	2,3556	7,2125	10,8268	2,3556	7,2125	10,8268	2,3556
Au	8,6550	13,3252	2,3556	8,6550	13,3252	2,3556	8,6550	13,3252	2,3556
Au	10,0975	15,8237	2,3556	10,0975	15,8237	2,3556	10,0975	15,8237	2,3556
Au	7,2125	5,8298	2,3556	7,2125	5,8298	2,3556	7,2125	5,8298	2,3556

Au	8,6470	8,3235	2,5240	8,6470	8,3235	2,5240	8,6470	8,3235	2,5240
Au	10,0773	10,8180	2,5362	10,0773	10,8180	2,5362	10,0773	10,8180	2,5362
Au	11,5300	13,3021	2,5347	11,5300	13,3021	2,5347	11,5300	13,3021	2,5347
Au	12,9825	15,8237	2,3556	12,9825	15,8237	2,3556	12,9825	15,8237	2,3556
Au	10,0975	5,8298	2,3556	10,0975	5,8298	2,3556	10,0975	5,8298	2,3556
Au	11,5223	8,3153	2,5359	11,5223	8,3153	2,5359	11,5223	8,3153	2,5359
Au	12,9630	10,8161	2,5315	12,9630	10,8161	2,5315	12,9630	10,8161	2,5315
Au	14,4360	13,3114	2,5370	14,4360	13,3114	2,5370	14,4360	13,3114	2,5370
Au	15,8675	15,8237	2,3556	15,8675	15,8237	2,3556	15,8675	15,8237	2,3556
Au	12,9825	5,8297	2,3556	12,9825	5,8297	2,3556	12,9825	5,8297	2,3556
Au	14,4000	8,3317	2,5355	14,4000	8,3317	2,5355	14,4000	8,3317	2,5355
Au	15,8602	10,8439	2,5366	15,8602	10,8439	2,5366	15,8602	10,8439	2,5366
Au	17,3100	13,3252	2,3556	17,3100	13,3252	2,3556	17,3100	13,3252	2,3556
Au	15,8675	5,8298	2,3556	15,8675	5,8298	2,3556	15,8675	5,8298	2,3556
Au	17,3100	8,3283	2,3556	17,3100	8,3283	2,3556	17,3100	8,3283	2,3556
Au	18,7525	10,8268	2,3556	18,7525	10,8268	2,3556	18,7525	10,8268	2,3556
Au	4,3275	9,1611	4,7112	4,3275	9,1611	4,7112	4,3275	9,1611	4,7112
Au	5,7700	11,6596	4,7112	5,7700	11,6596	4,7112	5,7700	11,6596	4,7112
Au	7,2125	14,1581	4,7112	7,2125	14,1581	4,7112	7,2125	14,1581	4,7112
Au	8,6550	16,6565	4,7112	8,6550	16,6565	4,7112	8,6550	16,6565	4,7112
Au	5,7700	6,6626	4,7112	5,7700	6,6626	4,7112	5,7700	6,6626	4,7112
Au	7,2418	9,1521	5,1036	7,2418	9,1521	5,1036	7,2418	9,1521	5,1036
Au	8,6544	11,6193	5,0736	8,6544	11,6193	5,0736	8,6544	11,6193	5,0736
Au	10,0998	14,1188	5,0136	10,0998	14,1188	5,0136	10,0998	14,1188	5,0136
Au	11,5400	16,6565	4,7112	11,5400	16,6565	4,7112	11,5400	16,6565	4,7112
Au	7,2125	4,1641	4,7112	7,2125	4,1641	4,7112	7,2125	4,1641	4,7112
Au	8,6623	6,6923	5,1047	8,6623	6,6923	5,1047	8,6623	6,6923	5,1047
Pd	10,1032	9,1645	4,9167	10,1032	9,1645	4,9167	10,1032	9,1645	4,9167
Au	11,5442	11,6202	5,1198	11,5442	11,6202	5,1198	11,5442	11,6202	5,1198
Au	13,0014	14,1110	5,0369	13,0014	14,1110	5,0369	13,0014	14,1110	5,0369
Au	14,4250	16,6565	4,7112	14,4250	16,6565	4,7112	14,4250	16,6565	4,7112
Au	10,0975	4,1641	4,7112	10,0975	4,1641	4,7112	10,0975	4,1641	4,7112
Au	11,5045	6,6819	5,0731	11,5045	6,6819	5,0731	11,5045	6,6819	5,0731
Au	12,9509	9,1839	5,1197	12,9509	9,1839	5,1197	12,9509	9,1839	5,1197
Pd	14,4040	11,6472	4,9093	14,4040	11,6472	4,9093	14,4040	11,6472	4,9093
Au	15,8672	14,1271	5,0513	15,8672	14,1271	5,0513	15,8672	14,1271	5,0513
Au	17,3100	16,6565	4,7112	17,3100	16,6565	4,7112	17,3100	16,6565	4,7112
Au	12,9825	4,1641	4,7112	12,9825	4,1641	4,7112	12,9825	4,1641	4,7112
Au	14,3912	6,6835	5,0142	14,3912	6,6835	5,0142	14,3912	6,6835	5,0142
Au	15,8357	9,1997	5,0366	15,8357	9,1997	5,0366	15,8357	9,1997	5,0366
Au	17,2831	11,6733	5,0509	17,2831	11,6733	5,0509	17,2831	11,6733	5,0509
Au	18,7525	14,1581	4,7112	18,7525	14,1581	4,7112	18,7525	14,1581	4,7112
Au	15,8675	4,1641	4,7112	15,8675	4,1641	4,7112	15,8675	4,1641	4,7112
Au	17,3100	6,6626	4,7112	17,3100	6,6626	4,7112	17,3100	6,6626	4,7112
Au	18,7525	9,1611	4,7112	18,7525	9,1611	4,7112	18,7525	9,1611	4,7112
Au	20,1950	11,6596	4,7112	20,1950	11,6596	4,7112	20,1950	11,6596	4,7112
C	10,5407	8,5989	7,4493	12,0075	9,2897	7,1639	10,1593	9,1781	6,9669
C	9,8896	9,7935	7,4479	10,6127	9,4392	7,2048	9,9678	10,1828	7,8270
H	8,8044	9,8466	7,5401	9,9927	8,7042	7,7298	10,0310	9,9755	8,9032
H	10,4464	10,7267	7,5332	10,1767	10,4433	7,1386	9,7378	11,2113	7,5451
H	11,6268	8,5601	7,5314	12,3825	8,3619	7,6153	10,3733	8,1737	7,3378
H	9,9994	7,6561	7,5401	12,7306	10,4704	7,0564	13,5865	11,2316	7,2684
O	13,1798	10,9391	6,4476	13,1474	11,6075	6,6449	14,4396	11,5896	6,9531

Ethylene dehydrogenation on OH/PdAu(111)

	IS			TS			FS		
	x	*y*	*z*	*x*	*y*	*z*	*x*	*y*	*z*
Au	7,2125	7,4954	0,0000	7,2125	7,4954	0,0000	7,2125	7,4954	0,0000
Au	8,6550	9,9939	0,0000	8,6550	9,9939	0,0000	8,6550	9,9939	0,0000
Au	10,0975	12,4924	0,0000	10,0975	12,4924	0,0000	10,0975	12,4924	0,0000
Au	11,5400	14,9909	0,0000	11,5400	14,9909	0,0000	11,5400	14,9909	0,0000
Au	10,0975	7,4954	0,0000	10,0975	7,4954	0,0000	10,0975	7,4954	0,0000
Au	11,5400	9,9939	0,0000	11,5400	9,9939	0,0000	11,5400	9,9939	0,0000
Au	12,9825	12,4924	0,0000	12,9825	12,4924	0,0000	12,9825	12,4924	0,0000
Au	14,4250	14,9909	0,0000	14,4250	14,9909	0,0000	14,4250	14,9909	0,0000
Au	12,9825	7,4954	0,0000	12,9825	7,4954	0,0000	12,9825	7,4954	0,0000
Au	14,4250	9,9939	0,0000	14,4250	9,9939	0,0000	14,4250	9,9939	0,0000
Au	15,8675	12,492	0,0000	15,8675	12,492	0,0000	15,8675	12,492	0,0000
Au	15,8675	7,4954	0,0000	15,8675	7,4954	0,0000	15,8675	7,4954	0,0000
Au	17,3100	9,9939	0,0000	17,3100	9,9939	0,0000	17,3100	9,9939	0,0000
Au	5,7700	8,3283	2,3556	5,7700	8,3283	2,3556	5,7700	8,3283	2,3556
Au	7,2125	10,8268	2,3556	7,2125	10,8268	2,3556	7,2125	10,8268	2,3556
Au	8,6550	13,3252	2,3556	8,6550	13,3252	2,3556	8,6550	13,3252	2,3556
Au	10,0975	15,8237	2,3556	10,0975	15,8237	2,3556	10,0975	15,8237	2,3556
Au	7,2125	5,8298	2,3556	7,2125	5,8298	2,3556	7,2125	5,8298	2,3556
Au	8,6470	8,3235	2,5240	8,6470	8,3235	2,5240	8,6470	8,3235	2,5240
Au	10,0773	10,8180	2,5362	10,0773	10,8180	2,5362	10,0773	10,8180	2,5362
Au	11,5300	13,3021	2,5347	11,5300	13,3021	2,5347	11,5300	13,3021	2,5347
Au	12,9825	15,8237	2,3556	12,9825	15,8237	2,3556	12,9825	15,8237	2,3556
Au	10,0975	5,8298	2,3556	10,0975	5,8298	2,3556	10,0975	5,8298	2,3556
Au	11,5223	8,3153	2,5359	11,5223	8,3153	2,5359	11,5223	8,3153	2,5359
Au	12,9630	10,8161	2,5315	12,9630	10,8161	2,5315	12,9630	10,8161	2,5315
Au	14,4360	13,3114	2,5370	14,4360	13,3114	2,5370	14,4360	13,3114	2,5370
Au	15,8675	15,8237	2,3556	15,8675	15,8237	2,3556	15,8675	15,8237	2,3556
Au	12,9825	5,8297	2,3556	12,9825	5,8297	2,3556	12,9825	5,8297	2,3556
Au	14,4000	8,3317	2,5355	14,4000	8,3317	2,5355	14,4000	8,3317	2,5355
Au	15,8602	10,8439	2,5366	15,8602	10,8439	2,5366	15,8602	10,8439	2,5366
Au	17,3100	13,3252	2,3556	17,3100	13,3252	2,3556	17,3100	13,3252	2,3556
Au	15,8675	5,8298	2,3556	15,8675	5,8298	2,3556	15,8675	5,8298	2,3556
Au	17,3100	8,3283	2,3556	17,3100	8,3283	2,3556	17,3100	8,3283	2,3556
Au	18,7525	10,8268	2,3556	18,7525	10,8268	2,3556	18,7525	10,8268	2,3556
Au	4,3275	9,1611	4,7112	4,3275	9,1611	4,7112	4,3275	9,1611	4,7112
Au	5,7700	11,6596	4,7112	5,7700	11,6596	4,7112	5,7700	11,6596	4,7112
Au	7,2125	14,1581	4,7112	7,2125	14,1581	4,7112	7,2125	14,1581	4,7112
Au	8,6550	16,6565	4,7112	8,6550	16,6565	4,7112	8,6550	16,6565	4,7112
Au	5,7700	6,6626	4,7112	5,7700	6,6626	4,7112	5,7700	6,6626	4,7112
Au	7,2418	9,1521	5,1036	7,2418	9,1521	5,1036	7,2418	9,1521	5,1036
Au	8,6544	11,6193	5,0736	8,6544	11,6193	5,0736	8,6544	11,6193	5,0736
Au	10,0998	14,1188	5,0136	10,0998	14,1188	5,0136	10,0998	14,1188	5,0136
Au	11,5400	16,6565	4,7112	11,5400	16,6565	4,7112	11,5400	16,6565	4,7112
Au	7,2125	4,1641	4,7112	7,2125	4,1641	4,7112	7,2125	4,1641	4,7112
Au	8,6623	6,6923	5,1047	8,6623	6,6923	5,1047	8,6623	6,6923	5,1047

Pd	10,1032	9,1645	4,9167	10,1032	9,1645	4,9167	10,1032	9,1645	4,9167
Au	11,5442	11,6202	5,1198	11,5442	11,6202	5,1198	11,5442	11,6202	5,1198
Au	13,0014	14,1110	5,0369	13,0014	14,1110	5,0369	13,0014	14,1110	5,0369
Au	14,4250	16,6565	4,7112	14,4250	16,6565	4,7112	14,4250	16,6565	4,7112
Au	10,0975	4,1641	4,7112	10,0975	4,1641	4,7112	10,0975	4,1641	4,7112
Au	11,5045	6,6819	5,0731	11,5045	6,6819	5,0731	11,5045	6,6819	5,0731
Au	12,9509	9,1839	5,1197	12,9509	9,1839	5,1197	12,9509	9,1839	5,1197
Pd	14,4040	11,6472	4,9093	14,4040	11,6472	4,9093	14,4040	11,6472	4,9093
Au	15,8672	14,1271	5,0513	15,8672	14,1271	5,0513	15,8672	14,1271	5,0513
Au	17,3100	16,6565	4,7112	17,3100	16,6565	4,7112	17,3100	16,6565	4,7112
Au	12,9825	4,1641	4,7112	12,9825	4,1641	4,7112	12,9825	4,1641	4,7112
Au	14,3912	6,6835	5,0142	14,3912	6,6835	5,0142	14,3912	6,6835	5,0142
Au	15,8357	9,1997	5,0366	15,8357	9,1997	5,0366	15,8357	9,1997	5,0366
Au	17,2831	11,6733	5,0509	17,2831	11,6733	5,0509	17,2831	11,6733	5,0509
Au	18,7525	14,1581	4,7112	18,7525	14,1581	4,7112	18,7525	14,1581	4,7112
Au	15,8675	4,1641	4,7112	15,8675	4,1641	4,7112	15,8675	4,1641	4,7112
Au	17,3100	6,6626	4,7112	17,3100	6,6626	4,7112	17,3100	6,6626	4,7112
Au	18,7525	9,1611	4,7112	18,7525	9,1611	4,7112	18,7525	9,1611	4,7112
Au	20,1950	11,6596	4,7112	20,1950	11,6596	4,7112	20,1950	11,6596	4,7112
C	10,3566	8,5871	7,5547	12,1914	9,2237	7,2216	10,1650	9,1696	6,9790
C	9,8403	9,8393	7,5583	10,8175	9,4365	7,3253	9,9112	10,1684	7,8382
H	8,7637	10,0063	7,6105	10,1754	8,7135	7,8412	10,0365	9,9876	8,9069
H	10,4807	10,7193	7,6282	10,3924	10,4391	7,2158	9,5708	11,1658	7,5464
H	11,4313	8,4153	7,6235	12,5360	8,2572	7,6125	10,4818	8,1858	7,3333
H	9,7158	7,7062	7,6088	14,4790	11,5024	7,7137	14,0417	10,7430	7,6125
O	13,3250	11,7247	6,8093	13,7869	11,3199	7,0498	14,4863	11,5629	7,3142
H	13,4579	10,8518	7,2309	13,0830	10,3158	7,2463	14,0175	12,2725	7,7752

Ethylene dehydrogenation on PdAu(100)

	IS			**TS**			**FS**		
	x	*y*	*z*	*x*	*y*	*z*	*x*	*y*	*z*
Au	4,0800	-2,0400	-2,4695	4,0800	-2,0400	-2,4695	4,0800	-2,0400	-2,4695
Au	2,0400	-4,0800	-2,4695	2,0400	-4,0800	-2,4695	2,0400	-4,0800	-2,4695
Au	4,0800	2,0400	-2,4695	4,0800	2,0400	-2,4695	4,0800	2,0400	-2,4695
Au	2,0400	0,0000	-2,4695	2,0400	0,0000	-2,4695	2,0400	0,0000	-2,4695
Au	0,0000	-2,0400	-2,4695	0,0000	-2,0400	-2,4695	0,0000	-2,0400	-2,4695
Au	-2,0400	-4,0800	-2,4695	-2,0400	-4,0800	-2,4695	-2,0400	-4,0800	-2,4695
Au	2,0400	4,0800	-2,4695	2,0400	4,0800	-2,4695	2,0400	4,0800	-2,4695
Au	0,0000	2,0400	-2,4695	0,0000	2,0400	-2,4695	0,0000	2,0400	-2,4695
Au	-2,0400	0,0000	-2,4695	-2,0400	0,0000	-2,4695	-2,0400	0,0000	-2,4695
Au	-4,0800	-2,0400	-2,4695	-4,0800	-2,0400	-2,4695	-4,0800	-2,0400	-2,4695
Au	-2,0400	4,0800	-2,4695	-2,0400	4,0800	-2,4695	-2,0400	4,0800	-2,4695
Au	-4,0800	2,0400	-2,4695	-4,0800	2,0400	-2,4695	-4,0800	2,0400	-2,4695
Au	6,1200	-2,0400	-0,4295	6,1200	-2,0400	-0,4295	6,1200	-2,0400	-0,4295
Au	4,0800	-4,0800	-0,4295	4,0800	-4,0800	-0,4295	4,0800	-4,0800	-0,4295
Au	2,0400	-6,1200	-0,4295	2,0400	-6,1200	-0,4295	2,0400	-6,1200	-0,4295
Au	6,1200	2,0400	-0,4295	6,1200	2,0400	-0,4295	6,1200	2,0400	-0,4295
Au	4,1303	0,0000	-0,4335	4,1303	0,0000	-0,4335	4,1303	0,0000	-0,4335
Au	2,0104	-2,0092	-0,2598	2,0104	-2,0092	-0,2598	2,0104	-2,0092	-0,2598
Au	-0.0005	-4,1513	-0,4582	-0.0005	-4,1513	-0,4582	-0.0005	-4,1513	-0,4582

Au	-2,0400	-6,1200	-0,4295	-2,0400	-6,1200	-0,4295	-2,0400	-6,1200	-0,4295
Au	4,0800	4,0800	-0,4295	4,0800	4,0800	-0,4295	4,0800	4,0800	-0,4295
Au	2,0105	2,0093	-0,2596	2,0105	2,0093	-0,2596	2,0105	2,0093	-0,2596
Au	-0.0001	0,0000	-0,2763	-0.0001	0,0000	-0,2763	-0.0001	0,0000	-0,2763
Au	-2,0115	-2,0087	-0,2588	-2,0115	-2,0087	-0,2588	-2,0115	-2,0087	-0,2588
Au	-4,0800	-4,0800	-0,4295	-4,0800	-4,0800	-0,4295	-4,0800	-4,0800	-0,4295
Au	2,0400	6,1200	-0,4295	2,0400	6,1200	-0,4295	2,0400	6,1200	-0,4295
Au	-0.0005	4,1509	-0,458	-0.0005	4,1509	-0,458	-0.0005	4,1509	-0,458
Au	-2,0116	2,0087	-0,2587	-2,0116	2,0087	-0,2587	-2,0116	2,0087	-0,2587
Au	-4,1298	0,0000	-0,4334	-4,1298	0,0000	-0,4334	-4,1298	0,0000	-0,4334
Au	-6,1200	-2,0400	-0,4295	-6,1200	-2,0400	-0,4295	-6,1200	-2,0400	-0,4295
Au	-2,0400	6,1200	-0,4295	-2,0400	6,1200	-0,4295	-2,0400	6,1200	-0,4295
Au	-4,0800	4,0800	-0,4295	-4,0800	4,0800	-0,4295	-4,0800	4,0800	-0,4295
Au	-6,1200	2,0400	-0,4295	-6,1200	2,0400	-0,4295	-6,1200	2,0400	-0,4295
Au	6,1200	-4,0800	1,6105	6,1200	-4,0800	1,6105	6,1200	-4,0800	1,6105
Au	4,0800	-6,1200	1,6105	4,0800	-6,1200	1,6105	4,0800	-6,1200	1,6105
Au	6,1200	0,0000	1,6105	6,1200	0,0000	1,6105	6,1200	0,0000	1,6105
Au	4,0420	-2,0081	1,8525	4,0420	-2,0081	1,8525	4,0420	-2,0081	1,8525
Au	2,0068	-4,0368	1,8579	2,0068	-4,0368	1,8579	2,0068	-4,0368	1,8579
Au	0,0000	-6,1200	1,6105	0,0000	-6,1200	1,6105	0,0000	-6,1200	1,6105
Au	6,1200	4,0800	1,6105	6,1200	4,0800	1,6105	6,1200	4,0800	1,6105
Au	4,0419	2,0082	1,8523	4,0419	2,0082	1,8523	4,0419	2,0082	1,8523
Pd	2,0426	0,0000	1,7918	2,0426	0,0000	1,7918	2,0426	0,0000	1,7918
Au	0,0000	-1,9640	1,9533	0,0000	-1,9640	1,9533	0,0000	-1,9640	1,9533
Au	-2,0073	-4,0364	1,8578	-2,0073	-4,0364	1,8578	-2,0073	-4,0364	1,8578
Au	-4,0800	-6,1200	1,6105	-4,0800	-6,1200	1,6105	-4,0800	-6,1200	1,6105
Au	4,0800	6,1200	1,6105	4,0800	6,1200	1,6105	4,0800	6,1200	1,6105
Au	2,0068	4,0367	1,8576	2,0068	4,0367	1,8576	2,0068	4,0367	1,8576
Au	0.0001	1,9640	1,953	0.0001	1,9640	1,953	0.0001	1,9640	1,953
Pd	-2,0432	0,000	1,7922	-2,0432	0,000	1,7922	-2,0432	0,000	1,7922
Au	-4,0427	-2,0083	1,8524	-4,0427	-2,0083	1,8524	-4,0427	-2,0083	1,8524
Au	-6,1200	-4,0800	1,6105	-6,1200	-4,0800	1,6105	-6,1200	-4,0800	1,6105
Au	0,0000	6,1200	1,6105	0,0000	6,1200	1,6105	0,0000	6,1200	1,6105
Au	-2,0073	4,0363	1,8574	-2,0073	4,0363	1,8574	-2,0073	4,0363	1,8574
Au	-4,0426	2,0084	1,8521	-4,0426	2,0084	1,8521	-4,0426	2,0084	1,8521
Au	-6,1200	0,000	1,6105	-6,1200	0,000	1,6105	-6,1200	0,000	1,6105
Au	-4,0800	6,1200	1,6105	-4,0800	6,1200	1,6105	-4,0800	6,1200	1,6105
Au	-6,1200	4,0800	1,6105	-6,1200	4,0800	1,6105	-6,1200	4,0800	1,6105
C	-2,6851	-0,5606	4,09978	-2,2322	-0,2577	3,8703	-2,1823	-0,1431	3,8246
C	-1,6200	0,3091	4,11036	-3,0403	0,3770	4,7250	-2,3128	0,8574	4,7002
H	-2,5256	-1,6317	4,22962	-1,6123	-1,0897	4,2116	-2,1068	-1,1779	4,1691
H	-3,7065	-0,1958	4,2105	-3,1359	0,0103	5,7542	1,0885	0,8767	2,8836
H	-1,7813	1,3797	4,24369	-3,6377	1,2512	4,4581	-2,3871	1,9099	4,4253
H	-0,6044	-0,0564	4,26218	-1,1520	0,9059	2,9321	-2,3422	0,6312	5,7745

Ethylene dehydrogenation on O/PdAu(100)

	IS			**TS**			**FS**		
	x	*y*	*z*	*x*	*y*	*z*	*x*	*y*	*z*
Au	4,0800	-2,0400	-2,4695	4,0800	-2,0400	-2,4695	4,0800	-2,0400	-2,4695
Au	2,0400	-4,0800	-2,4695	2,0400	-4,0800	-2,4695	2,0400	-4,0800	-2,4695
Au	4,0800	2,0400	-2,4695	4,0800	2,0400	-2,4695	4,0800	2,0400	-2,4695
Au	2,0400	0,0000	-2,4695	2,0400	0,0000	-2,4695	2,0400	0,0000	-2,4695
Au	0,0000	-2,0400	-2,4695	0,0000	-2,0400	-2,4695	0,0000	-2,0400	-2,4695

Au	-2,0400	-4,0800	-2,4695	-2,0400	-4,0800	-2,4695	-2,0400	-4,0800	-2,4695
Au	2,0400	4,0800	-2,4695	2,0400	4,0800	-2,4695	2,0400	4,0800	-2,4695
Au	0,0000	2,0400	-2,4695	0,0000	2,0400	-2,4695	0,0000	2,0400	-2,4695
Au	-2,0400	0,0000	-2,4695	-2,0400	0,0000	-2,4695	-2,0400	0,0000	-2,4695
Au	-4,0800	-2,0400	-2,4695	-4,0800	-2,0400	-2,4695	-4,0800	-2,0400	-2,4695
Au	-2,0400	4,0800	-2,4695	-2,0400	4,0800	-2,4695	-2,0400	4,0800	-2,4695
Au	-4,0800	2,0400	-2,4695	-4,0800	2,0400	-2,4695	-4,0800	2,0400	-2,4695
Au	6,1200	-2,0400	-0,4295	6,1200	-2,0400	-0,4295	6,1200	-2,0400	-0,4295
Au	4,0800	-4,0800	-0,4295	4,0800	-4,0800	-0,4295	4,0800	-4,0800	-0,4295
Au	2,0400	-6,1200	-0,4295	2,0400	-6,1200	-0,4295	2,0400	-6,1200	-0,4295
Au	6,1200	2,0400	-0,4295	6,1200	2,0400	-0,4295	6,1200	2,0400	-0,4295
Au	4,1303	0,0000	-0,4335	4,1303	0,0000	-0,4335	4,1303	0,0000	-0,4335
Au	2,0104	-2,0092	-0,2598	2,0104	-2,0092	-0,2598	2,0104	-2,0092	-0,2598
Au	-0.0005	-4,1513	-0,4582	-0.0005	-4,1513	-0,4582	-0.0005	-4,1513	-0,4582
Au	-2,0400	-6,1200	-0,4295	-2,0400	-6,1200	-0,4295	-2,0400	-6,1200	-0,4295
Au	4,0800	4,0800	-0,4295	4,0800	4,0800	-0,4295	4,0800	4,0800	-0,4295
Au	2,0105	2,0093	-0,2596	2,0105	2,0093	-0,2596	2,0105	2,0093	-0,2596
Au	-0.0001	0,0000	-0,2763	-0.0001	0,0000	-0,2763	-0.0001	0,0000	-0,2763
Au	-2,0115	-2,0087	-0,2588	-2,0115	-2,0087	-0,2588	-2,0115	-2,0087	-0,2588
Au	-4,0800	-4,0800	-0,4295	-4,0800	-4,0800	-0,4295	-4,0800	-4,0800	-0,4295
Au	2,0400	6,1200	-0,4295	2,0400	6,1200	-0,4295	2,0400	6,1200	-0,4295
Au	-0.0005	4,1509	-0,458	-0.0005	4,1509	-0,458	-0.0005	4,1509	-0,458
Au	-2,0116	2,0087	-0,2587	-2,0116	2,0087	-0,2587	-2,0116	2,0087	-0,2587
Au	-4,1298	0,0000	-0,4334	-4,1298	0,0000	-0,4334	-4,1298	0,0000	-0,4334
Au	-6,1200	-2,0400	-0,4295	-6,1200	-2,0400	-0,4295	-6,1200	-2,0400	-0,4295
Au	-2,0400	6,1200	-0,4295	-2,0400	6,1200	-0,4295	-2,0400	6,1200	-0,4295
Au	-4,0800	4,0800	-0,4295	-4,0800	4,0800	-0,4295	-4,0800	4,0800	-0,4295
Au	-6,1200	2,0400	-0,4295	-6,1200	2,0400	-0,4295	-6,1200	2,0400	-0,4295
Au	6,1200	-4,0800	1,6105	6,1200	-4,0800	1,6105	6,1200	-4,0800	1,6105
Au	4,0800	-6,1200	1,6105	4,0800	-6,1200	1,6105	4,0800	-6,1200	1,6105
Au	6,1200	0,0000	1,6105	6,1200	0,0000	1,6105	6,1200	0,0000	1,6105
Au	4,0420	-2,0081	1,8525	4,0420	-2,0081	1,8525	4,0420	-2,0081	1,8525
Au	2,0068	-4,0368	1,8579	2,0068	-4,0368	1,8579	2,0068	-4,0368	1,8579
Au	0,0000	-6,1200	1,6105	0,0000	-6,1200	1,6105	0,0000	-6,1200	1,6105
Au	6,1200	4,0800	1,6105	6,1200	4,0800	1,6105	6,1200	4,0800	1,6105
Au	4,0419	2,0082	1,8523	4,0419	2,0082	1,8523	4,0419	2,0082	1,8523
Pd	2,0426	0,0000	1,7918	2,0426	0,0000	1,7918	2,0426	0,0000	1,7918
Au	0,0000	-1,9640	1,9533	0,0000	-1,9640	1,9533	0,0000	-1,9640	1,9533
Au	-2,0073	-4,0364	1,8578	-2,0073	-4,0364	1,8578	-2,0073	-4,0364	1,8578
Au	-4,0800	-6,1200	1,6105	-4,0800	-6,1200	1,6105	-4,0800	-6,1200	1,6105
Au	4,0800	6,1200	1,6105	4,0800	6,1200	1,6105	4,0800	6,1200	1,6105
Au	2,0068	4,0367	1,8576	2,0068	4,0367	1,8576	2,0068	4,0367	1,8576
Au	0.0001	1,9640	1,953	0.0001	1,9640	1,953	0.0001	1,9640	1,953
Pd	-2,0432	0,000	1,7922	-2,0432	0,000	1,7922	-2,0432	0,000	1,7922
Au	-4,0427	-2,0083	1,8524	-4,0427	-2,0083	1,8524	-4,0427	-2,0083	1,8524
Au	-6,1200	-4,0800	1,6105	-6,1200	-4,0800	1,6105	-6,1200	-4,0800	1,6105
Au	0,0000	6,1200	1,6105	0,0000	6,1200	1,6105	0,0000	6,1200	1,6105
Au	-2,0073	4,0363	1,8574	-2,0073	4,0363	1,8574	-2,0073	4,0363	1,8574
Au	-4,0426	2,0084	1,8521	-4,0426	2,0084	1,8521	-4,0426	2,0084	1,8521
Au	-6,1200	0,000	1,6105	-6,1200	0,000	1,6105	-6,1200	0,000	1,6105
Au	-4,0800	6,1200	1,6105	-4,0800	6,1200	1,6105	-4,0800	6,1200	1,6105
Au	-6,1200	4,0800	1,6105	-6,1200	4,0800	1,6105	-6,1200	4,0800	1,6105
C	-2,4996	-0,5916	4,1135	-1,6295	0,0541	3,9531	-2,0378	-0,1184	3,8238
C	-1,6011	0,4469	4,0936	-2,2485	-1,0445	4,4759	-1,8736	0,8852	4,6962
H	-2,1592	-1,6202	4,2381	-1,9743	1,0327	4,3072	-2,2134	-1,1362	4,1819
H	-3,5670	-0,4067	4,2409	-1,9265	-2,0626	4,2488	-1,7161	1,9250	4,4070

H	-1,9451	1,4747	4,2200	-3,0535	-0,9487	5,2150	-1,9120	0,6793	5,7743
H	-0,5275	0,2758	4,2015	0,8571	0,5755	3,4175	1,2847	0,9917	3,5438
O	1,5202	1,2150	3,2699	-0,3210	0,1172	3,7042	0,6330	0,3960	3,9712

Ethylene dehydrogenation on OH/PdAu(100)

	R			**TS**			**P**		
	x	*y*	*z*	*x*	*y*	*z*	*x*	*y*	*z*
Au	4,0800	-2,0400	-2,4695	4,0800	-2,0400	-2,4695	4,0800	-2,0400	-2,4695
Au	2,0400	-4,0800	-2,4695	2,0400	-4,0800	-2,4695	2,0400	-4,0800	-2,4695
Au	4,0800	2,0400	-2,4695	4,0800	2,0400	-2,4695	4,0800	2,0400	-2,4695
Au	2,0400	0,0000	-2,4695	2,0400	0,0000	-2,4695	2,0400	0,0000	-2,4695
Au	0,0000	-2,0400	-2,4695	0,0000	-2,0400	-2,4695	0,0000	-2,0400	-2,4695
Au	-2,0400	-4,0800	-2,4695	-2,0400	-4,0800	-2,4695	-2,0400	-4,0800	-2,4695
Au	2,0400	4,0800	-2,4695	2,0400	4,0800	-2,4695	2,0400	4,0800	-2,4695
Au	0,0000	2,0400	-2,4695	0,0000	2,0400	-2,4695	0,0000	2,0400	-2,4695
Au	-2,0400	0,0000	-2,4695	-2,0400	0,0000	-2,4695	-2,0400	0,0000	-2,4695
Au	-4,0800	-2,0400	-2,4695	-4,0800	-2,0400	-2,4695	-4,0800	-2,0400	-2,4695
Au	-2,0400	4,0800	-2,4695	-2,0400	4,0800	-2,4695	-2,0400	4,0800	-2,4695
Au	-4,0800	2,0400	-2,4695	-4,0800	2,0400	-2,4695	-4,0800	2,0400	-2,4695
Au	6,1200	-2,0400	-0,4295	6,1200	-2,0400	-0,4295	6,1200	-2,0400	-0,4295
Au	4,0800	-4,0800	-0,4295	4,0800	-4,0800	-0,4295	4,0800	-4,0800	-0,4295
Au	2,0400	-6,1200	-0,4295	2,0400	-6,1200	-0,4295	2,0400	-6,1200	-0,4295
Au	6,1200	2,0400	-0,4295	6,1200	2,0400	-0,4295	6,1200	2,0400	-0,4295
Au	4,1303	0,0000	-0,4335	4,1303	0,0000	-0,4335	4,1303	0,0000	-0,4335
Au	2,0104	-2,0092	-0,2598	2,0104	-2,0092	-0,2598	2,0104	-2,0092	-0,2598
Au	-0.0005	-4,1513	-0,4582	-0.0005	-4,1513	-0,4582	-0.0005	-4,1513	-0,4582
Au	-2,0400	-6,1200	-0,4295	-2,0400	-6,1200	-0,4295	-2,0400	-6,1200	-0,4295
Au	4,0800	4,0800	-0,4295	4,0800	4,0800	-0,4295	4,0800	4,0800	-0,4295
Au	2,0105	2,0093	-0,2596	2,0105	2,0093	-0,2596	2,0105	2,0093	-0,2596
Au	-0.0001	0,0000	-0,2763	-0.0001	0,0000	-0,2763	-0.0001	0,0000	-0,2763
Au	-2,0115	-2,0087	-0,2588	-2,0115	-2,0087	-0,2588	-2,0115	-2,0087	-0,2588
Au	-4,0800	-4,0800	-0,4295	-4,0800	-4,0800	-0,4295	-4,0800	-4,0800	-0,4295
Au	2,0400	6,1200	-0,4295	2,0400	6,1200	-0,4295	2,0400	6,1200	-0,4295
Au	-0.0005	4,1509	-0,458	-0.0005	4,1509	-0,458	-0.0005	4,1509	-0,458
Au	-2,0116	2,0087	-0,2587	-2,0116	2,0087	-0,2587	-2,0116	2,0087	-0,2587
Au	-4,1298	0,0000	-0,4334	-4,1298	0,0000	-0,4334	-4,1298	0,0000	-0,4334
Au	-6,1200	-2,0400	-0,4295	-6,1200	-2,0400	-0,4295	-6,1200	-2,0400	-0,4295
Au	-2,0400	6,1200	-0,4295	-2,0400	6,1200	-0,4295	-2,0400	6,1200	-0,4295
Au	-4,0800	4,0800	-0,4295	-4,0800	4,0800	-0,4295	-4,0800	4,0800	-0,4295
Au	-6,1200	2,0400	-0,4295	-6,1200	2,0400	-0,4295	-6,1200	2,0400	-0,4295
Au	6,1200	-4,0800	1,6105	6,1200	-4,0800	1,6105	6,1200	-4,0800	1,6105
Au	4,0800	-6,1200	1,6105	4,0800	-6,1200	1,6105	4,0800	-6,1200	1,6105
Au	6,1200	0,0000	1,6105	6,1200	0,0000	1,6105	6,1200	0,0000	1,6105
Au	4,0420	-2,0081	1,8525	4,0420	-2,0081	1,8525	4,0420	-2,0081	1,8525
Au	2,0068	-4,0368	1,8579	2,0068	-4,0368	1,8579	2,0068	-4,0368	1,8579
Au	0,0000	-6,1200	1,6105	0,0000	-6,1200	1,6105	0,0000	-6,1200	1,6105
Au	6,1200	4,0800	1,6105	6,1200	4,0800	1,6105	6,1200	4,0800	1,6105
Au	4,0419	2,0082	1,8523	4,0419	2,0082	1,8523	4,0419	2,0082	1,8523
Pd	2,0426	0,0000	1,7918	2,0426	0,0000	1,7918	2,0426	0,0000	1,7918
Au	0,0000	-1,9640	1,9533	0,0000	-1,9640	1,9533	0,0000	-1,9640	1,9533
Au	-2,0073	-4,0364	1,8578	-2,0073	-4,0364	1,8578	-2,0073	-4,0364	1,8578
Au	-4,0800	-6,1200	1,6105	-4,0800	-6,1200	1,6105	-4,0800	-6,1200	1,6105
Au	4,0800	6,1200	1,6105	4,0800	6,1200	1,6105	4,0800	6,1200	1,6105
Au	2,0068	4,0367	1,8576	2,0068	4,0367	1,8576	2,0068	4,0367	1,8576

Au	0.0001	1,9640	1,953	0.0001	1,9640	1,953	0.0001	1,9640	1,953
Pd	-2,0432	0,000	1,7922	-2,0432	0,000	1,7922	-2,0432	0,000	1,7922
Au	-4,0427	-2,0083	1,8524	-4,0427	-2,0083	1,8524	-4,0427	-2,0083	1,8524
Au	-6,1200	-4,0800	1,6105	-6,1200	-4,0800	1,6105	-6,1200	-4,0800	1,6105
Au	0,0000	6,1200	1,6105	0,0000	6,1200	1,6105	0,0000	6,1200	1,6105
Au	-2,0073	4,0363	1,8574	-2,0073	4,0363	1,8574	-2,0073	4,0363	1,8574
Au	-4,0426	2,0084	1,8521	-4,0426	2,0084	1,8521	-4,0426	2,0084	1,8521
Au	-6,1200	0,000	1,6105	-6,1200	0,000	1,6105	-6,1200	0,000	1,6105
Au	-4,0800	6,1200	1,6105	-4,0800	6,1200	1,6105	-4,0800	6,1200	1,6105
Au	-6,1200	4,0800	1,6105	-6,1200	4,0800	1,6105	-6,1200	4,0800	1,6105
C	-2,9763	-0,5998	4,1628	-0,8471	1,1088	3,8983	-1,8536	-0,1879	3,8215
C	-1,7697	0,0488	4,1277	-1,6418	-0,0374	4,0161	-1,6103	0,7558	4,7491
H	-3,0234	-1,6797	4,3213	-1,3318	2,0171	4,2793	-2,0576	-1,2070	4,1623
H	-3,9130	-0,0464	4,2263	-2,6040	-0,0019	4,5388	-1,4248	1,8059	4,5161
H	-1,7110	1,1316	4,2386	-1,1719	-1,0318	4,0050	-1,6667	0,4941	5,8147
H	-0,8563	-0,5262	4,2973	0,5093	0,7419	3,9954	0,6884	0,1403	4,2755
O	1,4248	1,0680	3,5485	1,6640	0,3201	3,9344	1,6717	0,1359	4,1978
H	0,9061	0,4439	4,0893	1,7991	-0,4871	4,4642	1,9401	1,0447	4,4327

Cartesian coordinates of the preferred adsorption sites for O, OH, H and H_2O on PdAu(100) and (111).

O adsorption on PdAu(100) : Four-fold Hollow site

	x	*y*	*z*
Au	4,0800	-2,0400	-2,4695
Au	2,0400	-4,0800	-2,4695
Au	4,0800	2,0400	-2,4695
Au	2,0400	0,0000	-2,4695
Au	0,0000	-2,0400	-2,4695
Au	-2,0400	-4,0800	-2,4695
Au	2,0400	4,0800	-2,4695
Au	0,0000	2,0400	-2,4695
Au	-2,0400	0,0000	-2,4695
Au	-4,0800	-2,0400	-2,4695
Au	-2,0400	4,0800	-2,4695
Au	-4,0800	2,0400	-2,4695
Au	6,1200	-2,0400	-0,4295
Au	4,0800	-4,0800	-0,4295
Au	2,0400	-6,1200	-0,4295
Au	6,1200	2,0400	-0,4295
Au	4,1303	0,0000	-0,4335
Au	2,0104	-2,0092	-0,2598
Au	-0.0005	-4,1513	-0,4582
Au	-2,0400	-6,1200	-0,4295
Au	4,0800	4,0800	-0,4295
Au	2,0105	2,0093	-0,2596
Au	-0.0001	0,0000	-0,2763
Au	-2,0115	-2,0087	-0,2588
Au	-4,0800	-4,0800	-0,4295
Au	2,0400	6,1200	-0,4295
Au	-0.0005	4,1509	-0,458

Au	-2,0116	2,0087	-0,2587
Au	-4,1298	0,0000	-0,4334
Au	-6,1200	-2,0400	-0,4295
Au	-2,0400	6,1200	-0,4295
Au	-4,0800	4,0800	-0,4295
Au	-6,1200	2,0400	-0,4295
Au	6,1200	-4,0800	1,6105
Au	4,0800	-6,1200	1,6105
Au	6,1200	0,0000	1,6105
Au	4,0420	-2,0081	1,8525
Au	2,0068	-4,0368	1,8579
Au	0,0000	-6,1200	1,6105
Au	6,1200	4,0800	1,6105
Au	4,0419	2,0082	1,8523
Pd	2,0426	0,0000	1,7918
Au	0,0000	-1,9640	1,9533
Au	-2,0073	-4,0364	1,8578
Au	-4,0800	-6,1200	1,6105
Au	4,0800	6,1200	1,6105
Au	2,0068	4,0367	1,8576
Au	0.0001	1,9640	1,953
Pd	-2,0432	0,000	1,7922
Au	-4,0427	-2,0083	1,8524
Au	-6,1200	-4,0800	1,6105
Au	0,0000	6,1200	1,6105
Au	-2,0073	4,0363	1,8574
Au	-4,0426	2,0084	1,8521
Au	-6,1200	0,000	1,6105
Au	-4,0800	6,1200	1,6105
Au	-6,1200	4,0800	1,6105
O	-0.0193	-0.0001	2.9940

OH adsorption on PdAu(111) : PdAu Bridge site

	x	*y*	*z*
Au	4,0800	-2,0400	-2,4695
Au	2,0400	-4,0800	-2,4695
Au	4,0800	2,0400	-2,4695
Au	2,0400	0,0000	-2,4695
Au	0,0000	-2,0400	-2,4695
Au	-2,0400	-4,0800	-2,4695
Au	2,0400	4,0800	-2,4695
Au	0,0000	2,0400	-2,4695
Au	-2,0400	0,0000	-2,4695
Au	-4,0800	-2,0400	-2,4695
Au	-2,0400	4,0800	-2,4695
Au	-4,0800	2,0400	-2,4695
Au	6,1200	-2,0400	-0,4295
Au	4,0800	-4,0800	-0,4295
Au	2,0400	-6,1200	-0,4295
Au	6,1200	2,0400	-0,4295
Au	4,1303	0,0000	-0,4335
Au	2,0104	-2,0092	-0,2598
Au	-0.0005	-4,1513	-0,4582
Au	-2,0400	-6,1200	-0,4295
Au	4,0800	4,0800	-0,4295
Au	2,0105	2,0093	-0,2596

Au	-0.0001	0,0000	-0,2763
Au	-2,0115	-2,0087	-0,2588
Au	-4,0800	-4,0800	-0,4295
Au	2,0400	6,1200	-0,4295
Au	-0.0005	4,1509	-0,458
Au	-2,0116	2,0087	-0,2587
Au	-4,1298	0,0000	-0,4334
Au	-6,1200	-2,0400	-0,4295
Au	-2,0400	6,1200	-0,4295
Au	-4,0800	4,0800	-0,4295
Au	-6,1200	2,0400	-0,4295
Au	6,1200	-4,0800	1,6105
Au	4,0800	-6,1200	1,6105
Au	6,1200	0,0000	1,6105
Au	4,0420	-2,0081	1,8525
Au	2,0068	-4,0368	1,8579
Au	0,0000	-6,1200	1,6105
Au	6,1200	4,0800	1,6105
Au	4,0419	2,0082	1,8523
Pd	2,0426	0,0000	1,7918
Au	0,0000	-1,9640	1,9533
Au	-2,0073	-4,0364	1,8578
Au	-4,0800	-6,1200	1,6105
Au	4,0800	6,1200	1,6105
Au	2,0068	4,0367	1,8576
Au	0.0001	1,9640	1,953
Pd	-2,0432	0,000	1,7922
Au	-4,0427	-2,0083	1,8524
Au	-6,1200	-4,0800	1,6105
Au	0,0000	6,1200	1,6105
Au	-2,0073	4,0363	1,8574
Au	-4,0426	2,0084	1,8521
Au	-6,1200	0,000	1,6105
Au	-4,0800	6,1200	1,6105
Au	-6,1200	4,0800	1,6105
O	1,2659	0,9795	3,5498
H	0,6902	0,3327	4,0035

H adsorption on PdAu(100) : PdAu Bridge site

	x	*y*	*z*
Au	4,0800	-2,0400	-2,4695
Au	2,0400	-4,0800	-2,4695
Au	4,0800	2,0400	-2,4695
Au	2,0400	0,0000	-2,4695
Au	0,0000	-2,0400	-2,4695
Au	-2,0400	-4,0800	-2,4695
Au	2,0400	4,0800	-2,4695
Au	0,0000	2,0400	-2,4695
Au	-2,0400	0,0000	-2,4695
Au	-4,0800	-2,0400	-2,4695
Au	-2,0400	4,0800	-2,4695
Au	-4,0800	2,0400	-2,4695
Au	6,1200	-2,0400	-0,4295
Au	4,0800	-4,0800	-0,4295
Au	2,0400	-6,1200	-0,4295

Au	6,1200	2,0400	-0,4295
Au	4,1303	0,0000	-0,4335
Au	2,0104	-2,0092	-0,2598
Au	-0.0005	-4,1513	-0,4582
Au	-2,0400	-6,1200	-0,4295
Au	4,0800	4,0800	-0,4295
Au	2,0105	2,0093	-0,2596
Au	-0.0001	0,0000	-0,2763
Au	-2,0115	-2,0087	-0,2588
Au	-4,0800	-4,0800	-0,4295
Au	2,0400	6,1200	-0,4295
Au	-0.0005	4,1509	-0,458
Au	-2,0116	2,0087	-0,2587
Au	-4,1298	0,0000	-0,4334
Au	-6,1200	-2,0400	-0,4295
Au	-2,0400	6,1200	-0,4295
Au	-4,0800	4,0800	-0,4295
Au	-6,1200	2,0400	-0,4295
Au	6,1200	-4,0800	1,6105
Au	4,0800	-6,1200	1,6105
Au	6,1200	0,0000	1,6105
Au	4,0420	-2,0081	1,8525
Au	2,0068	-4,0368	1,8579
Au	0,0000	-6,1200	1,6105
Au	6,1200	4,0800	1,6105
Au	4,0419	2,0082	1,8523
Pd	2,0426	0,0000	1,7918
Au	0,0000	-1,9640	1,9533
Au	-2,0073	-4,0364	1,8578
Au	-4,0800	-6,1200	1,6105
Au	4,0800	6,1200	1,6105
Au	2,0068	4,0367	1,8576
Au	0.0001	1,9640	1,953
Pd	-2,0432	0,000	1,7922
Au	-4,0427	-2,0083	1,8524
Au	-6,1200	-4,0800	1,6105
Au	0,0000	6,1200	1,6105
Au	-2,0073	4,0363	1,8574
Au	-4,0426	2,0084	1,8521
Au	-6,1200	0,000	1,6105
Au	-4,0800	6,1200	1,6105
Au	-6,1200	4,0800	1,6105
H	0,9660	0,7896	2,8745

H_2O adsorption on PdAu(100) : Pd Top site

	x	*y*	*z*
Au	4,0800	-2,0400	-2,4695
Au	2,0400	-4,0800	-2,4695
Au	4,0800	2,0400	-2,4695
Au	2,0400	0,0000	-2,4695
Au	0,0000	-2,0400	-2,4695
Au	-2,0400	-4,0800	-2,4695

Au	2,0400	4,0800	-2,4695
Au	0,0000	2,0400	-2,4695
Au	-2,0400	0,0000	-2,4695
Au	-4,0800	-2,0400	-2,4695
Au	-2,0400	4,0800	-2,4695
Au	-4,0800	2,0400	-2,4695
Au	6,1200	-2,0400	-0,4295
Au	4,0800	-4,0800	-0,4295
Au	2,0400	-6,1200	-0,4295
Au	6,1200	2,0400	-0,4295
Au	4,1303	0,0000	-0,4335
Au	2,0104	-2,0092	-0,2598
Au	-0.0005	-4,1513	-0,4582
Au	-2,0400	-6,1200	-0,4295
Au	4,0800	4,0800	-0,4295
Au	2,0105	2,0093	-0,2596
Au	-0.0001	0,0000	-0,2763
Au	-2,0115	-2,0087	-0,2588
Au	-4,0800	-4,0800	-0,4295
Au	2,0400	6,1200	-0,4295
Au	-0.0005	4,1509	-0,458
Au	-2,0116	2,0087	-0,2587
Au	-4,1298	0,0000	-0,4334
Au	-6,1200	-2,0400	-0,4295
Au	-2,0400	6,1200	-0,4295
Au	-4,0800	4,0800	-0,4295
Au	-6,1200	2,0400	-0,4295
Au	6,1200	-4,0800	1,6105
Au	4,0800	-6,1200	1,6105
Au	6,1200	0,0000	1,6105
Au	4,0420	-2,0081	1,8525
Au	2,0068	-4,0368	1,8579
Au	0,0000	-6,1200	1,6105
Au	6,1200	4,0800	1,6105
Au	4,0419	2,0082	1,8523
Pd	2,0426	0,0000	1,7918
Au	0,0000	-1,9640	1,9533
Au	-2,0073	-4,0364	1,8578
Au	-4,0800	-6,1200	1,6105
Au	4,0800	6,1200	1,6105
Au	2,0068	4,0367	1,8576
Au	0.0001	1,9640	1,953
Pd	-2,0432	0,000	1,7922
Au	-4,0427	-2,0083	1,8524
Au	-6,1200	-4,0800	1,6105
Au	0,0000	6,1200	1,6105
Au	-2,0073	4,0363	1,8574
Au	-4,0426	2,0084	1,8521
Au	-6,1200	0,000	1,6105
Au	-4,0800	6,1200	1,6105
Au	-6,1200	4,0800	1,6105
O	1,9679	-0,0146	4,2304
H	1,3469	-0,7594	4,3518
H	1,4243	0,7836	4,3773

H adsorption on PdAu(111) : fcc Hollow site

	x	*y*	*z*
Au	7,2125	7,4954	0,0000
Au	8,6550	9,9939	0,0000
Au	10,0975	12,4924	0,0000
Au	11,5400	14,9909	0,0000
Au	10,0975	7,4954	0,0000
Au	11,5400	9,9939	0,0000
Au	12,9825	12,4924	0,0000
Au	14,4250	14,9909	0,0000
Au	12,9825	7,4954	0,0000
Au	14,4250	9,9939	0,0000
Au	15,8675	12,492	0,0000
Au	15,8675	7,4954	0,0000
Au	17,3100	9,9939	0,0000
Au	5,7700	8,3283	2,3556
Au	7,2125	10,8268	2,3556
Au	8,6550	13,3252	2,3556
Au	10,0975	15,8237	2,3556
Au	7,2125	5,8298	2,3556
Au	8,6470	8,3235	2,5240
Au	10,0773	10,8180	2,5362
Au	11,5300	13,3021	2,5347
Au	12,9825	15,8237	2,3556
Au	10,0975	5,8298	2,3556
Au	11,5223	8,3153	2,5359
Au	12,9630	10,8161	2,5315
Au	14,4360	13,3114	2,5370
Au	15,8675	15,8237	2,3556
Au	12,9825	5,8297	2,3556
Au	14,4000	8,3317	2,5355
Au	15,8602	10,8439	2,5366
Au	17,3100	13,3252	2,3556
Au	15,8675	5,8298	2,3556
Au	17,3100	8,3283	2,3556
Au	18,7525	10,8268	2,3556
Au	4,3275	9,1611	4,7112
Au	5,7700	11,6596	4,7112
Au	7,2125	14,1581	4,7112
Au	8,6550	16,6565	4,7112
Au	5,7700	6,6626	4,7112
Au	7,2418	9,1521	5,1036
Au	8,6544	11,6193	5,0736
Au	10,0998	14,1188	5,0136
Au	11,5400	16,6565	4,7112
Au	7,2125	4,1641	4,7112
Au	8,6623	6,6923	5,1047
Pd	10,1032	9,1645	4,9167
Au	11,5442	11,6202	5,1198
Au	13,0014	14,1110	5,0369
Au	14,4250	16,6565	4,7112
Au	10,0975	4,1641	4,7112
Au	11,5045	6,6819	5,0731
Au	12,9509	9,1839	5,1197
Pd	14,4040	11,6472	4,9093
Au	15,8672	14,1271	5,0513
Au	17,3100	16,6565	4,7112
Au	12,9825	4,1641	4,7112
Au	14,3912	6,6835	5,0142

Au	15,8357	9,1997	5,0366
Au	17,2831	11,6733	5,0509
Au	18,7525	14,1581	4,7112
Au	15,8675	4,1641	4,7112
Au	17,3100	6,6626	4,7112
Au	18,7525	9,1611	4,7112
Au	20,1950	11,6596	4,7112
H	11,2944	9,8527	5,9384

O adsorption on PdAu(111) : Fcc Hollow site

	x	*y*	*z*
Au	7,2125	7,4954	0,0000
Au	8,6550	9,9939	0,0000
Au	10,0975	12,4924	0,0000
Au	11,5400	14,9909	0,0000
Au	10,0975	7,4954	0,0000
Au	11,5400	9,9939	0,0000
Au	12,9825	12,4924	0,0000
Au	14,4250	14,9909	0,0000
Au	12,9825	7,4954	0,0000
Au	14,4250	9,9939	0,0000
Au	15,8675	12,492	0,0000
Au	15,8675	7,4954	0,0000
Au	17,3100	9,9939	0,0000
Au	5,7700	8,3283	2,3556
Au	7,2125	10,8268	2,3556
Au	8,6550	13,3252	2,3556
Au	10,0975	15,8237	2,3556
Au	7,2125	5,8298	2,3556
Au	8,6470	8,3235	2,5240
Au	10,0773	10,8180	2,5362
Au	11,5300	13,3021	2,5347
Au	12,9825	15,8237	2,3556
Au	10,0975	5,8298	2,3556
Au	11,5223	8,3153	2,5359
Au	12,9630	10,8161	2,5315
Au	14,4360	13,3114	2,5370
Au	15,8675	15,8237	2,3556
Au	12,9825	5,8297	2,3556
Au	14,4000	8,3317	2,5355
Au	15,8602	10,8439	2,5366
Au	17,3100	13,3252	2,3556
Au	15,8675	5,8298	2,3556
Au	17,3100	8,3283	2,3556
Au	18,7525	10,8268	2,3556
Au	4,3275	9,1611	4,7112
Au	5,7700	11,6596	4,7112
Au	7,2125	14,1581	4,7112
Au	8,6550	16,6565	4,7112
Au	5,7700	6,6626	4,7112
Au	7,2418	9,1521	5,1036
Au	8,6544	11,6193	5,0736
Au	10,0998	14,1188	5,0136
Au	11,5400	16,6565	4,7112
Au	7,2125	4,1641	4,7112
Au	8,6623	6,6923	5,1047

Pd	10,1032	9,1645	4,9167
Au	11,5442	11,6202	5,1198
Au	13,0014	14,1110	5,0369
Au	14,4250	16,6565	4,7112
Au	10,0975	4,1641	4,7112
Au	11,5045	6,6819	5,0731
Au	12,9509	9,1839	5,1197
Pd	14,4040	11,6472	4,9093
Au	15,8672	14,1271	5,0513
Au	17,3100	16,6565	4,7112
Au	12,9825	4,1641	4,7112
Au	14,3912	6,6835	5,0142
Au	15,8357	9,1997	5,0366
Au	17,2831	11,6733	5,0509
Au	18,7525	14,1581	4,7112
Au	15,8675	4,1641	4,7112
Au	17,3100	6,6626	4,7112
Au	18,7525	9,1611	4,7112
Au	20,1950	11,6596	4,7112
O	11,4004	9,9136	6,4155

OH adsorption on PdAu(111) : PdAu Bridge site

	x	*y*	*z*
Au	7,2125	7,4954	0,0000
Au	8,6550	9,9939	0,0000
Au	10,0975	12,4924	0,0000
Au	11,5400	14,9909	0,0000
Au	10,0975	7,4954	0,0000
Au	11,5400	9,9939	0,0000
Au	12,9825	12,4924	0,0000
Au	14,4250	14,9909	0,0000
Au	12,9825	7,4954	0,0000
Au	14,4250	9,9939	0,0000
Au	15,8675	12,492	0,0000
Au	15,8675	7,4954	0,0000
Au	17,3100	9,9939	0,0000
Au	5,7700	8,3283	2,3556
Au	7,2125	10,8268	2,3556
Au	8,6550	13,3252	2,3556
Au	10,0975	15,8237	2,3556
Au	7,2125	5,8298	2,3556
Au	8,6470	8,3235	2,5240
Au	10,0773	10,8180	2,5362
Au	11,5300	13,3021	2,5347
Au	12,9825	15,8237	2,3556
Au	10,0975	5,8298	2,3556
Au	11,5223	8,3153	2,5359
Au	12,9630	10,8161	2,5315
Au	14,4360	13,3114	2,5370
Au	15,8675	15,8237	2,3556
Au	12,9825	5,8297	2,3556
Au	14,4000	8,3317	2,5355
Au	15,8602	10,8439	2,5366
Au	17,3100	13,3252	2,3556
Au	15,8675	5,8298	2,3556
Au	17,3100	8,3283	2,3556

Au	18,7525	10,8268	2,3556
Au	4,3275	9,1611	4,7112
Au	5,7700	11,6596	4,7112
Au	7,2125	14,1581	4,7112
Au	8,6550	16,6565	4,7112
Au	5,7700	6,6626	4,7112
Au	7,2418	9,1521	5,1036
Au	8,6544	11,6193	5,0736
Au	10,0998	14,1188	5,0136
Au	11,5400	16,6565	4,7112
Au	7,2125	4,1641	4,7112
Au	8,6623	6,6923	5,1047
Pd	10,1032	9,1645	4,9167
Au	11,5442	11,6202	5,1198
Au	13,0014	14,1110	5,0369
Au	14,4250	16,6565	4,7112
Au	10,0975	4,1641	4,7112
Au	11,5045	6,6819	5,0731
Au	12,9509	9,1839	5,1197
Pd	14,4040	11,6472	4,9093
Au	15,8672	14,1271	5,0513
Au	17,3100	16,6565	4,7112
Au	12,9825	4,1641	4,7112
Au	14,3912	6,6835	5,0142
Au	15,8357	9,1997	5,0366
Au	17,2831	11,6733	5,0509
Au	18,7525	14,1581	4,7112
Au	15,8675	4,1641	4,7112
Au	17,3100	6,6626	4,7112
Au	18,7525	9,1611	4,7112
Au	20,1950	11,6596	4,7112
O	14,1041	11,7115	6,9405
H	14,3136	10,8212	7,2842

H_2O adsorption on PdAu(111) : Pd Top site

	x	*y*	*z*
Au	7,2125	7,4954	0,0000
Au	8,6550	9,9939	0,0000
Au	10,0975	12,4924	0,0000
Au	11,5400	14,9909	0,0000
Au	10,0975	7,4954	0,0000
Au	11,5400	9,9939	0,0000
Au	12,9825	12,4924	0,0000
Au	14,4250	14,9909	0,0000
Au	12,9825	7,4954	0,0000
Au	14,4250	9,9939	0,0000
Au	15,8675	12,492	0,0000
Au	15,8675	7,4954	0,0000
Au	17,3100	9,9939	0,0000
Au	5,7700	8,3283	2,3556
Au	7,2125	10,8268	2,3556
Au	8,6550	13,3252	2,3556
Au	10,0975	15,8237	2,3556
Au	7,2125	5,8298	2,3556
Au	8,6470	8,3235	2,5240
Au	10,0773	10,8180	2,5362

Au	11,5300	13,3021	2,5347
Au	12,9825	15,8237	2,3556
Au	10,0975	5,8298	2,3556
Au	11,5223	8,3153	2,5359
Au	12,9630	10,8161	2,5315
Au	14,4360	13,3114	2,5370
Au	15,8675	15,8237	2,3556
Au	12,9825	5,8297	2,3556
Au	14,4000	8,3317	2,5355
Au	15,8602	10,8439	2,5366
Au	17,3100	13,3252	2,3556
Au	15,8675	5,8298	2,3556
Au	17,3100	8,3283	2,3556
Au	18,7525	10,8268	2,3556
Au	4,3275	9,1611	4,7112
Au	5,7700	11,6596	4,7112
Au	7,2125	14,1581	4,7112
Au	8,6550	16,6565	4,7112
Au	5,7700	6,6626	4,7112
Au	7,2418	9,1521	5,1036
Au	8,6544	11,6193	5,0736
Au	10,0998	14,1188	5,0136
Au	11,5400	16,6565	4,7112
Au	7,2125	4,1641	4,7112
Au	8,6623	6,6923	5,1047
Pd	10,1032	9,1645	4,9167
Au	11,5442	11,6202	5,1198
Au	13,0014	14,1110	5,0369
Au	14,4250	16,6565	4,7112
Au	10,0975	4,1641	4,7112
Au	11,5045	6,6819	5,0731
Au	12,9509	9,1839	5,1197
Pd	14,4040	11,6472	4,9093
Au	15,8672	14,1271	5,0513
Au	17,3100	16,6565	4,7112
Au	12,9825	4,1641	4,7112
Au	14,3912	6,6835	5,0142
Au	15,8357	9,1997	5,0366
Au	17,2831	11,6733	5,0509
Au	18,7525	14,1581	4,7112
Au	15,8675	4,1641	4,7112
Au	17,3100	6,6626	4,7112
Au	18,7525	9,1611	4,7112
Au	20,1950	11,6596	4,7112
O	14,2603	11,5716	7,4341
H	14,1549	10,6103	7,5696
H	13,3606	11,9323	7,5535

-S5-

REFERENCES

(1) Ahlrichs, R; Bär, M.; Häser, M.; Horn, H.; Kölmel, C. *Chem. Phys. Lett.* **1989**, *162*, 165.
(2) Becke, A.D. *Physical Reviews A* **1988**, *38*, 3098.
(3) Perdew, J.P. *Physical Review B* **1986**, *33*, 8822.
(4) Eichkorn, K.; Treutler, O.; Öhm, H.; Häser M.; Ahlrichs, R. *Chem. Phys. Lett.* **1995**, *240*, 283.
(5) Eichkorn, F.; Weigend, O.; Treutler; Ahlrichs, R. *Theor. Chem. Acc.* **1997**, *97*, 119.
(6) Andrae, D.; Hæussermann, U.; Dolg, M.; Stoll, H.; Preuß, H. *Theor. Chim. Acta* **1990**, 77, 123. Schäfer, A.; Horn, H.; Ahlrichs, R. *J. Chem. Phys.* **1992**, 97, 2571.
(7) Schäfer, A.; Huber, C.; Ahlrichs, R. *J. Chem. Phys.* **1994**, 100, 5829.
(8) Rivalta I.; Mazzone G.; Russo N.; Sicilia E. *J. Chem. Theory Comput.*, **2009**, 5,1350.
(9) Mazzone G.; Rivalta I.; Russo N.; Sicilia E. *Chem. Commun.* **2009**, *14*, 1852.
(10) Eichkorn, F.; Weigend, O.; Treutler; Ahlrichs, R. *Theor. Chem. Acc.* **1997**, *97*, 119.
(11) Schäfer, A.; Horn, H.; Ahlrichs, R. *J. Chem. Phys.* **1992**, *97*, 2571.
(12) Boys, S.F.; Bernardi, F. *Mol. Phys.* **1970**, *19*, 553.

Manoscritto II

Gold(I)-Catalyzed Hydration of 1,2- Phenylacetylene: Computational Insights

Gloria Mazzone, Nino Russo, Emilia Sicilia

Manuscript

Gold(I)-Catalyzed Hydration of 1,2- Phenylacetylene: Computational Insights

*Gloria Mazzone, Nino Russo, Emilia Sicilia**

The hydration of unsatured carbon compounds is one of the most environmentally benign and economically attractive route to form carbon-oxygen bond. Unactivated alkynes are an abundant hydrocarbon resource and hydration represents an excellent means of functionalization, which has been extensively studied.[1]

It has long been known that water can be added quite easily to activated electron-rich alkynes in the presence of an acid catalyst.[2] The reaction of simple alkynes, instead, needs co-catalysts, typically mercury(II) salts, to enhance the reactivity.[3] Such catalysts have been extensively used in high-scale industrial processes[4] until the discovery of the toxicity of mercury salts. Moreover, under the reaction conditions the mercury(II) is quickly reduced to catalytically inactive metallic mercury. To avoid the use of toxic mercury salts there has been much effort aimed at the development of alternative synthetic strategies for the hydration of alkynes based on the use of metal catalytic systems,[5] but neither of them has shown activity comparable to that of those mercury salt containing systems. Among the alternative systems, gold compounds have gradually taken a prominent place, beneficially replacing mercury salts. Notably, at the end of ninety years, Teles and co-workers have reported the addition of methanol to alkynes efficiently catalyzed by coordinatively unsaturated cationic gold(I) species, of the type R_3PAu^+, generated in situ by the protonolysis of R_3PAuCH_3 with an acid and release of CH_4.[6] A remarkable result of Tales work stems from theoretical calculations that show how gold(I) directs the alcohol nucleophile to the side of the coordinated metal. This behavior is different from the usual attack of the nucleophile from the side opposite to the coordinated metal that is assumed for other electrophilic metals. In 2002 Tanaka et al. using similar reagents achieved the efficient hydration of a wide range of alkynes in aqueous methanol.[7] Good yields have been reported also by Laguna[8] and others[9] especially when gold(I) complexes were combined with strong acids under heating. Very recently, Leyva and Corma have carried out the efficient hydration of a wide range of alkynes to the corresponding ketones by using gold(I)-phosphine complexes as catalyst with no acidic cocatalyst.[10] Catalysts like R_3PAuX (X=trifluoromethanesulphonate $^-$OTf or other weakly coordinating counteranions), have been formed in situ by treatment of the corresponding chloride complex, R_3PAuCl, with a silver salt. The soft non coordinating anions makes the catalytic center acidic enough to bypass the use of additives. With the purpose to shed light on the proposed mechanistic hypotheses,[6-8] even

contradictory, for this reaction the authors have carried out a series of kinetic experiments using MeOH, H_2O or both as nucleophiles, diphenylacetylene as substrate and $AuPR_3X$ (PR_3:PPh_3, SPhos, P^tBu_3; X:Cl, OTf, NTf_2) as catalyst in THF solvent.

In this paper our goal is to investigate, with the aid of Density Functional Theory (DFT) calculations, the detailed mechanism of the alkyne hydration reaction by gold(I) complexes with the support of the experimental observations and mechanistic proposal. We expect this work could enhance further understanding and provide helpful information for chemists for the exploration of such kind of reactions.

The plausible mechanism proposed on the basis of experimental findings (Scheme 1) involves coordination of triple bond to Au(I) complex with formation of the Au-π-alkyne complex **I** and subsequent attack of the ROH (R=H, CH_3) nucleophile. ROH would coordinate to gold leading to formation of the intermediate **II**, before its addition to the triple bond (**III**) to afford, by protodeauration, the *E* isomer of the enol ether product **IV** together with the restored catalyst. Formation of the *Z* from the *E* isomer can occur by rotation about the C-C double bond[6] or in the next step of the overall process, that is addition of a second molecule of ROH to form the corresponding ketal **V**.

Elimination of a ROH molecule from the **V** would explain formation of both *Z* and *E* isomers, whereas subsequent reaction of ketal **V** with H_2O leads to the formation of the ketone final product. The authors suggest that the gold catalyst could come into play also in these last steps of the overall hydration process.

As the first step of a more comprehensive project, we have investigated here the detailed mechanism of the hydration of diphenylacetylene catalyzed by the $[(Ph_3P)Au]^+$ complex using pure water as nucleophile.

For the present study calculations have been performed at the Becke3-LYP (B3LYP) level of density functional theory [11,12] with the Gaussian03 computational package.[13] For Au the relativistic compact Stuttgart/Dresden effective core potential[14] has been used in conjunction with its split valence basis set. To reduce the computational cost of stationary points optimization for carbon and hydrogen atoms of phenyl rings standard 3-21G basis set of Pople have been used together with the augmented, correlation-consistent triple zeta basis sets of Dunning and co-workers[15] for the rest of the atoms. Preliminary test calculations have clearly shown that the use of triple zeta quality basis sets also for the phenyl rings atoms does not introduce any significant structural change. Therefore, final energies, including zero-point vibrational energy, have been calculated by performing single-point calculations on the

optimized geometries at the same level of theory and employing Dunning augmented triple zeta basis sets for all H, C, O and P atoms. To properly reproduce the experimental conditions, implicit solvent effects have been calculated through the polarisable continuum solvation model, PCM,[16] performing single point calculations in THF on fully optimized geometry of each stationary point along the reaction path. Energies in THF are shown in parentheses both in the text and Figures. Additional computational details are available in the Supporting Information.

B3LYP calculated energy profiles for the reaction pathways corresponding to the addition of the first and second H_2O molecules are shown in Figures 1 and 2, respectively. Structures of reactants, intermediates, transition states, and products of the reactions are depicted schematically in the same figures, whereas all detailed geometrical information on such stationary point is reported in the Supporting Information. Their relative energies in the gas and solution phases are calculated with respect to ground-state reactants asymptote, $[(Ph_3P)Au]^+ + C_2Ph_2 + H_2O$. In the same Figure 2 is also shown the energy profile for the direct addition of water in absence of the gold catalyst (see the Supporting Information).

From the energy profile in Figure 1, it is evident that the first step of the catalytic addition of water to the alkyne pathway involves a preliminary intermediate **I**, where the CC triple bond interacts with the gold atom. Intermediate **I** is formed without any barrier and is 41.3 kcal/mol (32.4 kcal/mol) lower in energy than the reactants. Several examples[17-21] of such a π-coordination to gold(I) have been theoretically studied to evaluate the extent of the π-to-metal σ-donation and metal-to-π* back-donation and the main conclusion is that $Au(I)^+$ cannot significantly participate to a Dewar-Chatt-Duncanson type bonding[22] as antibonding orbitals are too high in energy for significant backbonding to occur. Here the C1-C2 bond has lost a little of its triple bond character. Indeed, the C-C length increases from 1.205 Å, calculated for the free alkyne, to 1.229 Å and the deviation from linearity is measured by the value of 169.2 degrees of the C1-C2-C4. With these optimized geometries in hand, the natural bond order (NBO)[23] analysis have been used to investigate the nature of the metal-alkyne bond. Second-order perturbative analysis has revealed that π-to-metal σ-donation largely dominates (105.8 kcal/mol) over metal-to-π* back-donation (14.1 kcal/mol). In addition to NBO analysis also the frontier molecular orbitals have been examined (see the Supporting Information). As expected the LUMO contains the π*-metal interaction. Furthermore, from the calculation of the energies of the frontier orbitals of the two species $[(Ph_3P)Au]^+$ and C_2Ph_2 results that the HOMO of

diphenylacetylene is only 0.3 eV higher in energy than to the LUMO of gold(I) complex. The difference in energy, instead, between the HOMO of $[(Ph_3P)Au]^+$ and the LUMO of C_2Ph_2 is very large, that is 9.4 eV. The lack of backbonding from Au(I) enhances the electrophilicity of the ligand and favors the attack of the nucleophile. As a first step, the intermediate **II** is formed in which water is loosely precoordinated. This precoordination is computed to be exothermic by 18.2 kcal/mol and introduces some changes into the structure of the complex. The lengths of the two Au-C bonds, that are 2.307 Å, become different (Au-C1=2.423 Å and Au-C2=2.294 Å). The angle between phosphorus, gold, and the next C2 carbon of the triple bond changes from 165.1° to 179.5°. The Au-O bond is 3.021 Å and the P-Au-O angle is 89.8°.

The next step involves formation of intermediate **III** by coordination between the O-atom of water and one carbon atom of the diphenylacetylene concomitant with a movement of Au^+ to the other carbon. The calculated activation energy for rearrangement of **II** to **III** is 36.8 kal/mol (35.0 kcal/mol), and the intermediate **III** is located at -24.2 kcal/mol (-14.1 kcal/mol) with respect to $[(Ph_3P)Au]^+ + C_2Ph_2 + H_2O$ separated reactants. The further reaction towards formation of the *E* isomer of the enol involves an Au^+-assisted hydrogen migration from oxygen, via gold to the terminal carbon to finally afford the product complex **V** with a relative energy of -58.9 kcal/mol (-48.9 kcal/mol). The first step, that is migration to Au^+, has a computed activation energy of 10.8 kcal/mol (11.0 kcal/mol), and intermediate **IV** is formed that lies 14.6 kcal/mol (3.7 kcal/mol) lower in energy with respect to ground reactants asymptote. The next hydrogen shift from gold to the position *cis* to the OH group corresponds to a very low activation energy of about 1 kcal/mol. Our calculations show that the *Z* isomer formation occurs exclusively by rotation around the C-C double bond of the complex **V**. Indeed, all the attempts to directly transfer the hydrogen atom from oxygen to the position *trans* to the OH group have been unsuccessful. The transition state structure for the *E* to *Z* isomerization is located at a relative energy of -35.3 kcal/mol (-28.7 kcal/mol) and corresponds to an activation energy of 23.6 kcal/mol (20.2 kcal/mol) . The *Z* isomer is stabilized by 4.1 kcal/mol (3.9 kcal/mol) with respect to the *E* one. As pointed out in recent literature,[24,25] even if gold-alkene π-complexes are known since a long time, the number of such structurally characterized complexes is quite limited. From our computational analysis results that in both isomers the binding of Au^+ to the double bond is very asymmetric in that the gold atom is only attached to the C2 terminal carbon atom. The C1-C2 bond length is increased from 1.338 to 1.386 Å for the *E* isomer and from 1.342 to 1.383 Å for the *Z* isomer. The C1–C2–Au angle amounts to 89.2° and 87.6° in *E* and *Z* isomers, respectively. NBO analysis reveals that even if π-to-metal σ-donation plays a role,

electrostatic interactions are the primary origins of the bond. Both NBO and ESP[26] charge analyses show that the positive charge is significantly redistributed on the ligand and the gold atom carries a charge not larger than 0.29. An attractive interaction, therefore exists with the C2 atom of the alkene that carries a negative charge, whereas the C1 atom is positively charged due to the bond with the O atom. More details can be found in the Supporting Information. The catalytic cycle could be, then, closed by the release of the enol that is calculated to be endothermic by 40.8 kcal/mol (32.7 kcal/mol). As underlined by the authors[10] the catalyst could play also a role in the next steps of the whole process that involves the addition of a second water molecule. To evaluate which is the most favorable pathway we have calculated the energy profiles for the reaction occurring both in absence of and assisted by the gold catalyst. As it evident from Figure 2 the process takes great advantage of the assistance of the catalyst.

Both adducts, indicated as **V** and **VI**, formed by the *E* or *Z* isomers with the $[(Ph_3P)Au]^+$ complex can enter the subsequent catalytic cycle for the addition of a second water molecule. Indeed, the possibility that the isomerization from *E* to *Z* isomers occurs depends on how rapidly the final ketone product is formed. For that reason we have investigated the pathway for the addition of a second H_2O molecule starting from both **V** (pathway (a)) and **VI** (pathway (b)) intermediates.

The B3LYP calculated energy profiles show that the first step of the process is the loose coordination of H_2O that is calculated to be endothermic by about 77 kcal/mol (62 kcal/mol) with respect to the reactants asymptote along both (a) and (b) pathways. From an examination of Figure 2 results that along the path involving the *E* isomer the reaction proceeds by a 1,3-hydrogen migration and gold acts as a proton shuttle. Oxygen coordinates to C2 and one of the hydrogen atoms is transferred to Au to form the **VIII(a)** intermediate that lies 26.0 kcal/mol (14.0 kcal/mol) below $[(Ph_3P)Au]^+ + C_2Ph_2 + H_2O$ separated reactants. The barrier for this rearrangement is 53.6 kcal/mol (52.6 kcal/mol), whereas the barrier for the next hydrogen shift from Au to the carbon atom to form the corresponding gem-diol **IX** is very low and amounts to 1.3 kcal/mol (1.9 kcal/mol). Along pathway (b), instead, the intermediate **IX** formation takes place directly since the hydrogen atom is transferred from oxygen to carbon in one step and the barrier that is necessary to overcome is 53.6 kcal/mol (50.8 kcal/mol). The calculated barrier for the *E* to *Z* isomerization is lower than both the barrier that is necessary to overcome to generate from the *E* isomer the **IX** intermediate and the reverse barrier to go from **IX** to the *Z* isomer by elimination of a water molecule. In addition, the pathway that involves the *Z* isomer appears to

be slightly more favourable. Therefore, it should be concluded that formation of the Z isomer occurs preferentially by direct isomerization from *E* isomer. The final step of the reaction, that is formation of the ketone product from intermediate **IX** can occur both by direct elimination of a water molecule from the two OH groups and by the involvement of a third molecule of water. The transition states for the both pathways have been intercepted and, as can be clearly inferred from Figure 2, the process is calculated to be more favourable if the participation of a third water molecule is taken into consideration. The **TS7** transition state lies at 63.3 kcal/mol below the reactants asymptote and corresponds to a barrier of 6.0 kcal/mol (8.5 kcal/mol). The calculated imaginary frequency is associated to the movement of the third water molecule that approaches the complex and induces formation of the product by abstracting a hydrogen atom from one of the two OH groups and simultaneously transferring a hydrogen atom to the other OH. The elimination of a water molecule directly from the intermediate **IX** occurs through the **TS7'** transition state, whose formation is exothermic by 39.8 kcal (26.8 kcal/mol) relative to the reactants dissociation limit and the corresponding activation barrier amounts to 29.5 kcal/mol (29.4 kcal/mol). As a result a water molecule is eliminated and the carbonyl bond is formed. The formation of the adduct **X** with two directly interacting H_2O molecules is calculated to be more exothermic than the formation of the **X'** adduct with one water molecule, that is 96.3 kcal/mol (75.7 kcal/mol) *versus* 80.6 kcal/mol (64.5 kcal/mol), whereas to release the product and regenerate the catalyst it is required to overcome an energy barrier of 66.7 kcal/mol (47.0 kcal/mol) from intermediate **X**. The whole catalytic process is exothermic by 29.6 kcal/mol (28.7 kcal/mol) with respect to $[(Ph_3P)Au]^+ + C_2Ph_2 + H_2O$ reactants. Comparison in Figure 2 of the catalyzed and uncatalyzed pathways clearly shows that the intervention of the catalyst also in the second part of the process is crucial to lower the energy barriers and to act in such a way that all the stationary points along the reaction path lie below the energy of the reactants asymptote.

In conclusion, the investigation of the whole hydration process of 1,2-phenylacetylene catalyzed by the gold(I) $[(Ph_3P)Au]^+$ complex by addition of water to form the corresponding ketone has been carried out and the mechanistic hypotheses existing in the literature have been explored. Calculations confirm that the first molecule addition occurs with gold acting as a proton shuttle to transfer the migrating hydrogen in *cis* position with respect to OH group. From the formed *E* isomer the *Z* one could be easily formed by rotation around the C-C bond. The addition of the second water molecule to give the ketone final product occurs favorably with the support of the catalyst and involves a second hydrogen shift from oxygen to carbon. If the *E*

isomer is involved, gold directly participates to the reaction assisting the hydrogen transfer, whereas if the product is obtained starting from the *Z* isomer gold is not directly involved. The intervention of a third water molecule lowers the energy barrier for the elimination of a water molecule and formation of the π carbonyl bond. The theoretical insights presented in this work are expected to help us understand this gold-catalyzed hydration reactions as well as similar processes. In this perspective, work is in progress to carry out analogous calculations for the analysis of the mechanistic details of the 1,2-diphenylacetilene hydration with methanol as nucleophile.

References

[1] a) P. F. Hudrlik, A. M. Hudrlik in *The Chemistry of the Carbon-Carbon Triple Bond*, Part 1 (Ed.: S. Patai), Wiley, New York, **1978**, p. 199; b) G.H. Schmid, in *The Chemistry of the Carbon-Carbon Triple Bond*, Part 1 (Ed.: S. Patai), Wiley, New York, **1978**, p. 275; c) J. March, Advanced Organic Chemistry, Wiley, New York, 1992, p. 762; R. C. Larock, W. W. Leong in *Comprehensive Organic Synthesis*, Vol. 4 (Eds.: B. M. Trost, I. Fleming, M. F. Semmelhack), Pergamon, Oxford, **1991**, p. 269; d) I.V. Kozhevnikov, *Chem. Rev*. **1998**, *98*, 171.

[2] a) W. Drenth, H. Hogeveen, *Recl. Trav. Chim. Pays-Bas* **1960**, *79*, 1002; A.D. Allen, Y. Chiang, A.J. Kresge, T.T. Tidwell *J. Org. Chem.* **1982**, 47, 775, and references therein.

[3] a) H. D. Hinton, J. A. Niewland, *J. Am. Chem. Soc.* **1930**, *52*, 2892; b) D. B. Killian, G. F. Hennion, J. A. Niewland, *ibid.* **1934**, *56*, 1384; c) G. F. Hennion, J. A. Niewland, *ibid.* **1935**, *57*, 2006; d) D. B. Killian, G. F. Hennion, J. A. Niewland, *ibid.* **1936**, *58*, 1658; e) *ibid.* **1936**, *58*, 80; f) G. F. Hennion,W. S. Murray, *ibid.* **1942**, *64*, 1220; g) M. Bassetti, B. Floris, *J. Chem. Soc. Perkin Trans.* **1988**, *2* 227.

[4] Acetaldehyde. Ullmann's Encyclopedia of Industrial Chemistry, 7th ed.; Wiley-VCH: Weinheim, **2006**.

[5] L. Hintermann, A. Labonne, *Synthesis* **2007**, *8*, 1121.

[6] J.H. Teles, S. Brode, M. Chabanas, *Angew. Chem. Int. Ed.* **1998**, *37*, 1415.

[7] E. Mizushima, K. Sato, T. Hayashi, M. Tanaka, *Angew. Chem., Int. Ed.* **2002**, *41*, 4563.

[8] R. Casado, M. Contel, M. Laguna, P. Romero, S.Sanz, *J. Am. Chem. Soc.* **2003**, *125*, 11925.

[9] P. Roembke, H. Schmidbaur, S. Cronje, H. Raubenheimer, *J. Mol. Catal. A.* **2004**, *212*, 35.

[10] A. Leyva, A. Corma, *J. Org. Chem.* **2009**, *74*, 2067.

[11] A. D. Becke, J. Chem. Phys. **1993**, *98*, 5648-5652.

[12] P. J. Stephens, F. J. Devlin, C. F. Chabalowski, M. J. Frisch, *J. Phys. Chem.* **1994**, *98*, 11623-11627.

[13] GAUSSIAN 03, Revision A.1, Gaussian, .M.J. Frisch et al., see the Supporting Information.

[14] D. Andrae, U. Häußermann, M. Dolg, H. Stoll, H. Preuß, *Teor. Chim. Acta* **1990**, *77*, 123.

[15] R. A. Kendall, T. H. Dunning Jr., and R. J. Harrison, *J. Chem. Phys.* **1992** *96*, 6796.

[16] a) S. Miertus, E. Scrocco, J. Tomasi, *Chem. Phys.* **1981**, *55*, 117-129; b) S. Miertus J. Tomasi, *Chem. Phys.* **1982**, *65*, 239-245.

[17] N. D. Shapiro, F. D. Toste, *PNAS* **2008**, *105*, 2779.

[18] M. S. Nechaev, V. M. Rayón, G. Frenking, *J. Phys. Chem. A* **2004**, *108*, 3134.

[19] C.K. Kim, K.A. Lee, C.K. Kim, B. Lee, H.W. Lee, *Chem. Phys. Lett.* **2004**, *391*, 321.

[20] R.H. Hertwig, W. Koch, D. Schröder, H. Schwarz, J. Hrušák, P.J. Schwerdtfeger , *Phys. Chem.* **1996**, *100*, 12253.

[21] T. Ziegler, A. Rauk *Inorg. Chem.* **1979**, *18*, 1558.

[22] a) M. J. Dewar, S. *Bull. Soc. Chim. Fr.* **1951**, 79; b) J. Chatt,, L. A. Duncanson, *J. Chem. Soc.* **1953**, 2939.

[23] a) J. E. Carpenter, F. Weinhold, *J. Mol Struct. (THEOCHEM)* **1988**, *169*, 41; b) J. E. Carpenter, F. J. Weinhold, *The Structure of Small Molecules and Ions*; Plenum: New York, 1988.

[24] T. J. Brown, M. G. Dickens, R. A. Widenhoefer *J. Am. Chem. Soc.* **2009**, *131*, 6350–6351.

[25] H. V. R. Dias, J. Wu *Eur. J. Inorg. Chem.* **2008**, 509–522.

[26] (a) B. H. Besler, K. M. Merz Jr., and P. A. Kollman, *J. Comp. Chem.* **11**, 431 (1990); (b) U. C. Singh and P. A. Kollman, *J. Comp. Chem.* **5**, 129 (1984).

Supporting Information

Gold(I)-Catalyzed Hydration of 1,2- Phenylacetylene: Computational Insights

Gloria Mazzone, Nino Russo, Emilia Sicilia

1. **Gaussian03 Full Reference [13]**
2. **Additional computational details**
3. **Geometrical structures of all stationary points**
4. **HOMO and LUMO structures of the $[(Ph_3P)Au\text{-alkyne}]^+$ complex**
5. **Energy profile fort the uncatalized addition of a water molecule to the enol**
6. **Charge distribution analysis for the $[(Ph_3P)Au\text{-alkene}]^+$ complexes**

1. Full citation for reference [13]

M.J. Frisch, G.W. Trucks, H.B. Schlegel, G.E. Scuseria, M.A. Robb, J.R. Cheeseman, J.A. Montgomery, Jr., T. Vreven, K.N. Kudin, J.C. Burant, J. M. Millam, S.S. Iyengar, J. Tomasi, V. Barone, B. Mennucci, M. Cossi, G. Scalmani, N. Rega, G.A. Petersson, H. Nakatsuji, M. Hada, M. Ehara, K. Toyota, R. Fukuda, J. Hasegawa, M. Ishida, T. Nakajima, Y. Honda, O. Kitao, H. Nakai, M. Klene, X. Li, J.E. Knox, H.P. Hratchian, J.B. Cross, C. Adamo, J. Jaramillo, R. Gomperts, R.E. Stratmann, O. Yazyev, A.J. Austin, R. Cammi, C. Pomelli, J.W. Ochterski, P.Y. Ayala, K. Morokuma, G.A. Voth, P. Salvador, J.J. Dannenberg, V.G. Zakrzewski, S. Dapprich, A.D. Daniels, M.C. Strain, O. Farkas, D.K. Malick, A.D. Rabuck, K. Raghavachari, J.B. Foresman, J.V. Ortiz, Q. Cui, A.G. Baboul, S. Clifford, J. Cioslowski, B.B. Stefanov, G. Liu, A. Liashenko, P. Piskorz, I. Komaromi, R.L. Martin, D.J. Fox, T. Keith, M.A. Al-Laham, C.Y. Peng, A. Nanayakkara, M. Challacombe, P.M.W. Gill, B. Johnson, W. Chen, M.W. Wong, C. Gonzalez, J.A. Pople, GAUSSIAN 03, Revision A.1, Gaussian, Inc., Pittsburgh PA, **2003**.

2. Additional computational details

Solvent effects, both electrostatic and non electrostatic, have been implicitly included making use of the Tomasi's integral equation formalism for the polarizable continuum model (IEF-PCM)[1,2] as implemented in Gaussian03. All stationary points structures obtained from vacuum calculations have been re-optimised in implicit THF (ε = 7.58) with the above IEF-PCM method.

The solvation Gibbs free energies should be evaluated using the well-known thermodynamic cycle[3], where the reaction Gibbs free energy in solution, ΔG_{sol}, is calculated for each process as the sum of two contributions: a gas-phase reaction free energy, ΔG_{gas}, and a solvation reaction free energy term calculated with the continuum approach, ΔG_{solv}:

$\Delta G_{sol} = \Delta G_{gas} + \Delta G_{solv}$

The gas-phase reaction free energy is the sum of two parts: electronic plus nuclear repulsion energy (ΔE_{ele}) and thermal contribution including zero-point energy ($\Delta G_{gas} = \Delta H + T\Delta S$). The last term, $T\Delta S$, that is the thermal correction, is evaluated using the calculated quantum mechanical vibrational frequencies. Due to the formation of new adducts between the complex $[(Ph_3P)Au]^+$, the alkyne C_2Ph_2 and H_2O in the catalytic cycle, entropy effects should be taken into consideration. Since this reaction is carried out in solution, translation and rotation movements do not largely contribute to entropy. Here the entropy by vibrational frequencies is evaluated in a classical way, where vibrational frequencies are calculated by quadratic fitting of energy changes. However, the entropy effects by the vibrational frequencies do not significantly influence the energy change. Thus, the energy changes are given hereafter without entropy contribution.

3. Geometrical structures of all stationary points

First Hydration

I				II				TS1			
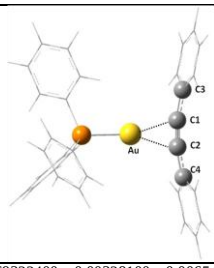				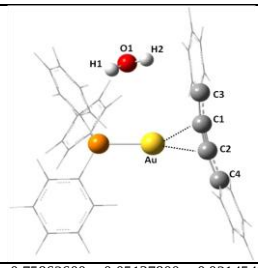				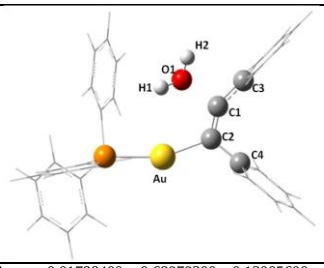			
Au	0.69322400	0.00328100	0.00654000	Au	-0.75862600	-0.05137800	-0.02145400	Au	-0.01788400	-0.68272300	0.13005600
P	-1.61528700	0.02035000	0.01781600	P	1.44516100	-0.73600300	-0.06343700	P	2.20672400	0.00235300	-0.01323500
C	-2.29916600	-0.66711700	1.54502400	C	1.72271000	-2.36642200	-0.78568700	C	3.30123900	-0.66424100	-1.28481800
C	-3.39360200	-0.06008800	2.18447800	C	2.83681300	-2.61056800	-1.60796600	C	4.04934500	0.17022700	-2.13467400
C	-1.74720200	-1.85102100	2.07072200	C	0.83351500	-3.41346300	-0.47750000	C	3.43319200	-2.06254600	-1.38021500
C	-3.93427200	-0.64152100	3.33405200	C	3.05988000	-3.89565900	-2.10762300	C	4.92148800	-0.39439200	-3.06804500
H	-3.81369000	0.85807800	1.78893700	H	3.51760200	-1.80324200	-1.85722200	H	3.94642000	1.24884600	-2.06969700
C	-2.29736100	-2.42556700	3.21554400	C	1.07024300	-4.69436800	-0.97501400	C	4.31132200	-2.61576100	-2.31161400
H	-0.89528000	-2.31789000	1.58398800	H	-0.03681600	-3.22450900	0.14532400	H	2.85190800	-2.70921700	-0.72871400
C	-3.39008500	-1.82116300	3.84691300	C	2.18198200	-4.93492800	-1.78937500	C	5.05365700	-1.78277400	-3.15508700
H	-4.77694700	-0.17205800	3.82762500	H	3.91639400	-4.08357300	-2.74428600	H	5.49669600	0.24812300	-3.72432400
H	-1.87338400	-3.33767500	3.61857700	H	0.38719800	-5.50085900	-0.73581300	H	4.41282000	-3.69205300	-2.38391700
H	-3.81161300	-2.26723300	4.73973300	H	2.35918300	-5.92984900	-2.18001100	H	5.73126200	-2.21603100	-3.88099700
C	-2.30101200	-0.95332700	-1.34357600	C	2.15225800	-0.75000400	1.59983900	C	3.16183200	0.09641900	1.51815500
C	-3.39805300	-1.80840600	-1.14157500	C	2.90412100	-1.84073900	2.06612900	C	4.56092800	0.24543500	1.49624500
C	-1.74448000	-0.81900300	-2.63010500	C	1.95092600	0.37558900	2.42586800	C	2.48410200	0.03443600	2.75032100
C	-3.93561600	-2.51302300	-2.22181200	C	3.45054400	-1.80469400	3.35249600	C	5.26510500	0.35194100	2.69649700
H	-3.82368200	-1.92236300	-0.15069500	H	3.05975200	-2.70692200	1.43245100	H	5.09300500	0.26130000	0.55090300
C	-2.29195300	-1.52199800	-3.70215200	C	2.50642900	0.40080800	3.70399100	C	3.19694900	0.14566400	3.94466200
H	-0.89075200	-0.16598100	-2.78855200	H	1.38726000	1.23003700	2.05999300	H	1.40783400	-0.11138500	2.76859100
C	-3.38665800	-2.36933400	-3.49793300	C	3.25244500	-0.68928500	4.16837100	C	4.58511500	0.30680200	3.91730800
H	-4.78070000	-3.17282500	-2.06474000	H	4.02925300	-2.64677100	3.71325800	H	6.34297000	0.46193900	2.67961500
H	-1.86514400	-1.41484500	-4.69237300	H	2.35983800	1.26839500	4.33697200	H	2.67381300	0.09367600	4.89236900
H	-3.80685200	-2.91846300	-4.33199900	H	.67816500	-0.66648100	5.16452400	H	5.13797400	0.38477100	4.84584600
C	-2.27935400	1.69492700	-0.14701700	C	2.40772600	0.48189500	-1.01059100	C	1.80840000	1.72682200	-0.50261000
C	-3.37040400	1.96244100	-0.99180200	C	3.58165800	1.03723200	-0.47676500	C	1.97875200	2.79946500	0.38421400
C	-1.71233000	2.73248500	0.61764700	C	1.87064100	1.00176200	-2.20395900	C	1.09583800	1.92894500	-1.70835300
C	-3.89087700	3.25731500	-1.06125100	C	4.19950000	2.11439700	-1.11904000	C	1.43415800	4.05423300	0.08181800
H	-3.80484300	1.16818800	-1.58895000	H	3.98343000	0.66411000	0.45851500	H	2.51769500	2.65160000	1.31343000
C	-2.24311100	4.01939600	0.54518700	C	2.49252900	2.07765900	-2.84022400	C	0.56403400	3.18699400	-2.00749900
H	-0.86224700	2.53144200	1.26373000	H	0.94843700	0.59409400	-2.60887600	H	0.95849300	1.10510900	-2.40490100
C	-3.33131600	4.28181800	-0.29427000	C	3.65174300	2.64211100	-2.29042700	C	0.72381600	4.24940600	-1.10453100
H	-4.73091400	3.46377500	-1.71389300	H	5.08868600	2.55831700	-0.68609200	H	1.56354600	4.87544700	0.77742100
H	-1.80707100	4.81675100	1.13523200	H	2.06459500	2.48966400	-3.74763800	H	0.03125800	3.33906600	-2.94156000
H	-3.73804900	5.28429800	-0.35286600	H	4.11444600	3.49907400	-2.76727500	H	0.30545700	5.22331700	-1.33347900
C	2.90584100	-0.64785500	-0.00926200	C	-3.06753700	0.33222000	0.04263900	C	-2.09104700	-0.58582300	0.09989800
C	2.92764300	0.58050200	-0.01024100	C	-2.51535800	1.42862700	0.03791000	C	-2.71883000	0.53895000	-0.00563900
C	3.21849700	1.97526700	-0.02188100	C	-2.05908900	2.78251800	0.03249000	C	-3.99921300	1.18899200	-0.09290400
C	3.57420200	2.62952400	1.17650200	C	-1.77981800	3.42973000	-1.18971400	C	-4.66405000	1.26010200	-1.33509800
C	3.17033000	2.69917400	-1.23208500	C	-1.81138500	3.45101900	1.24878100	C	-4.58517300	1.76398100	1.05459000
C	3.88439600	3.98723100	1.15472800	C	-1.25034300	4.72087100	-1.18862100	C	-5.90492200	1.88951900	-1.42046000
H	3.61027900	2.06700400	2.10406600	H	-1.96361400	2.90983300	-2.12456700	H	-4.20844900	0.80817900	-2.21175900
C	3.48105900	4.05632200	-1.23748100	C	-1.27983500	4.73960700	1.23856200	C	-5.82309200	2.39550000	0.95582700
H	2.89780800	2.18974900	-2.15098300	H	-2.01285000	2.94555700	2.18776000	H	-4.06653800	1.70159500	2.00734100
C	3.83727600	4.70065200	-0.04772800	C	-0.99458100	5.37549000	0.02429900	C	-6.48071500	2.45759900	-0.27873900
H	4.16675200	4.48940200	2.07248900	H	-1.02723400	5.21296000	-2.12905200	H	-6.42540200	1.93395900	-2.36988000
H	3.45042000	4.61212000	-2.16709600	H	-1.07306500	5.24338500	2.17566200	H	-6.28079900	2.83134900	1.83610200
H	4.08088500	5.75638700	-0.05822900	H	-0.56174600	6.37004100	0.02210200	H	-7.44578500	2.94559400	-0.34948300
C	3.14715800	-2.05202400	-0.02129700	C	-3.91207100	-0.81409700	0.06209200	C	-2.93320500	-1.81107900	0.18393800
C	3.07909900	-2.77198400	-1.23294600	C	-4.31324500	-1.37217700	1.29466700	C	-3.49306500	-2.20025200	1.41155200
C	3.47447300	-2.72013300	1.17753900	C	-4.35969400	-1.38383300	-1.14878600	C	-3.16008500	-2.59050000	-0.96242800
C	3.34200500	-4.13920600	-1.23912400	C	-5.15760700	-2.47935500	1.30776300	C	-4.27504600	-3.35528600	1.48658700
H	2.82847600	-2.25181400	-2.15203000	H	-3.96447100	-0.92973000	2.22253600	H	-3.31021700	-1.60418400	2.30140600
C	3.73715200	-4.08781000	1.15490300	C	-5.20352700	-2.49109900	-1.11916400	C	-3.94899200	-3.73938600	-0.87958500
H	3.52631500	-2.16048300	2.10610000	H	-4.04753200	-0.95015300	-2.09361600	H	-2.71782700	-2.29763100	-1.91101600
C	3.67022100	-4.79739900	-0.04890400	C	-5.60235500	-3.03891400	0.10495400	C	-4.50692400	-4.12426400	0.34331900
H	3.29586500	-4.69235700	-2.16968000	H	-5.47253100	-2.90501400	2.25316000	H	-4.70452300	-3.65193400	2.43697700
H	3.99777400	-4.60099800	2.07299300	H	-5.55403200	-2.92585800	-2.04774300	H	-4.12547700	-4.33505500	-1.76828100
H	3.87622600	-5.86108900	-0.06005200	H	-6.26055400	-3.89946400	0.12156900	H	-5.11599800	-5.01829200	0.40444300
				O	1.27732100	3.12657500	0.09026200	O	-1.61808800	1.96011200	-0.00662900
				H	0.49050000	3.59003600	-0.21879900	H	-2.10946400	2.68822800	-0.41416000
				H	1.70985800	2.81163000	-0.71088200	H	-0.77345300	1.86187700	-0.50097000

III				TS2				IV			
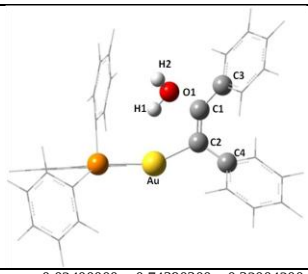				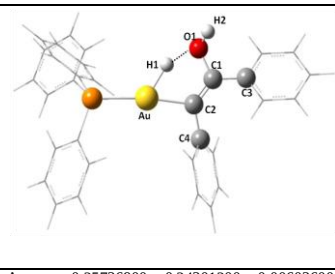				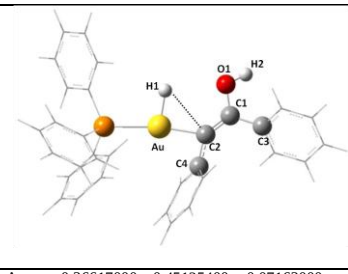			
Au	0.02400000	-0.74390300	0.32004200	Au	-0.25736900	-0.24301200	-0.00603600	Au	0.36617000	0.45125400	-0.07163000
P	2.24139500	-0.02229300	-0.03576900	P	2.14395300	-0.14575700	0.00471900	P	-2.02799400	0.19809600	-0.01330900
C	3.29224500	-0.73274900	-1.31809000	C	2.72142200	1.57015500	0.05388600	C	-2.55129000	-0.60961900	1.51903900
C	3.95991600	0.06483500	-2.26552700	C	3.73986200	1.97831400	0.93190800	C	-3.74824500	-0.24503400	2.16083700
C	3.47854600	-2.12824600	-1.31893100	C	2.13607500	2.50467000	-0.82360800	C	-1.74968500	-1.63242700	2.06122300
C	4.80594600	-0.53371400	-3.20117200	C	4.16907700	3.30819600	0.92488000	C	-4.14004900	-0.90826900	3.32589600
H	3.81462800	1.14062700	-2.27493600	H	4.18961000	1.26429300	1.61333100	H	-4.35966900	0.55416100	1.75587600
C	4.33134500	-2.71481100	-2.25364400	C	2.57541600	3.82798400	-0.82625800	C	-2.15088200	-2.28950800	3.22389900
H	2.96158500	-2.74652400	-0.58989300	H	1.34787400	2.19701900	-1.50659600	H	-0.81906800	-1.91387700	1.57568000
C	4.99284300	-1.91878300	-3.19389800	C	3.59052200	4.22985100	0.04893200	C	-3.34506500	-1.92791800	3.85570800
H	5.31874900	0.07941000	-3.93292200	H	4.95450400	3.62198700	1.60231400	H	-5.06180000	-0.62567100	3.82055700
H	4.47571600	-3.78857100	-2.25280500	H	2.12616800	4.54391800	-1.50427200	H	-1.53206500	-3.07527100	3.64079500
H	5.65057800	-2.37803400	-3.92204000	H	3.92690800	5.25969700	0.04840200	H	-3.65156800	-2.43593200	4.76225100
C	3.27781800	0.31152000	1.40595000	C	2.89081400	-0.90336700	-1.45851600	C	-2.60841200	-0.83238100	-1.38504200
C	4.62886900	0.68134300	1.26658700	C	3.96076100	-0.28575700	-2.12875300	C	-3.48098200	-1.91291100	-1.17423800
C	2.70813600	0.21299700	2.68957400	C	2.40727100	-2.14784100	-1.90627700	C	-2.15797500	-0.53910500	-2.68843200
C	5.38832700	0.96837700	2.40100200	C	4.54374200	-0.91504500	-3.23135800	C	-3.90043900	-2.68780400	-2.25943300
H	5.08437700	0.72819600	0.28280900	H	4.32911500	0.67714400	-1.79208400	H	-3.82697800	-2.14416100	-0.17274700
C	3.47579400	0.50563300	3.81810200	C	2.99906500	-2.76962200	-3.00506700	C	-2.58764000	-1.31424700	-3.76493400
H	1.67489900	-0.10429100	2.80085300	H	1.57667400	-2.62662800	-1.39535100	H	-1.48373200	0.29676300	-2.85898100
C	4.81272300	0.88536000	3.67307800	C	4.06615600	-2.15320600	-3.66749300	C	-3.45709400	-2.38995500	-3.54998600
H	6.42962600	1.24852300	2.29452000	H	5.36801700	-0.43795700	-3.74819300	H	-4.57494600	-3.52001700	-2.09557800
H	3.03652700	0.42487500	4.80553100	H	2.62732300	-3.72790000	-3.34802300	H	-2.24649600	-1.08280700	-4.76722700
H	5.40976000	1.10506500	4.55009000	H	4.52053500	-2.63629300	-4.52420700	H	-3.78703700	-2.99257200	-4.38772600
C	1.64635400	1.60784200	-0.66052600	C	2.85336800	-0.98055200	1.44366200	C	-2.94171800	1.75560700	-0.10525000
C	1.59407000	2.72543000	0.19449900	C	4.01255100	-1.76731100	1.32785600	C	-4.04469900	1.90300300	-0.96348600
C	0.95102400	1.64935300	-1.88895600	C	2.24583500	-0.81018600	2.70262800	C	-2.56022500	2.81960400	0.73527600
C	0.84073700	3.85176100	-0.16036300	C	4.56023200	-2.36641000	2.46492100	C	-4.75410600	3.10704600	-0.98048600
H	2.12400400	2.70598400	1.14118200	H	4.47707000	-1.91144600	0.35838700	H	-4.34458800	1.08577200	-1.61012800
C	0.19685800	2.77527300	-2.23745900	C	2.80370800	-1.40738400	3.83239900	C	-3.27873200	4.01415900	0.71485700
H	0.97343600	0.79271300	-2.55612000	H	1.34335400	-0.21226700	2.79713600	H	-1.71211000	2.71073300	1.40537100
C	0.12965500	3.87699500	-1.36690500	C	3.95992600	-2.18579000	3.71326000	C	-4.37294400	4.15906500	-0.14525400
H	0.80339100	4.70395800	0.50910100	H	5.45329900	-2.97339800	2.37438600	H	-5.60249500	3.22043500	-1.64501200
H	-0.33229700	2.79720100	-3.18561300	H	2.33645200	-1.27267300	4.80085400	H	-2.98522200	4.83098300	1.36371300
H	-0.45590300	4.75044400	-1.63740700	H	4.38817700	-2.65359800	4.59163300	H	-4.92494000	5.09113200	-0.16362900
C	-2.05025400	-0.54403400	0.28746900	C	-2.33251600	-0.05848200	0.00272800	C	2.41664200	0.31860100	-0.11838000
C	-2.54883700	0.66873400	0.09648300	C	-3.13757200	-1.11960500	-0.04191900	C	3.38774600	1.22703600	-0.01226500
C	-3.84705000	1.25731200	-0.18860200	C	-4.59192200	-1.21070900	0.06928700	C	4.82662000	0.93465200	-0.10085000
C	-4.72327700	0.59667700	-1.07339600	C	-5.31311700	-0.29366000	0.85964800	C	5.72327100	1.61602400	0.74792100
C	-4.24970000	2.47075100	0.40698800	C	-5.28823500	-2.23453100	-0.60630300	C	5.32799700	0.00413600	-1.02865000
C	-5.97385200	1.14234700	-1.35283800	C	-6.69646200	-0.40503500	0.97309800	C	7.09298900	1.36300500	0.66752000
H	-4.41976300	-0.34310900	-1.52144800	H	-4.78431900	0.49574800	1.38159800	H	5.34347700	2.31508000	1.48921100
C	-5.50423600	3.00806600	0.11980000	C	-6.67498500	-2.33341500	-0.49227800	C	6.69871600	-0.23819900	-1.10678400
H	-3.59181400	2.97491200	1.10897600	H	-4.74522800	-2.92961300	-1.23989500	H	4.64313700	-0.50569400	-1.69790400
C	-6.36614800	2.34708400	-0.75994900	C	-7.37980100	-1.42295700	0.29890400	C	7.58197800	0.43902300	-0.26035400
H	-6.64290100	0.63004900	-2.03427600	H	-7.24350800	0.29823900	1.58993400	H	7.77639500	1.88115700	1.33027000
H	-5.81261400	3.93606300	0.58749100	H	-7.20444800	-3.11686600	-1.02207100	H	7.07983300	-0.94633700	-1.83310000
H	-7.34021000	2.76720000	-0.98096400	H	-8.45633000	-1.50510200	0.39066400	H	8.64676700	0.24950800	-0.32524400
C	-2.93609800	-1.71378200	0.40487000	C	-2.66764000	1.35639900	-0.08905900	C	2.33210500	-1.11479200	-0.00684800
C	-3.93981000	-1.75835200	1.39107600	C	-3.32097000	1.86876000	-1.23210500	C	1.46415800	-1.78571700	-0.93395100
C	-2.76748500	-2.81989100	-0.44971700	C	-2.29015700	2.24824500	0.94106300	C	2.79345000	-1.84051800	1.12684500
C	-4.76145600	-2.87997300	1.50846200	C	-3.60600500	3.22883300	-1.32650300	C	1.07283100	-3.12117900	-0.70986600
H	-4.06329200	-0.91762900	2.06760100	H	-3.60121100	1.18993100	-2.03191100	H	1.23220600	-1.30953000	-1.88575600
C	-3.60537400	-3.93005900	-0.33990400	C	-2.57881100	3.60972900	0.83688900	C	2.41586700	-3.16006900	1.31217700
H	-1.98302200	-2.80009200	-1.20223800	H	-1.79904200	1.85927100	1.82994200	H	3.43574800	-1.33830600	1.84264700
C	-4.60243600	-3.96368300	0.63997800	C	-3.23691300	4.10081200	-0.29425600	C	1.54244400	-3.80071500	0.40533600
H	-5.52575100	-2.90823200	2.27695300	H	-4.11625500	3.61268500	-2.20257200	H	0.43078400	-3.61842600	-1.42835300
H	-3.47500000	-4.77199800	-1.01053200	H	-2.29690400	4.28426200	1.63730900	H	2.78877000	-3.70942300	2.16944400
H	-5.24443800	-4.83181500	0.73133900	H	-3.46237000	5.15785600	-0.37320600	H	1.25576000	-4.83168500	0.57526600
O	-1.52154100	1.80065700	0.21873100	O	-2.48277300	-2.34737900	-0.23769400	O	3.05352200	2.53159800	0.18364400
H	-1.37809900	2.32501300	-0.60568300	H	-2.83746300	-3.02495800	0.35902500	H	3.81256700	3.08617800	-0.03320300
H	-0.64790100	1.35985500	0.40959800	H	-1.10716100	-1.63648800	-0.15609500	H	0.45178300	1.99092100	0.19053500

TS3				V				TS4			
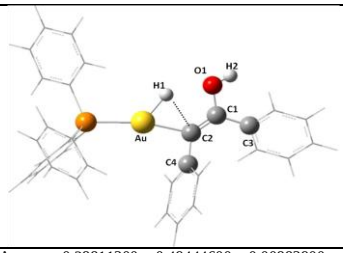				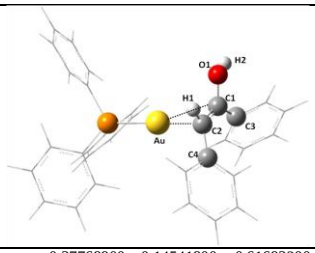				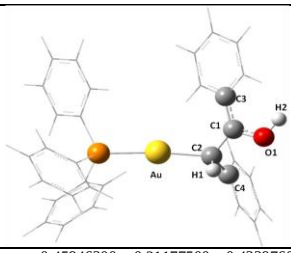			
Au	0.28811300	-0.49444600	-0.00883900	Au	0.37768900	0.14541800	-0.61693200	Au	0.45946300	-0.21177500	0.43397600
P	-2.08835300	-0.15042300	0.01557900	P	-1.80563300	-0.09503200	0.09935400	P	-1.82552300	0.00260400	0.00109600
C	-2.63509600	0.88606700	-1.36443800	C	-2.89108500	-0.68153400	-1.22383300	C	-2.81696700	0.30370800	1.48990500
C	-3.80929300	0.58796000	-2.07667800	C	-3.88435400	-1.64433900	-0.97306000	C	-3.89175300	1.20943900	1.49197900
C	-1.87598000	2.02145800	-1.70727500	C	-2.76044000	-0.12770000	-2.51173700	C	-2.51760000	-0.42623100	2.65600200
C	-4.22167000	1.42620900	-3.11546700	C	-4.74215200	-2.03885800	-2.00292100	C	-4.65984300	1.37414500	2.64764800
H	-4.38867000	-0.29339100	-1.82388800	H	-3.98250300	-2.08056400	0.01504700	H	-4.12299300	1.78045900	0.59918900
C	-2.29897700	2.85440600	-2.74234600	C	-3.62453100	-0.52487400	-3.53107600	C	-3.29368900	-0.26008500	3.80241700
H	-0.96117200	2.25318500	-1.16722900	H	-1.98763500	0.60919000	-2.71205500	H	-1.68205000	-1.12058500	2.66099700
C	-3.47066100	2.55667700	-3.44639100	C	-4.61472400	-1.48025100	-3.27675600	C	-4.36405100	0.64043600	3.79885000
H	-5.12593500	1.19438400	-3.66564500	H	-5.50696800	-2.78174300	-1.80938500	H	-5.48782700	2.07343900	2.64700900
H	-1.71434000	3.72806700	-3.00498300	H	-3.52355200	-0.09694500	-4.52143200	H	-3.06228800	-0.82552800	4.69750300
H	-3.79321600	3.20199200	-4.25468100	H	-5.28129200	-1.79109200	-4.07228600	H	-4.96242400	0.77174900	4.69255900
C	-2.63774600	0.66997500	1.53300700	C	-2.49833800	1.47069200	0.68474000	C	-2.51955400	-1.49570100	-0.75110000
C	-3.55793300	1.73135100	1.49579900	C	-3.80151000	1.86290700	0.33353600	C	-3.78427800	-1.98310400	-0.37906400
C	-2.14129500	0.21556000	2.77103000	C	-1.72180400	2.28975900	1.52699400	C	-1.77558800	-2.16913500	-1.73868800
C	-3.98046400	2.32498800	2.68817100	C	-4.32179600	3.06102400	0.82972800	C	-4.30043700	-3.12340500	-0.99950800
H	-3.93685700	2.08822500	0.54429700	H	-4.39841500	1.23960900	-0.32302200	H	-4.35367000	-1.47877600	0.39385000
C	-2.57319100	0.81175100	3.95526900	C	-2.25306200	3.47984600	2.02200500	C	-2.30181100	-3.30276300	-2.35756100
H	-1.42982200	-0.60534300	2.80680500	H	-0.70865500	1.99779900	1.78964700	H	-0.78822400	-1.80921000	-2.01385800
C	-3.49170200	1.86654700	3.91369900	C	-3.55186000	3.86591800	1.67250200	C	-3.56362700	-3.77992600	-1.98831100
H	-4.69063000	3.14295000	2.65811100	H	-5.32563800	3.36415800	0.55650000	H	-5.27432900	-3.49911200	-0.70811900
H	-2.19420200	0.45801000	4.90688200	H	-1.65539400	4.10808600	2.67185700	H	-1.72643400	-3.81890300	-3.11715400
H	-3.82284400	2.33010000	4.83524800	H	-3.95940600	4.79490000	2.05295900	H	-3.96704800	-4.66539300	-2.46494600
C	-3.00498200	-1.70477300	-0.10171100	C	-1.96647100	-1.27749500	1.46038300	C	-2.22732400	1.36253600	-1.13357800
C	-4.13255200	-1.94677200	0.70174000	C	-2.76976900	-0.99260300	2.57743700	C	-3.08815700	1.18149700	-2.22845400
C	-2.59335500	-2.66699800	-1.04365600	C	-1.30485800	-2.51718800	1.36983700	C	-1.67439000	2.63398700	-0.88498000
C	-4.84173500	-3.14200300	0.55659300	C	-2.91219400	-1.94531300	3.58984000	C	-3.39472800	2.26252600	-3.06023100
H	-4.44854200	-1.21113500	1.43360000	H	-3.27622700	-0.03669500	2.65252100	H	-3.51521000	0.20458400	-2.42613900
C	-3.31212900	-3.85324500	-1.18458800	C	-1.45857500	-3.46333900	2.38204700	C	-1.99432400	3.70912000	-1.71355500
H	-1.71858800	-2.48604800	-1.66189400	H	-0.67864500	-2.73784100	0.50964000	H	-1.00737700	2.77808400	-0.03913200
C	-4.43434100	-4.09126100	-0.38370500	C	-2.26108000	-3.17699800	3.49231700	C	-2.85308700	3.52334000	-2.80285200
H	-5.70931200	-3.33014900	1.17798000	H	-3.53119300	-1.72440700	4.45139700	H	-4.05949800	2.11881300	-3.90402400
H	-2.99579100	-4.59255800	-1.91085200	H	-0.95309400	-4.41913600	2.30916100	H	-1.57965900	4.69000300	-1.51087200
H	-4.98663300	-5.01717600	-0.49065200	H	-2.37528300	-3.91251100	4.27963700	H	-3.09863100	4.35954100	-3.44677400
C	2.36617400	-0.32561700	0.02336700	C	2.40888700	0.70258900	-1.44022800	C	2.49409500	-0.58905100	0.91411700
C	3.31433700	-1.26300500	-0.02793300	C	2.74955300	-0.64082700	-1.45406900	C	3.51842800	0.46740400	0.90375000
C	4.76080900	-1.02684000	0.09405500	C	3.41015100	-1.44034800	-0.41169700	C	3.45526000	1.77845100	0.31141700
C	5.64665300	-1.75123800	-0.72976900	C	4.49263700	-2.26029500	-0.79574700	C	2.60973100	2.03216200	-0.79351700
C	5.27847400	-0.11248400	1.02866600	C	3.00157800	-1.42375100	0.93525500	C	4.27717200	2.82701000	0.80704200
C	7.02359700	-1.55729600	-0.61742700	C	5.15247700	-3.04069400	0.15510700	C	2.62070300	3.28018200	-1.40936800
H	5.25404900	-2.43882500	-1.47471100	H	4.83940000	-2.25504400	-1.82623300	H	1.97314100	1.24051700	-1.16968000
C	6.65623800	0.06881400	1.13999700	C	3.65999100	-2.21216300	1.87522700	C	4.25727400	4.07658300	0.20434300
H	4.60156900	0.43748000	1.67300100	H	2.16147600	-0.80442900	1.23718500	H	4.87889700	2.68451100	1.70218000
C	7.52940200	-0.65096500	0.31867700	C	4.73538800	-3.02036000	1.48815800	C	3.43915400	4.29965800	-0.91333900
H	7.69969700	-2.10833800	-1.26083800	H	5.99274100	-3.65626900	-0.14368900	H	1.98882400	3.45965800	-2.27051800
H	7.04995600	0.76538700	1.87075000	H	3.33277600	-2.20220500	2.90838800	H	4.86449600	4.88064600	0.60168900
H	8.59953600	-0.50714300	0.40863900	H	5.24571200	-3.63041600	2.22388600	H	3.43634700	5.27352400	-1.38852400
C	2.42825600	1.12256600	-0.08570500	C	2.92872300	1.78390800	-0.57761500	C	3.05585100	-1.80646100	0.22080300
C	1.94499100	1.93706800	0.97211000	C	2.27276600	3.03189500	-0.64186600	C	3.22515100	-3.01499200	0.91790600
C	2.85282400	1.74505000	-1.28542200	C	4.06907800	1.66211300	0.23790300	C	3.42821200	-1.74422800	-1.13603500
C	1.90484800	3.32718500	0.83388800	C	2.72840200	4.11695800	0.10488300	C	3.74296500	-4.13731900	0.26928300
H	1.64396500	1.46946900	1.90653200	H	1.40637900	3.14526800	-1.29013900	H	2.94630100	-3.07320200	1.96753300
C	2.81857600	3.13015600	-1.40685100	C	4.52238600	2.75318200	0.98084000	C	3.96165000	-2.86471700	-1.77608000
H	3.20779900	1.12615800	-2.10371500	H	4.61064900	0.72483200	0.28202200	H	3.29014800	-0.82116900	-1.69517300
C	2.34163700	3.92294400	-0.35151400	C	3.85313200	3.97901300	0.92342700	C	4.11865300	-4.06396000	-1.07626800
H	1.54660800	3.94079800	1.65248800	H	2.21509000	5.06963200	0.04060300	H	3.85738300	-5.06782300	0.81413400
H	3.16257100	3.59959200	-2.32140200	H	5.40935900	2.64927000	1.59549200	H	4.24792900	-2.80357600	-2.82027300
H	2.31741800	5.00132700	-0.45585800	H	4.21385700	4.82272400	1.49954900	H	4.52775000	-4.93476300	-1.57431700
O	2.94520000	-2.56470700	-0.21988600	O	2.55258200	-1.27158500	-2.62852300	O	4.61484900	0.14000400	1.53831600
H	3.64421700	-3.15181900	0.09529900	H	2.61693600	-2.22714400	-2.50331300	H	5.32399200	0.79157900	1.42511300
H	1.06960100	-1.84538500	-0.28074200	H	2.04663000	1.03584900	-2.40783000	H	2.42037800	-0.82458100	1.98282600

VI				enol				
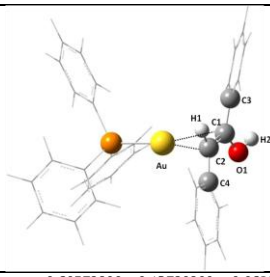				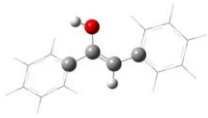				
Au	0.60579900	0.13780900	-0.06287000	C	0	-0.50055500	-0.40904900	0.12467500
P	-1.67760500	-0.17533600	-0.01814300	C	0	0.49752900	0.46514900	-0.07899900
C	-2.19744100	-1.64592800	-0.93496700	C	0	1.92159900	0.11101700	-0.02330700
C	-3.20991300	-2.48692200	-0.44139700	C	0	2.85131900	1.01477500	0.53095600
C	-1.60501000	-1.91848900	-2.18251800	C	0	2.39312500	-1.11001600	-0.54178000
C	-3.62796400	-3.58485400	-1.19780100	C	0	4.21042700	0.70003400	0.56978700
H	-3.66228800	-2.28448200	0.52335600	H	0	2.49961300	1.94685900	0.96722200
C	-2.03250700	-3.01390100	-2.93137600	C	0	3.75137900	-1.42062800	-0.49656700
H	-0.81494900	-1.27622200	-2.56137900	H	0	1.68922000	-1.79669000	-1.00134600
C	-3.04322700	-3.84683400	-2.43895800	C	0	4.66418800	-0.51718400	0.05666900
H	-4.40830200	-4.23321000	-0.81698500	H	0	4.91253600	1.39918300	1.01034000
H	-1.57706600	-3.22164200	-3.89240900	H	0	4.10144400	-2.36118000	-0.90695000
H	-3.37028700	-4.70023000	-3.02088500	H	0	5.72017200	-0.75935500	0.08449700
C	-2.54988300	1.22956100	-0.75223400	C	0	-1.94112600	-0.23646600	0.07763000
C	-3.65848400	1.03397100	-1.59424600	C	0	-2.74197900	-1.36787200	0.36127300
C	-2.12458300	2.53581900	-0.44290300	C	0	-2.59968800	0.97524700	-0.23521900
C	-4.33957300	2.13935900	-2.11003400	C	0	-4.13192200	-1.29679400	0.33176000
H	-3.98039700	0.02933200	-1.84574700	H	0	-2.25023400	-2.30684100	0.60624800
C	-2.81526000	3.63172600	-0.95840700	C	0	-3.99173400	1.03822600	-0.26491200
H	-1.25710900	2.69117900	0.19260800	H	0	-2.01300200	1.85796300	-0.44921300
C	-3.92193000	3.43369800	-1.79121100	C	0	-4.76476700	-0.09101300	0.01704700
H	-5.19289400	1.98846300	-2.76070700	H	0	-4.72275800	-2.17880400	0.55407700
H	-2.48769500	4.63637800	-0.71872900	H	0	-4.47724300	1.97740800	-0.50742700
H	-4.45266500	4.28736600	-2.19549000	H	0	-5.84695000	-0.03236700	-0.00606400
C	-2.31492900	-0.36431900	1.66553800	O	0	0.22816000	1.78972100	-0.33044800
C	-3.46149600	0.32749700	2.09046200	H	0	1.02388600	2.20425100	-0.67954500
C	-1.65966700	-1.24389400	2.54840200	H	0	-0.16873000	-1.40074500	0.39768300
C	-3.94798700	0.13326800	3.38618900					
H	-3.96511800	1.01111300	1.41602900					
C	-2.15603200	-1.43518000	3.83667100					
H	-0.76918700	-1.77488400	2.22308600					
C	-3.29921000	-0.74535900	4.25617000					
H	-4.83126400	0.66891700	3.71348600					
H	-1.65293600	-2.11419000	4.51503100					
H	-3.67906700	-0.89089300	5.26032200					
C	2.77260900	0.75090000	-0.34817000					
C	3.11037800	-0.24023400	0.55489000					
C	3.45307400	-1.61409900	0.16153200					
C	3.05327700	-2.69479600	0.97417900					
C	4.22724500	-1.86100700	-0.98665100					
C	3.41302400	-3.99770900	0.63353900					
H	2.42711200	-2.51952700	1.84718200					
C	4.58718100	-3.16755500	-1.31768500					
H	4.57433600	-1.03113500	-1.59480800					
C	4.18051600	-4.23478900	-0.51163300					
H	3.09151700	-4.82687500	1.25290900					
H	5.19659800	-3.35147500	-2.19467800					
H	4.46420800	-5.24753600	-0.77138700					
C	2.73642400	2.20959900	-0.17054500					
C	2.66907900	2.98867300	-1.34753500					
C	2.75276100	2.86924300	1.07793000					
C	2.63270800	4.37923900	-1.28239300					
H	2.65265500	2.49016200	-2.31441100					
C	2.71288000	4.26270800	1.13276400					
H	2.79892700	2.29766400	1.99566800					
C	2.65436200	5.02100000	-0.04018000					
H	2.59171700	4.96184400	-2.19555600					
H	2.73427400	4.75904700	2.09643100					
H	2.62909100	6.10292600	0.01289100					
O	3.23155500	0.05764600	1.86155700					
H	3.60707700	-0.69637600	2.33346800					
H	2.84472300	0.42388400	-1.37737000					

Second Hydration

VII(a)

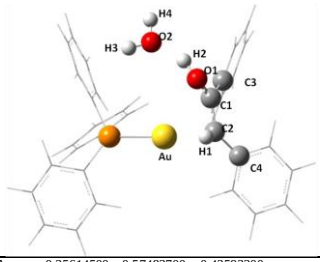

Au	0.35614500	0.57483700	-0.43593300
P	-1.84426300	0.16715100	0.14617800
C	-2.31669300	-1.29317400	-0.84468200
C	-2.77831700	-2.47180100	-0.23879700
C	-2.07184500	-1.27498100	-2.23375600
C	-2.97736700	-3.62324900	-1.01018500
H	-2.95763600	-2.49943100	0.83002900
C	-2.28664300	-2.42164800	-3.00134100
H	-1.68656600	-0.37657900	-2.70838500
C	-2.72946400	-3.60296200	-2.38607200
H	-3.31960200	-4.53508500	-0.53333100
H	-2.08426600	-2.40387500	-4.06741400
H	-2.87178500	-4.50094800	-2.97784500
C	-3.02984000	1.47284400	-0.23786900
C	-4.26643900	1.18266600	-0.84075200
C	-2.71786000	2.79701700	0.12496700
C	-5.18119800	2.21228600	-1.07441600
H	-4.50795900	0.16415500	-1.12633400
C	-3.64091800	3.81608500	-0.10695900
H	-1.76015500	3.02461300	0.58515000
C	-4.87035900	3.52408300	-0.70750100
H	-6.13312200	1.98995400	-1.54200900
H	-3.40129600	4.83510900	0.17272000
H	-5.58240200	4.31944000	-0.89237900
C	-2.09866300	-0.28961100	1.87719700
C	-3.28465800	0.05497700	2.54937500
C	-1.10636000	-1.03611200	2.54177900
C	-3.47662800	-0.35653000	3.87041700
H	-4.04362000	0.64450400	2.04645400
C	-1.31214500	-1.44799300	3.85809300
H	-0.18107100	-1.28956500	2.03174100
C	-2.49587900	-1.10862800	4.52175400
H	-4.38867600	-0.08700900	4.38972700
H	-0.54964800	-2.02470900	4.36893900
H	-2.64927100	-1.42355800	5.54705300
C	2.42038900	0.80359300	-1.32811900
C	2.44045300	-0.59029400	-1.25198900
C	2.96597600	-1.42630900	-0.15859600
C	3.62320100	-2.62595900	-0.49816000
C	2.82532900	-1.08037200	1.19930200
C	4.12446100	-3.46066700	0.50232900
H	3.76056600	-2.88614400	-1.54413100
C	3.32062900	-1.92140200	2.19207600
H	2.32611000	-0.15504700	1.47264500
C	3.96889600	-3.11374900	1.84671600
H	4.64211000	-4.37417900	0.23232600
H	3.20771600	-1.64791300	3.23523400
H	4.35677900	-3.76347300	2.62255800
C	3.25065200	1.78205200	-0.59458300
C	2.81258100	3.12182400	-0.56044700
C	4.48657600	1.46082800	-0.00538700
C	3.57333400	4.10552700	0.06950900
H	1.87218900	3.38619900	-1.03996100
C	5.24700200	2.45010500	0.62068400
H	4.85820000	0.44299100	-0.04202600
C	4.79204500	3.77060400	0.66703900
H	3.22228600	5.13104600	0.08796900
H	6.20245300	2.19064000	1.06254300
H	5.38775500	4.53422000	1.15279400
O	2.02179000	-1.24555800	-2.33921400
H	1.58266900	-2.09042600	-2.08122400
H	2.08044700	1.14686200	-2.30078300
H	0.42787400	-4.08055400	-1.24242600
O	0.35566900	-3.13772100	-1.40939200
H	-0.56278800	-2.97871500	-1.67449300

VII(b)

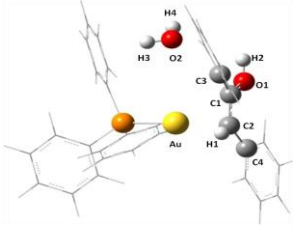

Au	-0.54778600	0.34818100	0.34580000
P	1.69167900	-0.15656400	0.15216000
C	2.62052300	-0.17059600	1.70171600
C	3.52941000	-1.20047200	1.99979400
C	2.45549700	0.90226300	2.59881600
C	4.26848700	-1.15113700	3.18437300
H	3.65557900	-2.03126400	1.31383900
C	3.20258900	0.94481300	3.77506800
H	1.74918900	1.69707800	2.37433500
C	4.10745600	-0.08152600	4.06817900
H	4.96750200	-1.94638700	3.41516700
H	3.07643900	1.77111100	4.46461600
H	4.68179300	-0.04819600	4.98624300
C	2.55232400	0.97557000	-0.96448700
C	3.88599900	1.35268600	-0.72859100
C	1.88085900	1.44649100	-2.10940100
C	4.54209100	2.18312000	-1.64059600
H	4.39981100	1.00628900	0.16171700
C	2.54692100	2.27115000	-3.01532600
H	0.84481100	1.17026100	-2.28558700
C	3.87656400	2.63830200	-2.78147400
H	5.56898200	2.47658300	-1.45716500
H	2.02931700	2.63419400	-3.89573700
H	4.38933300	3.28497500	-3.48352800
C	1.85488300	-1.81551600	-0.58373000
C	2.65925000	-2.03503400	-1.71375400
C	1.06325500	-2.86556100	-0.07724100
C	2.66800100	-3.29081800	-2.33140700
H	3.25116900	-1.22519500	-2.12506900
C	1.08639300	-4.11916600	-0.69055400
H	0.40513600	-2.69150700	0.76955700
C	1.88440800	-4.33107900	-1.82315300
H	3.27728200	-3.45052500	-3.21402000
H	0.46348600	-4.91945300	-0.30616300
H	1.87921300	-5.29720000	-2.31560600
C	-2.70619800	1.00312600	0.44856400
C	-3.01333000	-0.07054400	-0.37495600
C	-3.42137800	-1.38841100	0.13218700
C	-3.06575900	-2.55292300	-0.58073100
C	-4.21975200	-1.49919500	1.28616800
C	-3.50085300	-3.80136400	-0.13692800
H	-2.40552700	-2.49257200	-1.44402200
C	-4.65003300	-2.75272800	1.72076600
H	-4.53409600	-0.60659900	1.81780100
C	-4.29256700	-3.90340200	1.01148600
H	-3.22082900	-4.69374000	-0.68540100
H	-5.27749000	-2.83015100	2.60099000
H	-4.63518700	-4.87437200	1.34910200
C	-2.61591900	2.43579000	0.12403700
C	-2.50876700	3.32550900	1.21736400
C	-2.61871000	2.96988200	-1.18295700
C	-2.41146800	4.69966200	1.01394200
H	-2.50876700	2.92567900	2.22936000
C	-2.52022600	4.34830400	-1.37622700
H	-2.70553100	2.31318900	-2.03827600
C	-2.41479300	5.21596800	-0.28575100
H	-2.33861500	5.36786700	1.86445100
H	-2.53344400	4.74703000	-2.38444900
H	-2.34125700	6.28498800	-0.44598900
O	-3.02991500	0.09944800	-1.70305600
H	-3.25594300	-0.73125000	-2.14147200
H	-2.87623000	0.79292100	1.49633900
H	0.22348400	-2.59108700	-2.25479300
O	-0.52001700	-2.22033100	-2.74779600
H	-0.28119000	-2.33240200	-3.67118700

TS5(a)

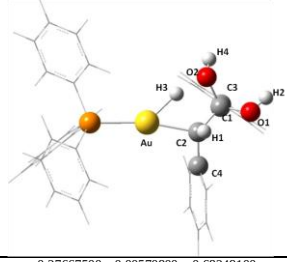

Au	0.27667500	0.00570800	-0.68249100
P	-1.97013000	-0.11186600	0.10055000
C	-2.91184400	1.35017500	-0.40323800
C	-4.20634300	1.23830800	-0.93791800
C	-2.33336700	2.62190800	-0.22412100
C	-4.91466400	2.39206000	-1.28420600
H	-4.65121500	0.25989500	-1.08278200
C	-3.05086200	3.76686500	-0.56725500
H	-1.33086400	2.71458700	0.18660300
C	-4.34027600	3.65176500	-1.09847800
H	-5.91227900	2.30556500	-1.69839200
H	-2.60569600	4.74487500	-0.42764600
H	-4.89305200	4.54299600	-1.37050300
C	-2.11277000	-0.21445700	1.90247900
C	-3.07845000	0.53129100	2.59997800
C	-1.25548900	-1.08153100	2.60676300
C	-3.18755500	0.40037000	3.98668300
H	-3.73392700	1.20855900	2.06329100
C	-1.37654100	-1.21003200	3.98980900
H	-0.50141100	-1.65296800	2.07247000
C	-2.34186600	-0.46871900	4.67975400
H	-3.93221500	0.97665800	4.52303900
H	-0.71801700	-1.88000600	4.53014900
H	-2.43031400	-0.56604800	5.75517800
C	-2.84391300	-1.54880200	-0.56919700
C	-3.68780900	-2.32832900	0.24013400
C	-2.69366300	-1.86336500	-1.93384200
C	-4.37783800	-3.40859500	-0.31646200
H	-3.80103100	-2.09290800	1.29282400
C	-3.39278800	-2.93871900	-2.48088700
H	-2.03696300	-1.26741300	-2.56173900
C	-4.23308300	-3.71188700	-1.67215800
H	-5.02729700	-4.01014900	0.30860400
H	-3.28032200	-3.17658600	-3.53210000
H	-4.77070400	-4.55016400	-2.09890100
C	2.26871000	0.53852300	-1.33776700
C	3.27787400	-0.60354800	-1.53610600
C	3.85603700	-1.26106200	-0.31044300
C	3.14425000	-2.24989200	0.39339500
C	5.11669400	-0.85658100	0.15718900
C	3.70010900	-2.84197000	1.52989100
H	2.15228700	-2.55630300	0.06863100
C	5.66724700	-1.45217700	1.29407900
H	5.65488500	-0.06769500	-0.36032300
C	4.96330000	-2.44651800	1.97847700
H	3.15183800	-3.61340000	2.05917900
H	6.64333900	-1.13813800	1.64535100
H	5.39597900	-2.91061400	2.85678200
C	2.56345500	1.64905000	-0.40061700
C	2.76015700	1.45668600	0.98513300
C	2.60812600	2.96212100	-0.91672300
C	3.01401200	2.54693000	1.81740500
H	2.71922600	0.45627700	1.40413200
C	2.86527900	4.04681700	-0.07914800
H	2.45587000	3.11935200	-1.98255100
C	3.06969000	3.84102100	1.28915000
H	3.16746600	2.38837200	2.87897900
H	2.91225100	5.04839200	-0.49149600
H	3.27010700	4.68379600	1.94019600
O	4.24794700	-0.10820900	-2.39473800
H	4.94760100	-0.76245800	-2.50971700
H	2.10626300	0.93450600	-2.33715300
H	2.70864300	-2.48489600	-2.06547000
O	2.44194000	-1.57798000	-2.26959400
H	1.30019400	-0.98370100	-1.63394400

TS5(b)				VIII(a)				TS6(a)			
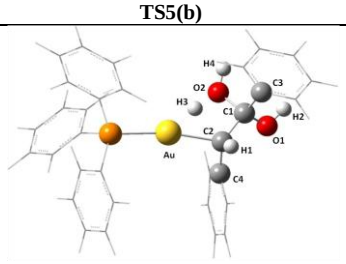				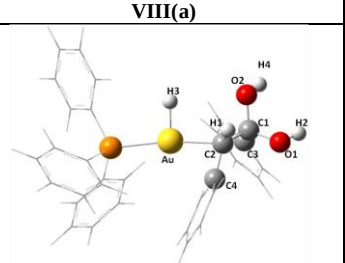				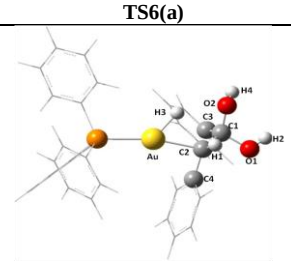			
Au	0.37848200	-0.06084500	-0.08184200	Au	0.48317600	0.28677600	-0.84101500	Au	0.41433100	0.15793700	-0.84845300
P	-1.96262500	0.26475300	0.02334300	P	-1.70554000	-0.23924000	0.01041200	P	-1.78173900	-0.18505200	0.03348100
C	-2.66926800	-0.44836200	1.53045100	C	-2.83462900	1.15637100	-0.20889700	C	-2.85962500	1.22923300	-0.30262500
C	-3.65073500	0.23657700	2.26728900	C	-4.17586200	0.95517500	-0.57962200	C	-4.18103900	1.04941500	-0.74564700
C	-2.23923900	-1.72320600	1.94778300	C	-2.35872900	2.46070900	0.02438600	C	-2.36175300	2.52902500	-0.08782400
C	-4.19954600	-0.35544300	3.40758600	C	-5.03154500	2.05209200	-0.70442900	C	-4.99654800	2.16310700	-0.96236300
H	-3.97712300	1.22198400	1.95278500	H	-4.54105800	-0.04761500	-0.77387300	H	-4.56343700	0.05007300	-0.92263700
C	-2.79790500	-2.30711600	3.08442400	C	-3.22214700	3.54836100	-0.10045200	C	-3.18560200	3.63309000	-0.30189100
H	-1.47630700	-2.25512500	1.38507800	H	-1.32066000	2.62194400	0.30307700	H	-1.33753300	2.67534000	0.24652100
C	-3.77614800	-1.62318800	3.81436600	C	-4.55732700	3.34434700	-0.46481100	C	-4.50203400	3.45029600	-0.73962200
H	-4.95537300	0.17336400	3.97630600	H	-6.06487500	1.89741500	-0.99182900	H	-6.01465600	2.02428200	-1.30645400
H	-2.46834000	-3.28880700	3.40350500	H	-2.85576800	4.55242300	0.07820200	H	-2.80266400	4.63300500	-0.13538600
H	-4.20351000	-2.07683300	4.70059100	H	-5.22440200	4.19192700	-0.56721400	H	-5.13767000	4.31059400	-0.91189200
C	-2.82105700	-0.50710200	-1.37056200	C	-1.68055000	-0.62602800	1.77876700	C	-1.78374700	-0.42105000	1.82910200
C	-3.98749100	-1.26604000	-1.17627700	C	-2.65540500	-0.11027100	2.64980500	C	-2.74370400	0.20406600	2.64309900
C	-2.31576000	-0.31854000	-2.67147500	C	-0.66882000	-1.46910400	2.27971800	C	-0.81975100	-1.27031500	2.40672600
C	-4.64310100	-1.82344400	-2.27723700	C	-2.62073300	-0.44394900	4.00627300	C	-2.74156800	-0.02823200	4.02092200
H	-4.37461700	-1.42111500	-0.17519100	H	-3.43074500	0.54605800	2.26966700	H	-3.48146700	0.86562800	2.20200800
C	-2.98093200	-0.87344200	-3.76379500	C	-0.64647900	-1.79987600	3.63455500	C	-0.82930300	-1.49848400	3.78247000
H	-1.40955200	0.26088400	-2.82552700	H	0.09500700	-1.86515100	1.61518100	H	-0.07050600	-1.75256700	1.78404900
C	-4.14343700	-1.62682300	-3.56656400	C	-1.62159700	-1.28731700	4.49763400	C	-1.78931300	-0.87760200	4.58918900
H	-5.54147400	-2.41025300	-2.12625500	H	-3.37423500	-0.04664000	4.67617500	H	-3.48309700	0.45321700	4.64758500
H	-2.59254900	-0.72591300	-4.76461300	H	0.12963600	-2.45224500	4.01749200	H	-0.08987500	-2.15531600	4.22551100
H	-4.65468100	-2.06250200	-4.41663700	H	-1.59990200	-1.54404400	5.55001700	H	-1.79215600	-1.05444500	5.65811600
C	-2.43022400	2.01284000	0.01350700	C	-2.47115000	-1.65037900	-0.82279000	C	-2.58998600	-1.63972600	-0.67664500
C	-3.52073100	2.46868300	-0.74665100	C	-3.05315500	-2.70015900	-0.09229000	C	-3.34176700	-2.51266100	0.12869400
C	-1.70743400	2.91694700	0.81523800	C	-2.50661700	-1.67304200	-2.23128700	C	-2.49464000	-1.86966300	-2.06259100
C	-3.88587000	3.81651400	-0.69600600	C	-3.65853300	-3.76363500	-0.76816500	C	-3.99615000	-3.60137600	-0.45327500
H	-4.07418100	1.77605400	-1.37157900	H	-3.03571300	-2.68526900	0.99190300	H	-3.41101800	-2.34299600	1.19772500
C	-2.08395400	4.25864500	0.86401100	C	-3.11940000	-2.73468800	-2.89498900	C	-3.15713200	-2.95560700	-2.63398700
H	-0.85969300	2.56927900	1.39966700	H	-2.06511000	-0.86191100	-2.80349800	H	-1.90719900	-1.20293500	-2.68737300
C	-3.17204900	4.70833800	0.10781800	C	-3.69149700	-3.78195400	-2.16379000	C	-3.90607300	-3.82144900	-1.82976700
H	-4.72656100	4.16734100	-1.28292400	H	-4.10502800	-4.57342600	-0.20319900	H	-4.57442200	-4.27498300	0.16816800
H	-1.53057300	4.95253700	1.48594800	H	-3.14863600	-2.74818700	-3.97823500	H	-3.08559400	-3.13015800	-3.70105400
H	-3.45967100	5.75231000	0.14393600	H	-4.16140200	-4.60861500	-2.68301400	H	-4.41472700	-4.66754700	-2.27613100
C	2.48713100	-0.62854800	0.13619600	C	2.42498500	0.98554600	-1.35759600	C	2.39908600	0.83523600	-1.36037500
C	3.56859400	-0.00157500	-0.77288800	C	3.56308600	-0.03212400	-1.40310200	C	3.54178300	-0.18815100	-1.40371900
C	4.10911400	1.29700800	-0.23155400	C	3.67420300	-1.00805700	-0.24721900	C	3.67428500	-1.15659000	-0.24483300
C	3.40466800	2.50557200	-0.37901300	C	2.90189300	-2.18382900	-0.24563200	C	2.86086600	-2.30336500	-0.18663200
C	5.30915400	1.28342100	0.49954300	C	4.54424700	-0.75420700	0.82451500	C	4.61912900	-0.93247900	0.76877500
C	3.91448900	3.68630200	0.16719900	C	3.00119500	-3.08971900	0.81374600	C	2.99181800	-3.20789300	0.86982600
H	2.45424300	2.53611100	-0.90682300	H	2.24178400	-2.39578700	-1.08279800	H	2.13765100	-2.49806200	-0.97428100
C	5.81194200	2.46722700	1.04300100	C	4.64119000	-1.66473300	1.88168100	C	4.74792500	-1.84222500	1.82262500
H	5.84038000	0.34720700	0.65020600	H	5.13740500	0.15586000	0.82883000	H	5.24458400	-0.04566100	0.73000600
C	5.11926700	3.66939400	0.87343800	C	3.87081600	-2.83063400	1.87863500	C	3.93556500	-2.97780700	1.87591400
H	3.37210400	4.61628500	0.03887200	H	2.41954500	-4.00547000	0.79705700	H	2.37317000	-4.09854800	0.89723600
H	6.74249700	2.45019300	1.59854600	H	5.32316400	-1.46680600	2.70098800	H	5.48682100	-1.66667400	2.59634200
H	5.51503800	4.58684000	1.29226200	H	3.95804800	-3.54041500	2.69305400	H	4.04513400	-3.68570200	2.68918100
C	2.39922400	-2.10976000	0.20025300	C	2.17599200	1.89424300	-0.23787700	C	2.27773500	1.84533300	-0.29827800
C	2.41488500	-2.73209300	1.46341900	C	1.87720700	1.37682800	1.06737900	C	2.27721100	1.51833100	1.08504000
C	2.28078200	-2.91173900	-0.95370900	C	1.93562600	3.27728300	-0.48139900	C	2.05591800	3.19502200	-0.67649800
C	2.32094600	-4.12163400	1.57221600	C	1.39057500	2.23375800	2.07552000	C	2.09539100	2.51851100	2.04342200
H	2.51455100	-2.12098600	2.35865400	H	2.15286500	0.35770500	1.32259700	H	2.44939500	0.49498600	1.39961600
C	2.19096900	-4.29693000	-0.84024900	C	1.47773700	4.10265100	0.53126700	C	1.88773400	4.18132300	0.28793300
H	2.26936600	-2.44741600	-1.93619700	H	2.14211700	3.67498200	-1.47139000	H	2.04906200	3.45222200	-1.73297200
C	2.21032800	-4.90547400	0.42153000	C	1.19654700	3.58224900	1.81304200	C	1.90766700	3.84525400	1.65038900
H	2.34377000	-4.58943000	2.55007100	H	1.18941300	1.83006400	3.06145000	H	2.10714600	2.26000100	3.09606200
H	2.10940800	-4.90636800	-1.73336900	H	1.33684500	5.16068200	0.34069600	H	1.75030100	5.21355300	-0.01305400
H	2.14286200	-5.98385600	0.50362000	H	0.83897900	4.24301600	2.59396100	H	1.77890300	4.61846400	2.39860400
O	4.54561800	-0.93403900	-1.04257500	O	4.70823900	0.80335900	-1.47817700	O	4.67217600	0.65838900	-1.50642200
H	5.30186300	-0.49716200	-1.45210900	H	5.49175400	0.25456200	-1.60191000	H	5.43496400	0.12564700	-1.76069100
H	2.61817000	-0.21565600	1.13222900	H	2.41431900	1.48823500	-2.31646900	H	2.36391800	1.28640400	-2.34417200
H	1.69063900	0.18008900	-1.20611700	H	3.94668800	-1.48651900	-2.65214100	H	3.81522600	-1.72765400	-2.58609100
O	2.79733400	0.26823100	-2.02193500	O	3.36143400	-0.72199000	-2.62020600	O	3.33761400	-0.89162200	-2.61611200
H	3.08538200	1.09082700	-2.44324700	H	0.35800100	-0.55987800	-2.15920600	H	1.09108600	-0.55097800	-2.10404000

IX	TS7	TS7’
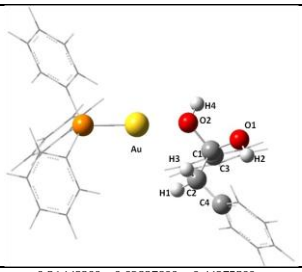	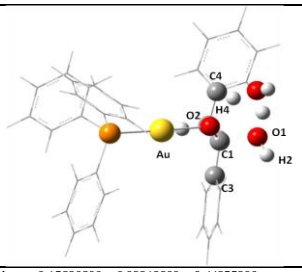	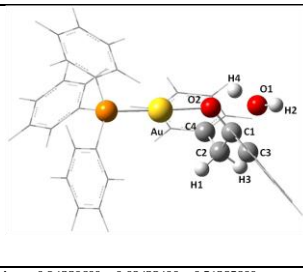

Au	-0.31448800	0.02887600	-0.44975300
P	1.87861000	0.32155400	0.03384600
C	2.41147400	-0.64093800	1.46851800
C	3.62092900	-1.35619600	1.45028900
C	1.61771000	-0.63382700	2.63162600
C	4.03259100	-2.04993600	2.59147600
H	4.23176400	-1.37022600	0.55434800
C	2.04099800	-1.32326800	3.76666000
H	0.67806900	-0.08870000	2.64647100
C	3.24767700	-2.03173500	3.74643800
H	4.96498800	-2.60186500	2.57649000
H	1.43207300	-1.31299500	4.66305300
H	3.57193500	-2.57040500	4.62877900
C	2.26487800	2.05174900	0.39270900
C	3.13030500	2.39369900	1.44613100
C	1.72698900	3.06000600	-0.43017400
C	3.45580100	3.73459800	1.66711700
H	3.54168000	1.62041900	2.08554700
C	2.06255900	4.39390900	-0.20409700
H	1.05381100	2.79866800	-1.24189300
C	2.92561200	4.73103400	0.84464700
H	4.12160300	3.99831600	2.48031100
H	1.65110200	5.16918100	-0.83967300
H	3.18029800	5.76927000	1.02089600
C	2.92698700	-0.16873500	-1.35596200
C	4.02760300	0.61638900	-1.73950800
C	2.64654100	-1.36800700	-2.03864200
C	4.84281200	0.19734100	-2.79399000
H	4.23866300	1.54604400	-1.22260300
C	3.46893800	-1.77857400	-3.08676600
H	1.78966200	-1.97077600	-1.75030500
C	4.56573700	-0.99600700	-3.46476500
H	5.68976400	0.80416200	-3.09156900
H	3.25312000	-2.70086800	-3.61302200
H	5.19852200	-1.31441400	-4.28449700
C	-3.73356700	-0.24445500	1.01170800
C	-3.31730000	-1.01392500	-0.24824700
C	-2.56821200	-2.30477700	-0.03303600
C	-1.98211000	-2.93056500	-1.15145000
C	-2.50619500	-2.93300500	1.21794000
C	-1.34224600	-4.16278700	-1.01250300
H	-2.02285500	-2.44972200	-2.12727000
C	-1.86331000	-4.16754300	1.35156100
H	-2.96350000	-2.47475700	2.08875600
C	-1.28176700	-4.78234800	0.24061700
H	-0.89939200	-4.64288900	-1.87822300
H	-1.82553700	-4.65084200	2.32112700
H	-0.79104800	-5.74257900	0.34713800
C	-4.24208900	1.12463800	0.66832000
C	-5.58040400	1.32207400	0.29031800
C	-3.34995400	2.21344400	0.60847800
C	-6.00798200	2.57019400	-0.16692800
H	-6.27772400	0.49018400	0.33641400
C	-3.78007100	3.46132300	0.14413900
H	-2.32105700	2.08956400	0.94496000
C	-5.10817500	3.63778600	-0.25016000
H	-7.04283600	2.71066000	-0.45763800
H	-3.08570800	4.29356300	0.11000500
H	-5.44518300	4.60411800	-0.60632500
O	-4.45800900	-1.18951500	-1.02427500
H	-4.31540900	-1.89750500	-1.66240200
H	-4.49545800	-0.83392400	1.51725500
O	-2.39836500	-0.14142500	-1.03489800
H	-2.83664300	0.72713000	-1.10133500
H	-2.87485800	-0.18513500	1.67659800

Au	0.15890800	-0.02219900	-0.44255900
P	-2.04197200	-0.27020500	0.02235000
C	-2.93716000	-1.17662900	-1.26491100
C	-3.86488000	-2.17937600	-0.93524800
C	-2.72359200	-0.83594700	-2.61435300
C	-4.57392100	-2.82875100	-1.94948600
H	-4.02804600	-2.45037700	0.10211500
C	-3.44080100	-1.48527500	-3.61821500
H	-2.00245800	-0.06540700	-2.87261500
C	-4.36474000	-2.48219900	-3.28604300
H	-5.28757200	-3.60324200	-1.69416800
H	-3.27748300	-1.22022500	-4.65621400
H	-4.91631000	-2.98922800	-4.06872800
C	-2.89403600	1.31579400	0.21430700
C	-4.18080200	1.51500100	-0.31418000
C	-2.26819700	2.34433100	0.94390000
C	-4.83566600	2.73137300	-0.10453300
H	-4.66094100	0.72771300	-0.88489200
C	-2.93330200	3.55162900	1.15375000
H	-1.26698400	2.19849500	1.33968700
C	-4.21593700	3.74539300	0.62945800
H	-5.82716200	2.88508500	-0.51400300
H	-2.45153100	4.34160100	1.71783000
H	-4.72813000	4.68670500	0.78954100
C	-2.30950900	-1.17853900	1.56711700
C	-3.27235000	-0.75739300	2.49972600
C	-1.55647600	-2.34212800	1.81577700
C	-3.47998400	-1.49859700	3.66610100
H	-3.84979600	0.14191300	2.31616500
C	-1.77491900	-3.07818300	2.97946800
H	-0.80637900	-2.66593400	1.09952400
C	-2.73543100	-2.65560800	3.90535100
H	-4.22124700	-1.17085900	4.38544300
H	-1.19542700	-3.97419500	3.16868400
H	-2.89848400	-3.22590500	4.81200200
C	3.40667200	0.14238800	1.19595500
C	3.02814600	0.87521200	-0.09999500
C	2.59562200	2.31349800	0.06104200
C	2.04922400	2.96929700	-1.06006200
C	2.76564800	3.02815500	1.25667900
C	1.69108400	4.31581800	-0.98604500
H	1.88908200	2.41308900	-1.98075600
C	2.39492900	4.37455700	1.32918000
H	3.17749700	2.54604600	2.13680800
C	1.86456300	5.02041100	0.21000800
H	1.27360500	4.81340200	-1.85446100
H	2.52769300	4.91786500	2.25803400
H	1.58764200	6.06658700	0.26800300
C	3.93997900	-1.23399200	0.93596700
C	5.32290200	-1.42666500	0.77772300
C	3.07418500	-2.31805800	0.71311600
C	5.82438500	-2.65871900	0.35054100
H	6.00395700	-0.59973800	0.96844000
C	3.57532700	-3.54966600	0.28331500
H	2.00413000	-2.18955500	0.85926600
C	4.94976600	-3.71713900	0.08749700
H	6.89349200	-2.79309200	0.22578600
H	2.89714600	-4.37798000	0.10671400
H	5.33795700	-4.67156800	-0.24961200
O	4.38352100	0.95716500	-0.87672000
H	4.38706700	1.79613600	-1.35697700
H	4.14204600	0.73404200	1.73397300
O	2.19737000	0.15156900	-0.90990600
H	3.07460400	-0.88896500	-1.69538000
H	2.50538400	0.12602000	1.80825000
H	4.39752700	-0.05703300	-1.61811000
O	4.00764500	-1.06234000	-2.09161700
H	3.96227700	-1.05570600	-3.05493100

Au	-0.24330600	-0.08433400	-0.51385900
P	1.94996600	-0.20700200	0.03147600
C	2.25837400	-1.40169200	1.35640500
C	3.37127500	-2.25867200	1.31176800
C	1.38581600	-1.44385500	2.46025800
C	3.60977300	-3.14112200	2.36856400
H	4.03899700	-2.23780500	0.45744500
C	1.63487600	-2.32429600	3.51205800
H	0.51743800	-0.79188700	2.49034600
C	2.74647200	-3.17297100	3.46604200
H	4.46739100	-3.80248600	2.33238300
H	0.96290100	-2.35469000	4.36172000
H	2.93476500	-3.86020800	4.28219200
C	2.60069100	1.38268900	0.60464800
C	3.43090100	1.46331800	1.73544500
C	2.29503500	2.54704100	-0.12641800
C	3.95463600	2.69942800	2.12444500
H	3.66335000	0.56954700	2.30393300
C	2.83015100	3.77378300	0.26504000
H	1.64383500	2.49029500	-0.99412700
C	3.65829400	3.85017600	1.39070300
H	4.59339500	2.76090400	2.99759400
H	2.60254900	4.66765000	-0.30405800
H	4.06861300	4.80566400	1.69504900
C	2.98411200	-0.70867700	-1.36671200
C	4.21046700	-0.07231600	-1.62314700
C	2.56362900	-1.77703900	-2.18157000
C	5.00885100	-0.50825400	-2.68375900
H	4.53279300	0.75641100	-1.00254200
C	3.37034800	-2.20808700	-3.23358700
H	1.61092800	-2.26317800	-1.99109300
C	4.59166900	-1.57315500	-3.48538300
H	5.95314200	-0.01539500	-2.88268800
H	3.04644500	-3.03041500	-3.86048400
H	5.21300000	-1.90591000	-4.30820400
C	-3.49467700	0.87437700	0.85454400
C	-3.41508100	-0.09909700	-0.31073300
C	-3.90384800	-1.48674100	-0.03570200
C	-3.23186300	-2.58529000	-0.59876800
C	-5.05633500	-1.70614500	0.74444800
C	-3.69842100	-3.88221900	-0.37532400
H	-2.34523800	-2.41749400	-1.20099900
C	-5.52181400	-3.00423600	0.95490700
H	-5.59805000	-0.87334100	1.18271200
C	-4.84257200	-4.09265200	0.39836800
H	-3.17124000	-4.72584900	-0.80606600
H	-6.41116600	-3.16693800	1.55286300
H	-5.20500300	-5.09972200	0.56751400
C	-3.08270900	2.28325700	0.56034400
C	-3.97710500	3.17272800	-0.05821800
C	-1.79227400	2.73014200	0.88278300
C	-3.57441200	4.47116700	-0.37848300
H	-4.98779300	2.84694900	-0.29089100
C	-1.39128200	4.03144400	0.56705900
H	-1.10307200	2.06372600	1.39693300
C	-2.27917100	4.89979500	-0.07193900
H	-4.27253700	5.15002800	-0.85512100
H	-0.39276300	4.36368000	0.82834500
H	-1.97148600	5.91020100	-0.31468800
O	-4.28975400	0.51022100	-1.50350700
H	-4.81294000	-0.20922900	-1.89145300
H	-4.50623700	0.83425600	1.25083600
O	-2.27455000	-0.01008400	-1.09463500
H	-3.18049700	0.47557100	-1.88690100
H	-2.86829800	0.42901300	1.62879800

X				X'				ketone			
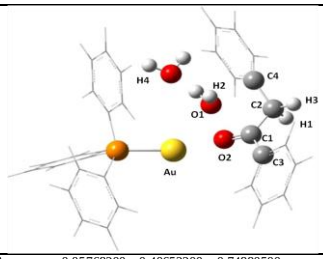				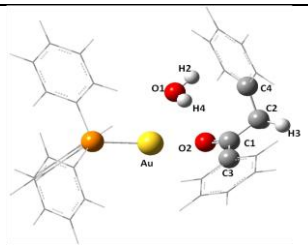				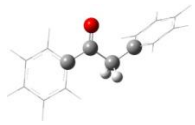			
Au	-0.05768200	0.40652200	-0.74880500	Au	-0.04553500	0.15041600	-0.83893500	C	-0.48579500	-0.81852800	0.11091400
P	2.01251700	0.00936300	0.06009400	P	2.02505000	-0.02904000	0.05103800	C	0.44837400	0.37941200	-0.02966700
C	1.76498500	-1.15348500	1.44113900	C	2.14839500	-1.43265500	1.18469000	C	1.91758800	0.12994500	-0.01211700
C	1.98635400	-2.52798200	1.25738900	C	3.35569300	-2.14521600	1.30562800	C	2.77877600	1.23469500	-0.15252800
C	1.14469500	-0.69902000	2.62205900	C	1.04062300	-1.78166900	1.98113800	C	2.47148700	-1.15429400	0.13916700
C	1.56569600	-3.44229500	2.23187500	C	3.45656400	-3.18405000	2.23326600	C	4.15938600	1.05760400	-0.14150900
H	2.45552300	-2.88694500	0.34792100	H	4.20122500	-1.89457800	0.67402300	H	2.33539400	2.21811000	-0.26804100
C	0.74303200	-1.61316500	3.59607500	C	1.15699000	-2.81951600	2.90740400	C	3.85631000	-1.32843700	0.15068800
H	0.95958800	0.36127400	2.76735200	H	0.09111200	-1.26673000	1.86989000	H	1.82576700	-2.01882800	0.24810100
C	0.93730400	-2.98722100	3.39675900	C	2.36206900	-3.51688700	3.03628700	C	4.70009200	-0.22451700	0.01047600
H	1.72505700	-4.50469500	2.07684100	H	4.38587900	-3.73377100	2.32535600	H	4.81676400	1.91274900	-0.25035900
H	0.26515800	-1.25995400	4.50379900	H	0.30430200	-3.08483700	3.52182800	H	4.27538200	-2.32118200	0.26813200
H	0.60341200	-3.69658200	4.14697400	H	2.44607600	-4.32408100	3.75442800	H	5.77546600	-0.36103500	0.01906800
C	2.91868200	1.43167400	0.70350400	C	2.46063100	1.45673100	0.99145800	C	-1.93983700	-0.47543700	0.06337300
C	3.73337200	1.32718100	1.84563000	C	2.95136800	1.36888800	2.30429900	C	-2.61480800	-0.07324500	1.22506200
C	2.86116300	2.64428800	-0.00812000	C	2.31761800	2.71740500	0.37874600	C	-2.64039500	-0.51769600	-1.15027700
C	4.48153800	2.42921100	2.26560900	C	3.29989200	2.53396600	2.99395200	C	-3.96407100	0.27989600	1.17385400
H	3.77611700	0.39697800	2.40288600	H	3.05865000	0.40094600	2.78066600	H	-2.07543400	-0.02954100	2.16918300
C	3.61660500	3.73669600	0.41640800	C	2.67567800	3.87227800	1.07203100	C	-3.99032000	-0.16513600	-1.20274000
H	2.22790000	2.72613200	-0.88683500	H	1.93473700	2.78952800	-0.63578700	H	-2.12158800	-0.82346300	-2.05678500
C	4.42502900	3.62969900	1.55258600	C	3.16511100	3.78076800	2.38054100	C	-4.65416300	0.23407800	-0.04036300
H	5.10687500	2.35010300	3.14715800	H	3.67767400	2.46466900	4.00722600	H	-4.47591000	0.59171200	2.07757800
H	3.57302500	4.66945800	-0.13332700	H	2.57476500	4.84093900	0.59639000	H	-4.52225600	-0.20057400	-2.14707500
H	5.00735800	4.48154700	1.88291400	H	3.43964500	4.68052500	2.91816800	H	-5.70223900	0.50795300	-0.07996600
C	3.09254200	-0.81641000	-1.13438700	C	3.32007100	-0.25289900	-1.19175500	O	0.01020600	1.50365300	-0.15184100
C	4.48912900	-0.80742300	-0.96156100	C	4.54081700	0.43768900	-1.10149200	H	-0.23715700	-1.32529200	1.04596600
C	2.52724000	-1.50742100	-2.22185800	C	3.11007800	-1.17531200	-2.23422200	H	-0.23159100	-1.52986600	-0.67706900
C	5.30333500	-1.49674900	-1.86095900	C	5.54250500	0.19939900	-2.04629500				
H	4.93526100	-0.25541700	-0.14102100	H	4.70269000	1.15481500	-0.30408900				
C	3.35022800	-2.19651600	-3.11403600	C	4.11743400	-1.40867700	-3.16878300				
H	1.45113200	-1.49531600	-2.36884100	H	2.16372400	-1.70342300	-2.31064800				
C	4.73574100	-2.19280700	-2.93258600	C	5.33271300	-0.72129000	-3.07527100				
H	6.37893700	-1.48531300	-1.72993700	H	6.48294400	0.73334800	-1.97791600				
H	2.91261200	-2.72486600	-3.95309000	H	3.95506700	-2.11804500	-3.97159100				
H	5.37346800	-2.72231800	-3.63035600	H	6.11133600	-0.90066000	-3.80699400				
C	-4.35731100	-0.12329800	-0.95283800	C	-4.23899700	-0.45752200	-1.82128300				
C	-3.14332300	0.77595500	-0.92407600	C	-3.16064700	0.50351700	-1.36449500				
C	-3.24546600	2.17171700	-0.49996800	C	-3.46010300	1.69252100	-0.56629500				
C	-2.35025100	3.11326300	-1.05047300	C	-2.41650000	2.56802900	-0.18816500				
C	-4.19955400	2.59609100	0.44551400	C	-4.77992700	2.00124000	-0.16705000				
C	-2.40999400	4.44809400	-0.66130800	C	-2.68092800	3.69523700	0.58020900				
H	-1.63315800	2.79195600	-1.80005800	H	-1.39981700	2.35935400	-0.50438300				
C	-4.23622200	3.92895000	0.85146300	C	-5.04037900	3.13002500	0.60699100				
H	-4.88419700	1.88361300	0.89204100	H	-5.60491300	1.36515100	-0.46110300				
C	-3.34691900	4.85480200	0.29652900	C	-3.99308700	3.97563800	0.98384100				
H	-1.73734100	5.17350100	-1.10450800	H	-1.87292500	4.35991300	0.86257800				
H	-4.95833500	4.24787500	1.59402000	H	-6.05637800	3.35616500	0.90789800				
H	-3.38820700	5.89336300	0.60382700	H	-4.19792700	4.85584800	1.58193500				
C	-4.08996700	-1.54461500	-0.53865300	C	-4.23975700	-1.61594100	-0.84669600				
C	-4.43658900	-1.97112000	0.75282500	C	-5.11135400	-1.63040000	0.25342500				
C	-3.46037100	-2.44883100	-1.40828500	C	-3.25110500	-2.60870300	-0.94698000				
C	-4.15540700	-3.27538300	1.17126900	C	-4.97797200	-2.60114300	1.25245700				
H	-4.91850400	-1.27723400	1.43702300	H	-5.88385200	-0.87183600	0.34449100				
C	-3.17162300	-3.75150800	-0.99063400	C	-3.11343900	-3.57508600	0.05286500				
H	-3.18680400	-2.12959800	-2.40996100	H	-2.56932700	-2.60254900	-1.79269700				
C	-3.51864500	-4.17103900	0.30102800	C	-3.96973800	-3.56674100	1.16069800				
H	-4.42973200	-3.59209900	2.17249000	H	-5.64929200	-2.59485900	2.10431000				
H	-2.68129200	-4.43976400	-1.67110900	H	-2.33369300	-4.32503300	-0.02571400				
H	-3.30673500	-5.18733600	0.62123600	H	-3.84953800	-4.30333400	1.94743100				
O	-2.08680800	0.20260600	1.64684500	O	-2.20229300	-0.83990700	1.55721200				
H	-2.14847400	0.34891100	2.59364700	H	-2.76246700	-0.17574900	1.96661700				
H	-5.15964000	0.31305900	-0.36882400	H	-5.21224800	0.01261500	-1.89130300				
O	-2.09242200	0.30981200	-1.38903400	O	-2.00595300	0.18482800	-1.68944800				
H	-1.83851200	-2.91067800	0.84248100	H	-3.95985000	-0.78836100	-2.81843600				
H	-4.70191400	-0.08127300	-1.99119000	H	-2.81198600	-1.53030400	1.25876600				
H	-1.75479200	-0.71326700	1.53355600								
O	-1.13581000	-2.26298800	0.99384900								
H	-0.46449300	-2.69424000	1.53630900								

4. HOMO and LUMO structures of the $[(Ph_3P)Au\text{-alkyne}]^+$ complex

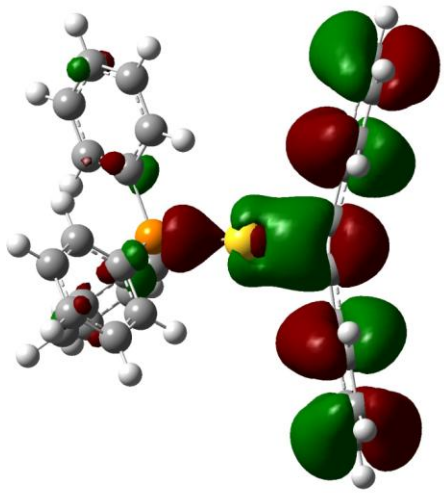

Structure of the Highest Occupied Molecular orbital of the $[(Ph_3P)Au\text{-alkyne}]^+$ complex.

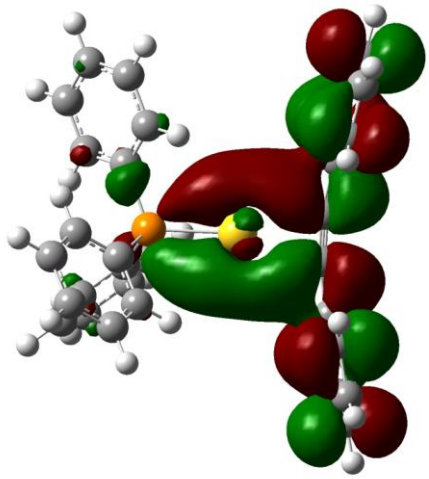

Structure of the Loweest Occupied Molecular orbital of the $[(Ph_3P)Au\text{-alkyne}]^+$ complex.

5. Energy profile for the uncatalized addition of a water molecule to the enol intermediate

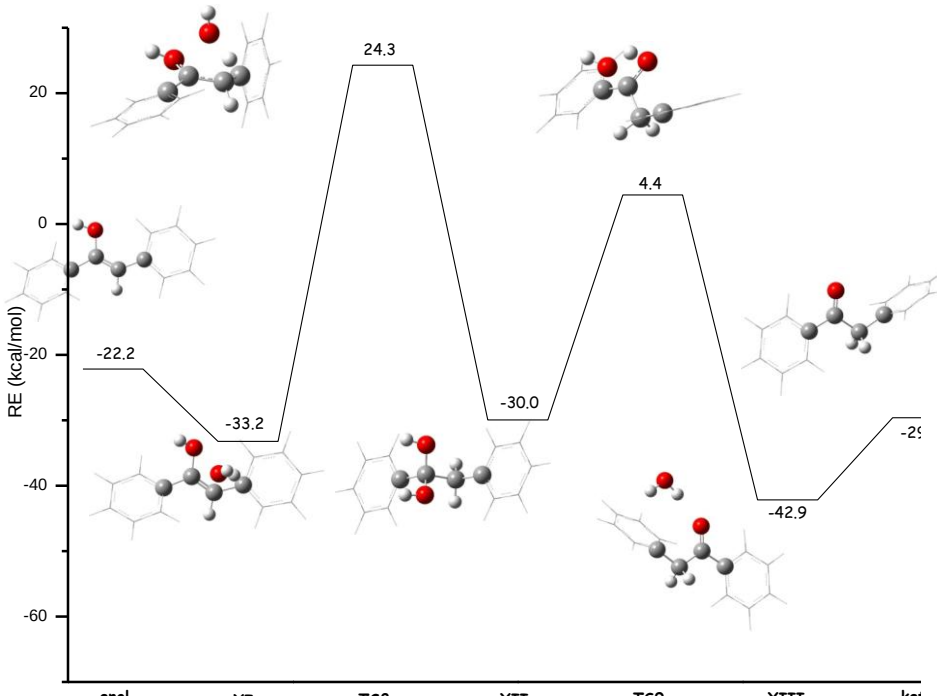

6. Charge distribution analysis for the [(Ph$_3$P)Au-alkene]$^+$ complexes

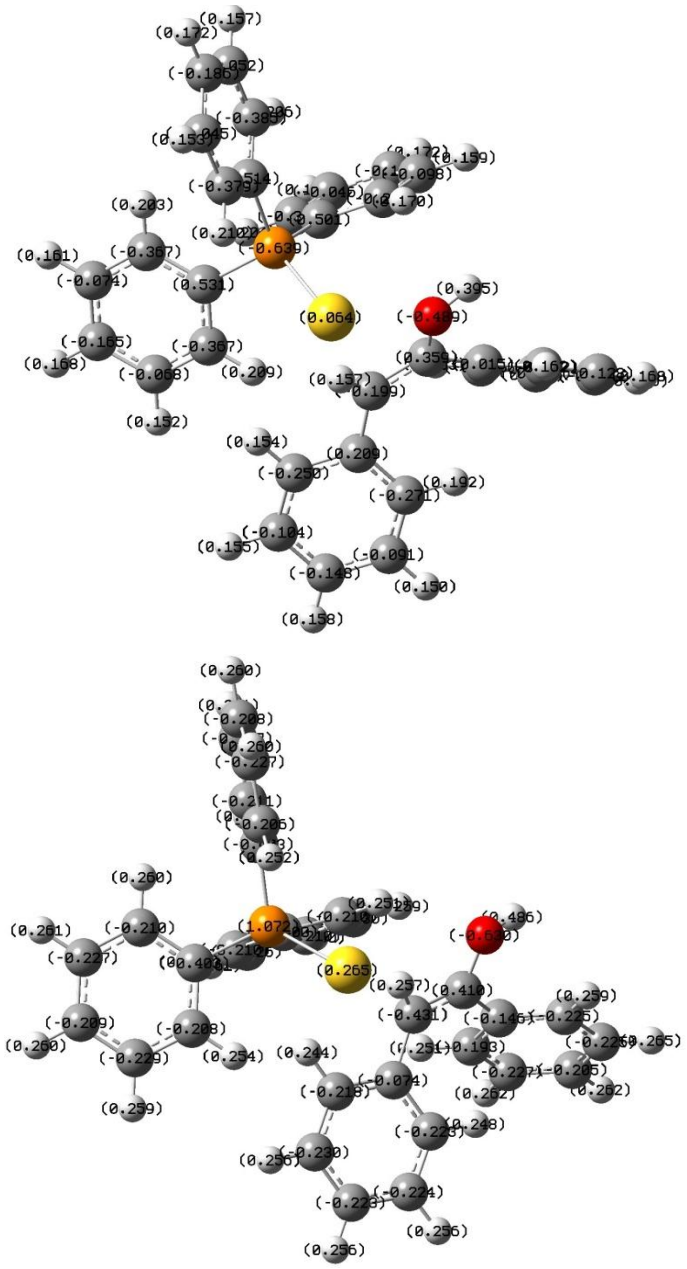

NBO and ESP charge distributions for the *E* isomer of the enol coordinated to the [(Ph$_3$P)Au]$^+$ complex

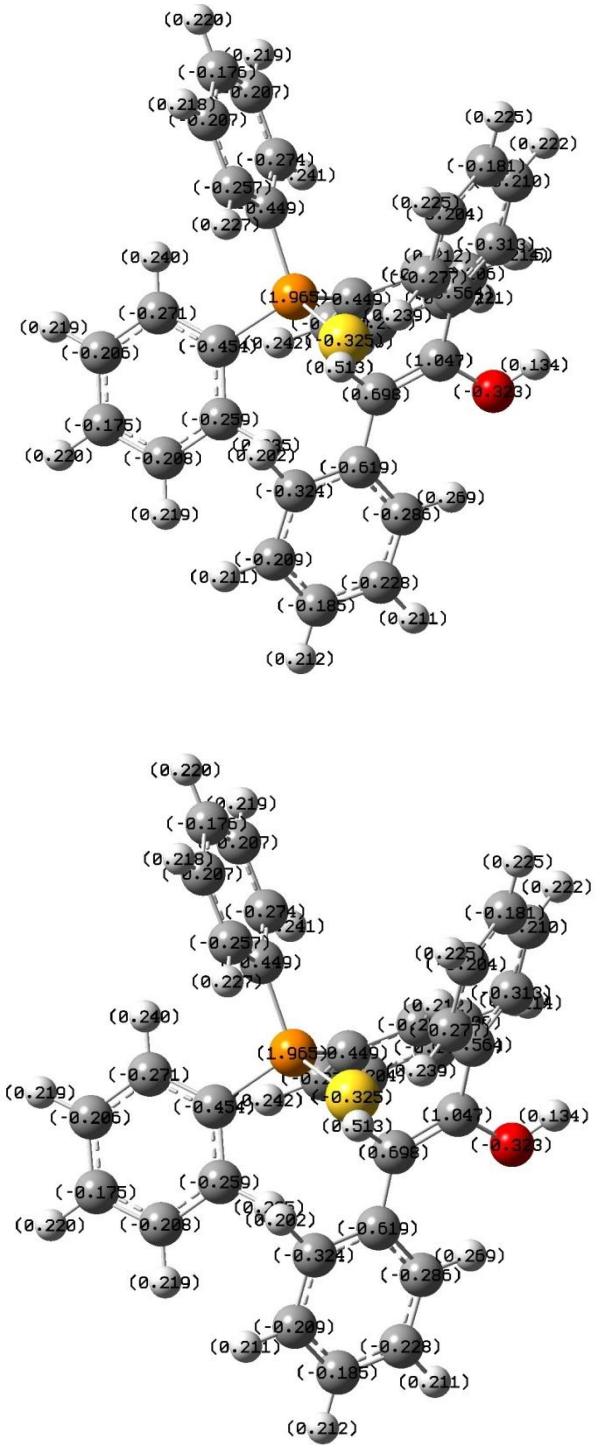

NBO and ESP charge distributions for the *Z* isomer of the enol coordinated to the $[(Ph_3P)Au]^+$ complex

[1] Cancès, M.; Mennucci, B.; Tomasi, J. *J. Chem. Phys.* **1997, *107*,** 3032-3041.

[2] Mennucci, B.; Cancès, E.; Tomasi, J. *J. Phys. Chem. B* **1997, *101*,** 10506-10507.

[3] Kollaman, P. *Chem. Rev.* **1993**, *93*, 2395.